Université catholique de Louvain

Ecole Polytechnique de Louvain

Institut de la matière condensée et des nanosciences

Bio- and Soft Matter

THERMOPLASTIC AS CARRIER FOR DELIVERING CARBON NANOTUBES AND LAYERED CLAY IN EPOXY RESIN FOR COMPOSITE APPLICATIONS

February 2013

Jury Members

Prof. J. Devaux (UCL, IMCN, supervisor)

Dr. D. Daoust (UCL, IMCN, supervisor)

Prof. T. Pardoen (UCL, iMMC)

Dr. B. Poulaert (Sonaca, Belgium)

Prof. C. Bailly (UCL, IMCN)

Dr. J. Cinquin (EADS, France)

Prof. I. Verpoest (KU Leuven, Belgium)

Prof. E. Gaigneaux (UCL, IMCN, chairperson)

I would like to express my sincere gratitude to all the people who made this thesis possible.

First of all, my thanks go to my supervisors Prof. Jacques Devaux and Dr. Daniel Daoust for their confidence, their availability and their enthusiasm and for having shared their expertise to improve the quality of this work.

I also would like to thank the members of my thesis committee, Prof. Thomas Pardoen from Institute of Mechanics, Materials and civil engineering (UCL-iMMC) and Dr. Bernard Poulaert from Sonaca, such as Prof. Christan Bailly for accompanying me during my thesis, for their advices and for the interesting discussions.

I am also grateful to Prof. Ignaas Verpoest from KU Leuven and Dr. Jacques Cinquin from EADS for accepting to be a member of my thesis jury and to Prof. Eric Gaigneaux for consenting to preside it.

My acknowledgments also go to Fonds pour la Formation à la Recherche dans l'Industrie et dans l'Agriculture (FRIA) for the financial support and to "Région Wallonne" for funding several projects that have benefited to accomplishment of this work. I give thanks to industrial partners Sonaca, Sabca and Techspace Aero for their valuable collaborations.

This thesis would not have been possible without teammates working on aeronautic composites. I really appreciate sharing information and debates with Waël Ballout, Remi Berben, François Cordenier, Benoît Coulon, Raphaël Debleser, Gauthier Finné, Edwin Henry, Michel Sclavons, Pascal Van Velthem and Quentin Voleppe.

Thank you to students from UCL and Institut Paul Lambin (IPL), Grégory, Minh, Christophe, François, Michael, Cédric and Kevin, who worked with me and have contributed to the achievement of this work:

I would like to give thanks to all members of the laboratory and especially to Aurore, Colette, Florian, Pascale and Sabine for their help and to Ali, Anne-Christine, Eric, Evelyne, Jun, Naïma and Nicolas for the excellent atmosphere they brought in the office.

I also wish to express my gratitude and thanks to several people and groups for their kind collaborations: Dr David Seveno from Université de Mons (UMons) for the considerable work concerning simulation, Michel Lenoble from InChem Corporation, Dr. Stefan Kuypers from JEOL, Dr. Giuseppe Canepa from Lonza, Nanocyl and Certech. Many thanks also to UCL groups of Prof. Charles-André Fustin, of Prof. Isabelle Huynen from Institute of Information and Communication Technologies, Electronics and Applied Mathematics (ICTEAM) and to pole of Materials and Processes Engineering (IMAP) from iMMC.

Last but not least, I would like to thank my family for their support and Mélissa for her daily encouragements giving me the motivation required to complete this work.

ABSTRACT

Thermoplastic and nanofiller additives have already shown their potential benefit on mechanical, thermal or electrical properties of composites. An original method to incorporate simultaneously a thermoplastic phase and nanoparticles in laminates processed by resin transfer molding (RTM) is proposed in the study. Introduction of nanocomposite prepared by melt blending in the dry preform intends to deliver both additives in the thermoset matrix during the process. The thesis explores the concept to determine if a soluble thermoplastic is exploitable to disperse and distribute nanofillers in epoxy resin and understand the key parameters controlling the mechanism.

First, this work focuses on the behavior of two thermoplastics, poly(ether sulfone) (PES) and poly(hydroxyether of bisphenol A) (phenoxy) in epoxy resin. Influence of these amorphous thermoplastics differing significantly by their glass transition temperature (T_g) on blend microstructure induced by reaction induced phase separation (RIPS) and on blend modulus is discussed in Chapter 1. As compared to PES, phenoxy generates smaller submicrometric nodules dispersed in the continuous epoxy resin-rich phase at low thermoplastic content. Phenoxy presents also the advantage to induce phase inversion at higher phenoxy concentration superior to 30 wt % in binary blends. Nevertheless, due to its lower T_g, phenoxy causes modulus drop around 90 °C and reduces thus thermomechanical properties of the crosslinked network. Effect of both thermoplastics on crosslinking kinetics is also studied by several techniques and shows that phenoxy plays a catalytic role while moderate PES contents do not affect reaction kinetics.

Then, solubility of PES and phenoxy in epoxide and diamine precursors and in reactive formulations like RTM6 resin qualified for aeronautics is investigated. Improved diffusion of lower molecular weight resin precursors into thermoplastic leading to dissolution at lower temperature is demonstrated in Chapter 2. Apparent migration of the thermoplastic macromolecules depending on their swelling by the resin precursors is also evidenced. Composition gradients and microstructures induced by PES and phenoxy filaments in epoxy resin are then detailed in Chapter 3. Interdiffusion favored for phenoxy chains characterized by a higher mobility produces wider thermoplastic distribution than for PES and contributes thus to prevention of phase inversion on a larger distance interval.

While the first part of this work considers only epoxy resin and thermoplastic, the second part of the study takes into account incorporation of nanofillers in the systems. Its objective is to prove that nanocomposite prepared with unmodified multiwalled carbon nanotubes (MWNTs) or organomodified layered clay allows to distribute both thermoplastic and nanofillers in epoxy resin. Two distinct stages are considered to achieve this goal. Nanofillers are first dispersed in the thermoplastic by melt blending and a thermal treatment is subsequently applied to the processed nanocomposites in the form of filaments in RTM6 resin.

Microstructures and properties of the produced nanocomposites are first investigated in Chapter 4 to control if the nanofillers are properly dispersed and homogeneously distributed in thermoplastic. Fine and homogeneous dispersion of MWNTs are reached in PES and phenoxy without severe process conditions. A good dispersion of organoclay platelets with intercalated-exfoliated morphology is also obtained in phenoxy. Then, location of the nanofillers and conservation of their dispersion is verified in Chapter 5 once nanocomposites are blended with RTM6 resin. The mechanisms controlling location of the nanoparticles in polymer blends are discussed on basis of thermodynamic predictions and other kinetics considerations. In order to complete the demonstration, Chapter 6 examines nanocomposite filaments during thermal treatment in epoxy resin and resulting composition gradients to confirm nanofiller delivery and to determine the interdiffusion mechanism. Identical distribution profiles of thermoplastic and nanofillers in the resin evidence that swelling of PES or phenoxy controls delivery of entangled nanofillers. The results validate that these amorphous polymers act as carrier for distribution of tubular and lamellar nanoparticles into epoxy resin and that, once RIPS takes place, a microstructure gradient is generated with, locally, thermoplastic nodules and nanofillers being dispersed in the epoxy resin continuous phase.

Finally, transposition of the concept to production of composite panels by RTM process is demonstrated by interleaving of nanocomposite films in the preform. Effect of the carbon fiber layers on thermoplastic and MWNT distribution is inspected. A considerable increase of mode I interlaminar fracture toughness is achieved thanks to phenoxy while PES and nanofillers do not lead to the same improvement.

TABLE OF CONTENTS

LIST OF ABBREVIATIONS AND SYMBOLS

A: 1) Absorbance; 2) Hamaker constant
ADSC: Alternating differential scanning calorimetry
AFP: Automated fiber placement
APC: Avion Plus Composite project
a.u.: Arbitrary units
BSMA: Bio- and Soft Matter pole from UCL-IMCN
CAI: Compression after impact
CCVD: Catalytic carbon vapor deposition
CDD: Charge-coupled device
CFRP: Carbon fiber reinforced polymer
CNTs: Carbon nanotubes
COMPASS: Condensed phase optimized molecular potentials of atomic simulation studies
CTE: Coefficient of thermal expansion (10^{-6}/°C)
CVD: Chemical vapor deposition
D: Diffusion coefficient (m^2/s)
D peak: Peak from disordered graphite
DCB: Double cantilever beam
DDS: 4,4'-diaminodiphenylsulfone
DETDA: 3,5-diethyltoluene-2,4-diamine and 3,5-diethyltoluene-2,6-diamine
DGEBA: Diglycidyl ether of bisphenol A
DMA: Dynamic mechanical analysis
DRI: Differential refractometer
DSC: Differential scanning calorimetry
DWNT: Double-walled carbon nanotube
EADS: European Aeronautic Defence and Space company
ECOM: Engine Composite project
ECOTAC: Efficient composite technologies for aircraft components project
Epoxy resin: Reactive formulation (epoxide and diamine hardener)
ESC: Environmental stress cracking
FRIA: Fonds pour la Formation à la Recherche dans l'Industrie et dans l'Agriculture
FRP: Fiber reinforced polymer
FTIR: Fourier transform infrared spectroscopy
G*: Complex modulus; G': Storage modulus; G'': Loss modulus (Pa)
G_{IC}: Energy release rate required for crack propagation in mode I ($J\ m^{-2}$)

h: Planck constant (6.63 x 10^{-34} J s)
H: enthalpy or heat of reaction (J)
HPLC: High performance liquid chromatography
ICTEAM: Institute of Information and Communication Technologies, Electronics and Applied Mathematics from UCL
IFSS: Interfacial shear strength (Pa)
ILSS: Interlaminar shear strength (Pa)
IMAP: Pole of Materials and Processes Engineering from UCL-iMMC
IMCN: Institute of Condensed Matter and Nanosciences from UCL
iMMC: Institute of Mechanics, Materials and civil engineering from UCL
IPL: Institut Paul Lambin
k_B: Boltzmann constant (1.38 x 10^{-23} J K^{-1})
K_{IC}: Fracture toughness (Pa $m^{1/2}$)
KU Leuven: Katholieke Universiteit Leuven
LCM: Liquid composite molding
LL: Line-line
LRI: Liquid resin infusion
M: Molar mass (g/mol); $\overline{M}_n$: Number average molar mass; $\overline{M}_w$: Weight average molar mass
MCDEA: 4,4'-methylenebis-(2,6-chlorodiethylaniline)
MDEA: 4,4'-methylenebis-(2,6-diethyl)-aniline
MMIPA: 4,4'-methylenebis-(2-isopropyl-6-methyl)-aniline
MSC: Multiplicative scatter correction
MSD: Mean square displacement
MWNT: Multiwalled carbon nanotube
n: refractive index
NDT: Non-destructive testing
NIR: Near infrared
NPT: Isothermic isobaric
NVT: Isothermic isovolume
PDI: Polydispersity index
PEI: Poly(ether imide)
PES: Poly(ether sulfone)
Phenoxy: Poly(hydroxyether of bisphenol A)
PLS: Partial least square regression
POLY: Polymer physics and chemistry laboratory from UCL
PPE: Poly(phenylene ether)
PS: Polystyrene

PSf: Polysulfone
RFI: Resin film infusion
RIPS: Reaction induced phase separation
RTM: Resin transfer molding
S: Solvent
SEC: Size exclusion chromatography
SEM: Scanning electron microscopy
SOLTEX: Soluble chain-extendable-polymer-filaments in textile preforms for in-situ resin toughening using rtm-technique project
SQRTM: Same qualified resin transfer molding
SWNT: Single-walled carbon nanotube
TEM: Transmission electron microscopy
T_g: Glass transition temperature
TGA: Thermogravimetric analysis
TGAP: Triglycidyl para-aminophenol
TGMDA: Tetraglycidyl-4,4'-methylenedianiline
THF: Tetrahydrofuran
TP: Thermoplastic
UCL: Université catholique de Louvain
UMons: Université de Mons
VARTM: Vacuum assisted resin transfer molding
VDW: van der Waals
VNA: Vector network analyzer
wt %: Mass percentage
XPS: X-ray photoelectron spectroscopy
XRD: X-ray diffraction
α: Conversion rate of resin crosslinking
γ: Interfacial energy (J m^{-2}); γ_d: Dispersive part of γ; γ_p: Polar part of γ
δ: Loss angle; tan δ: Damping factor
ε: Dielectric constant
θ: Bragg angle (between incident ray and scattering planes)
σ': Real part of the electrical conductivity (S m^{-1})
Φ: Volume fraction
ω: 1) Angular frequency (rad/s); 2) Wetting coefficient

LIST OF SCIENTIFIC COMMUNICATIONS

The present work has contributed to writing of several publications and to oral communications or exhibition of posters during conferences. This scientific output is listed here.

Publications

- **Dumont D**, Daoust D, Sclavons M, Devaux J. Microstructure control of epoxy resin blended with thermoplastic yarns. Proceedings of Polymer Processing Society 25 th Annual Meeting, (PPS-25) 2009;GS-V OP4 (Films & Fibers).
- **Dumont D**, Daoust D, Sclavons M, Devaux J, Seveno D, de Coninck J. Thermoplastic reinforcement for thermoset composites: Solubility measurements in epoxy resins, Proceedings of Vth International Conference on Science and Technology of Composite Materials (COMATCOMP'09) 2009:55-8 (Polymer-matrix composites).
- Seveno D, de Coninck J, **Dumont D**, Daoust D, Sclavons M, Devaux J. Solubility and diffusion of thermoplastic reinforcement in epoxy resins: a molecular dynamics study, Proceedings of Vth International Conference on Science and Technology of Composite Materials (COMATCOMP'09) 2009:59-62 (Polymer-matrix composites).
- **Dumont D**, Daoust D, Sclavons M, Devaux J. Dissolution and diffusion of nanofilled thermoplastic yarns in epoxy resins. Proceedings of Polymer Processing Society 26 th Annual Meeting (PPS-26) 2010;G09-335 (Polymer Blends and Alloys).
- **Dumont D**, Daoust D, Sclavons M, Devaux J. Thermoplastic yarns filled with carbon nanotubes for reinforcement of epoxy resins-based composites. Proceedings of European Conference on Composite Materials ECCM14 2010;991-ECCM14 (Nanocomposites).
- Van Velthem P, Berben R, Cordenier F, **Dumont D**, Henry E, Sclavons M, Daoust D. Phenoxy as carrier of additives at nano-scale: A way to improve properties of composites produced by resin transfer moulding. Proceedings of the 3rd International Carbon Composites Conference (IC3) 2011;(Carbon nanotubes and nanocomposites).
- Henry E, Berben R, Cordenier F, **Dumont D**, Sclavons M, Van Velthem P, Daoust D. Toward a new generation of aeronautic composite materials using nanofilled thermoplastic as reinforcement. Proceedings of the 2nd International Conference on Thermosets 2011:173-176 (Fiber Reinforced Thermosets).
- **Dumont D**, Seveno D, De Coninck J, Bailly C, Devaux J, Daoust D. Interdiffusion of thermoplastics and epoxy resin precursors: Investigations by experimental and molecular dynamics methods. Polymer International

2012;61(8):1263-71.

- **Dumont D**, Berben R, Cordenier F, Henry H, Sclavons M, Van Velthem P, Daoust D. Phenoxy for carbon nanotube dispersion into epoxy matrices of RTM-processed composites. Proceedings of Sampe Europe 33rd International Conference and Forum (SEICO12) 2012; Paper 67 (Material): 327-32.
- Henry E, Bailly C, Berben R, Bourbigot S, Cordenier F, Dumont D, Sclavons M, Van Velthem P, Daoust D. Thermoplastic as carrier of nanofillers into carbon fibre-epoxy resin composites: Influence of thermoplastic solubility on carbon nanotubes distribution. Proceedings of the 15th European Conference on Composite Materials (ECCM15) 2012; Nanocomposites;ID869 (Preparation and characterization).
- Dumont D, Bailly C, Baudouin AC, Cordenier F, Daoust D, Henry H, Sclavons M, Van Velthem P, Devaux J. Phenoxy as carrier for delivery of carbon nanotube in epoxy resin. In preparation

Oral presentations

- **Dumont D**, Daoust D, Sclavons M, Devaux J. Thermoplastic yarns in epoxy resins: dissolution, diffusion and induced microstructures. Sampe Benelux Student Seminar, 12-13 January 2009, Bergeijk (Netherlands).
- **Dumont D**, Daoust D, Sclavons M, Devaux J. Microstructure control of epoxy resin blended with thermoplastic yarns. Polymer Processing Society 25th Annual Meeting (PPS-25), 1-5 March 2009, Goa (India).
- **Dumont D**, Daoust D, Sclavons M, Devaux J, Seveno D, de Coninck J. Themoplastic reinforcement of thermoset composites: Solubility measurements in Epoxy Resins. Vth International Conference on Science and Technology of Composite Materials (COMATCOMP 2009), 7-9 October 2009, San Sebastian.
- **Dumont D**, Daoust D, Sclavons M, Devaux J. Nanofilled thermoplastic as reinforcement for thermoset composites: solubility and diffusion in epoxy resins" SAMPE Benelux Fall Seminar 2009, 19 November 2009, Louvain-la-Neuve.
- **Dumont D**, Daoust D, Sclavons M, Devaux J. Thermoplastic yarns filled with carbon nanotubes for reinforcement of epoxy resins-based composites. European Conference on Composite Materials ECCM14, 7-10 June 2010, Budapest.
- **Dumont D**, Daoust D, Sclavons M, Devaux J. Dissolution and diffusion of nanofilled thermoplastic yarns in epoxy resins. Polymer Processing Society Annual Meeting PPS-26, 4-8 July 2010, Banff (Canada).
- **Dumont D**, Henry E, Berben R, Bailly C, Cordenier F, Sclavons M, Van Velthem P, Daoust D. Nanofillers: to a new generation of aerospace composites. BPG Annual Meeting 2011, 12-13 May 2011, Houffalize.
- **Dumont D**, Berben R, Cordenier F, Henry E, Sclavons M, Van Velthem P, Daoust D. Phenoxy for carbon nanotube dispersion into epoxy matrices of RTM-processed composites. Sampe Europe 33rd International Conference and Forum (SEICO12), 26-29 march 2012, Paris.

Posters

- **Dumont D**, Daoust D, Sclavons M, Souvereyns G, Devaux J. Influence of thermoplastic content on the crosslinking reaction of an epoxy resin. BPG Annual Meeting 2008, 22-23 May 2008, De Haan.
- Finné G, Cordenier F, **Dumont D**, Van Velthem P, Bailly C, Daoust D, Sclavons M. Preparation and characterization of a nanoclay composite based on poly(hydroxyl ether of bisphenol A) matrix. BPG Annual Meeting 2008, 22-23 May 2008, De Haan.
- Van Velthem P, Baudouin AC, Daoust D, **Dumont D**, Cordenier F, Bailly C, Hubin F, Huynen I, Sclavons M. Preparation and characterization of carbon nanotubes/phenoxy nanocomposite. 5th international ECNP conference, 15-17 April 2009, Paris.
- **Dumont D**, Daoust D, Lê M, Rubay C, Sclavons M, Devaux J. Themoplastic reinforcement of thermoset composites: Solubility and diffusion in epoxy resins. BPG Annual Meeting 2009, 14-15 May 2009, Houffalize.
- **Dumont D**, Billard F, Coulon B, Devaux J, Sclavons M, Daoust D. Epoxy resins blended with soluble thermoplastic fibre containing carbon nanotubes. BPG Annual Meeting 2010, 25-26 May 2010, Blankenberge.
- **Dumont D**, Kuypers S, Devaux J, Sclavons M, Daoust D. FIB, Ion slicing and ultramicrotomy for TEM morphology of aerospace nanocomposite materials. Journées Miscroscopie Electronique à Transmission, 9-10 November 2010, Louvain-la-Neuve.
- Berben R, Henry E, Cordenier F, **Dumont D**, Sclavons M, Van Velthem P, André S, Ben Moussa N, Destoop V, Doneux C, Mestrez Q, Pardoen T, Devaux J, Bailly C, Daoust D, Gueuning D, Paquay E. Poulaert B. Nanofiller: a key to a new generation of aeronautic composite materials. Nanowall (journée inaugurale), 10 December 2010, Louvain-la-Neuve.
- Henry E, Bailly C, Berben R, Cordenier F, **Dumont D**, Sclavons M, Van Velthem P, Daoust D, Gueuning D, Paquay E, Poulaert B, Taquet P. Phenoxy resin as carrier of nanofillers: A novel method to improve properties of aeronautic composites produced by resin transfer moulding. JEC show composites, 28-31 March 2011, Paris.
- Van Velthem P, Bailly C, Berben R, Collignon K, Cordenier F, Devaux J, **Dumont D**, Henry E, Sclavons M, Daoust D. How phenoxy improves the fracture toughness of RTM-manufactured composites?, JEC show composites, 26-29 march 2012, Paris.

Introduction

This introductive part describes first the general context in which the present work has been realized. Then, state of the art concerning methods developed to reinforce composite laminates processed by liquid composite molding (LCM) technologies by introduction of thermoplastic or carbon nanotubes (CNTs) additives is reported. Finally, objectives and methodology of the study are detailed.

1. General context

Fiber reinforced composites have grown a lot since their limited use in military aircraft in the 1960's. Important growth in civil aviation in the last decades has been followed progressively by commercial application of composites in secondary components and more recently in load carrying structural parts to reach more than 50 wt % in the new generation of civil aircrafts. In addition to being lightweight, carbon fiber reinforced polymer (CFRP) parts also have advantageous thermomechanical stability and resistance to corrosion and fatigue. Increasing concern for the environment, not to mention rising fuel cost, means that the aerospace industry has much to gain by using these composites more extensively in commercial aircrafts. However, strict airworthiness requirements serve as a barrier to large scale changes in material use. Major challenges also come from poor resistance to impact damage and delamination, low thermal and electrical conductivities, moisture uptake and moderate resistance to some chemical agents as well as high manufacturing costs for less mature technologies.

Therefore, development of new composite materials and process technologies has been continuously pursued for applications of the aerospace field or other various demanding sectors among marine, automotive and civil engineering. In this framework, the polymer physics and chemistry laboratory (POLY) and then, the division of Bio- and Soft Matter of the Institute of Condensed Matter and Nanosciences (IMCN-BSMA) of UCL have been partners of several research projects about liquid molded composites for more than ten years.

Indeed, UCL was involved in a European research project (Growth Project GRD1 - 2000 - 25264) called "Soluble chain-extendable-polymer-filaments in textile preforms for in-situ resin toughening using rtm-technique" (SOLTEX) from 2001 until 2006. The novel soluble chain-extendable polymer yarns being incorporated in tailored textile preforms intended to

contribute to expand the performance of composites in terms of toughness, strength and surface quality while allowing manufacturing of durable and cost competitive structures by common resin injection technologies with low viscosity systems.

Several projects of "Région Wallonne" were also started during this period and some of them are still currently under progress. These projects are a joint venture between different entities from UCL, other universities, research centers, small and medium-sized enterprises and large enterprises as industrial partners of the aerospace community (Sonaca, Sabca and Techspace Aero) under the larger umbrella of the aerospace cluster Skywin in the frame of Plan Marshall:

- The project "Avion Plus Composite" (APC, 2007-2011) aimed to accelerate transition of the aeronautic industry in "Région Wallonne" from metal to composite by demonstrating the technical and economical potential of composite technologies. This partnership has fastened the competitiveness of composite structures and components by reducing their cost, improving their performance and decreasing their mass. The study has investigated the design of structures with integrated functionalities by using advanced materials with optimized resins and reinforcements, by developing characterization techniques, simulation tools and low cost LCM technologies like resin transfer molding (RTM), resin film infusion (RFI) or liquid resin infusion (LRI) and by optimizing automated fiber placement (AFP).
- The "Engine Composite" project (ECOM, 2008-2013) aims to develop new materials and fabrication methods meeting specifications of motor parts subject to a large range of mechanical solicitations, vibrations, friction, important temperature fluctuations and even extreme conditions in case of fan blade out. A technological breakthrough is required to reduce noise level, costs and emissions generated by the engine while sustaining high operating temperatures and mechanical constraints. Solutions are implemented to improve turbofan efficiency and decrease rotation speed by use of aerodynamic alternatives, new designs and innovative materials. In this context, the switch to composite materials becomes generalized and ECOM research proposes different methods based on APC results to improve the low pressure compressor and motor equipment by using RTM composites processed with high thermal resistance resins.
- The project entitled "Efficient composite technologies for aircraft components" (ECOTAC, 2011-2014) extends developments initiated during the APC project by exploring three new technological axes: AFP, same

qualified resin transfer molding (SQRTM) and nondestructive inspection. The AFP technology, which allows automation for complex geometries, is rapidly expanding but is still poorly controlled and its limitations and influence on properties are not yet well known. SQRTM offers possibilities of RTM with additional advantages of pre-impregnated fibers like the possibility of automation for preform fabrication or opportunity to use high performance prepregs.

Thanks to these research projects, IMCN-BSMA has acquired expertise in processing of composite panels by LRI, RTM and SQRTM and in physico-chemical characterization of composites and their constituents. Moreover, research and development activities have examined an original method to reinforce epoxy resin matrices of composite processed by RTM with thermoplastic and nanofiller additives. In parallel with these tasks of the projects having for objective to conceive advanced composite materials with improved properties, a more fundamental scientific study has been achieved in order to understand the key mechanisms involved at the nano- and micro-scales when the developed method is applied to simplified systems. Contribution to this study comes essentially from the PhD thesis supported by "Fonds pour la Formation à la Recherche dans l'Industrie et dans l'Agriculture" (FRIA) reported in the present document compiling its main results.

2. State of the art

As mentioned previously, CFRPs crosslinked with high functionality epoxy resin have excellent in-plane properties like thermomechanical stability and chemical resistance. However, high crosslink density of the epoxy matrices results in a brittle behavior of the composite and thus in limited fracture toughness while the lack of reinforcement in the out of plane direction leads to poor interlaminar properties. Therefore, many attempts have been made to perfect performance of composite laminates like resistance to failure due to interlaminar crack propagation but also impact damage resistance, fatigue life, wear behavior, thermal and electrical conductivities or barrier properties to water, solvents and fire degradation products. Several strategies can be exploited in order to try to achieve some of these goals. Indeed, development of new composite materials can be performed by improving the fiber preform, the polymer matrix or their interface. Complex preform architectures can be designed or reinforcement of the interface between

carbon fibers and epoxy resin can be privileged by their chemical functionalization, use of sizing agents or insertion of binders but the present work has chosen to focus on modification of the thermoset matrix.

Among different potential modifiers for epoxy resin, high performance thermoplastics and nanoparticles are two interesting options to improve composite properties. Unlike rubber toughening agents, high glass transition temperature (T_g) thermoplastic additives blended with epoxy resin are considered as they can enhance fracture resistance of the crosslinked network without compromising its thermomechanical stability [1]. The morphology created in the thermoplastic-epoxy resin blends by reaction induced phase separation (RIPS) can contribute to toughening at low thermoplastic concentration generating microstructures with thermoplastic-rich particles dispersed in the continuous epoxy-rich matrix but mainly for higher thermoplastic fractions producing bicontinuous or for phase inverted morphologies, since a crack must advance through fracture of the ductile continuous thermoplastic-rich phase to damage the blend. Improvement of epoxy resin performances has also been largely researched by dispersion of nanoparticles in the reactive resin formulation. Due to their high aspect ratio combined with their outstanding properties, CNTs discovered in 1991 by Sumio Iijima [2] have demonstrated their benefit for fracture toughness [3-8] or electrical conductivity [3,9-11] of epoxy resin even at very low content for optimized dispersion. Similarly, since researchers have discovered the possibility to produce a nanocomposite with layered silicates [12], remarkable improvement of thermal [13-14], mechanical [6,15-19] and fluid barrier [20-21] properties have been achieved for nanocomposites with exfoliated or at least intercalated morphologies as compared to neat epoxy resin or conventional composites by well dispersing montmorillonite clay layers in the thermoset matrix.

The following part of this section therefore reviews incorporation of thermoplastic or one kind of nanoparticles, CNTs, in composites processed by RTM or other LCM technologies.

2.1. Incorporation of thermoplastic in composites processed by LCM

Out-of-autoclave technologies like RTM or LRI, which are emerging cost effective alternatives to prepreg in order to manufacture composite parts in an automated and versatile way, require injectable resins with low viscosity

to ensure infiltration throughout the fabric and preform impregnation, which are essential for a final structure free of voids. Therefore, only small amounts of high molecular weight thermoplastic tougheners can be dissolved into the resin prior to infusion without sacrificing the flowability due to an important viscosity increase of the blend as compared to the neat resin. Moreover, if solid thermoplastic particles dispersed in the epoxy resin are considered, thermoplastic filtration forming agglomerates at undesirable locations during infusion becomes a critical issue. In order to maintain a low resin viscosity during injection and ensure easy resin impregnation, reinforcement of composite materials can be achieved by the introduction of solid thermoplastic additives into the preform without changing processing conditions. Effect of these thermoplastic tougheners, soluble or insoluble in the resin formulation, on the composite laminates properties is discussed here.

2.1.1. Insoluble thermoplastic additives

Some studies have highlighted enhanced performance in mode I crack opening, the dominant failure mode in compression after impact (CAI), by means of insoluble thermoplastic yarns that only soften in the epoxy matrix formulation during the liquid molding process. Insoluble thermoplastic in the fibrous form, commingled with the structural fibers of the laminate [22-23] or stitched onto the preform [24-25], inhibits crack propagation in these fiber hybrid composites during CAI testing. Fiber bridging with fiber pullout and extensive plastic deformation of the individual thermoplastic fibers contribute to the toughening mechanism. Similar improvements have been observed when thermoplastic veils [23,25] or films [26] are interposed as interleaf layers in the laminate. Thanomsilp and Hogg [22] have demonstrated that insoluble polypropylene and polyamide fibers commingled with structural glass fibers increases critical energy release rate required for crack initiation in mode I (G_{IC}) in laminates infused with low viscosity epoxy resin. The same behavior has been observed by Beier et al. [24-25] for composites processed by vacuum assisted resin transfer molding (VARTM) with a preform containing a combination of polyamide yarns and non-woven mats (**Fig. 1**). Stitching yarns as well as non-woven mats used as binders between the fabric layers contributes to the preform stabilization. The experimental data presented in this study have demonstrated a generally high mechanical property level for composites stitched and bindered with thermoplastic that soften in the matrix during preforming and subsequent

RTM process. Potential reduction of the in-plane mechanical composite properties induced by stitching and/or addition of binders is outweighed by cost savings and improvement of the out-of-plane performance. However, such thermoplastic reinforcements, insoluble in the epoxy matrix, have little effect on the initial formation of delamination during impact dominated by mode II shear cracking. The interfaces created by thermoplastic yarns or interleaving binder can also reduce resistance to fluids and hot-wet mechanical properties of the composite like shown with polyamide favoring water absorption. For these reasons, modification of the preform with amorphous thermoplastics soluble in epoxy resin during the liquid molding process has also been investigated by several authors like reported in the next subsection.

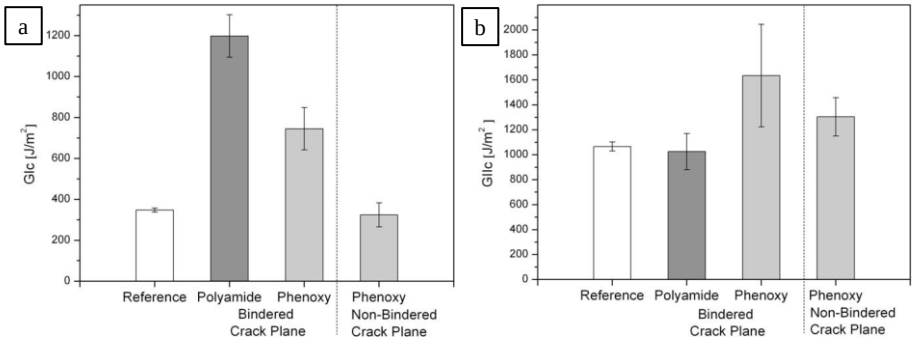

Fig. 1. Comparative plots of the energy release rates (a) G_{IC} and (b) G_{IIC} of the various composites (reference without thermoplastic, composite stitched and bindered by polyamide, composite stitched and bindered by phenoxy in the plane with or without binder) [25].

2.1.2. Soluble thermoplastic additives

Thermoplastics soluble in the epoxy resin formulation have been selected in many cases as localized toughening agents of the curable resin in the form of yarns commingled with the structural fibers of the laminate or stitched onto the preform [22,24-25,27] or chopped fibers [28], films [29], membranes [30] and non woven mats [23,25,31] interposed as interleaf layers in the laminate. Initially, the thermoplastic modifier is intended to remain insoluble during resin infusion to prevent thermoplastic flushing by the resin flow and avoid consecutive viscosity increase and reduction of the preform wettability. After complete mold filling by the injectable resin and as a result of the temperature increase applied to the system, the thermoplastic becomes

subsequently miscible and is distributed in the epoxy resin prior to substantial onset of curing and gelation. It is expected that these toughening concepts based on soluble thermoplastic can lead to improved damage tolerance for thermoset composites without compromising processability, mechanical or thermal properties. In addition to the potential stabilization of the dry preform improving its handling, the blend microstructure generated by phase separation can provide a localized toughening of the matrix hybrid composite by improving mode I fracture toughness and by delaying the initial formation of delamination during impact dominated by mode II shear cracking. Moreover, dissolution of the thermoplastic incorporated into the composite preform prevents macroscopic interfaces and reduces kinking and misalignment of structural fibers compared to insoluble thermoplastic elements. Fiber break is therefore hampered such as the formation of brittle resin-rich regions that affect in-plane properties of the composite.

Indeed, Thanomsilp and Hogg [22] have shown that the situation for which insoluble fibers increase G_{IC} but have little effect on G_{IIC} changes if the thermoplastic fibers dissolve in epoxy resin during the curing cycle. The addition of soluble modified polyethylene terephthalate does not improve G_{IC} but can substantially increase G_{IIC}. Beier et al. [24-25] have observed the same results by comparing effect of insoluble polyamide and phenoxy, which is soluble into RTM6 resin and can improve fracture toughness (K_{IC}) of this resin by more than 20 % when blended with 10 wt % phenoxy (**Table 1**). While G_{IC} is more enhanced by polyamide than by phenoxy, this second thermoplastic leads to a significant improvement of G_{IIC} not occuring with polyamide (**Fig. 1**).

Table 1. Properties of neat epoxy resin and resin-phenoxy blends [28].

Phenoxy (wt.%)	Tensile property		
	Modulus (GPa)	Strength (MPa)	Strain (%)
0	3.26 (0.13)	82.3 (13.1)	3.21 (0.68)
5	3.28 (0.18)	80.3 (10.5)	2.80 (0.56)
10	3.54 (0.26)	99.7 (8.2)	4.78 (1.08)

Phenoxy (wt.%)	Fracture toughness		T_g	
	K_{1c} (MPa$\sqrt{m}$)	G_{1c} (kJ m^{-2})	Phenoxy (°C)	Epoxy (°C)
0	1.01 (0.08)	218.2 (24.0)	n/a	122.8
5	1.15 (0.03)	224.9 (64.3)	65.2	123.1
10	1.23 (0.11)	270.7 (28.6)	65.2	125.6

Phenoxy has also been tested by Wong et al. [28] in composites prepared by a vacuum infusion process by positioning soluble thermoplastic fibers in the composite structure within the interlaminar region, where they are the most needed. Chopped fiber interleaves introduced between the carbon fiber plies dissolved in epoxy resin and forming a phase separated morphology with phenoxy-rich secondary phase upon curing allows localized toughening. Significant improvements of G_{IC} have been measured for global amounts of phenoxy fibers around 5 and 10 wt % of the total matrix content while other properties such as Young's modulus, tensile strength and thermal stability are not adversely affected despite the limited T_g of this thermoplastic (**Fig. 2**).

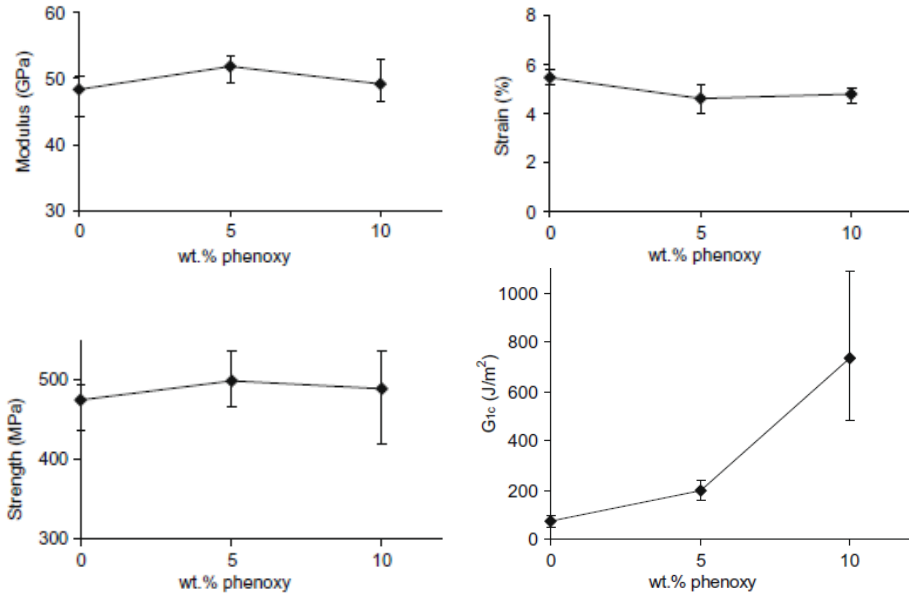

Fig. 2. Mechanical properties of carbon fiber-epoxy resin composite laminate modified with phenoxy fiber mats between each fabric layer [28].

Thermoplastic fibers soluble in the epoxy matrix of composites are commercialized under the trademark PRIFORM® developed by Cytec Engineering Materials for liquid resin infusion processes [32]. The Cytec patent claims that a phenoxy fiber can be used as toughening agent [33]. Phenoxy fiber is marketed by EMS-Griltech as a bonding fiber which has a toughening effect [34].

In situ dissolution of thermoplastic films for production of modified composites processed by RTM has also been studied by Naffakh et al. and has revealed that poly(ether imide) (PEI) films generates dispersed PEI nodules between the fiber glass layers [29]. Yun et al. [35] have shown that a morphology spectrum is obtained by inserting a polysulfone (PSf) film in carbon fiber reinforced epoxy prepreg before cure (**Fig. 3**). The relative rates of dissolution and apparent diffusion of polysulfone in the epoxy resin determine the composition gradient and consequently the gradual change of morphological feature changing from a sea-island to a phase inverted nodular structure as the thermoplastic concentration increases. Fracture toughness of the composite modified with 20 wt% PSf film 2.7 times higher than the one of the unmodified composite has been ascribed to the plastic deformation of the continuous thermoplastic-rich phase in the semi-interpenetrating network.

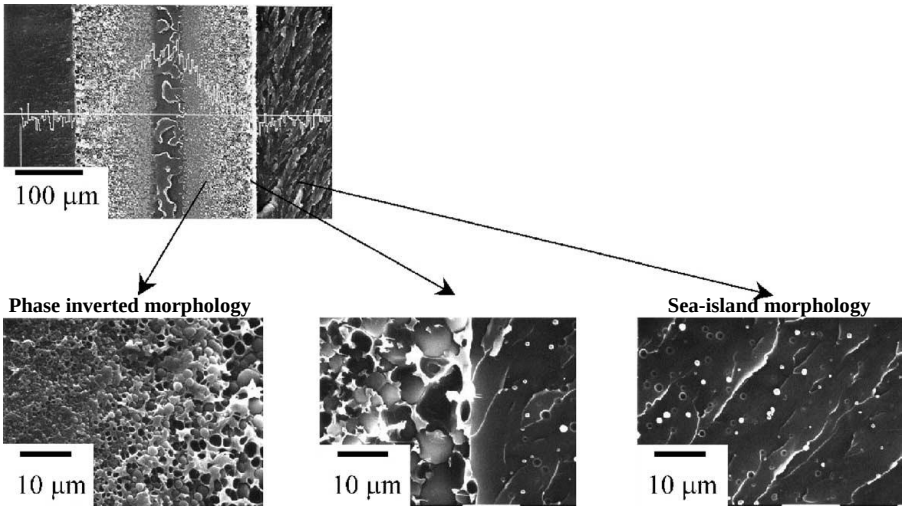

Fig. 3. Sulfur concentration profile determined by energy dispersive X-ray spectroscopy (EDAX) and SEM micrographs of the morphology spectrum induced by a polysulfone film in a carbon fiber composite [35].

The microstructure gradient has also been studied in the case of a PSf film modified epoxy resin [36]. For the same global PSf concentration, a higher improvement of the fracture toughness has been measured for the epoxy resin with morphology spectrum than for the resin with a uniform thermoplastic distribution. This higher capacity for absorbing fracture energy has been attributed to plastic deformation of the continuous thermoplastic-rich phase induced by high thermoplastic concentrations generated locally by

the films. Although phase inverted morphology improves the fracture toughness more efficiently, it can result in a local decrease of other properties as the high crosslinked epoxy resin is no more the continuous phase everywhere in the blend. Therefore, lower thermoplastic concentrations assuring sea-island or cocontinuous morphologies for all the material can be preferred even if to the detriment of the toughness increase.

From a mechanistic point of view, thermal dissolution occurs through swelling of the amorphous thermoplastic by the diffusing resin monomers and dissolution of the disentangled polymer chains into the epoxide-diamine reactive solution. Several regions can be identified in the composition gradient induced between the glassy polymer and the pure liquid solvent according to the amount of decreasing polymer concentration. An infiltration layer, a gel layer containing swollen polymer in a rubberlike state and a liquid layer containing (semi)-diluted solution with relatively free macromolecules have been identified in the literature [37-38] (**Fig. 4**). The thickness of the gel layer with swollen thermoplastic results from the balance between penetration velocity of the resin precursors and dissolution rate induced during mutual diffusion at the glassy thermoplastic-resin precursor interface.

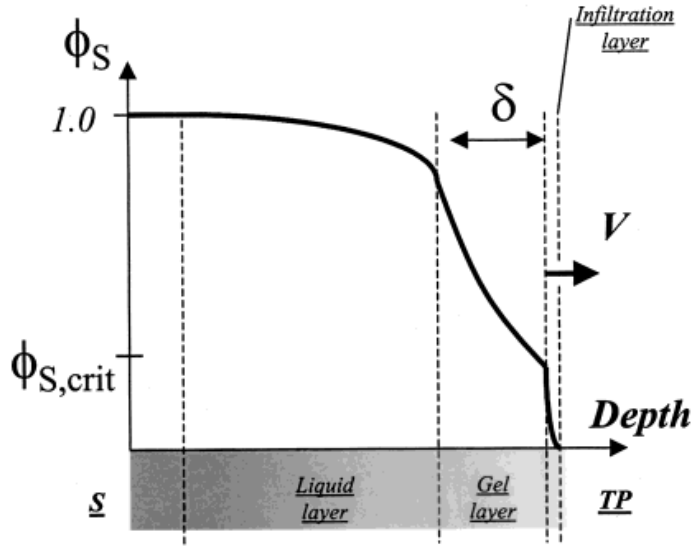

Fig. 4. Solvent (S) concentration profile for a case II diffusion with dissolution of thermoplastic (TP) at the interface between the gel layer and the liquid layer [38].

After interdiffusion between the thermoplastic and the resin precursors, phase separation induced by the curing reaction generates a morphology gradient with a microstructure distribution being function of the local blend composition like shown with PSf films [35-36]. Interdiffusion coupled with dissolution and miscibility of thermoplastic with epoxy resins has also been studied by Lestriez et al. [38] by observing the structure of the interfaces/interphases between poly(phenylene ether) (PPE) or PEI and epoxide-diamine networks at different conversions. The morphology spectrum resulting from the composition gradient between PEI (darker phase) and diglycidyl ether of bisphenol A (DGEBA) crosslinked with 4,4'-methylenebis-(2,6-chlorodiethylaniline) (MCDEA) (brighter phase) is presented in **Fig. 5**. The blend microstructure evolves on a distance interval of less than 50 µm from a sea-island morphology with PEI nodules dispersed in the continuous epoxy resin-rich phase (**Fig. 5.d**) to a phase inverted morphology with epoxy resin inclusions contained in the PEI continuous phase (**Fig. 5.a**) as the PEI concentration increases. A morphology close to co-continuity (**Fig. 5.b**) can also be observed locally in the interphase for intermediate PEI contents.

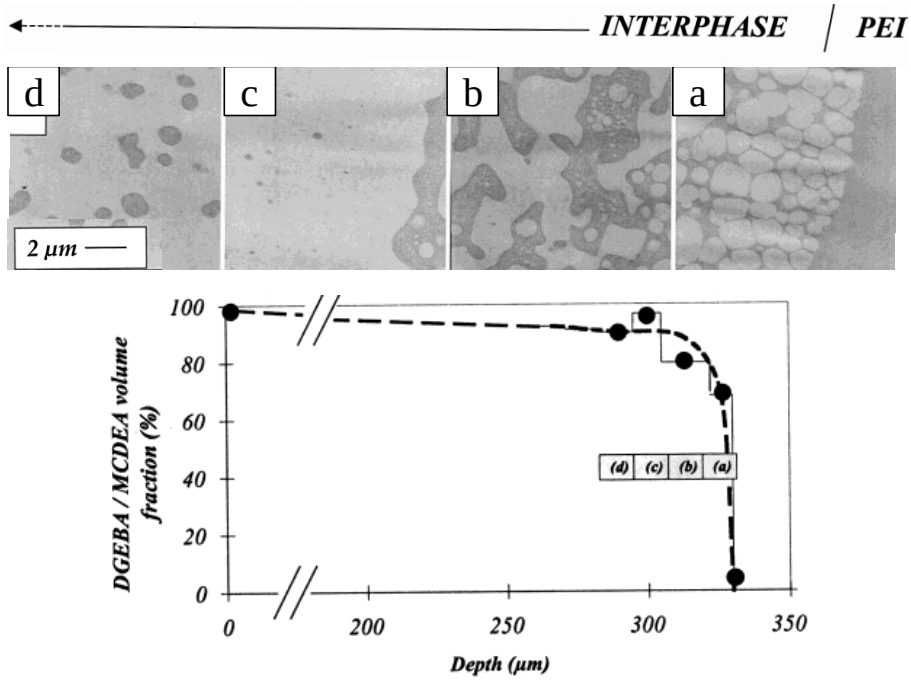

Fig. 5. Interface between a DGEBA-MCDEA resin and PEI after complete curing: (a-d) Transmission electron microscopy (TEM) micrographs and concentration profile determined from image analysis [38].

2.2. Incorporation of CNTs in composites processed by LCM

Different ways have been tested to introduce CNTs into composite laminates processed by LCM. The principal methods proposed in the literature are reviewed in this section and are illustrated in **Fig. 6**. Property improvements achieved in a selection of studies investigating these different ways of CNT incorporation into composite are summarized in **Table 2**. Some works [39-45] have also studied incorporation of clay in fiber reinforced polymers (FRP) produced by RTM, LRI or related processes, mainly by dispersing the layered silicate in epoxy resin prior to injecting the nanofilled resin, but are not detailed here.

Table 2. Effect of CNTs on composite properties like ILSS, interfacial shear strength (IFSS), electrical conductivity, T_g, coefficient of thermal expansion (CTE) and G_{IC} in a selection of studies.

	Way of introduction	**CNT type and concentration**	**ILSS**	**IFSS**	**Electrical conductivity**	**T_g**	**CTE**	**G_{IC} Crack initiation/ crack propagation**
Gojny et al. [46]	Dispersed in resin	0.3 wt % DWNT-NH_2 in resin	+20 %					
Beykarova et al. [47]	Dispersed in resin	0.5 wt % SWNT-COOH in resin	+40 %					
Fan et al. [48]	Dispersed in resin	2 wt % oxidized MWNTs in resin	+33 %					
Qian et al. [58]	Grown on fibers			+57 %				
Sager et al. [59]	Grown on fibers ● Randomly oriented ● Aligned	MWNTs		+71 % +11 %				
Garcia et al. [63]	Grown on the fibers	Aligned MWNTs: ● ~5 wt % in matrix ● ~2 wt % in matrix	+69 %		x10^6 in-plane x10^8 through-thickness			
Beykarova et al. [64]	Deposited by electrophoresis	~0.25 wt % with regard to carbon fabric ● MWNTs ● SWNTs	+27 %		+~30 % through-thickness +~100 % through-thickness			
Zhu et al. [66]	Sprayed on fibers	0.015 wt % SWNTs in composite	+35 %					
Godara et al. [67]	● In fiber sizing ● Dispersed in resin ● In fiber sizing + dispersed in resin	0.5 wt % MWNT-NH_2 in sizing and/or in resin		+92 % +48 % +32 %				
Warrier et al. [69]	● In fiber sizing ● Dispersed in resin ● In fiber sizing + dispersed in resin	0.5 wt % MWNT-NH_2 in sizing and/or in resin				+11 % +8 % +6 %	-31 % -12 % -17 %	+10 %/-53 % +25 %/-51 % +28 %/-34 %
Gorbatikh et al. [71]	Dispersed in resin	0.25 wt % modified MWNTs in resin						+75 %/+83 %

Among the different suggested strategies, dispersion of CNTs in the injectable resin (**Fig. 6.a**) followed by infusion of the nanophased matrix through the composite preform has been studied by several authors [46-55]. They have demonstrated improved matrix-dominated properties like interlaminar shear strength (ILSS) [46-48] and flexural strength [49,52], while fiber-dominated properties like tensile modulus and strength were not affected by the nanofillers. Nevertheless, in most cases the CNT content added to epoxy resin has been limited to less than 0.5 wt % to prevent processing problems like poor fiber impregnation due to the dramatic viscosity increase caused by the nanofillers. This low CNT amount explains electrical conductivity remaining one order of magnitude lower in the out-of-plane direction than in the plane direction reported by Gojny et al. [46]. In addition to challenge to disperse nanofillers in epoxy resin and to limitations related to viscosity increase, the composite preform can also generate a potential filtering effect during injection of the nanofilled resin [56-57] and can lead to an inhomogeneous nanofiller distribution in the composite matrix depending on permeability of the fibrous porous medium.

Due to these drawbacks, other methods have been explored to reinforce the matrix-rich regions of composites processed via LCM by introducing CNTs in the fiber fabric. Growth of CNTs randomly (**Fig. 6.b**) or radially (**Fig. 6.c**) oriented on the surface of carbon fibers by chemical vapor deposition (CVD) process has been exploited to produce fibrous substrates destined to be used in composite preforms [58-60]. Garcia et al. have produced composites with hybrid architecture of CNTs, advanced fibers and epoxy resin matrix by LRI using aligned CNTs grown on an alumina fiber cloth (**Fig. 6.d**) via CVD [63]. By using this fabric with a hierarchical reinforcing structure in place of the corresponding woven fabric without grafted CNTs, they have shown that electrical conductivity of the composite laminate can be increased by factors 10^6 and 10^8 respectively in-plane and through-thickness. Aligned CNT forests (**Fig. 6.e**), which can be handled like films since CNT are held together by physical entanglement and van der Waals forces, have been created by Wardle et al. [61-62] by a CVD method. Multiscale hybrid composites with improved out-of-plane electrical conductivity have also been successfully processed by infiltration of CNT-coated carbon fabrics with epoxy resin using VARTM [64]. In this case, electrophoresis has been utilized to integrate CNTs into the carbon fiber bundles (**Fig. 6.f**). All these methods have achieved significant improvements of ILSS. However, even if these processes may enable to overcome problems like aggregation of CNTs

and viscosity increase, significant technical challenges still remain like difficulty to upgrade these methods to large scale process. In the case of CVD, difficulty to remove metal catalysts may cause negative effects on composite properties and weight while harsh conditions for CNTs growth may reduce tensile properties of the carbon fibers.

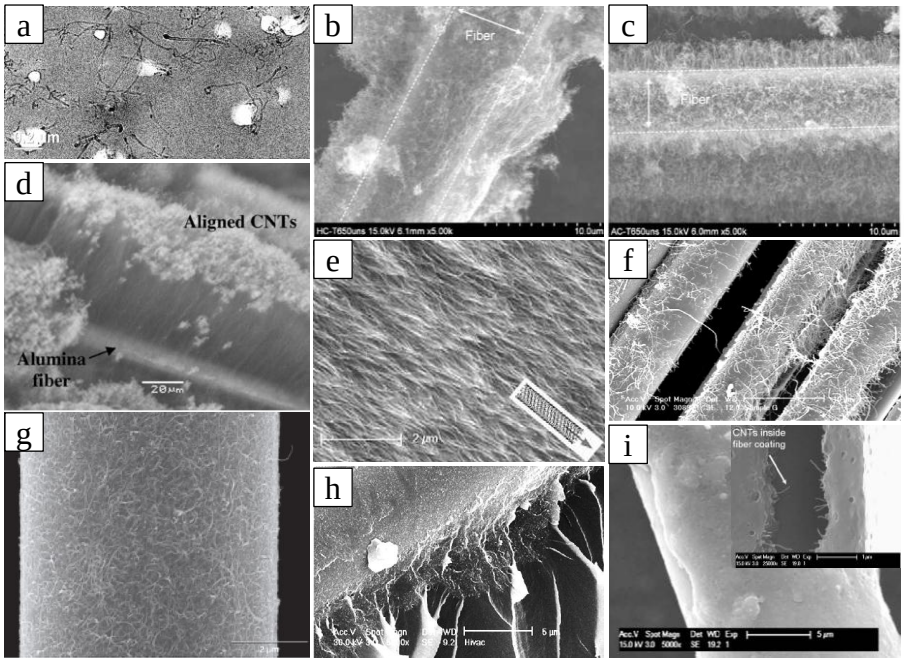

Fig. 6. TEM and SEM micrographs illustrating the different strategies investigated to incorporate CNTs in composites processed by LCM: (a) CNTs dispersed in injectable epoxy resin (image of composite matrix) [48]; (b) randomly oriented CNTs grown on carbon fiber [59]; (c) radially oriented CNTs grown on carbon fiber [59]; (d) aligned CNTs grown on alumina fiber [63]; (e) aligned CNTs forest (image of 20 wt % CNTs infiltrated with epoxy resin followed by nanocomposite curing) [62]; (f) CNTs deposited on carbon fibers by electrophoresis [64]; (g) epoxy sized carbon fibers coated with polyelectrolyte (polyethyleneimine) treated CNTs [65]; (h) thin CNT layer sprayed onto glass fibers (image of fracture surface of glass fiber/vinyl ester composite with silane functionalized CNTs) [66]; (i) CNTs dispersed in the sizing agent of glass fibers [67].

Kamae et al. [65] have developed a method to realize a uniform CNT coating on carbon fibers enabling the scalable fabrication of CNT containing carbon fiber/epoxy composites by each conventional molding process. CNTs

are treated by cationic polymers and then coated to carbon fibers by immersion into a CNT/water suspension. Covalent bonds between the cationic polymer treated CNTs and both carbon fibers and epoxy resin matrix are expected to be formed by the reactive functional groups of the cationic polymer and carboxyl groups or amine groups. The results show that the combination of epoxy resin sizing and polyethyleneimine treated CNT coating (**Fig. 6.g**) results in high IFSS. A spray process (**Fig. 6.h**) has also been proposed by Zhu et al. to deposit a thin layer of CNTs onto surface of woven glass fabrics, which can subsequently be used to fabricate CNTs enhanced vinyl ester/glass fiber composites with enhanced interface properties by VARTM [66].

In addition to the CNT grafting and coating methods listed previously, an alternative approach to deliver CNTs to the fiber surface has been examined by dispersing CNTs in the fiber sizing formulation [67-71] (**Fig. 6.i**). The sizing agent plays the role of vehicle for introduction CNTs in reinforced thermoset polymer composites. Phenoxy, silanes or copolymers have been suggested as polymer binders to transfer CNTs from coating to epoxy resin precursors [68]. Godara et al. [67] have coated glass fibers with a CNT containing sizing without removal of the commercial sizing by drawing the fibers through a water dissolved, epoxy-compatible phenoxy-based formulation filled with 0.5 wt % CNTs. Composite laminates prepared with CNT-glass fiber prepregs have shown that CNTs increase IFSS by more than 90 %. Introduction of CNTs in the sizing combined with their dispersion in the thermoset matrix has also been tested but the maximum gain has been achieved for CNTs incorporated solely in the sizing. Improvement of other composite properties like T_g, crack initiation fracture toughness or damage initiation threshold during tensile loading and reduction of thermal expansion has also been shown by addition of CNTs in the glass fiber sizing [69,71].

3. Objectives and methodology

As above mentioned in the literature review, either thermoplastic or CNTs have been frequently incorporated by different ways in composite laminates processed using LCM and have shown their benefits on properties of the reinforced composites. Nevertheless, simultaneous introduction of both additives has been suggested only by few studies apart from dispersion of CNTs in the thermoplastic sizing agent of the fibers. A strategy consisting in

addition of soluble thermoplastic veils potentially filled with nanoparticles in the composite preform is described in a patent application [31] like the same approach using exfoliated phyllosilicates nanodispersed in thermoplastic films [72]. Song has also considered thermoplastic films made of poly(ethylene oxide) miscible with epoxy resin to process multiscale fiber reinforced composites [73].

Therefore, the present study aims to investigate and develop this innovative and commercially viable toughening method using nanofilled thermoplastic elements added to the composite preform as carrier to vehicle nanoparticles everywhere or more locally in carbon fiber-reinforced laminates processed by RTM. Beyond the advantage to combine positive effects of both thermoplastic and nanofillers additives on the composite properties, this alternative route for delivery of nanoparticles in the epoxy resin matrix of composites allows to preliminary disperse nanoparticles in thermoplastic and consequently prevents difficulties related to injection of a stable nanofiller dispersion in the liquid resin.

The main objective of the thesis is thus to prove, on the one hand, that thermoplastic carriers are adapted to deliver nanofillers into epoxy resin before important crosslinking with their distribution depending among others on thermoplastic solubility and, on the other hand, that once RIPS takes place, nanofillers are dispersed in the epoxy resin-rich phase while thermoplastic forms another phase. The study does not intends to evidence property improvement but focuses on demonstration of the concept and aims to explain the mechanisms controlling composition gradients resulting from in situ dissolution and interdiffusion and to establish their link with the generated microstructure. Indeed, such considerations have not been considered previously but are primordial for a future transposition of the concept to process of composites with controlled nanofiller and thermoplastic distributions.

This document is divided into two distinct parts, which corresponds to the principal stages required to validate the concept. The first part investigates the behavior of the thermoplastic carrier in epoxy resin or in the epoxide and diamine precursors while the second part takes into account nanofiller introduction in the systems.

The first part of this work explores binary blends prepared with epoxy resin and two amorphous thermoplastics, poly(ether sulfone) (PES) and poly(hydroxyether of bisphenol A) (phenoxy). PES was selected as thermoplastic modifier for epoxy resin due to its high T_g assuring preservation of high thermomechanical properties of highly crosslinked thermoset networks required to sustain high operating temperatures for example in parts of jet engine like the low pressure compressor. The behavior of PES is compared to that of another amorphous thermoplastic, i.e. phenoxy presenting a chemical structure inducing a much lower T_g. Both thermoplastics were selected to determine influence of thermoplastic solubility on composition and microstructure gradients induced by a single filament in contact with the resin. Indeed, in situ dissolution and interdiffusion between thermoplastic and resin precursors considered separately or in the reactive resin formulation are inspected using these model systems. Composition gradients resulting from competition between interdiffusion and crosslinking reaction are discussed such as local morphologies generated by RIPS. An innovative aspect of the study is thus that the selected systems are completely characterized at all the stages of the process from thermoplastic solubility in resin precursors to final morphology spectrum via intermediate stages like thermoplastic behavior in reactive resin during interdiffusion and induced composition gradient. The originality of this work is also that, thanks to the material choice, not only extreme cases with totally soluble or insoluble thermoplastics are studied but the complete range of partial solubility is investigated by varying thermoplastic nature (PES or phenoxy), resin formulation and thermal cycle. Moreover, both thermoplastics and epoxy resin on which the study focuses, i.e. HexFlow® RTM6 resin, are commercial products evaluated without prior chemical modification. Besides the RTM6 resin which is qualified for aerospace applications, other epoxide-diamine formulations are also inspected to evidence influence of lower molar mass precursors.

While the first part of this work concentrates on systems composed of epoxy resin and soluble thermoplastic, the second part of the study considers additional incorporation of nanofillers. Two distinct stages are required to disperse and distribute nanoparticles into epoxy resin. Nanofillers are first dispersed in the thermoplastic by melt blending and the processed nanocomposites are subsequently blended with the RTM6 resin before significant crosslinking. Curing of the modified resin and reaction induced phase separation should then lead to the desired microstructure with both a

thermoplastic phase and nanofillers dispersed in the continuous epoxy resin phase. The main objective of this part is to demonstrate that the investigated concept allows to take advantage of thermoplastic solubility in the resin precursors to use nanocomposites for dispersion and delivery of nanofillers in the composite matrix and more specifically in the epoxy resin-rich phase after RIPS. In order to check that this method is suitable for nanofiller incorporation, microstructures and properties of the nanocomposites prepared by melt blending are first investigated to control if the nanofillers are properly dispersed and homogeneously distributed in the thermoplastics. Then, location of the nanofillers and conservation of their dispersion is verified when nanocomposites are blended with RTM6 resin. The mechanisms controlling location of the nanoparticles in polymer blends are discussed on basis of thermodynamic predictions and other kinetics considerations. Next, composition profiles resulting from thermal treatment of nanocomposite filaments in epoxy resin are examined and correlated to local microstructures to confirm nanofiller delivery and evidence the migration mechanism of the nanofillers. Different kinds of nanofillers are considered, i.e., unfunctionalized multiwalled carbon nanotubes (MWNTs) but also layered clay organomodified or not, in order to potentially evidence an effect of the nanoparticule shape (tubular or lamellar) on the involved mechanisms. Finally, application of the studied concept to composite laminates with a preform interleaved with nanocomposite films is tested in order to verify if a transposition to process of composite parts by RTM is possible.

References

[1] Hodgkin JH, Simon GP, Varley RJ. Thermoplastic toughening of epoxy resins: a critical review. Polymer for Advanced Technologies 1998;9(1):3-10.
[2] Iijima S. Helical microtubules of graphitic carbon. Nature 1991;354:56-8.
[3] Thostenson ET, Chou TW. Processing-structure-multi-functional property relationship in carbon nanotube/epoxy composites. Carbon 2006;44(14):3022-9.
[4] Gojny FH, Wichmann MHG, Fiedler B, Schulte K. Influence of different carbon nanotubes on the mechanical properties of epoxy matrix composites - A comparative study. Composites Science and Technology 2005;65:2300-13.
[5] Yu N, Zhang ZH, He SY. Fracture toughness and fatigue life of MWCNT/epoxy composites. Materials Science and Engineering: A 2008;494:380-4.
[6] Ganguli S, Aglan H, Dean D. Microstructural origin of strength and toughness of epoxy nanocomposites. Journal of Elastomers and Plastics 2005;37(1):19-35.

[7] Ganguli S, Bhuyan M, Allie L, Aglan H. Effect of multi-walled carbon nanotube reinforcement on the fracture behavior of a tetrafunctional epoxy. Journal of Materials Science 2005;40(13):3593-5.
[8] Karapappas P, Vavouliotis A, Tsotra P, Kostopoulos V, Paipetis A. Enhanced fracture properties of carbon reinforced composites by the addition of multi-wall carbon nanotubes. Journal of Composite Materials 2009;43(9):977-85.
[9] Sandler J, Shaffer MSP, Prasse T, Bauhofer W, Schulte K, Windle AH. Development of a dispersion process for carbon nanotubes in an epoxy matrix and the resulting electrical properties. Polymer 1999;40:5967-71.
[10] Gojny FH, Wichmann MHG, Fiedler B, Kinloch IA, Bauhofer W, Windle AH, Schulte K. Evaluation and identification of electrical and thermal conduction mechanisms in carbon nanotube/epoxy composites Polymer 2006;47:2036-45.
[11] Song YS, Youn JR. Influence of dispersion states of carbon nanotubes on physical properties of epoxy nanocomposites. Carbon 2008;43(7):1378-85.
[12] Usuki A, Kojima Y, Kawasumi M, Okada A, Fukushima Y, Kurauchi T, Kamigaito O. Synthesis of nylon 6-clay hybrid. Journal of Materials Research 1993;8(5):1179-84.
[13] Park SJ, Seo BS, Lee JR, Surface modification of montmorillonite on surface acid-base characteristicsof clay on thermal stability of epoxy/clay nanocomposites. Journal of Colloid and Interface Science 2002;251:160-5.
[14] Lakshmi MS, Narmadha B, Reddy BSR, Enhanced thermal stability and structural characteristics of different MMT-Clay/epoxy-nanocomposite materials. Polymer Degradation and Stability 2008;93(1):201-13.
[15] Lan T, Pinnavaia TJ. Clay-reinforced epoxy nanocomposites. Chemistry of Materials 1994;6(12):2216-9.
[16] Kornmann X, Lindberg H, Berglund LA, Synthesis of epoxy-clay nanocomposites. Influence of the nature of the curing agent on structure. Polymer 2001;42(10):4493-9.
[17] Becker O, Varley, Simon G. Morphology, thermal relaxations and mechanical properties of layered silicate nanocomposite based upon high functionality epoxy resins. Polymer 2002;43:4365-73.
[18] Qi B, Zhang QX, Bannister M, Mai YW. Investigation of the mechanical properties of DGEBA-based epoxy resin with nanoclay additives. Composite Structures 2006;75(1-4):514-9.
[19] Ha SR, Ryu SH, Park SJ, Rhee KY. Effect of clay surface modification and concentration on the tensile performance of clay/epoxy nanocomposites. Materials Science and Engineering: A 2007. 448(1-2):264-8.
[20] Wang Z, Massam J, Pinnavaia TJ. Epoxy-clay nanocomposites. In: Pinnavaia TJ, Beall GW, editors. Polymer clay nanocomposites. Chichester:Wiley;2000:127-48.
[21] Becker O, Varley RJ, Simon GP. Thermal stability and water uptake of high performance epoxy layered silicate nanocomposites. European Polymer Journal 2004;40:187-95.

[22] Thanomsilp C, Hogg PJ. Interlaminar fracture toughness of hybrid composites based on commingled filament fabrics. Composites Science and Technology 2005;65(10):1547-63.
[23] Hogg PJ. Toughening of thermosetting composites with thermoplastic fibers. Materials Science and Engineering A 2005;412(1-2):97-103.
[24] Beier U, Wolff-Fabris F, Fischer F, Sandler JKW, Altstädt V, Hulder G, Schmachtenberg E, Spanner H, Weimer C, Roser T, Buchs W. Mechanical performance of carbon fiber-reinforced composites based on preforms stitched with innovative low-melting temperature and matrix soluble thermoplastic filaments. Composites Part A: Applied Sc. and Manufact. 2008; 39(9):1572-81.
[25] Beier U, Sandler JKW, Altstädt V, Spanner H, Weimer C. Mechanical performance of carbon fiber-reinforced composites based on stitched and bindered preforms. Composites: Part A 2009;40(11):1756-63.
[26] Li L, Lee-Sullivan P, Liew KM. The Influence of Thermoplastic Film Interleaving on the Interlaminar Shear Strength and Mode I Fracture of Laminated Composites. Journal of Engineering Materials and Technology 1996;118(3):302-9.
[27] Carter JT, LoFaro C, Maskell RK, McGrail PT. Flexible polymer element as toughening agent in prepregs. U.S. Pat. Appl. Publ. US 2004/0041128 A1, 2004.
[28] Wong DWY, Lin L, McGrail PT, Peijs T, Hogg PJ. Improved fracture toughness of carbon fiber/epoxy composite laminates using dissolvable thermoplastic fibers. Composites Part A: Applied Science and Manufacturing 2010;41:759-67.
[29] Naffakh M, Dumon M, Gérard JF. Study of a reactive epoxy-amine resin enabling in situ dissolution of thermoplastic films during resin transfer molding for toughening composites. Composites Science and Technology 2006;66(10):1376-84.
[30] Mortimer S, Cawse JL. A thermoplastic toughening material and related method. PCT Int. Appl. Publ. WO 2007/110617 A1, 2007.
[31] LoFaro C, Abusafieh A, Webb WE, Doyle M. Resin-soluble veil for composite materials. U.S. Pat. Appl. Publ. US 2006/0252334 A1, 2006.
[32] http://www.cytec.com/engineered-materials/Priform.htm.
[33] Carter JT, Lo Faro C, Maskell RK, Mcgrail PT. Cytec Technology Corp. Flexible polymer element as toughening agent in prepregs. US patent number 7192634, Wilmington, DE, US, 2007.
[34] http://www.emsgriltech.com/.
[35] Yun NG, Won YG, Kim SC. Toughening of carbon fiber/epoxy composite by inserting polysulfone film to form morphology spectrum. Polymer 2004;45(20):6953-8.
[36] Min HS, Kim SC. Fracture toughness of polysulfone/epoxy semi-IPN with morphology spectrum. Polymer Bulletin 1999;42(2):221-27.
[37] Ueberreiter K, The Solution Process, in Diffusion in Polymers, ed by Crank J and Park GS. Academic Press, New York, pp 219-257 (1968).

[38] Lestriez B, Chapel JP, Gérard JF. Gradient interphase between reactive epoxy and glassy thermoplastic from dissolution process, reaction kinetics, and phase separation thermodynamics. Macromolecules 2001;34(5):1204-13.
[39] Chowdhury FH, Hosur MV, Jeelani S. Studies on the flexural and thermomechanical properties of woven carbon/nanoclay-epoxy laminates. Materials Science and Engineering A 2006;421(1-2):298-306.
[40] Lin LY, Lee JH, Hong CE, Yoo GH, Advani SG. Preparation and characterization of layered silicate/glass fiber/epoxy hybrid nanocomposites via vacuum-assisted resin transfer molding (VARTM). Composites Science and Technology 2006;66(13):2116-25.
[41] Subramaniyan AK, Sun CT. Enhancing compressive strength of unidirectional polymeric composites using nanoclay. Composites Part A: Applied Science and Manufacturing 2006;37(12):2257-68.
[42] Zhou Y, Pervin F, Rangari VK, Jeelani S. Influence of montmorillonite clay on the thermal and mechanical properties of conventional carbon fiber reinforced composites. Journal of Materials Processing Technology 2007;191(1-3):347-51.
[43] Zhao A, Gou J, Bietto S, Ibeh C, Hui D. Fire retardancy of clay/carbon nanofiber hybrid sheet in fiber reinforced polymer composites. Composites Science and Technology 2009;69(13):2081-7.
[44] Mohan TP, Kanny K. Water barrier properties of nanoclay filled sisal fibre reinforced epoxy composites. Composites Part A: Applied Science and Manufacturing 2011;42(4):385-393.
[45] Quaresimin M, Salviato M, Zappalorto M. Fracture and interlaminar properties of clay-modified epoxies and their glass reinforced laminates Engineering Fracture Mechanics 2012;81:80-93.
[46] Gojny FH, Wichmann MHG, Fiedler B, Bauhofer W, Schulte K. Influence of nano-modification on the mechanical and electrical properties of conventional fibre-reinforced composites. Composites Part A: Applied Science and Manufacturing 2005;36(11):1525-35.
[47] Bekyarova E, Thostenson ET, Yu A, Itkis ME, Fakhrutdinov D, Chou TW, Haddon RC. Functionalized single-walled carbon nanotubes for carbon fiber-epoxy composites. Journal of Physical Chemistry C 2007;111(48):17865-71.
[48] Fan Z, Santare MH, Advani SG. Interlaminar shear strength of glass fiber reinforced epoxy composites enhanced with multi-walled carbon nanotubes. Composites Part A: Applied Science and Manufacturing 2008;39(3):540-554.
[49] Zhou Y, Pervin F, Lewis L, Jeelani S. Fabrication and characterization of carbon/epoxy composites mixed with multi-walled carbon nanotubes. Materials Science and Engineering A 2008;475(1-2):157-65.
[50] Fernberg P, Nilsson G, Joffe R. Piezoresistive performance of long-fiber composites with carbon nanotube doped matrix. Journal of Intelligent Material Systems and Structures 2009;20(9):1017-1023.

[51] Gao L, Thostenson ET, Zhang Z, Chou TW. Sensing of damage mechanisms in fiber-reinforced composites under cyclic loading usin carbon nanotubes. Advanced Functional Materials 2009;19(1):123-30.
[52] Kim M, Park YB, Okoli OI, Zhang C. Processing, characterization, and modeling of carbon nanotube-reinforced multiscale composites. Composites Science and Technology 2009;69(3-4):335-42.
[53] Chandrasekaran VCS, Advani SG, Santare MH. Role of processing on interlaminar shear strength enhancement of epoxy/glass fiber/multi-walled carbon nanotube hybrid composites. Carbon 2010;48(13):3692-9.
[54] Wang S, Qiu J. Enhancing thermal conductivity of glass fiber/polymer composites through carbon nanotubes incorporation. Composites Part B: Engineering 2010;41(7):533-6.
[55] De Greef N, Gorbatikh L, Godara A, Mezzo L, Lomov SV, Verpoest I. The effect of carbon nanotubes on the damage development in carbon fiber/epoxy composites. Carbon 2011;49(14):4650-64.
[56] Fan Z, Hsiao KT, Advani SG. Experimental investigation of dispersion during flow of multi-walled carbon nanotube/polymer suspension in fibrous porous media. Carbon 2004;42(4):871-6.
[57] Baets J, Godara A, Devaux J, Verpoest I. Toughening of polymerized cyclic butylene terephthalate with carbon nanotubes for use in composites. Composites Part A: Applied Science and Manufacturing 2008;39(11):1756-61.
[58] Qian H, Bismarck A, Greenhalgh ES, Kalinka G, Shaffer MSP. Hierarchical composites reinforced with carbon nanotube grafted fibers: The potential assessed at the single fiber level. Chemisty of Materials 2008;20(5):1862-9.
[59] Sager RJ, Klein PJ, Lagoudas DC, Zhang Q, Liu J, Dai L, Baur JW. Effect of carbon nanotubes on the interfacial shear strength of T650 carbon fiber in an epoxy matrix. Composites Science and Technology 2009;69(7-8):898-904.
[60] Lomov SV, Gorbatikh L, Kotanjac Z, Koissin V, Houlle M, Rochez O, Karahan M, Mezzo L, Verpoest I. Compressibility of carbon woven fabrics with carbon nanotubes/nanofibres grown on the fibres. Composites Science and Technology 2011;71(3):315-25.
[61] Wardle BL, Saito DS, Garcia EJ, Hart AJ, Guzmán de Villoria R, Verploegen EA. Fabrication and characterization of ultrahigh-volume-fraction aligned carbon nanotube–polymer composites. Advanced Materials 2008;20(14):2707-14.
[62] Cebeci H, Guzman de Villoria R, Hart AJ, Wardle BL. Multifunctional properties of high volume fration aligned carbon nanotube polymer composites with controlled morphology. Composites Science and Technology 2009:69(15-16):2649-56.
[63] Garcia EJ, Wardle BL, Hart AJ, Yamamoto N. Fabrication and multifunctional properties of a hybrid laminate with aligned carbon nanotubes grown *In Situ*. Composites Science and Technology 2008;68(9):2034-41.

[64] Bekyarova E, Thostenson ET, Yu A, Kim H, Gao J, Tang J, Hahn HT, Chou TW, Itkis ME, Haddon RC. Multiscale carbon nanotube-carbon fiber reinforcement for advanced epoxy composites. Langmuir 2007;23(7):3970-4.
[65] Kamae T, Drzal LT. Carbon fiber/epoxy composite property enhancement through incorporation of carbon nanotubes at the fiber–matrix interphase – Part I: The development of carbon nanotube coated carbon fibers and the evaluation of their adhesion. Composites Part A: Applied Science Manufacturing 2012;43(9):1569-77.
[66] Zhu J, Imam A, Crane R, Lozano K, Khabashesku VN, Barrera EV. Processing a glass fiber reinforced vinyl ester composite nanotube enhancement of interlaminar shear strength. Composites Science and Technology 2007;67(7-8):1509-17.
[67] Godara A, Gorbatikh L, Kalinka G, Warrier A, Rochez O, Mezzo L, Luizi F, van Vuure AW, Lomov SV, Verpoest I. Interfacial shear strength of a glass fiber/epoxy bonding in composites modified with carbon nanotubes. Composites Science and Technology 2010;70(9):1346-52.
[68] Mezzo L, Godara A, Rochez O, Luizi F, Warrier A, Verpoest I, Lomov S. Method for the preparation of a reinforced thermoset polymer composite. PCT Int. Appl. WO 2010/007163 A1, 2010.
[69] Warrier A, Godara A, Rochez O, Mezzo L, Luizi F, Gorbatikh L, Lomov SV, VanVuure AW, Verpoest I. The effect of adding carbon nanotubes to glass/epoxy composites in the fibre sizing and/or the matrix. Composites Part A: Applied Science and Manufacturing 2010;41(4):532-8.
[70] Gao L, Chou TW, Thostenson ET, Zhang Z, Coulaud M. *In situ* sensing of impact damage in epoxy/glass fiber composites using percolating carbon nanotube networks. Carbon 2011;49(10):3382-5.
[71] Gorbatikh L, Lomov SV, Verpoest I. Nano-engineered composites: a multiscale approach for adding toughness to fibre reinforced composites. Procedia Engineering 2011;10:3252-8.
[72] Luinge H, Wachinger G. Method for the production of a fiber composite component, and semifinished textile product therefor. PCT Int. Appl. WO 2010/020237 A2, 2010.
[73] Song YS. Multiscale fiber-reinforced composites prepared by vacuum-assisted resin transfer molding. Polymer Composites 2007;28(4):458-61.

Part 1

MODIFICATION OF EPOXY RESIN WITH SOLUBLE THERMOPLASTICS TOWARDS TOUGHENING OF COMPOSITE MATRICES

Since toughening of epoxy thermosets with thermoplastics is an important avenue towards improved properties of high performance systems, the first part of this work explores binary blends prepared with epoxy resin and two amorphous thermoplastics, poly(ether sulfone) (PES) and poly(hydroxyether of bisphenol A) (phenoxy). In order to transpose the studied systems to composite production by Resin Transfer Molding (RTM) process, in situ dissolution of thermoplastic in epoxy resin during thermal treatment is required before resin crosslinking. Therefore, the study intends to investigate the interdiffusion mechanism between thermoplastics and resin precursors up to the formation of the morphology gradient resulting from reaction induced phase separation. The final objective is to define thermoplastic-epoxy resin combinations and thermal conditions favoring interdiffusion and thus improving thermoplastic dissolution and distribution into epoxy resin to minimize compositions inhomogeneities in the generated blends. Moreover, a microstructure with thermoplastic nodules dispersed in a continuous epoxy resin-rich phase is desired through the morphology spectrum derived from the concentration gradients. Finally, transposability to liquid composite molding using thermoplastic elements like filaments, films, veils or

membranes interleaved in the composite preform must be guaranteed such as thermomechanical properties at least equivalent to the neat RTM6 resin.

PES was selected as thermoplastic modifier for epoxy resin due to its high glass transition temperature (T_g) assuring preservation of high thermomechanical properties of highly crosslinked thermoset networks. The behavior of PES is compared to that of another amorphous thermoplastic, i.e. phenoxy presenting a chemical structure inducing a much lower T_g. The originality of this work is also that both thermoplastics and epoxy resin on which the study focuses, i.e. HexFlow® RTM6 resin, are commercial products evaluated without prior chemical modification. Besides the RTM6 resin which is qualified for aerospace applications, other epoxide-diamine formulations are also inspected to evidence influence of lower molar mass precursors.

The first part of the work is divided into three chapters:
- The first chapter *"Blends of highly crosslinked epoxy resins with phenoxy and poly(ether sulfone): Network characterization of neat and thermoplastic-modified resins and influence of thermoplastic incorporation on cure reaction"* describes important characteristics of neat epoxy resins and resins modified with fixed contents of both thermoplastics like thermomechanical properties, viscosity, crosslinking kinetics and morphology.
- The second chapter *"Interdiffusion of thermoplastics and epoxy resin precursors: Investigations by experimental and molecular dynamics methods"* studies experimentally temperature intervals for dissolution of a fixed amount of thermoplastic into the epoxide and diamine precursors and interdiffusion using a model system consisting in a single filament in contact with the resin precursors. Diffusion coefficient are also computed by molecular simulation and correlated to the experimental results.
- The third chapter *"Swelling of phenoxy and poly(ether sulfone) in epoxy resin: Resulting composition and microstructure gradients"* examines swelling of thermoplastic filaments in the reactive resins and thermoplastic distribution into epoxy resin resulting from competition between interdiffusion and crosslinking reaction. Local morphologies induced by the composition gradient are also discussed.

Chapter 1

BLENDS OF HIGHLY CROSSLINKED EPOXY RESIN WITH PHENOXY AND POLY(ETHER SULFONE): NETWORK CHARACTERIZATION OF NEAT AND THERMOPLASTIC-MODIFIED RESINS AND INFLUENCE OF THERMOPLASTIC INCORPORATION ON CURE REACTION

Abstract

In order to exploit epoxy resin as matrix of continuous fiber reinforced composites for high performance applications, good thermomechanical and chemical resistances combined with high fracture toughness of the polymer material are required. High functionality epoxide-diamine resin formulations modified with soluble amorphous thermoplastics are therefore promising systems to reach such properties thanks to the highly crosslinked thermoset network and the ductile thermoplastic-rich domains resulting from resin curing and reaction induced phase separation (RIPS).

The present work compares the HexFlow® RTM6 resin largely used by aerospace industries to other resin formulations prepared by mixing stoichiometric amounts of tetraglycidyl methylene dianiline (TGMDA) or triglycidyl p-aminophenol (TGAP) with a liquid diamine hardener, i.e. diethyltoluenediamine (DETDA). These low viscosity epoxy resins adapted to produce complex composite parts in an economical way by a process like Resin Transfer Molding (RTM) are characterized in terms of flexural modulus of the cured resins and evolution of the resin viscosity and crosslinking conversion during isothermal curing. Viscosity decrease of the unreacted resin, faster reaction kinetics and higher density networks leading to higher modulus are evidenced with DETDA hardener.

Addition of a high glass transition temperature (T_g) thermoplastic, poly(ether sulfone) (PES) and a lower T_g thermoplastic, phenoxy into these epoxy resins is investigated. Influence of PES and phenoxy amounts on the microstructure of the thermoset-thermoplastic blends is described. As compared to resins modified with PES, formation of smaller nodules at low thermoplastic content and higher critical compositions before phase inversion are observed for phenoxy-modified resins. Reduction of the blend modulus generated above thermoplastic T_g takes place at a temperature by far inferior with this lower T_g thermoplastic than with PES. Moreover, catalytic effect of phenoxy incorporation on the crosslinking kinetics is verified while the cure reaction is not influenced by moderate PES contents. Finally, the potential of Raman spectroscopy to evaluate the local PES and phenoxy amount in a blend with epoxy resin is demonstrated.

1. Introduction

The high crosslink density of epoxy resins makes them ideal candidates as matrices for high performance fiber-reinforced composites. Cured epoxy networks exhibit high tensile modulus and strength, good thermal stability and high T_g, excellent chemical and solvent resistance and good adhesion properties. These characteristics, desired in many commercial applications, combined with the low weight of the resin have led to a widespread use of fiber-reinforced epoxy resin matrix composite as engineering materials to replace metals in structural parts of aircrafts. However, due to their high crosslink density, epoxy matrices are inherently rather brittle and have poor fracture toughness. Therefore, many attempts have been made to improve resistance to failure due to interlaminar crack propagation in laminated fiber-reinforced composites. The modification of the thermosetting resin matrix with a thermoplastic can contribute to composite toughening.

Blends of epoxy resins with various amounts of high performance engineering thermoplastics have been widely investigated [1]. Unlike rubber toughening agents, high T_g thermoplastic additives can enhance the fracture resistance of epoxy resins without compromising the thermomechanical stability of the network. Effective toughness improvement has been obtained for amorphous thermoplastics miscible with the uncured resin formulations like poly(ether imide) (PEI) [2-5], polysulfone (PSf) [6-8] and PES [9-14] without sacrificing the glass transition temperature. It has been established that the morphology created in the thermoplastic-epoxy resin blends by the RIPS can contribute to some toughening at low thermoplastic concentration generating microstructures with thermoplastic-rich particles dispersed in the continuous epoxy-rich matrix. For higher thermoplastic fractions (from 15 wt % thermoplastic) producing bicontinuous morphologies or for phase inverted morphologies, significant improvement of the fracture toughness is achieved since a crack must advance through fracture of the ductile continuous thermoplastic-rich phase to damage the blend. Nevertheless, handling of such thermoplastic concentrations can be prevented due to important viscosity increase of the thermosetting resin-thermoplastic blend and potential decrease of other mechanical properties and limited resistance to fluids and to environmental stress cracking (ESC) of the thermoplastic phase.

This work specially examines an amorphous thermoplastic with a high T_g, PES and a lower T_g thermoplastic, poly(hydroxyether of bisphenol A) (phenoxy) introduced within several highly crosslinked epoxy networks adapted for high performance applications on a large temperature interval (up to more than 150 °C). Due to its high T_g, no degradation of thermomechanical properties of the PES-modified epoxy resins is expected. In spite of its lower T_g, phenoxy has demonstrated ability to improve fracture toughness in two-phase morphology blends without significant reduction of other properties of the epoxy network [15-18]. Several authors have considered toughening of epoxy resins based on tetrafunctional and trifunctional epoxide precursors using PES modifier and diaminodiphenyl sulfone (DDS) [9,11-12] or aromatic anhydride [10] curing agents. The few investigations that have been conducted for epoxy resins based on high functionality precursors blended with phenoxy have explored the tetraepoxide-DDS formulation [19] and the commercially important Hexflow® RTM6 resin qualified for aeronautic applications, for which K_{IC} has been improved by 20 % with only 10 wt % phenoxy [17].

In the present study, influence of epoxy resin modification with different amounts of PES or phenoxy on flexural modulus, blend microstructure and cure kinetics is examined for RTM6 resin and for resin formulations based on either tetraepoxide or triepoxide and the monoaromatic diamine DETDA as curing agent. These epoxy resins are proposed in this work as alternative epoxide-diamine formulations to RTM6 resin since they are intended to have at least equivalent thermomechanical properties. Indeed, the low molar volume of the DETDA hardener should produces highly crosslinked epoxy networks fulfilling the severe requirements of the aeronautic sector. Moreover, limited viscosities of the resin precursors make the selected resins injectable and adapted for RTM process.

At first, this work characterizes neat epoxy resins. On the one hand, some structural properties of the different cured epoxy networks are compared and on the other hand, evolutions of the resin viscosity and reaction conversion during isothermal cure treatments are monitored. Indeed, screening of resin crosslinking is an essential prerequisite to processing of composites based on these polymer matrices and polymerization kinetics controls the time window during which the resin precursors remains miscible with a thermoplastic modifier. Second, microstructures of the epoxy resin-thermoplastic blends depending on the system composition are discussed.

Influence of PES and phenoxy incorporation on modulus, viscosity and cure kinetics of the modified resins is also investigated. Potential of Raman spectroscopy for determination of local composition is finally described.

2. Experimental

2.1. Materials

2.1.1. Neat resins

The HexFlow® RTM6 monocomponent resin from Hexcel specifically developed to fulfill the requirements of the aerospace industry in advanced RTM process, which is composed of a tetraepoxide and a blend of two diamine hardeners [20], was compared to epoxy resin formulations similarly composed of tetraglycidyl-4,4'-methylenedianiline (TGMDA, Araldite® MY 721 from Huntsman) or based on triglycidyl para-aminophenol (TGAP, Araldite® MY 0510 from Huntsman). Both TGMDA tetraepoxide and lower viscosity TGAP triepoxide were crosslinked with DETDA (Lonzacure® DETDA 80 from Lonza, 77–81 % 3,5-diethyltoluene-2,4-diamine and 18–22 % 3,5-diethyltoluene-2,6-diamine) in these alternative resin formulations. Chemical structures and molar masses of the epoxide and diamine precursors and some of their characteristics provided in the supplier technical data sheets [21-24] are summarized in **Table 1**.

Table 1. Epoxy resin formulations and characteristics of their precursors.

Resin	Epoxide precursor	Diamine hardener
HexFlow® RTM6 Monocomponent resin specifically developed to fulfill the requirements of the aerospace and space industries in advanced RTM process	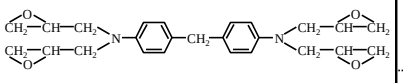 N, N, N', N' tetraglycidyl -4,4'-methylene dianiline (TGMDA) Tetraepoxide, M = 422 g/mol Viscosity: 3000-6000 mPa s at 50 °C	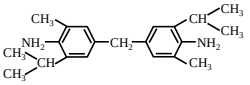 4,4'-methylenebis-(2-isopropyl-6-methyl)-aniline (MMIPA) M = 310 g/mol 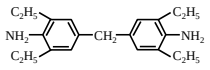 4,4'-methylenebis-(2,6-diethyl)-aniline (MDEA) M = 310 g/mol, melting point: 87-89 °C
TGMDA-DETDA Stoichiometric ratio (1 mol TGMDA for 1 mol DETDA)		
TGAP-DETDA Stoichiometric ratio (4 mol TGAP for 3 mol DETDA)	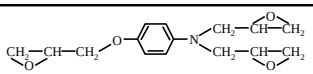 Triglycidyl para-aminophenol (TGAP) Triepoxide, M = 277 g/mol Viscosity: 550-850 mPa s at 25 °C	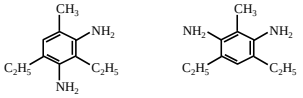 77-81% 3,5-diethyltoluene-2,4-diamine 18-22% 3,5-diethyltoluene-2,6-diamine Diethyltoluenediamine (DETDA) M = 178 g/mol, liquid at ambient

The TGMDA-DETDA and TGAP-DETDA reactive resins were prepared by stirring stoichiometric amounts of epoxide monomers and DETDA monoaromatic diamine (two oxirane rings for one amine group reacting two times) at ambient until homogeneous mixtures were obtained.

2.1.2. Resin-thermoplastic blends

The PES (Radel® A-200 NT from Solvay Advanced Polymers) and phenoxy (InChemRez® Phenoxy Resin PKHP-200 from InChem Corporation) thermoplastics were blended with RTM6, TGMDA-DETDA and TGAP-DETDA resins. The chemical structures, average molar masses and T_g of these amorphous thermoplastics are presented in **Table 2**. Phenoxy characteristics are data from the supplier [25]. The weight-average molar mass of PES was measured by size exclusion chromatography (SEC) using two PSS Gram columns (porosity of 100 and 1000 Å). N,N-dimethylformamide with 5 mmol/L ammonium hexafluorophosphate was used as carrier solvent (0.5 mL/min, 35 °C) and the detector was a Waters 410 differential refractometer (DRI). The PES T_g was measured by differential scanning calorimetry (DSC) during runs from 25 to 300 °C at a heating rate of 10 °C/min on a DSC 821e from Mettler Toledo. Phenoxy and PES selected as thermoplastic modifiers are distinguished by their molecular structures and their very different T_g, respectively of 92 °C and 220 °C while their weight-average molar masses are very close.

Thermoplastic was blended with TGMDA-DETDA and TGAP-DETDA resins by dissolving between 10 and 50 wt % PES or phenoxy powder in the epoxide monomers at 140 °C under mechanical stirring during 60 minutes. After thermal dissolution of the thermoplastic, the DETDA curing agent was mixed with the solution at 80 °C and the blends were immediately cooled after homogenization to minimize the curing reaction.

In order to introduce PES in the reactive RTM6 resin, dissolution was achieved in dichloromethane solvent (unstabilized grade for HPLC from BioSolve BV) at room temperature. The residual solvent was subsequently eliminated under vacuum. Preparation of phenoxy-RTM6 blends was differently executed by homogenization and dissolution of the phenoxy content in the resin during the cure treatment before gelation.

Table 2. Chemical formula and characteristics of PES and phenoxy thermoplastics.

Poly(ether sulfone) (PES)	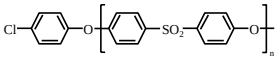	T_g = 220 °C $\overline{M}_n$ = 24,700 ; $\overline{M}_w$ = 49,400 g/mol (PS equivalent)
Poly(hydroxyether of bisphenol A) (phenoxy)	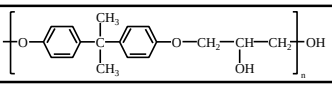	T_g = 92 °C $\overline{M}_n$ = 13,000 ; $\overline{M}_w$ = 52,000 Daltons

2.2. Characterization techniques

2.2.1. Dynamic mechanical analysis (DMA)

Samples were prepared in a steel mold coated with 2 layers of Frekote 700-NC mold release agent from Loctite. For neat TGMDA-DETDA and TGAP-DETDA resins and for resin-thermoplastic blends with 10 wt % phenoxy or PES, an isothermal curing of 80 minutes at 140 °C was applied to limit crosslinking kinetics and exothermicity while for RTM6 resin, a 1.5 °C/min temperature ramp from 105 to 200 °C adapted to process of composite parts was used. For all samples, the cure cycle was completed by a post-cure at an arbitrary chosen temperature of 200 °C during 30 minutes after which the reaction does not further progress. The sample specimens cut by a diamond saw into rectangular bars measuring approximately 60 mm × 6 mm x 2 mm were analyzed in the three-point bending mode on a DMA/STDA 861e from Mettler Toledo operating at an oscillation frequency of 1 Hz. Data were collected from room temperature to 250 °C at a scanning rate of 3 °C/min and results were averaged on 5 samples. A 3 N pre-stressing was applied to the specimens and maximal 10 µm displacement (maximum strain rate of 5.9 10^{-5} s^{-1}) and 0.1 N force (maximum stress of 0.28 MPa) were imposed in order to be located in the linear stress-strain domain.

2.2.2. Rheological measurements

Shear rheology was performed using a Bohlin Gemini II rheometer from Malvern Instruments with a 40 mm diameter parallel-plate geometry and a gap of 0.5 mm to measure the initial viscosity of the neat epoxy resins and the complex viscosity change of the resins and resin-thermoplastic blends during isothermal curing. A 10 % deformation was applied to the samples at a frequency of 1 Hz.

2.2.3. Differential scanning calorimetry (DSC)

Uncured resins or blends were placed in 40 µm aluminum pans with sample weights between 10 and 20 mg and crosslinked during isothermal runs on a DSC 821e from Mettler Toledo. The residual reaction enthalpy of the crosslinked samples was subsequently measured by alternating DSC (ADSC) at 2 °C/min up to 300 °C with an amplitude of 0.5 °C and a period of 48 s as modulation conditions. The same temperature scans were applied to the unreacted resin in order to measure the total reaction enthalpy.

2.2.4. Near infrared (NIR) spectroscopy

The progress of the crosslinking reaction of an epoxy resin during an isothermal curing was continuously followed using NIR spectroscopy by fitting the uncured epoxide-diamine resin formulation with or without thermoplastic modifier between two disposable glass slides into a homemade heated cell. Since glass is transparent in the NIR spectral region, monitoring of the curing reaction was achieved in situ by real time spectrum acquisitions with a Perkin Elmer NIR-FT Raman 2000R System spectrometer configured to operate in the NIR spectral region with a tungsten light source with a quartz envelope, a KBr beam splitter and a MIR TGS detector. Spectra were acquired every 60 s in the range 8000-4000 cm^{-1} at a 4 cm^{-1} resolution by coadding 8 scans during the isothermal curing until sample vitrification. A post-curing at 250 °C was afterwards completed in order to collect the NIR spectrum of the fully crosslinked epoxy resin.

2.2.5. Scanning electron microscopy (SEM)

Observations of the blend microstructures were performed on cryofractured surfaces of cured samples using a SEM LEO 982 (Zeiss) operating at 1 kV. The thermoplastic-modified resins were cured during 120 minutes at 140 °C and solvent etching of the thermoplastic phase was achieved before analysis to reveal the blend microstructures. The phenoxy and PES extractions were carried out respectively in tetrahydrofuran (THF) and dichloromethane (unstabilized grades for HPLC from BioSolve BV) during 24 hours.

2.2.6. Raman spectroscopy

Raman spectra of neat thermoplastics and of epoxy resins and blends cured at 140 °C were acquired with a DXR SmartRaman Spectrometer from Thermo Scientific operating in the microscopic mode with a 2048 pixel charge-coupled device (CDD) detector. A laser with an incident excitation wavelength of 780 nm and a power of 10 mW, a 50 µm slit aperture and a 10 times magnification objective were used.

3. *Results and discussion*

3.1. Characterization of neat epoxy resins

The following section compares RTM6, TGMDA-DETDA and TGAP-DETDA resin formulations in terms of properties of the crosslinked network and evolution of the curing reaction. Elastic modulus of the cured epoxy resins measured in the 3-point bending mode by DMA is first presented. Rheological characterization of the different epoxy resins is subsequently detailed. Initial viscosity of the uncured resins and increase of the viscosity during isothermal curing leading to gel time evaluation are discussed. Then, monitoring of the resin crosslinking is completed by assessment of the cure conversion on basis of the reaction heat flow measured by DSC and the concentration in reactive chemical groups revealed by NIR spectroscopy. Finally, results generated by these different techniques enabling cure follow up are compared.

3.1.1. Flexural elastic modulus

The modulus values evaluated by DMA must be carefully considered due their strong dependence on the specimen geometry leading to an important measurement variability (standard deviation up to 400 MPa despite repetition of the measurement at least 5 times) and their potential overestimation induced by the experimental conditions. Moreover, even if the same post-cure treatment was applied, the different cure cycle used for RTM6 resin as compared to other resin formulations can influence the crosslinked network architecture and consequently, the resin modulus. However, some main tendencies can be identified by comparing evolution of the modulus during thermal scanning.

When DETDA reacts with TGMDA epoxide, the storage modulus of the induced network is higher than for the RTM6 resin like shown in **Fig. 1**. Flexural modulus of the TGMDA-DETDA resin post-cured at 200 °C reaches approximately 4700 MPa at room temperature and remains superior by more than 500 MPa over the entire 25-250 °C temperature range to modulus of RTM6 resin cured by means of a classical temperature profile (ramp at 1.5 °C/min) used for composite manufacturing and post-cured in the same conditions as the TGMDA-DETDA resin. High crosslink density of the TGMDA-DETDA resin also increases T_g until around 230 °C but should reduce material ductility and justify even more the need to incorporate a more ductile thermoplastic phase in the thermoset network.

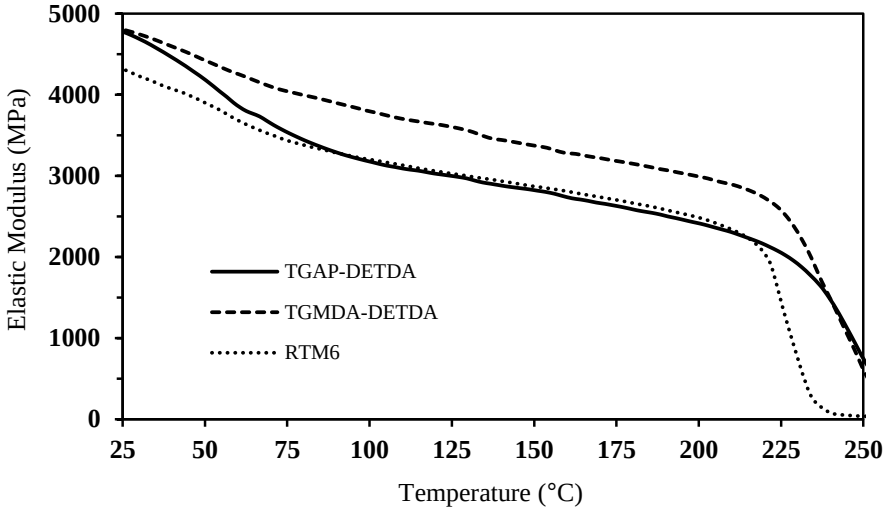

Fig. 1. Elastic modulus of the TGAP-DETDA, TGMDA-DETDA and RTM6 resins measured by DMA in 3 point bending mode from 25 to 250 °C.

Substitution of TGMDA tetraepoxide by TGAP triepoxide significantly reduces elastic modulus of the TGAP-DETDA resin as compared to TGMDA-DETDA resin. Nevertheless, since decrease of the network stiffness induced by TGAP epoxide is counterweighted by the DETDA hardener, modulus of the TGAP-DETDA resin remains in the same range than for RTM6 resin on a large temperature interval and is even higher below 75 °C and at high temperature where heat deflection is postponed. These results confirm that the TGMDA-DETDA and TGAP-DETDA resin are adapted like RTM6 resin for applications requiring high

thermomechanical performance. It must also be remarked that TGAP-DETDA resin shows a faster modulus decrease between 30 and 80 °C after which the modulus curve presents the same slope than the other resins. This low-temperature transition seems to evidence a different chemical structure of the resin network generated by triepoxide as compared to tetrafunctional resins.

3.1.2. Rheological behavior

The rheological characterization of epoxy resins aims to evaluate the viscosity evolution of the TGAP-DETDA and TGMDA-DETDA formulations by comparison with the RTM6 resin. In order to preserve resin injectability during a liquid composite molding process, viscosity has to remain below an upper limit of approximately 0.5 Pa s [26], which is recommended in order to prevent poor preform wettability and the need of excessive pressures to ensure the resin flow during resin injection. The RTM6 resin is typically injected between 80 and 100 °C to fulfill these requirements. This moderate injection temperature allows to limit the crosslinking reaction during the mold filling. A viscosity of the uncured RTM6 resin inferior to 0.5 Pa s in the 80 to 100 °C interval is confirmed in **Fig. 2** while the slow resin crosslinking kinetics in this temperature range ensures a sufficient time window to manage the resin injection without appearance of a significant viscosity increase.

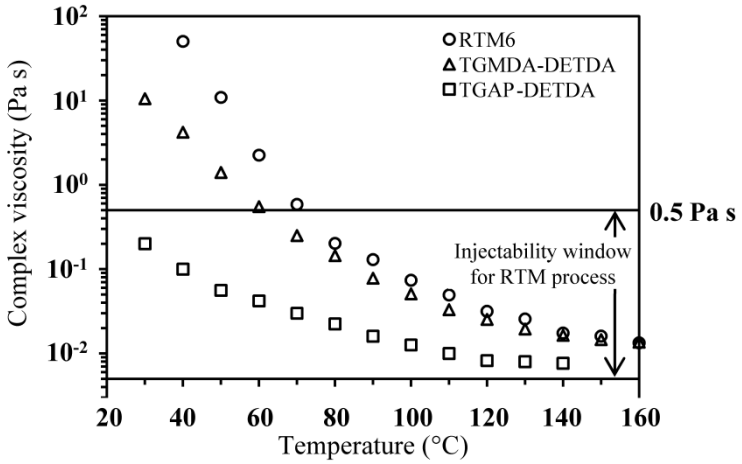

Fig. 2. Complex viscosity of the unreacted TGAP-DETDA, TGMDA-DETDA and RTM6 resins versus temperature between 30 °C and 160 °C.

The slight decrease of the initial viscosity between the TGMDA-DETDA and the RTM6 resins caused by the substitution of the RTM6 diamine hardeners by the liquid monoaromatic DETDA diamine allows only limited reduction of the injection temperature. When the main resin component, the TGMDA tetraepoxide, is replaced by the lower molecular weight TGAP triepoxide, a larger reduction of the viscosity takes place, which makes injection of the TGAP-DETDA resin possible even at room temperature.

The rheological measurements performed on reactive resins demonstrate an important temperature dependence of the complex viscosity evolution (**Fig. 3**) and accordingly gel time of the epoxide-diamine formulation. The correspondence between steady state shear viscosity and complex viscosity assumed to express the rheological data is an implicit application of the Cox-Merz rule [27]. Gel time values reported in this study correspond to the time period required to increase the initial resin viscosity by a 10^3 factor but other methods provide almost the same results like measurement of the time required to attain a storage modulus higher than the loss modulus.

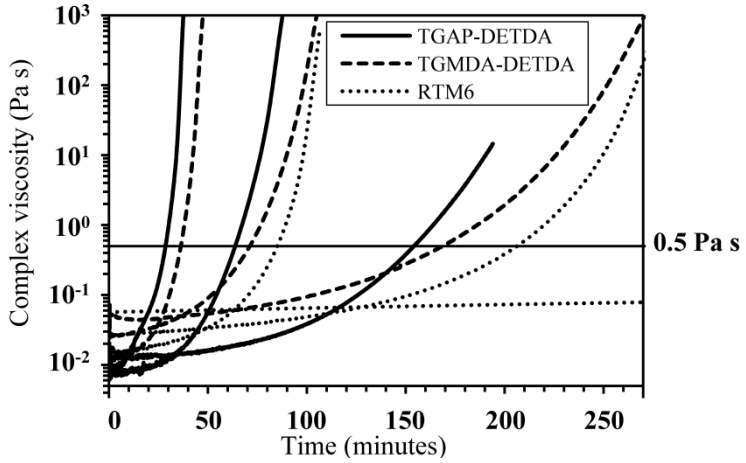

Fig. 3. Evolution of the complex viscosity of the TGAP-DETDA, TGMDA-DETDA and RTM6 epoxy resins during isotherms at 100 °C, 120 °C and 140 °C (right to left).

The gel time of the RTM6 resin varies from around 95 minutes at 140 °C to 4 hours at 120 °C and more than 10 hours at 100 °C. Despite the lower viscosities of the TGMDA-DETDA and mainly TGAP-DETDA resin formulations as compared to RTM6 resin, their higher reactivities, which induces a faster viscosity increase reduces considerably the time available

for the resin injection in equivalent thermal conditions. The faster crosslinking kinetics of the alternative resin formulations reduces the gel time at 140 °C from about 95 minutes for RTM6 resin to respectively 42 and 30 minutes for TGMDA-DETDA and TGAP-DETDA resins. Nevertheless, adequate time intervals for the injection are preserved at 80 °C since more than 3 hours are required to double the viscosity of both resins which remains in the injectability window during this time period. Furthermore, thanks to lower initial viscosities of the TGAP-DETDA and TGMDA-DETDA resins, a decrease of the temperature applied during the mold filling by these resins is still achievable in order to delay the cure initiation without hindering the flowability.

3.1.3. Crosslinking kinetics

The need to quantify the kinetics of the curing reaction is explained by the important influence of the curing process of the epoxy resin on both manufacturing and structure of epoxy resin-based composites. Features like resin injectability, final conversion rate of the cured resin and epoxy network properties are affected by the crosslinking. Therefore, in addition to measurement of the viscosity by rheometry, the curing progress was also been followed in terms of heat flow emitted by the exothermic crosslinking reaction using DSC on the one hand and concentrations in reactive functional groups by NIR spectroscopy on the other hand.

Extent of the curing process is provided by DSC assuming that the heat of reaction is proportional to the epoxide group consumption. Evolution of the conversion $\alpha(t)$ during an isothermal run can be calculated by the following expression:

$$\alpha(t) = \alpha_{final} \frac{\Delta H(t)}{\Delta H_{final}} \qquad \text{with} \qquad \alpha_{final} = 1 - \frac{\Delta H_{resid}}{\Delta H_0}$$

where $\Delta H(t)$ is the heat of reaction released during time *t* of isothermal cure, ΔH_{final} is the total heat release throughout the isotherm, α_{final} is the conversion rate reached after the isothermal treatment, ΔH_0 is the maximum enthalpy measured during a dynamic scan from 25 to 300 °C for an initially unreacted sample and ΔH_{resid} is the residual heat of reaction after isothermal cure determined by applying the same dynamic scan. Linear

baselines were chosen to integrate the exothermic reaction peaks and ADSC was used in order to separate enthalpy of the irreversible resin crosslinking from the reversible signal due to devitrification, which takes place in the same temperature range upon heating to 300 °C. Reaction enthalpy measured during isotherms, residual heats of reaction and calculated conversions are presented in **Fig. 4** for the TGAP-DETDA resin in a temperature range from 80 to 160 °C.

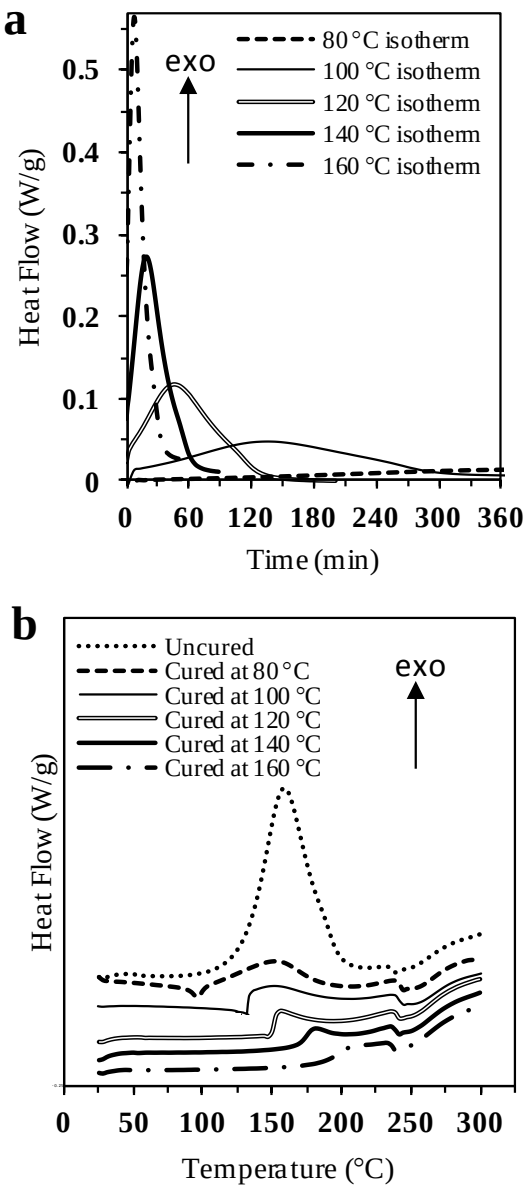

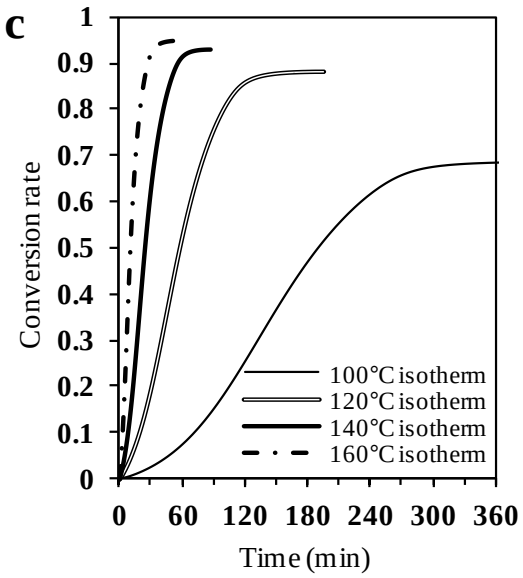

Fig. 4. TGAP-DETDA resin cured at 80, 100, 120, 140 and 160 °C: (a) Reaction enthalpy measured by DSC during isothermal cure; (b) Irreversible heat flow measured by ADSC during a dynamic scan from 25 to 300 °C corresponding to the residual reaction enthalpy after isothermal cure; (c) Calculated conversion rate during an isothermal cure.

The earlier heat releases of TGAP-DETDA and TGMDA-DETDA resins as compared to the RTM6 resin, which are reported in **Fig. 5** during a 140 °C isothermal cure, demonstrate their faster crosslinking kinetics. Reaction conversions calculated considering respectively total reaction enthalpies of 560, 470 and 450 J/g for TGAP-DETDA, TGMDA-DETDA and RTM6 resins corroborate these differences of resin reactivity. Moreover, the autocatalytic nature of the curing process caused by the formation of hydroxyl groups catalyzing the amine addition reaction is identifiable by the shape of the conversion curves. These results also evidence limited final conversions after the isothermal curing reaction due to vitrification that prevents to fully crosslink the epoxy network and justify why a postcuring stage is required to reach conversion higher than 95 %.

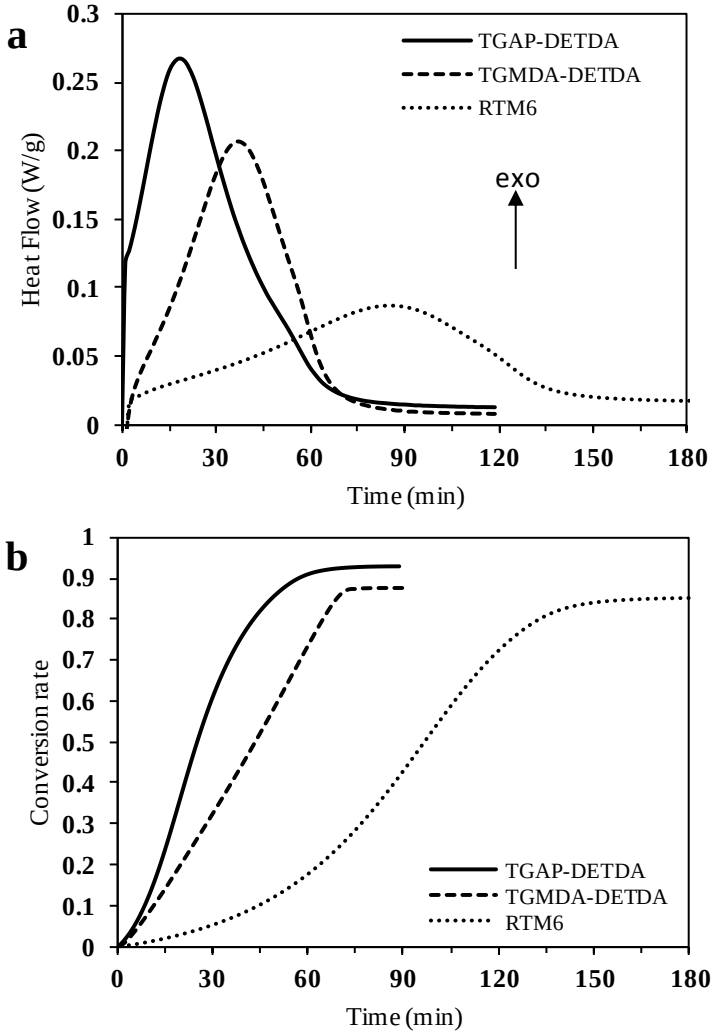

Fig. 5. (a) Reaction enthalpy and (b) conversion rate of TGAP-DETDA, TGMDA-DETDA and RTM6 resins during 140 °C isotherms.

Although DSC turns out to be an appropriate reference technique to evidence effect of the resin formulation on the crosslinking kinetics, the method described here prevents accurate determination of the reaction conversion. Indeed, several sources of potential errors [28] are due to the fact that:

- Residual unreacted epoxide moieties at the end of the dynamic scan up to 300 °C cannot be excluded, especially for the samples containing thermoplastic. Such incomplete reaction results in a value of ΔH_0 smaller than the full reaction enthalpy.

- The heat released by ring opening is not the same for each type of reaction, i.e., epoxide with primary amine, secondary amine or hydroxyl. As the proportion of each type of reaction is not preserved with etherification being more probable during the dynamic run up to 300 °C, the actual value of reaction enthalpy should be higher than ΔH_0 and calculated conversions would be overestimated.
- Degradation at high temperature could influence the measurement of ΔH_0 and ΔH_{resid}.
- Initial instability of the heat flow during isothermal runs is a source of measurement inaccuracy.

Therefore, monitoring of the global reaction heat generally leads to overestimation of the epoxide conversion. As an alternative, NIR spectroscopy exploits the fundamental advantages of the Fourier transform infrared spectroscopy (FTIR) technique to assess the real chemical group concentrations throughout polymerization, from the liquid epoxide-diamine mixture to the glassy epoxy resin. Access to the concentrations in epoxide, primary amine and secondary amine is quite direct by following the intensity changes of the absorption bands of these functional groups in the NIR spectral region from 8000 to 4000 cm^{-1} [29]. In this wavenumber domain, the absorption bands are due to the combination and the overtone of fundamental vibrations. Only CH, NH and OH vibrations are active in epoxy resins. Consequently, NIR absorption spectra are less complex than in the mid-infrared region and overlappings of the absorption bands are reduced. From an experimental point of view, in situ monitoring of the curing reaction was achieved by real time acquisitions of NIR spectra performed on samples presenting a 1 mm path length defined by the gap separating the glass slides maintaining the liquid resin in the heated cell, which are transparent in the NIR region.

The evolution of the NIR spectrum of the TGAP-DETDA epoxy resin during isothermal curing at 140 °C (**Fig. 6**) shows intensity variation of the absorption band of the reactive functional groups involved in the curing process. The intensity of the peaks assigned to primary amines rapidly decreases due to their addition on oxirane rings of the TGAP molecules. The secondary amine groups created by this reaction lead to the formation of a peak shoulder around 6600 cm^{-1}, whose intensity initially increases. Then, when reaction with the TGAP epoxide groups takes place, its intensity

decreases as the secondary amine amount is reduced. Both primary and secondary amine additions occurring during the curing process contribute to the decrease in the epoxide absorption band intensity and the formation of hydroxyl peaks derived from the oxirane ring-opening. Moreover, it can be assumed that influence of etherification on the kinetics remains insignificant for the reaction of epoxide monomers and aromatic diamine curing agents in stoichiometric conditions and at moderate temperature.

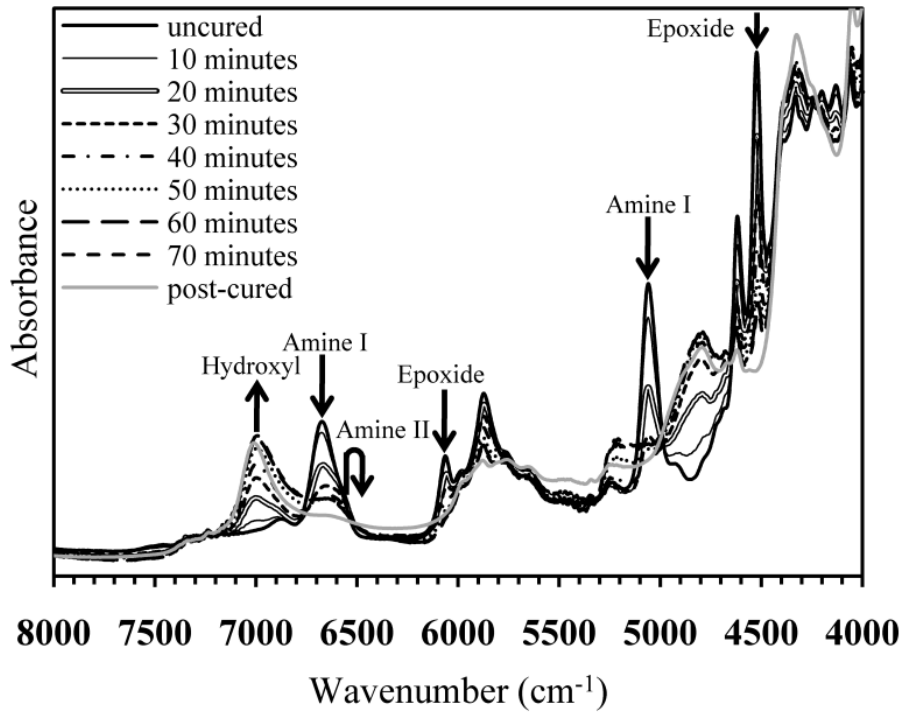

Fig. 6. NIR spectra of the TGAP-DETDA resin during an isothermal curing at 140 °C.

Concentration of the epoxide and amine functional groups of the epoxy resins is determined on basis of absorbance of the bands located in the region of combination of the fundamental vibrations between 5100 and 4000 cm^{-1}. According the Beer-Lambert law, conversion rates of the epoxide and primary amine reactive moieties are calculated at a reaction time *t* by the mathematical expression

$$\alpha(t) = \frac{A(0) - A(t)}{A(0) - A(\infty)}$$

where $A(0)$ is the initial absorbance of the functional group characteristic band and $A(\infty)$ represents its residual absorbance measured on the fully crosslinked resin post-cured at 250 °C.

The epoxide conversion during a 140 °C isotherm is presented in **Fig. 7** for the TGAP-DETDA and TGMDA-DETDA resins. The conversion curves confirm the faster crosslinking kinetics of the formulation based on the TGAP triepoxide. Slower kinetics of the RTM6 resin compared to epoxy resins cured with the DETDA diamine hardener is also clearly apparent. In the early stages of the reaction, the perfect balance between primary amine and epoxide consumptions (0.5 ratio between epoxide and amine I conversions) shows that the epoxide reaction is only due to the primary amine addition. At higher epoxide conversion, addition reactions of the primary amine and secondary amine are in competition as supported by initiation of the secondary amine conversion computed by deducting the epoxide conversion from the primary amine conversion.

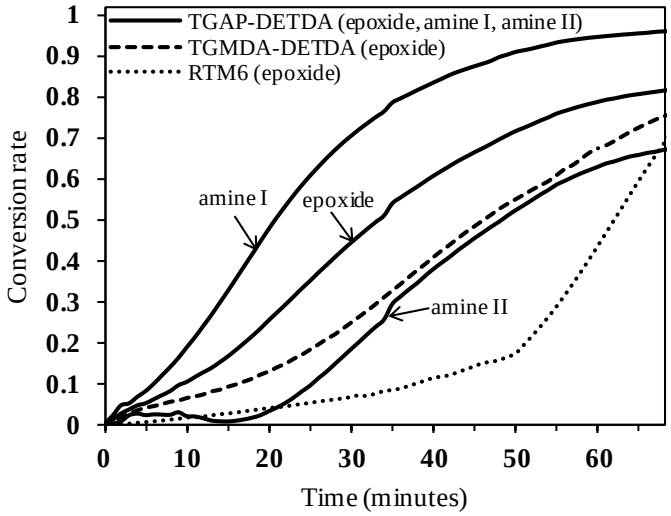

Fig. 7. Conversion of the epoxide, primary amine and secondary amine groups of the TGAP-DETDA resin and conversion of the epoxide moieties of TGMDA-DETDA and RTM6 resins versus time at 140 °C measured by NIR spectroscopy.

Comparison of the reaction conversions derived from DSC and NIR spectroscopy measurements and associated viscosity increase are presented in **Fig. 8** for RTM6 resin crosslinked at 140 °C. Overestimation of the

conversion based on evaluation of the exothermal reaction heat flow is evidenced. Moreover, the initial slow increase of resin viscosity can be related to the induction period of the autocatalytic reaction during which moderate crosslinking kinetics induces slower conversion growth. For longer curing times, viscosity increase becomes exponential simultaneously with theoretical gel time determined by NIR spectroscopy at conversion of 33.3 % for a tetrafunctional epoxide reacting with a diamine hardener according to Flory's expression [30].

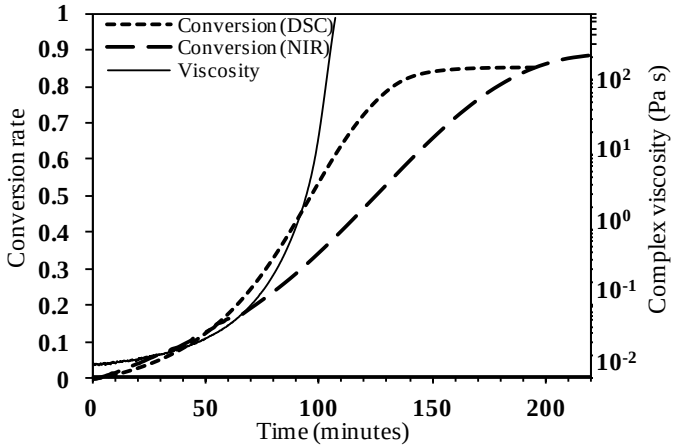

Fig. 8. Viscosity of the RTM6 resin cured at 140 °C and conversion measured by DSC and NIR spectroscopy.

Some of the main resin characteristics assessed by monitoring the cure reaction are summarized in **Table 3** showing that significant variation of the measured gel time value depending on the analysis technique can appear. Gel time values determined by NIR spectroscopy and DSC are equivalent to the time interval required to reach a conversion of 33.3 % for the TGMDA-DETDA resin and 40.8 % for the TGAP-DETDA resin corresponding to theoretical gel times derived from Flory's expression. Each method clearly emphasizes influence of the cure temperature on gel time and T_g of the crosslinked network and evidences shorter gel times and higher final conversions induced by TGAP triepoxide and mainly DETDA hardener as compared respectively to TGMDA tertraepoxide and MMIPA/MDEA diamines composing RTM6 resin.

Table 3. Gel times, final conversions and glass transition temperatures of TGAP-DETDA, TGMDA-DETDA and RTM6 resins resulting from 80, 100, 120 and 140 isothermal cures.

Resin	Temperature (°C)	Gel time (minutes)			Final conversion (DSC)	T_g (DSC)
		Rheometry	NIR	DSC		
RTM6	100	> 600				
	120	257				
	140	95	96	81	0.85	
	160	45			0.91	173
TGMDA-DETDA	80	650				
	100	245				
	120	93				
	140	43	35	31	0.87	172
TGAP-DETDA	80	512				
	100	192		162	0.69	131
	120	75		50	0.88	147
	140	34	28	22	0.93	171

3.2. Characterization of epoxy resin-thermoplastic blends

This section presents first SEM microstructures of epoxy resin-thermoplastic blends induced by RIPS depending on PES or phenoxy amounts dissolved in the different epoxide-diamine formulations. Effect of PES and phenoxy on elastic modulus of the thermoplastic-modified resins is then discussed. Finally, influence of PES and phenoxy modifiers on resin crosslinking is reported.

3.2.1. Blend microstructures

The microstructure resulting from RIPS in epoxy resin toughened with a thermoplastic significantly influences the properties of the polymer blend. Morphologies are controlled by many factors such as miscibility between the blend components, thermoplastic concentration or temperature cycle controlling the reaction rate. Therefore, a study of the morphology of PES or phenoxy-modified resins is necessary to adapt the thermoplastic content in order to generate the desired microstructure type.

Location of the initial blend composition with respect to the critical composition is the most important consideration influencing the blend microstructure. For off-critical compositions, the system enters first in the metastable region located between the binodal and spinodal lines as the cure

reaction progresses. Due to influence of kinetic factors, the phase separation mechanism can deviate from the behavior predicted by thermodynamics and follow different trajectories in the metastable region depending on the ratio between phase separation rate and cure reaction rate [31-32]. If phase separation rate is much faster, equilibrium is rapidly reached and a nucleation and growth mechanism is initiated with composition evolving along the binodal branch (trajectory a in **Fig. 9)**. Nevertheless, phase separation rate is in general insufficient to reach the equilibrium composition. For rapid crosslinking kinetics, phase separation does not occur in the metastable region but takes place in the unstable region (trajectory b in **Fig. 9**). In this case, the system demixes spontaneously by spinodal decomposition against concentration gradient as soon as it reaches the spinodal curve. The epoxy resin-thermoplastic system is more likely to cross the metastable region and to dephase by spinodal decomposition for blend compositions close to the critical value while for sufficiently off-critical mixtures, the probability of nucleation and growth is higher. Structures formed at the beginning of phase separation show some connectivity whereas at later stages, coalescence and coarsening can be observed.

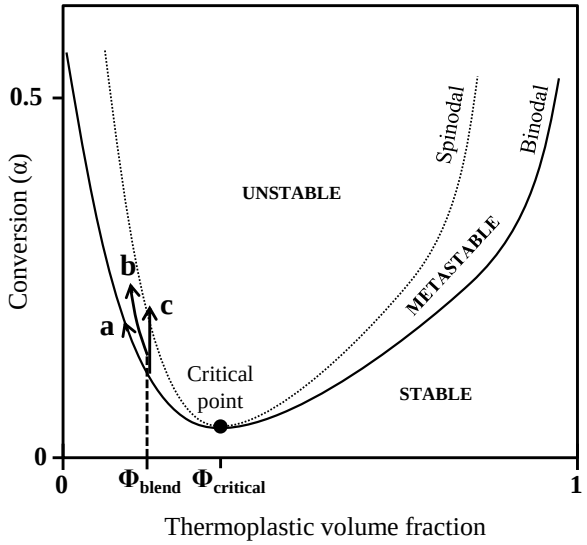

Fig. 9. Conversion-composition diagram showing trajectories followed upon curing of a blend: (a) Phase separation rate >> cure reaction rate; (b) phase separation rate close to cure rate; (c) phase separation rate << cure rate.

The microstructures created by introduction of 10 wt % phenoxy or PES in the TGMDA-DETDA resin are compared in **Fig. 10.a** and **Fig. 10.b**. Sea

(epoxy resin-rich phase)-island (thermoplastic-rich nodules) morphologies can be observed in both cases. While nodules of the phenoxy-rich phase with a size distribution mainly comprised between 100 and 200 nm are dispersed in the continuous epoxy-rich phase, the phase separation produces larger PES nodules characterized by a diameter around 500 nm. The similarity of the chemical structures of the epoxide monomers and the repetitive unit of the phenoxy macromolecules, which improves compatibility between the epoxy network and phenoxy can be a factor explaining the lower size of the phenoxy nodules. Indeed, a lower initial miscibility with the resin precursors can lead to a phase separation process occuring at higher conversions for phenoxy than for PES and consequently to presence of smaller phenoxy-rich particles because mass diffusion is hindered by the increasing viscosity of the medium as crosslinking proceeds.

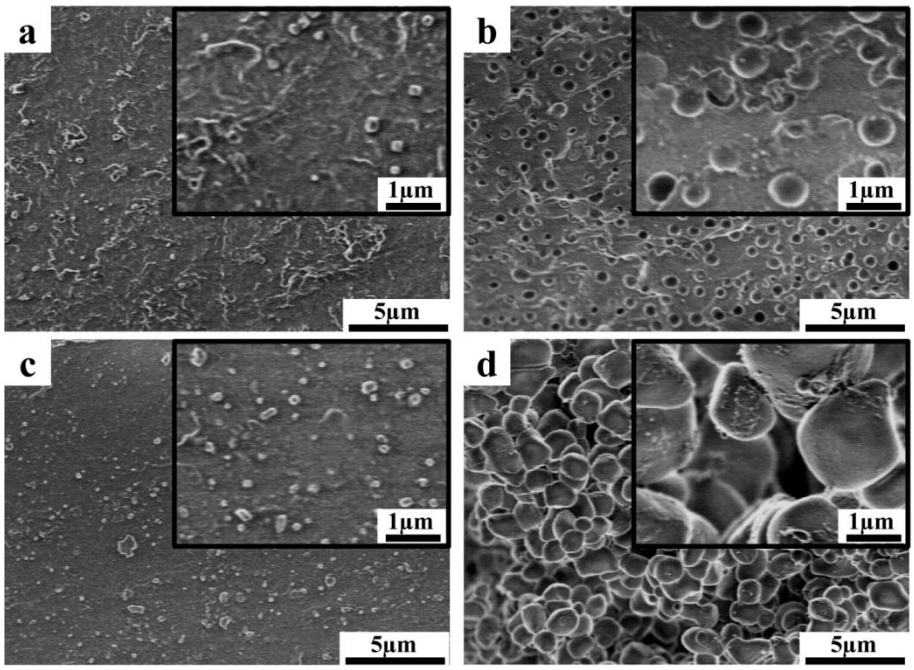

Fig. 10. SEM micrographs of the solvent etched fracture surface of cured blends of TGMDA-DETDA resin with (a) 10 wt % phenoxy, (b) 10 wt % PES, (c) 20 wt % phenoxy and (d) 20 wt % PES.

Addition of 20 wt % phenoxy to the TGMDA-DETDA resin increases the nodule concentration without significant modification of their average dimensions (**Fig. 10.c**). At this thermoplastic concentration, the blend

microstructure is totally different for the PES-modified resin and reflects the formation of a phase inverted morphology (**Fig. 10.d**). The solvent extraction of the continuous PES-rich phase clearly emphasizes a globular morphology with epoxy resin-rich inclusions attaining more than 1 µm.

An identical microstructure type is exhibited for TGAP-DETDA and RTM6 resins in **Fig. 11**, which confirms the higher critical composition in epoxy resin-phenoxy blends.

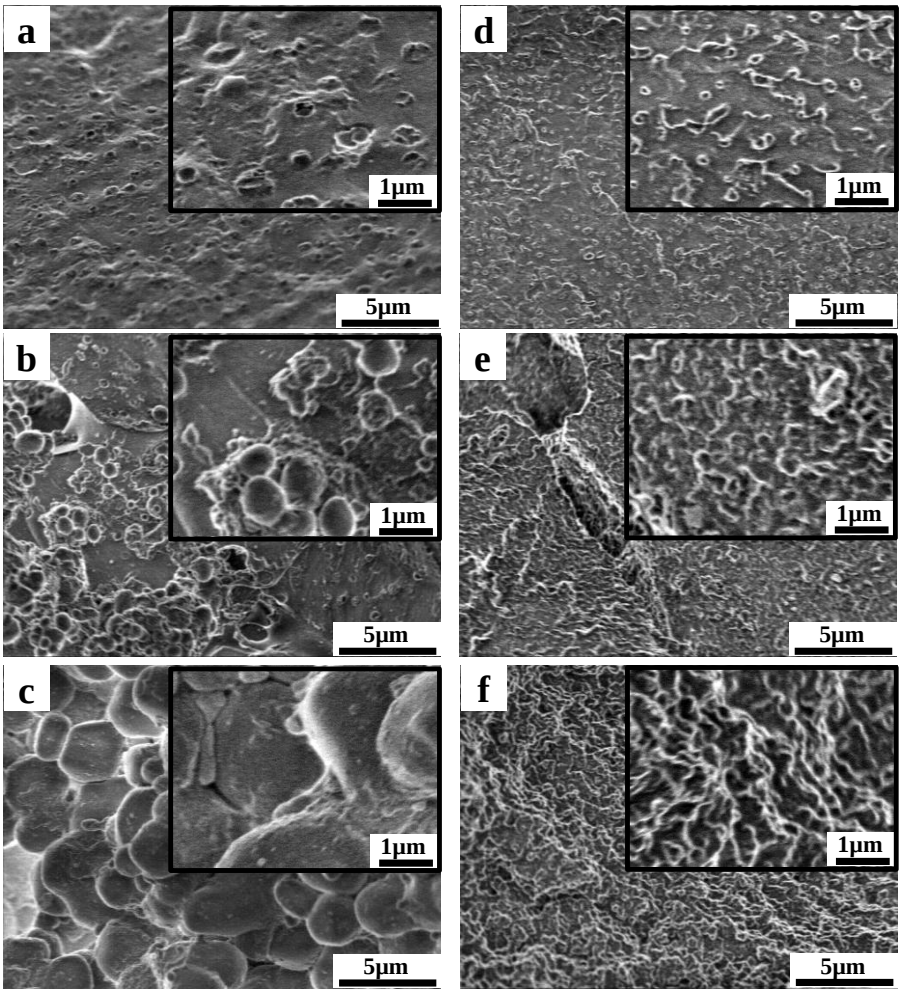

Fig. 11. SEM micrographs of the solvent etched fracture surface of cured blends of TGAP-DETDA resin with (a) 10 wt % PES, (b) 15 wt % PES, (c) 20 wt % PES and RTM6 resin with (d) 20 wt % phenoxy, (e) 30 wt % phenoxy, (f) 40 wt % phenoxy.

Phase inversion is initiated between 30 and 40 wt % of phenoxy in the RTM6 resin like in the TGMDA-DETDA resin while the appearance of continuous PES-rich phase was observed around 15 wt % in each epoxy resin studied.

3.2.2. Influence of thermoplastic on flexural elastic modulus

Addition of 10 wt % PES to epoxy resin has low effect on elastic modulus as shown in **Fig. 12** comparing neat and PES-modified TGAP-DETDA resins. Indeed, for limited PES contents generating blend morphologies with dispersed thermoplastic-rich nodules, elastic modulus is governed by the continuous resin-rich phase before temperature becomes higher than T_g of the PES-rich phase. Moreover, values of the tensile moduli of PES (2900 MPa [33]) and RTM6 resin (3300 MPa [34]) at 25 °C communicated by the material suppliers are close to each other. Around 220 °C, heat deflection is initiated but does not reduce considerably the blend performance since this transition occurs only slightly before T_g of the neat resin around 230 °C. Therefore, each epoxy resin investigated in this study can be modified with PES while maintaining modulus values equivalent to neat RTM6 resin.

Although addition of 10 wt % phenoxy (flexural modulus of 2700 MPa [25]) to TGMDA-DETDA resin decreases elastic modulus at room temperature, influence of phenoxy becomes more critical above its T_g at 92 °C where transition in the blend modulus evolution is apparent and considerably reduces the modulus value at higher temperatures. Such variation of the modulus is consistent with formation of a two-phase microstructure with respective compositions of the nodular phenoxy-rich phase and continuous epoxy resin-rich phase close to pure phenoxy and epoxy resin as glass transitions takes place at temperatures close to T_g of the blend components. Despite modulus reduction induced by the dispersed phenoxy phase, TGMDA-DETDA resin modified with phenoxy preserves a suitable modulus for high temperature applications, which is in the same range as for the neat RTM6 resin. On the contrary, PES is preferred to phenoxy modifier with TGAP-DETDA resin due to the lower modulus of this resin formulation. If the thermoplastic moduli were known on the temperature interval, it would also have been interesting to exploit micromechanics by evaluating if predictions of homogenization by the Mori-Tanaka method [35] follow experimental data.

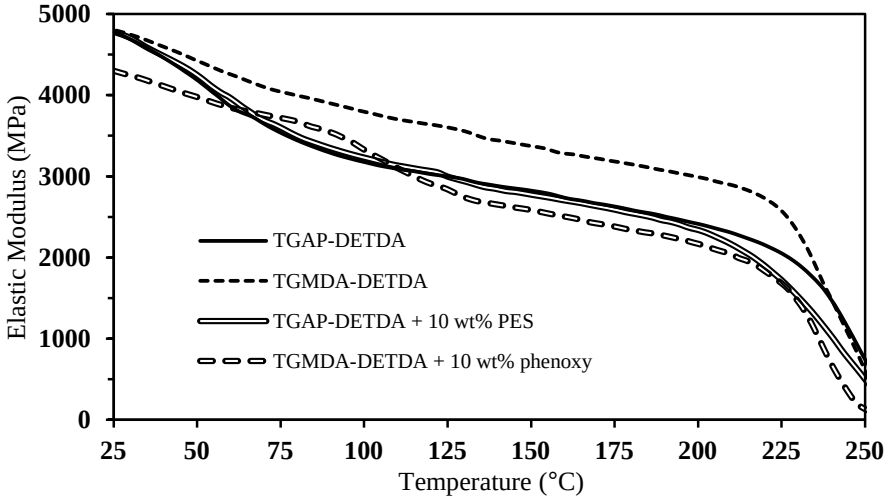

Fig. 12. Elastic modulus of neat and 10 wt% PES-modified TGAP-DETDA resin and of neat and 10 wt% phenoxy-modified TGMDA-DETDA resin measured by DMA in 3 point bending mode from 25 to 250 °C.

3.2.3. Influence of thermoplastic on the crosslinking reaction

The effect of PES or phenoxy addition on viscosity of the homogeneous resin-thermoplastic blends is evidenced in **Fig. 13**, which shows the important viscosity increase accompanying the dissolution of high molecular weight macromolecules of thermoplastic in the resin monomers.

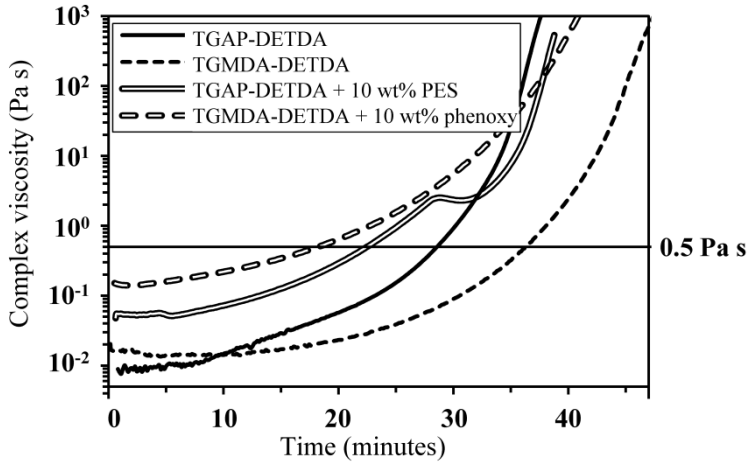

Fig. 13. Evolution of the complex viscosity of the TGAP-DETDA resin and its blend with 10 wt % PES and the TGMDA-DETDA resin and its blend with 10 wt % phenoxy during an isotherm at 140 °C.

Even with a limited thermoplastic content of 10 wt % in the epoxy resin, the initial viscosity of the uncured blend is approximately multiplied by a factor 10 preventing injection of the modified resins. Indeed, the system viscosity becoming higher than the injectability limit of 0.5 Pa s cannot be counteracted by a temperature increase without considerably reducing the time window available for injection. These results confirm that either very low thermoplastic concentrations can be added to the injectable epoxy resin or a different way must be exploited in order to introduce the thermoplastic and preserve a satisfactory processability by RTM.

Considering epoxy resin blended with 10 wt % thermoplastic, it appears that the influence of PES on the cure progress remains limited while phenoxy catalyzes the crosslinking reaction since the gel time is clearly reduced. Unlike the neat resins and phenoxy-modified resin, an interruption of the exponential increase of the viscosity takes place during the isothermal temperature treatment for the PES-modified resin with even a slight decrease of the viscosity. This intermediate viscosity plateau occurring in the TGAP-DETDA resin with 10 wt % PES after 25 to 30 minutes at 140 °C reveal a phase separation in the polymer blend before gelation. The reduction of the concentration of PES macromolecules in the continuous epoxy phase associated to the formation of a blend morphology with PES-rich nodules explains this temporary drop in viscosity before it rises again as crosslinking continues.

Independent measurements of the influence of the phenoxy content in the epoxy resin on the extent of the curing process have been provided by DSC. The conversion curves of the neat and phenoxy-modified TGMDA-DETDA resin at 140 °C are given in **Fig. 14** that shows also the catalytic effect of phenoxy on the reaction kinetics. Epoxide ring opening is favored by an increase of the initial amount of hydroxyl groups in the epoxide-diamine mixture for phenoxy concentrations contained in the blend up to 30 wt %. At higher phenoxy concentration, the dilution effect due to decreasing content of resin precursors starts to counterweigh the catalytic effect. Phenoxy addition must thus be taken into account to possibly adapt the process conditions since the gel time is considerably reduced in presence of phenoxy. Indeed, gel time of the TGMDA-DETDA resin at 140 °C derived from DSC measurements decreases from 31 minutes for the neat resin to 26 minutes for the resin modified with 10 wt % phenoxy and less than 18 minutes with 30 wt % phenoxy.

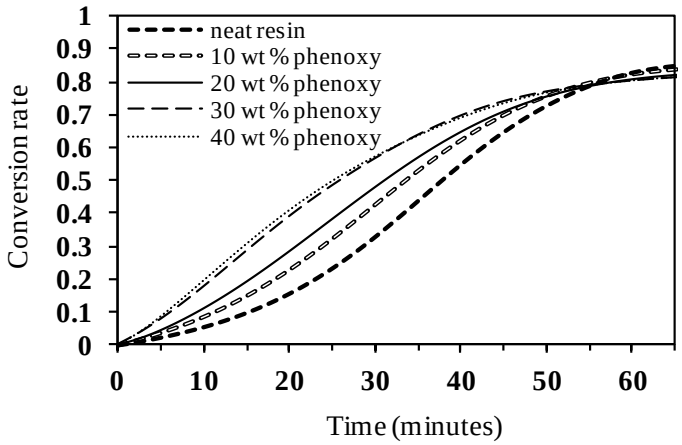

Fig. 14. Conversion of the TGMDA-DETDA resin and its blend with 10 to 40 wt % phenoxy versus time measured by DSC at 140 °C.

Crosslinking kinetics of epoxide-diamine mixtures blended with thermoplastics are also assessable by monitoring intensities of the NIR absorption bands during curing. For phenoxy-modified resins (**Fig. 15**), conversion of the functional groups can be rapidly derived from untreated spectra without any spectrum normalization required like for neat epoxy resins. Indeed, hypothesis of a linear relation between NIR peak height and concentration of the reactive group is relevant as the sample thickness remains constant throughout in situ acquisitions of the NIR spectra.

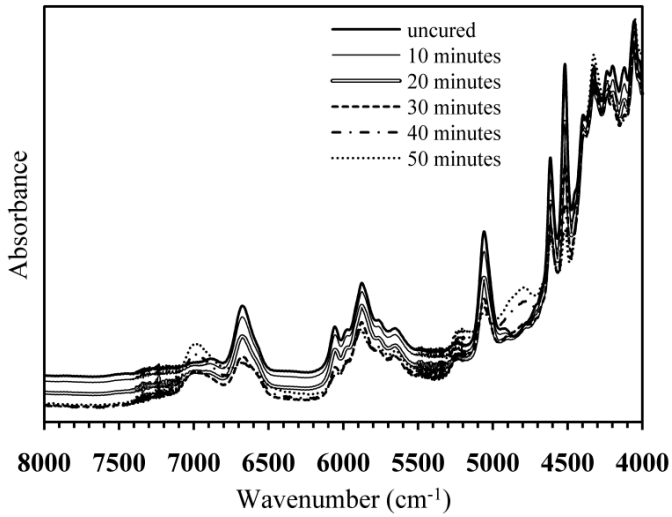

Fig. 15. NIR spectra of the TGMDA-DETDA resin blended with 10 wt % phenoxy during an isotherm curing at 140 °C.

For PES-modified resins, a variation of the spectrum baseline takes place during the resin curing as shown in **Fig. 16.a**. This baseline change is initiated after 27 minutes at 140 °C for the TGAP-DETDA resin blended with 10 wt % PES. It corresponds to the phase separation time deduced from rheological measurements. Interfaces between the epoxy resin and the PES-rich phases are created by the development of the blend microstructure and induce an increase of the light scattering and consequently, a reduction of the sample transmittance. Therefore, the evolution of the spectrum absorbance is also exploitable to detect initiation of phase separation in PES-modified resins but not for the epoxy resins containing phenoxy. This difference is explained by the size of the PES nodules (around 500 nm) dispersed in the epoxy resin being close to the NIR wavelength region investigated (785 to 1570 nm) and to significant disparities of refractive indexes between epoxy resin and PES. A higher scattering intensity and consequently, a more important baseline shift are thus induced, mainly at high wavenumbers as compared to lower size phenoxy nodules.

Due to such an important shift towards higher absorbance values during the resin crosslinking, pre-treatment of the NIR spectra is first required in order to compute conversion in the epoxy resin-PES blends via Equation 2. Multiplicative Scatter Correction (MSC) was used to compensate the light scattering by removing amplification and offset effects from the raw spectral signals as well as to prevent them from dominating over the chemical signals. Spectra of the PES-modified TGAP-DETDA resin are shown in **Fig. 16.b** after application of a full MSC treatment with the software The Unscrambler® X Version 10.0.1 allowing further evaluation of the chemical group conversion.

Since PES shows no reactivity with the epoxide or diamine precursors, crosslinking kinetics of PES-modified resins remains nearly unchanged at moderate PES concentration compared to neat resins as demonstrated in **Fig. 17** by the close epoxide conversions of the unmodified TGAP-DETDA resin and the homogeneous blend containing 10 wt % PES. Only a dilution effect hindering the reaction kinetics in the blend is expected for increasing PES concentrations.

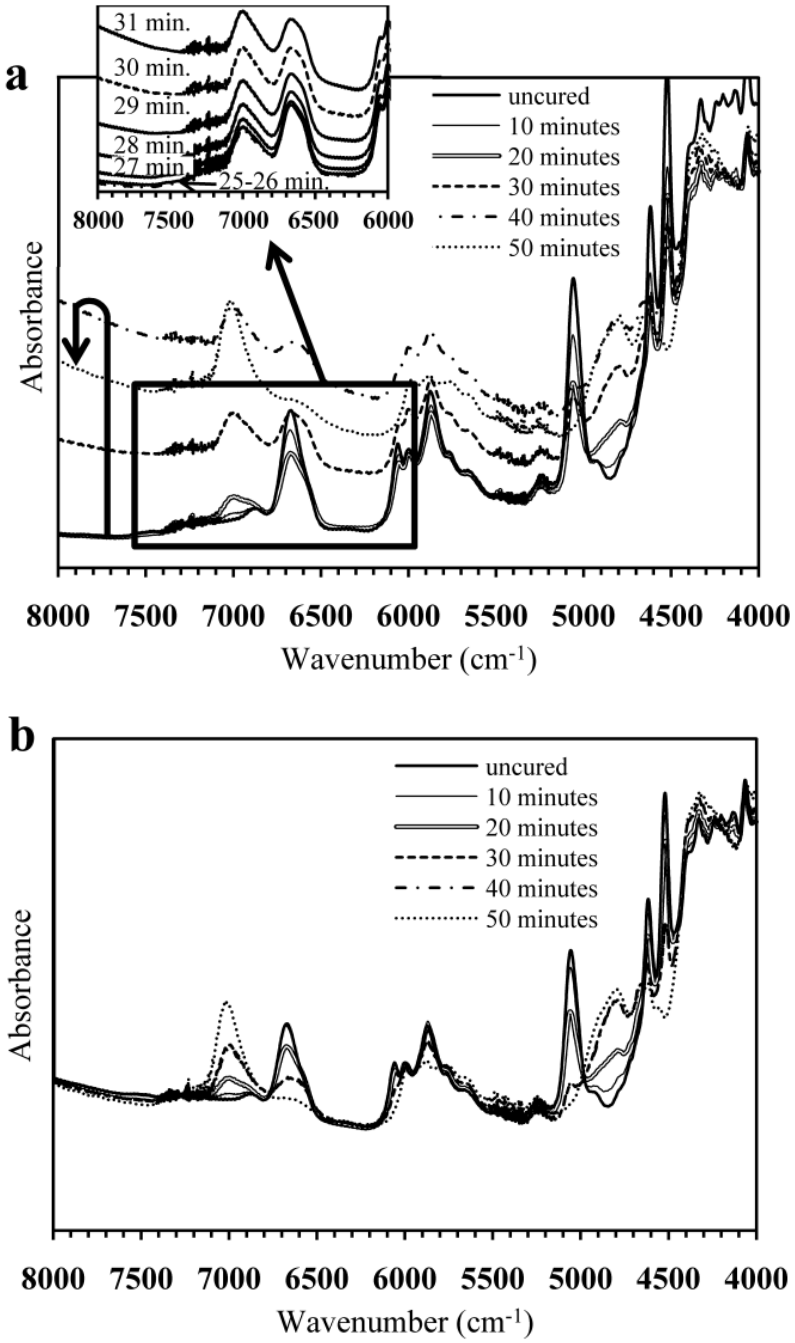

Fig. 16. NIR spectra of the TGAP-DETDA resin blended with 10 wt % PES during an isotherm curing at 140 °C; (a) untreated spectra (b) spectra after MSC treatment.

In contrast, the overall curing reaction rate apparently enhanced by the presence of phenoxy confirms the results based on DSC heat flows. Faster curing reaction rates of phenoxy-modified resins are attributed to the hydroxyl group in phenoxy chains exerting a catalytic effect for diamine addition whereas the reaction mechanism remains autocatalytic and unchanged in the phenoxy-epoxy resin system [19]. Indeed, the –OH groups of phenoxy shows little reactivity with epoxide at the early stages of the cure when the amine hardener is still abundant and reaction with the residual epoxide groups becomes only possible when the diamine moieties are sufficiently depleted at later cure stages. The unaffected initial cure mechanism has been confirmed in the present study by an absence of reaction heat flow measured by DSC between TGAP and TGMDA epoxides and phenoxy in the typical temperature interval used for resin curing.

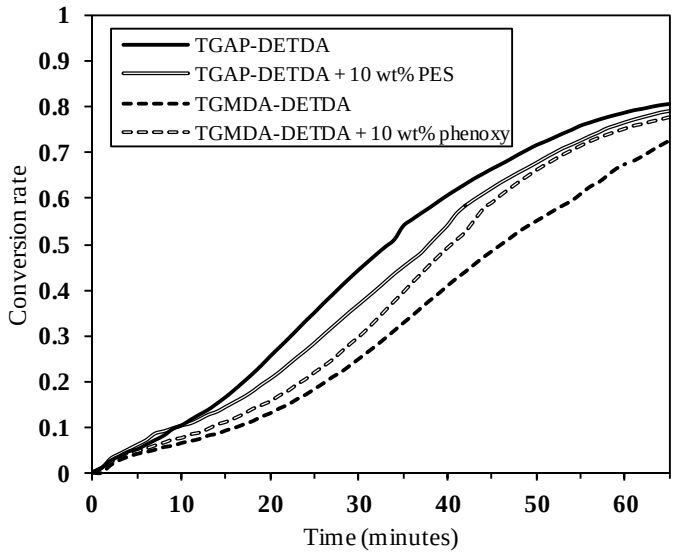

Fig. 17. Conversion of the epoxide groups of the TGAP-DETDA resin, TGAP-DETDA resin-10 wt % PES blend, the TGMDA-DETDA resin and the TGMDA-DETDA resin-10 wt % phenoxy blend versus time at 140 °C measured by NIR spectroscopy.

3.2.4. Quantification of thermoplastic content in an epoxy resin

Raman spectroscopy can be exploited to assess the phenoxy or PES concentration in an epoxy resin-thermoplastic blend of unknown composition similarly to what has been reported for determination of the

local thermoplastic content within epoxy resin-copolyethersulfone blends [36-37]. PES and phenoxy are characterized by intense spectral bands centered respectively at 1148 cm^{-1} and 1111 cm^{-1} while no Raman band of the epoxide-diamine formulation appears in this region of the spectrum as illustrated in **Fig. 18**. Therefore, the local thermoplastic concentration in an epoxy resin is quantifiable on the basis of the normalized intensity of such thermoplastic characteristic bands. Nevertheless, for more accuracy in composition prediction, multivariable analysis of the spectra should be preferred.

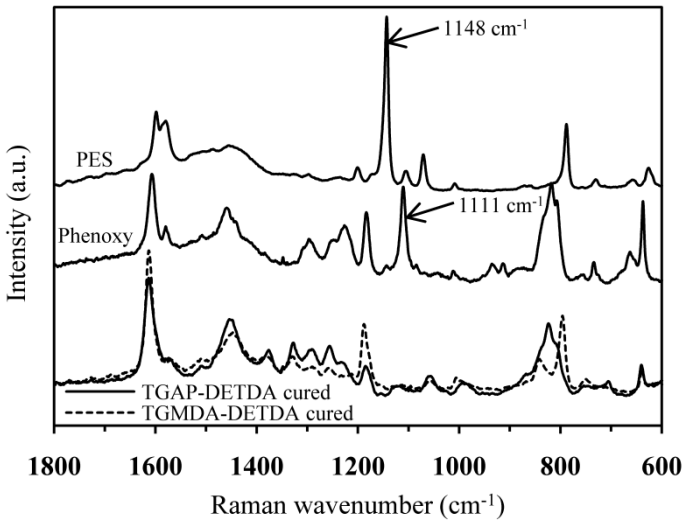

Fig. 18. Raman spectra of PES and phenoxy thermoplastics and TGAP-DETDA and TGMDA-DETDA resins cured at 140 °C.

A calibration set of data for prediction of thermoplastic amount in epoxy resin was defined by acquiring Raman spectra of resin-thermoplastic blends with PES or phenoxy fraction up to 50 wt %. Spectra were recorded in 5 different sample spots randomly selected using the lower magnification objective (10 times, resulting in a 3.81 µm spot diameter) and higher aperture (50 µm slit) available with the micro-Raman device. Such a setup was exploited to maximize the volume analyzed since spatial resolution is not valuable for these calibration samples and spectra corresponding to average blend composition without influence of the local microstructure are desired. Dependence of the 1111 cm^{-1} band intensity on phenoxy concentration in the blend is illustrated in **Fig. 19** for the TGMDA-DETDA resin-phenoxy system. The blend spectra confirms that monitoring of this

characteristic band of the phenoxy spectrum allow evaluation of the phenoxy content in epoxy resin.

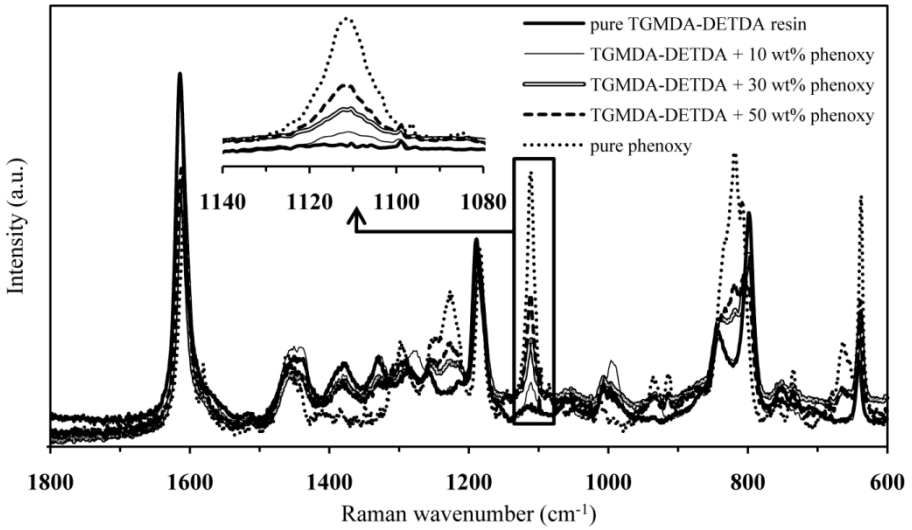

Fig. 19. Raman spectra of pure TGMDA-DETDA resin, TGMDA-DETDA resin blended with 10, 30 and 50 wt % phenoxy and pure phenoxy.

4. Conclusions

In order to maximize the thermoplastic content contributing to epoxy resin toughening while maintaining a continuous epoxy resin-rich phase in the thermoplastic-modified resin, PES and phenoxy concentrations of respectively 15 wt % and 30 wt % are recommended since they allow to reach compositions of the thermoset-thermoplastic blend close to the critical point. Incorporation of PES in epoxy resin can be achieved without compromising the blend modulus regardless the resin formulation and can for that reason be implemented for high T_g applications. In contrast, phenoxy induces drop of the blend modulus above its T_g. Consequently, toughening of epoxy resin with phenoxy is more suitable for an epoxide-diamine formulation characterized by high modulus values like TGMDA-DETDA than for RTM6 or TGAP-DETDA resins for which modulus decrease is prohibited. Indeed, the higher resin modulus resulting from hardening of TGMDA epoxide with low molecular weight DETDA compensates reduction of the modulus due to phenoxy and preserves its value in the same range than for neat RTM6 resin.

Although reaction kinetics is faster for resins crosslinked with DETDA as curing agent than for RTM6 resin, TGMDA-DETDA and TGAP-DETDA resins remain adapted for RTM injection, which can be achieved at lower temperature thanks to their reduced viscosities. Moreover, even if phenoxy catalyzes the curing process, monitoring of the cure reaction by several techniques has shown that low thermoplastic amounts have a limited influence on crosslinking kinetics. However, important viscosity increase caused by the thermoplastic macromolecules prevents injection of modified resins even at low PES or phenoxy content.

Therefore, a different method like in situ dissolution of the thermoplastic in the epoxy resin during the cure cycle [38-39] is suggested in order to preserve processability by RTM. The following chapters investigate thus interdiffusion between the thermoplastics and the resin precursors and composition gradients induced by thermal treatment of thermoplastic in reactive resins. In this context, Raman spectroscopy has demonstrated that it can be exploited to determine the local PES or phenoxy content in an epoxy resin-thermoplastic blend.

References

[1] Hodgkin JH, Simon GP, Varley RJ. Thermoplastic toughening of epoxy resins: a critical review. Polymer for Advanced Technologies 1998;9(1):3-10.
[2] Cho JB, Hwang JW, Cho K, An JH, Park CE. Effects of morphology on toughening of tetrafunctional epoxy resins with poly(ether imide). Polymer 1993;34(23):4832-36.
[3] Hourston DJ, Lane JM, Zhang HX. Toughening of Epoxy Resins with Thermoplastics: 3. An Investigation into the Effects of Composition on the Properties of Epoxy Resin Blends. Polymer International 1997;42(4):349-355.
[4] Bonnet A, Lestriez B, Pascault JP, Sautereau H. Intractable high Tg thermoplastics processed with epoxy resin: Interfacial adhesion and mechanical properties of the cured blends. Journal of Polymer Science Part B: Polymer Physics 2001;39(3):363-73.
[5] Shin S, Jang J. Toughness improvement of high-performance epoxy resin using aminated polyetherimide. Journal of Applied Polymer Science 1997;65(11):2237-46.
[6] Hedrick JL, Yilgoer I, Wilkes GL, McGrath JE. Chemical modification of matrix resin networks with engineering thermoplastics. 1. Phenolic hydroxyl-terminated poly(aryl ether sulfone)-epoxy systems. Polymer Bulletin 1985;13:201-8.
[7] Min HS, Kim SC. Fracture toughness of polysulfone/epoxy semi-IPN with morphology spectrum. Polymer Bulletin 1999;42(2):221-27.

[8] Martinez I, Martin MD, Eceiza A, Oyanguren P, Mondragon I. Phase separation in polysulfone-modified epoxy mixtures. Relationships between curing conditions, morphology and ultimate behavior. Polymer 2000;41(3):1027-35.
[9] Bucknall CB, Partridge, IK. Phase separation in epoxy resins containing polyethersulphone. Polymer 1983;24(5):639-44.
[10] Raghava RS. Development and characterization of thermosetting-thermoplastic polymer blends for applications in damage-tolerant composites. Journal of Polymer Science: Polym. Phys. Ed. 1988;26(1):65-81.
[11] Akay M, Cracknell JG. Epoxy resin-polyethersulphone blends. Journal of Applied Polymer Science 1994;52(5):663-88.
[12] MacKinnon AJ, Jenkins SD, McGrail PT, Pethrick RA. Cure and physical properties of thermoplastic-modified epoxy resins based on polyethersulfone. Journal of Applied Polymer Science 1995;58:2345-55.
[13] Andrés MA, Garmendia J, Valea A, Eceiza A, Mondragon I. Fracture toughness of epoxy resins modified with polyethersulfone: Influence of stoichiometry on the morphology of the mixtures. Journal of Applied Polymer Science 1998;69(1):183-191.
[14] Mimura K, Ito H, Fujioka H. Improvement of thermal and mechanical properties by control of morphologies in PES-modified epoxy resins. Polymer 2000;41(12):4451-59.
[15] Teng KC, Chang FC. Single-phase and multiple-phase thermoplastic/thermosetting polyblends: 2. Morphologies and mechanical properties of phenoxy/epoxy blends. Polymer 1996;37(12):2385-94.
[16] Siddhamali SK, Kyu T. Toughening of thermosetting/thermoplastic composites via reaction-induced phase separation: Epoxy/phenoxy blends. Journal of Applied Polymer Science 2000;77(6):1257-68.
[17] Beier U, Wolff-Fabris F, Fischer F, Sandler JKW, Altstädt V, Hulder G, Schmachtenberg E, Spanner H, Weimer C, Roser T, Buchs W. Mechanical performance of carbon fibre-reinforced composites based on preforms stitched with innovative low-melting temperature and matrix soluble thermoplastic filaments. Composites Part A: Applied Sc. and Manufact. 2008; 39(9):1572-81.
[18] Wong DWY, Lin L, McGrail PT, Peijs T, Hogg PJ. Improved fracture toughness of carbon fiber/epoxy composite laminates using dissolvable thermoplastic fibers. Composites Part A: Applied Science and Manufacturing 2010;41:759-67.
[19] Hseih HK, Su CC, Woo EM. Cure kinetics and inter-domain etherification in an amine-cured phenoxy/epoxy system. Polymer 1998;39(11):2175-83.
[20] Kiuna N, Lawrence CJ, Fontana QPV, Lee PD, Selerland T, Spelt PDM. A model for resin viscosity during cure in the resin transfer moulding process. Composites Part A: Applied Science and Manufacturing 2002;33(11):1497-503.
[21] Araldite® MY 721 datasheet (Huntsman).
[22] Araldite® MY 0510 datasheet (Huntsman).
[23] Lonzacure® DETDA 80 datasheet (Lonza).

[24] Lonzacure® M-DEA kr datasheet (Lonza).
[25] http://www.phenoxy.com/products/pkhp-200.html.
[26] Puckett M, Petervary M. Materials. In: Kruckenberg TM, Paton R, editors. Resin Transfer Molding for Aerospace Structures, Kluwer Academic Publishers: Dordrecht (The Netherlands), 1998.
[27] Cox WP, Merz EH. Correlation of dynamic and steady flow viscosities. Journal of Polymer Science 1958;28(118):619-22.
[28] Van Overbeke E, Devaux J, Legras R, Carter JT, McGrail PT, Carlier V. Raman spectroscopy and DSC determination of conversion in DDS-cured epoxy resin: Application to epoxy-copolyethersulfone blends. Applied Spectroscopy 2001;55(5):540-51.
[29] Billaud C, Vandeuren M, Legras R, Carlier V. Quantitative analysis of epoxy resin curing reaction: A study by near-infrared spectroscopy. Applied Spectroscopy 2002;56(11):1413-21.
[30] Flory PJ. Principles of polymer chemistry. Ithaca, NY, USA: Cornell University Press; 1953.
[31] Van Overbeke E. Curing and phase separation in epoxy resin - thermoplastic blends: Characterisation based on micro-Raman spectroscopy and multivariate analysis. PhD Thesis, Université catholique de Louvain, 2001.
[32] Williams RJJ, Rozenberg BA, Pascault JP. Reaction-induced phase separation in modified thermosetting polymers. Advances in Polymer Science 1997;128:95-156.
[33] Radel A datasheet (Solvay Advanced Polymers).
[34] HexFlow RTM6 datasheet (Hexcel).
[35] Mori T, Tanaka K. Average stress in matrix and average elastic energy of materials with misfitting inclusions. Acta Metallurgica 1973;21(5):571-4.
[36] Van Overbeke E, Devaux J, Legras R, Carter JT, McGrail PT, Carlier V. Raman spectroscopy determination of the thermoplastic content within epoxy resin-copolyethersulfone. Applied Spectroscopy 2001;55(11):1514-22.
[37] Van Overbeke E, Devaux J, Legras R, Carter JT, McGrail PT, Carlier V. Phase separation in epoxy-copolyethersulphone blends; morphologies and local characterization by micro-Raman spectroscopy. Polymer 2003;44(17):4899-908.
[38] Naffakh M, Dumon M, Gérard JF. Study of a reactive epoxy-amine resin enabling in situ dissolution of thermoplastic films during resin transfer molding for toughening composites. Composites Science and Technology 2006;66(10):1376-84.
[39] Wong DWY, Lin L, McGrail PT, Peijs T, Hogg PJ. Improved fracture toughness of carbon fiber/epoxy composite laminates using dissolvable thermoplastic fibers. Composites Part A: Applied Science and Manufacturing 2010;41:759-67.

Chapter 2

INTERDIFFUSION OF THERMOPLASTICS AND EPOXY RESIN PRECURSORS: INVESTIGATIONS BY EXPERIMENTAL AND MOLECULAR DYNAMICS METHODS

Abstract

The main focus of this chapter is to study the complex issue of interdiffusion between thermoplastics and epoxy resin precursors, by a combination of experimental and numerical simulation methods, in order to understand the key parameters driving the process. Temperature intervals during which thermoplastic dissolution takes place through interdiffusion with the resin precursors have been compared on basis of heat flows measured during dynamic heating for several thermoplastic-precursors systems. Diameter changes of thermoplastic filaments in contact with epoxide and diamine precursors have also been followed and an original approach using carbon nanotubes as tracers of the filament swelling front has been developed. These methods show that the improved mobility of the low molecular weight resin monomers as well as the higher mobility of the lower T_g phenoxy as compared to poly(ether sulfone) control the dissolution by favoring the penetration of precursors into the thermoplastic and lead to both swelling of

the outer part of the filaments and reduction of the inner unaffected core. Simulation by molecular dynamics supports the idea that diffusion of polymer macromolecules remains limited compared to the dominant effect of precursor diffusion. Indeed, low diffusion coefficients have been predicted for thermoplastic oligomers compared to the resin monomers. For the latter, the calculated values correlate well with the experimental data measured during interdiffusion.

A publication has been extracted from this chapter: Dumont D, Seveno D, De Coninck J, Bailly C, Devaux J, Daoust D. Interdiffusion of thermoplastics and epoxy resin precursors: investigations using experimental and molecular dynamics methods. Polymer International 2012;61(8):1263-71.

My thanks go to Dr. David Seveno from Laboratory of Surface and Interfacial Physics, Université de Mons, Place Du Parc, 20, B-7000 Mons, Belgium for the molecular simulation results and his important collaboration to this work.

1. Introduction

The high thermomechanical properties and the excellent chemical resistance of epoxy resins have contributed to their widespread use as polymer matrix in high-performance fiber-reinforced composites. However, due to the high crosslink density of the cured network, high functionality epoxide monomers crosslinked with diamine hardeners are intrinsically rather brittle and show poor fracture toughness. Many attempts have been made to improve the damage resistance of epoxy resins by modification with glassy thermoplastic polymers like polysulfone (PSf) [1-2], poly(ether sulfone) (PES) [3-5], poly(ether imide) (PEI) [6-8] or poly(hydroxyether of bisphenol A) (phenoxy) [9-10], initially soluble in the uncured resin formulation and subject to reaction induced phase separation (RIPS) during the cure reaction. Effective toughness improvement has been obtained in two-phase morphology blends without sacrificing desirable properties of the neat resin such as modulus, yield strength or glass transition temperature (T_g) usually induced when rubbers are used.

In order to effectively incorporate a thermoplastic additive in a reactive resin by thermal solubilization, the blend should be heated at a temperature allowing complete dissolution of the thermoplastic before the mobility of the diffusing moieties is hampered by the molecular weight increase and crosslinking of the resin. In practice, the manufacturing of tough composite parts by way of a liquid composite molding process, such as Resin Transfer Molding (RTM), requires in-situ dissolution of solid thermoplastic elements added to the composite preform [11-18]. Indeed, for these cost effective out-of-autoclave technologies, predissolving the thermoplastic in the liquid resin results in excessive viscosity increase and prevents correct injection through the preform.

Competition between thermoplastic dissolution in a reactive resin and the concurrent crosslinking reaction is therefore an important feature to consider for the application of this toughening approach. The selection of epoxide and diamine monomers as precursors of toughenable resin formulations must, for that reason, consider their ability to dissolve thermoplastic additives at temperatures low enough to prevent significant resin crosslinking. Dissolution occurs at the interface between the thermoplastic and the resin precursors through swelling and disentanglement of the initially glassy

polymer by the low molecular weight reactive monomers. Since interdiffusion between the low molecular weight resin precursors and the polymer macromolecules is strongly affected by the system composition, important disparities between dissolution kinetics are expected depending on the association between the thermoplastic and the epoxy resin. Lestriez et al. [19] have observed the structure of interphases between thermoplastics and epoxy networks at different cure conversions. They have highlighted that the thickness of the mixed layer containing both thermoplastic and thermosetting moieties is controlled by their compatibility coupled with the mutual diffusion between the resin precursors and the thermoplastic chains. Although there is an influence of the thermoplastic nature and the resin precursors on their initial miscibility [20], it has been suggested that the molecular dynamics of the low molecular weight diffusing moieties controls the diffusion and explains the location of the diffusion fronts. Several authors [21-24] have studied the diffusion of resin precursors into amorphous thermoplastics. These works have demonstrated significant diffusivity differences of epoxide precursors compared to diamine hardeners.

The objective of the present chapter is to investigate interdiffusion between different epoxide and diamine resin precursors presented in **Table 1** and two thermoplastics characterized by a large difference of T_g, i.e. PES and phenoxy, in order to understand its role in the dissolution process. Consequently, precursors-thermoplastic combinations promoting solubilization can be determined. Experimental tests were performed in parallel with numerical simulations to evaluate the behavior of thermoplastic-precursor blends at the molecular level. Indeed, with the huge breakthrough in computer power over the last decades, simulation has become a complementary method to experimentation. Several modeling approaches have already been used to predict the behavior of polymers into solvents, such as molecular dynamics [25-30] or coarse-grained simulations [25]. These techniques are able to predict both the energetics and the mobility of the molecules and can thus orient the selection of thermoplastics and resin precursors without the corresponding experimental, cost and health-related issues.

This paper is organized as follows. First, a thermal method to assess thermoplastic solubility in the resin monomers based on the heat flow associated to the solubilization is described. This approach provides a fast route to comparisons between resin precursors for a given thermoplastic and

vice-versa. Then, the interdiffusion mechanism leading to swelling and dissolution of the thermoplastic is observed by microscopic methods and discussed. The diffusion fronts of the thermoplastic and one resin precursor are examined simultaneously at the interface between a thermoplastic filament and each resin precursor. An original method using carbon nanotubes as tracers to continuously follow the apparent thermoplastic migration has been developed. Finally, in addition to this experimental technique, molecular dynamics simulations enabling calculation of diffusion coefficients are described and used to predict the influence of both the energetic interactions and molecule sizes on the dissolution.

2. Experimental

2.1. Materials

Tetraglycidyl-4,4'-methylenedianiline (TGMDA) tetrafunctional epoxide (Araldite® MY 721 from Huntsman), and two aromatic diamines, 4,4'-methylenebis-(2,6-diethyl)-aniline (MDEA, Lonzacure® M-DEA kr manufactured by Lonza) and 4,4'-methylenebis-(2-isopropyl-6-methyl)-aniline (MMIPA from Acros organics), were the resin precursors initially selected as potential solvents for PES (Radel® A-200 from Solvay Advanced Polymers) and phenoxy (InChemRez® Phenoxy Resin PKHP-200 from InChem Corporation) thermoplastics. These monomers are the epoxide and diamine precursors of the HexFlow® RTM6 resin from Hexcel [31] developed to fulfill the requirements of the aerospace industries in RTM. The PES and phenoxy amorphous thermoplastics were similarly tested with an alternative diamine hardener, monoaromatic liquid diethyltoluenediamine (DETDA, Lonzacure® DETDA 80 from Lonza, an isomer mixture composed by 77–81% 3,5-diethyltoluene-2,4-diamine and 18–22% 3,5-diethyltoluene-2,6-diamine) and with the lower viscosity triglycidyl para-aminophenol (TGAP) triepoxide (Araldite® MY 0510 from Huntsman). The chemical structures and characteristics of the above-mentioned resin monomers and thermoplastics are listed in **Table 1**.

Density, melting point and T_g values are data from the supplier technical data sheets [32-37]. The molar mass of the epoxide and diamine precursors is derived from the chemical structure of the monomers and the molar volume is calculated on basis of the molar mass and density values. The

weight average molar mass of the polymers was measured by SEC. For phenoxy, a set of four Waters Styragel HR5, HR4, HR3 and HR2 columns was used with tetrahydrofuran as mobile phase at a 1 ml/min flow rate. For PES, two PSS Gram columns (porosity of 100 Å and 1000 Å) were used and the carrier solvent (0.5 ml/min, 35 °C) was N, N-dimethylformamide with 5 mM ammonium hexafluorophosphate. The detector was a Waters 410 differential refractometer (DRI) in both cases.

Table 1. Chemical formula and characteristics of the resin precursors and thermoplastics.

Epoxides		
Tetraglycidyl -4,4'-methylene dianiline (TGMDA)	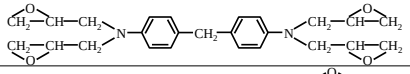	M = 422 g/mol Density at ambient: 1.15-1.18 g/cm^3 Molar volume: 3.86 10^{-4} m^3
Triglycidyl para-aminophenol (TGAP)	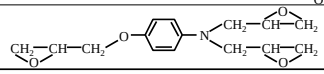	M = 277 g/mol Density at ambient: 1.21-1.22 g/cm^3 Molar volume: 2.47 10^{-4} m^3
Diamines		
4,4'-methylenebis-(2,6-diethyl)-aniline (MDEA)	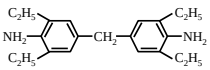	Melting point: 82-90 °C M= 310 g/mol Density at ambient: 0.9 g/cm^3 Molar volume: 3.44 10^{-4} m^3
4,4'-methylenebis-(2-isopropyl-6-methyl)-aniline (MMIPA)	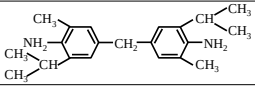	Melting point: 70-73 °C M = 310 g/mol Density at ambient: 0.99 g/cm^3 Molar volume: 3.13 10^{-4} m^3
Diethyltoluenediamine (DETDA)	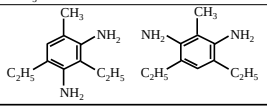	Liquid at ambient M = 178 g/mol Density at ambient: 1 g/cm^3 Molar volume: 1.78 10^{-4} m^3
Thermoplastics		
Poly(ether sulfone) (PES)	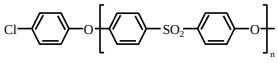	T_g = 220 °C $\overline{M}_w$ = 49,400 g/mol (PS eq) Density at ambient: 1.37 g/cm^3
Poly(hydroxyether of bisphenol A) (phenoxy)	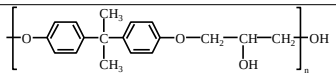	T_g = 92 °C $\overline{M}_w$ = 51,500 g/mol (PS eq) Density at ambient: 1.18 g/cm^3

Unmodified Nanocyl^{TM} NC 7000 multiwall carbon nanotubes (MWNTs) from Nanocyl S.A., with a purity of 90% were used as nanofillers in PES and phenoxy polymers for the preparation of nanocomposite filaments. These MWNTs include about 7 graphene shells and their average diameter and length are respectively 9.5 nm and 1.5 μm.

2.2. Manufacturing of thermoplastic and nanocomposite filaments

In order to draw thermoplastic filaments, a DSM Xplore Fiber Spin Line was used in combination with a corotating twin-screw batch-type micro-compounder (DSM Xplore 15 ml). The PES and phenoxy polymers were first dried at 80 °C during 12 hours under vacuum prior to compounding at

220 °C for phenoxy and at 340 °C for PES. Subsequently, the winding unit was exploited to process monofilaments with a diameter controlled by the winding speed and the winding torque as well as the thermoplastic flow and the die dimensions (5 or 0.5 mm diameter).

Nanocomposite filaments containing 0.1 and 1 wt % MWNTs used as tracers for the follow-up of the apparent thermoplastic migration were manufactured using the same processing conditions as for the pure thermoplastic filaments. A fine and homogeneous dispersion of the MWNTs was achieved for a residence time of 5 minutes in the mixing chamber using a rotation speed of the screws of 150 rpm [38]. Nanofiller dispersion in the thermoplastic filaments was examined by means of Transmission Electron Microscopy (TEM) by cutting ultrathin sections of approximately 95 nm in thickness with a Reichert Microtome using a histodiamond knife with a cut angle of 45 ° from Diatome at ambient temperature. The ultrathin sections were subsequently collected on 300 mesh copper grids and inspected with a LEO 922 transmission electron microscope operating at 200 kV.

2.3. Characterization techniques

2.3.1. Differential scanning calorimetry (DSC)

Calorimetric measurements of dissolution temperatures and enthalpy changes were performed with the help of a differential scanning calorimeter (Mettler Toledo DSC822E). Indium and zinc were used for calibrations. A temperature ramp from 25 to 200 °C was applied at various heating speeds (1, 5 and 10 °C/min) on 40 µl aluminum sealed pans containing thermoplastic powder homogeneously dispersed in a single resin component, either an epoxide or a diamine precursor. The sample weights were comprised between 15 and 20 mg.

2.3.2. Hot stage microscopy

A 100 µm diameter thermoplastic fiber (95 < diameter < 105 µm) of about 1 cm length was placed in 50 mg epoxide or diamine between two microscope glass slides and fitted into a Mettler FP82HT hot stage monitored by a Mettler FP90 central processor. On the one hand, dissolution of the thermoplastic filament was continuously observed with an Olympus BX51

optical microscope connected to a ColorviewI camera during an isothermal temperature treatment at 90 °C. On the other hand, in the case of a nanocomposite filament, extent of the apparent MWNT diffusion was evaluated from the progression of a darker area containing carbon nanotubes towards the resin precursor.

3. Experimental results and discussion

3.1. Thermoplastic solubilization in epoxide and diamine precursors

A fast and convenient dynamic calorimetric method is introduced in this section in order to assess the solubility of a thermoplastic polymer in an epoxide or diamine precursor. This approach is an alternative to other thermal methods like cloud-point curve determination with a light transmission device [20] used for the evaluation of thermoplastic solubility in epoxy resins. However, the DSC method described here is limited in most cases to the evaluation of thermoplastic solubility in the resin reactants considered separately. Indeed, for reactive formulations, the cure reaction starts before the thermoplastic is completely dissolved and as consequence, the large crosslinking exotherm prevents the detection of the much smaller (endo or exo) dissolution peak.

The thermoplastic, in solid powder form, is initially insoluble in the chosen epoxide and diamine monomers at ambient temperature. During the heating scan, swelling of the polymer particles and the corresponding dilution and disentanglement of the thermoplastic chains by low molecular weight monomers takes place. Depending on the system, the thermoplastic can be fully or only partially soluble in the resin components, leading to biphasic sol-gel mixtures in some cases. For moderate thermoplastic contents, dissolution is accompanied by an enthalpy change until it is complete, corresponding to the saturation temperature for this composition. To ensure an equilibrium measurement, slow heating rates must be used for accurate solubility prediction. However, such low heating rates lead to very weak power signals with insufficient signal to noise ratio. Hence, a compromise has to be found when selecting the heating rate. It should be, on the one hand, as low as possible to minimize the dissolution rate effect and on the other, high enough to provide a sharp thermal effect for exact solubility determination in a reasonable amount of time. The effect of the heating rate on the heat flow signal width and strength is evidenced for the dissolution of

10 wt % PES in TGAP in **Fig. 1** where amplification of the heat flow and delay to higher temperatures can be observed for increasing heating rates. Below 0.5 °C/min, the heating rate becomes too slow to differentiate the enthalpy change from the signal baseline. In order to calculate the equilibrium saturation temperature, the dissolution offset temperature (i.e. the end-temperature of the peak based on the baseline tangent) can be extrapolated to "zero" heating rate [39].

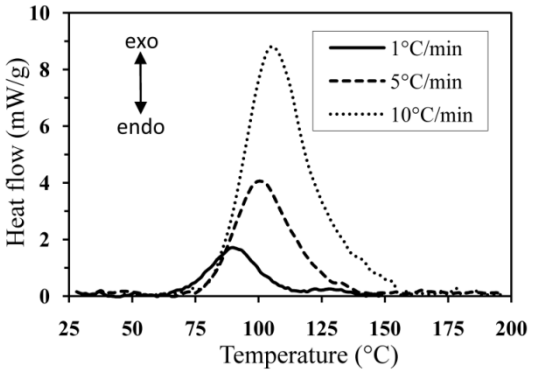

Fig. 1. Influence of the heating rate (1, 5 and 10 °C/min) on the dissolution heat flow curve of 10 wt % PES in the TGAP triepoxide.

The wide temperature windows observed for thermoplastic solubilizations combined with the low intensity of the residual heat flows prevent accurate determination of the dissolution offset. As a consequence, precise evaluation of saturation temperatures at equilibrium is difficult. Nevertheless, reproducibility tests have revealed lower standard deviations for onset and peak temperatures, in the range of 1.5 °C for the latter. Therefore, a comparison on temperature intervals and maxima of the dissolution heat flow is possible in order to evidence the promoting or inhibiting influence of particular epoxides and diamine hardeners on thermoplastic solubilization.

Peak values of the weak exothermic heat flow signal and intervals of dissolution are reported as a function of the heating rate (1, 5 and 10 °C/min) in **Fig. 2** for 10 wt % PES in TGAP and TGMDA epoxides. The onset temperatures measured on basis of the baseline tangent indicate that PES dissolution is initiated in TGAP about 40 °C lower than in TGMDA. Whatever the heating rate, the higher solubility of PES in the triepoxide compared to the tetraepoxide is confirmed by the lower temperature of the maximal dissolution heat flow in TGAP.

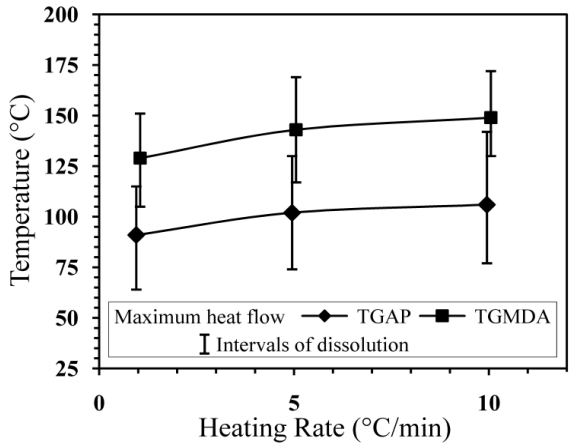

Fig. 2. Temperatures of the maximum heat flows and dissolution intervals for 10 wt % PES in TGAP and TGMDA epoxides as a function of the heating rate.

Trends in the capacity of the aromatic diamines to dissolve PES are similarly evidenced in **Fig. 3** for the same amount of PES powder added to the diamine hardeners. At any finite heating rate, the dissolution intervals of PES in DETDA are centered more than 50 °C lower than in MDEA and MMIPA. Whereas DETDA promotes PES solubility in an epoxy resin formulation owing to its low dissolution temperature, MDEA and MMIPA diamines show on the contrary higher PES dissolution temperatures than the epoxides (and hence do not significantly promote PES dissolution).

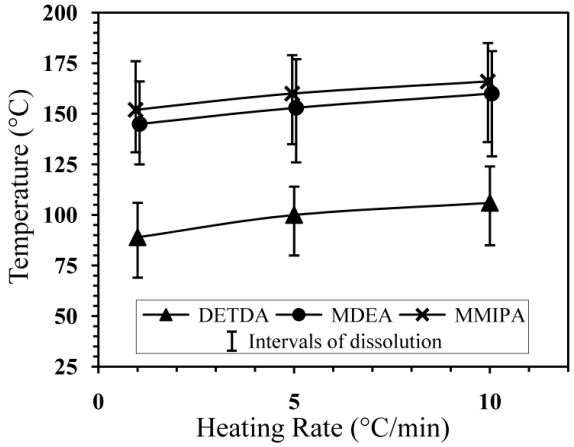

Fig. 3. Temperatures of the maximum heat flows and dissolution intervals for 10 wt % PES in DETDA, MDEA and MMIPA diamines as a function of the heating rate.

Complementary measurements have shown no significant effect of the thermoplastic concentration on the measured dissolution temperature. However, at high polymer contents the equilibrium structure becomes biphasic, with a diluted sol phase and a concentrated gel phase. For TGAP and DETDA precursors, the specific dissolution enthalpy of PES (**Fig. 4**) initially decreases until a concentration of about 20 wt % PES. This decrease reflects the transition from a sol phase dominated structure to a gel-phase dominated one. The increasing relative contribution of PES swelling to the total heat flow explains the reduction of the normalized enthalpy variation. It justifies the choice of limited concentrations of 10 wt % polymer powder to measure temperature intervals for thermoplastic dissolution. At PES concentration above 20 %, the normalized enthalpy levels out since the majority of the thermoplastic remains in the swollen state. Finally, beyond 60 wt % PES, a new decrease of the normalized heat flow is observed due to the presence of residual glassy PES, which is confirmed by a thermal transition corresponding to the T_g of pure PES (220 °C) still detectable after the dissolution process. For the TGMDA and MDEA precursors characterized by lower enthalpy change accompanying the PES swelling and dissolution, this transition is observable earlier, for concentrations above 40 wt % PES. These results corroborate the higher solubility of PES for DETDA and TGAP as compared to MDEA and TGMDA.

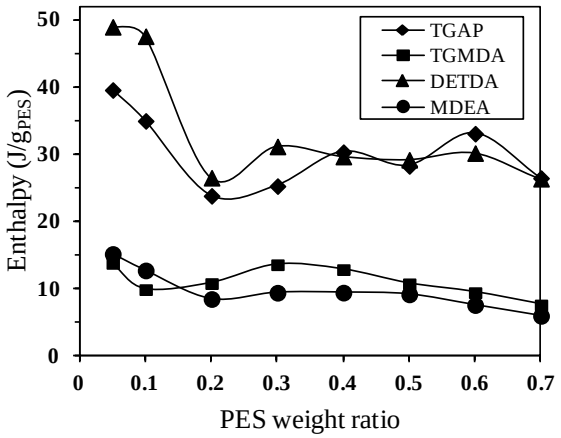

Fig. 4. Enthalpy variation measured during swelling and dissolution of PES (10 to 70 wt %) in the epoxide and diamine monomers with a heating rate of 5 °C/min.

In contrast with the exothermicity of PES dissolution, the thermal heat flow resulting from solubilization of phenoxy is endothermic due to its molecular structure leading to different interactions with the resin precursors. Temperature dissolution intervals and maxima measured during heating of 10 wt % phenoxy (and PES for comparison) in TGMDA are reported in **Fig. 5.** Dissolution of low T_g phenoxy takes place at a lower temperature than of high T_g PES. A similar trend is evidenced for TGAP epoxide and the diamines, except in the case of the quasi-athermic dissolution of MDEA for which no data are assessable.

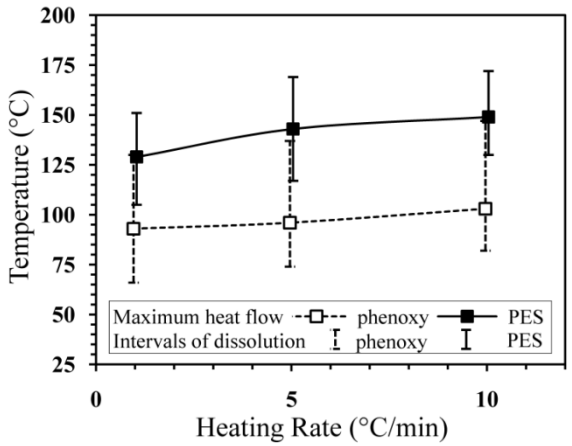

Fig. 5. Temperatures of the maximum heat flows and dissolution intervals for 10 wt % thermoplastic in the TGMDA tetraepoxide as a function of the heating rate.

The temperature intervals measured by the thermal method described here above, which provides an easy approach to select resin precursors and thermoplastics promoting dissolution, are synthetically compared in **Fig. 6** for a thermoplastic concentration of 10 wt %. These experimental results illustrate that dissolution is highly dependent on the nature of both thermoplastic and precursor. Thermodynamic considerations based on compatibility and molecular dynamics driven by mobility of the molecules are the main factors susceptible to influence the thermoplastic dissolution.

The main observations can be summarized as follows:
(i) A lower dissolution temperature in TGMDA is observed for phenoxy compared to PES. In the other precursors, the temperature decrease exists but is less pronounced.

(ii) A higher solubility of both thermoplastics in TGAP triepoxide and DETDA diamine is clearly established, especially for PES, in comparison, respectively, with TGMDA tetraepoxide and MDEA or MMIPA diamines. It demonstrates that TGAP and DETDA monomers can be chosen as precursors of alternative resin formulations to the RTM6 resin in order to reduce the dissolution temperature of thermoplastic additives.

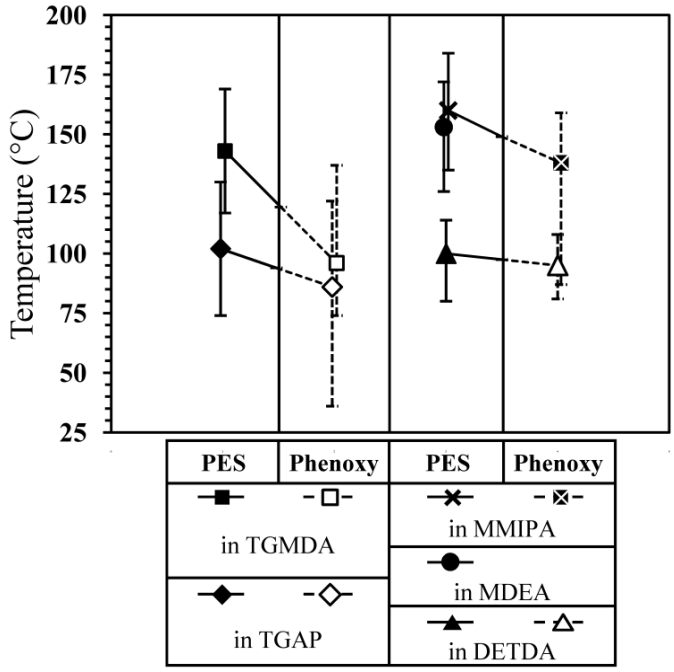

Fig. 6. Comparison of dissolution temperatures (maximum value of enthalpy and interval) for 10 wt% thermoplastic with a 5 °C/min heating rate.

3.2. Thermoplastic and nanocomposite filaments in the epoxide and diamine precursors

In order to evidence the mechanisms controlling the solubilization at the interface between the thermoplastic and a resin precursor, the behavior of neat thermoplastic and nanocomposite filaments dispersed in epoxide and diamine precursors were observed under isothermal conditions. A single 100 µm diameter-thermoplastic fiber in an epoxide or a diamine precursor was used as experimental model system to justify the differences in dissolution temperatures evidenced by DSC. The diameter decrease of PES and phenoxy filaments was followed by optical microscopy during heating at 90 °C. The

dissolution progress is illustrated for a phenoxy filament in the TGAP triepoxide by the temporal sequence illustrated in **Fig. 7**. The diameter initially decreases quite regularly all along the thermoplastic filament. Subsequently, it becomes thinner with Rayleigh instability becoming observable and finally, the fiber breaks. Afterwards, the remaining inclusions of pure thermoplastic rapidly disappear.

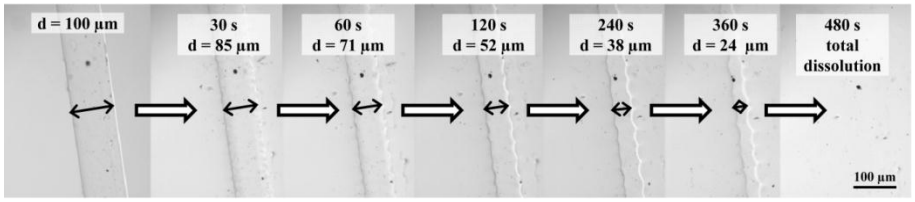

Fig. 7. Images from hot stage microscopy of a phenoxy filament in TGAP epoxide at 90°C.

During dissolution of the filament, its diameter, which is delimited by the location of the apparent interfaces, decreases continuously as a result of interdiffusion between the low molecular weight resin precursor and the polymer chains. Several regions can be identified in the composition gradient induced between the glassy polymer and the pure liquid solvent according to the amount of decreasing polymer concentration. An infiltration layer, a gel layer containing swollen polymer in a rubberlike state and a liquid layer containing (semi)-diluted solution with relatively free macromolecules have been identified in literature [19,40]. The interface detectable by this optical technique can be considered as the diffusion front of the epoxy resin precursor and delineates the thermoplastic area still unaffected by precursor molecules. The abrupt reduction of the TGAP precursor concentration that takes place in the infiltration layer between the pure thermoplastic and the gel layer makes the interface clearly visible due to the sharp transition of refractive index induced by the front.

The diameter evolution of 100 µm diameter-phenoxy and PES filaments in TGMDA tetraepoxide and DETDA diamine at 90 °C is reported in **Fig. 8**. The quicker movement of the filament interface observed for phenoxy, which is also noticeable with the other precursors considered, demonstrates faster diffusion kinetics of the TGMDA and DETDA precursors into phenoxy than into PES under the same conditions. This effect of the thermoplastic nature is especially apparent for the TGMDA precursor. Indeed, no dissolution of the PES filament occurs in TGMDA at 90 °C

whereas dissolution of the phenoxy filament progresses regularly. Temperature should be increased in order to provide a sufficient mobility to the molecules of the mixed layer containing TGMDA and PES to initiate interdiffusion. A slowdown of the diameter reduction of the phenoxy filament can also be observed at increasing diffusion times in TGMDA, leading to an incomplete dissolution of the filament. The interdiffusion process becomes inhibited as the width of the mixed layer rises and the concentration gradient decreases, lowering the mobility of the diffusing monomers and the diffusion driving force. The preferential diffusion of the TGMDA and DETDA precursors in phenoxy as compared to PES can be explained by its lower T_g inducing an improved mobility of the phenoxy macromolecules. The linear phenoxy and PES chains are characterized by close average molecular weights but the weight fraction of penetrating diamine or epoxide molecules required for transition of the thermoplastic-precursor blend from glassy to rubbery state is much lower for phenoxy than for PES due to their T_g difference. Consequently, mobility of the phenoxy chains in the resulting gel layer is considerably enhanced and promotes the precursor diffusion.

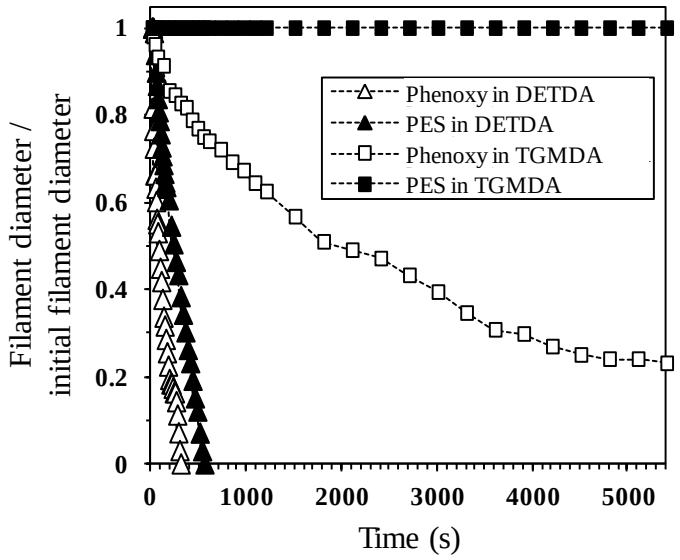

Fig. 8. Evolution of the diameter of PES and phenoxy filaments in TGMDA and DETDA precursors at 90 °C.

In addition to the molecular structure of the thermoplastic, the nature of the resin precursors also reveals an obvious influence on the interdiffusion

kinetics. The filament diameter decreases faster for TGAP than for TGMDA. The lower molecular volume of the triepoxide molecules compared to the tetraepoxide ones explains their faster diffusion into the thermoplastics. Similarly, the hot stage microscopy results demonstrate that the monoaromatic DETDA diamine exhibits a higher diffusion coefficient in the thermoplastics than the MDEA diaromatic diamine. These findings are illustrated in **Fig. 9** for a phenoxy filament of 100 µm diameter respectively in TGMDA, TGAP, MDEA and DETDA precursors at 90 °C. A linear relation between the evolution of the filament diameter and the square root of the isothermal contact time is evident during the initial stages of interdiffusion. The penetration distance of the different diffusing monomers into phenoxy being proportional to the square root of time is characteristic of an apparent Fickian diffusion in the infiltration layer.

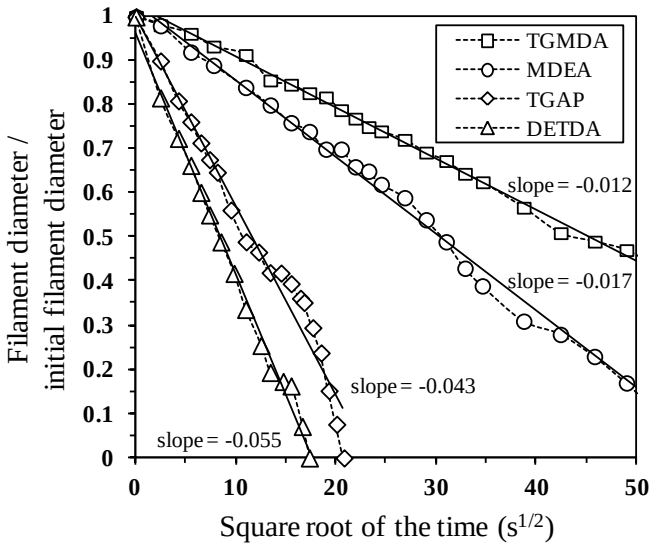

Fig. 9. Evolution of the diameter of a phenoxy filament in the different resin precursors as a function of the square root of the time at 90 °C.

The measurement of the filament diameter provides a straightforward assessment of the diffusion of the epoxide or diamine moieties toward the polymer but nevertheless does not give any indication on the apparent diffusion of the thermoplastic chains in the opposite direction. Therefore, in order to fully characterize the mutual diffusion between a thermoplastic filament and a resin precursor, MWNTs were exploited for the monitoring of

the apparent thermoplastic migration into each epoxy resin monomer via hot stage microscopy.

In this case, the MWNTs homogeneously dispersed in the nanocomposite filament (**Fig. 10.a**) play the role of tracers to follow the progress of the thermoplastic front into the different precursors. MWNTs were used on the one hand because the front of their apparent migration can be easily followed by optical microscopy techniques and, on the other hand because complementary investigations have revealed that MWNT and thermoplastic distributions are similar after interdiffusion and that MWNTs have no important effect on the apparent migration of the thermoplastic macromolecules [38].

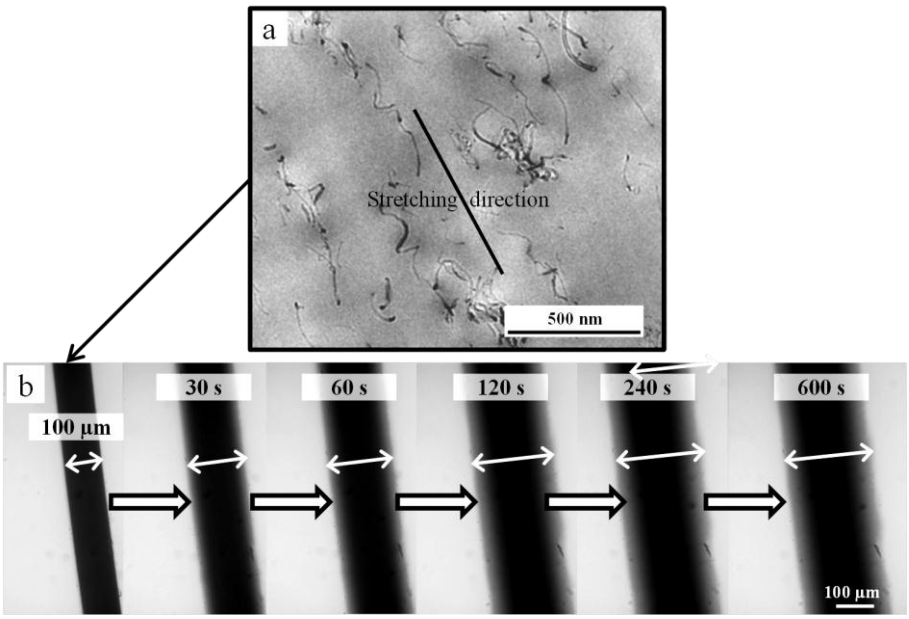

Fig. 10. (a) TEM micrograph of a phenoxy filament filled with MWNTs and (b) images from hot stage microscopy of a nanocomposite filament (phenoxy + 1 wt % MWNTs) in TGAP precursor at 90 °C.

Nanocomposite filaments filled with 0.1 wt % MWNTs allow following simultaneously the apparent migration of the carbon nanotubes and the diameter reduction of the filament during the initial stages of the interdiffusion process. However, for increasing durations of the isothermal contact, the local MWNT concentration becomes too low to detect a well-

defined front of the expanding dark zone containing the nanotubes. A MWNT concentration of 1 wt % in the nanocomposite filament is for that reason more appropriate to evaluate the thermoplastic movement. The limits of the black area containing MWNTs, which is delimited by the white arrow on the different images from hot stage microscopy (**Fig. 10.b**), indicate the extent of the apparent thermoplastic migration.

The distance between these MWNT fronts is reported as a function of the square root of the contact time at 90 °C in **Fig. 11** for a 100 µm diameter phenoxy-MWNT filament in the different epoxide and diamine precursors. The curves evidence a faster apparent migration of phenoxy in the lower molecular volume DETDA and TGAP monomers.

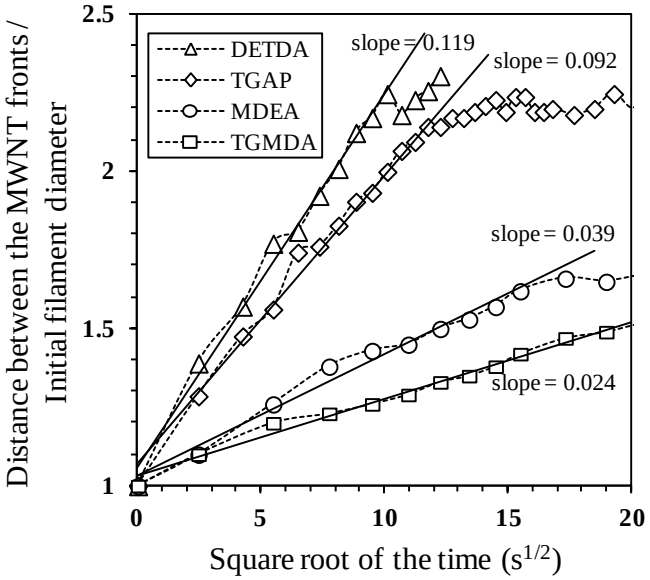

Fig. 11. Evolution of the distance between the fronts of the zone containing MWNTs for a nanocomposite filament based on phenoxy in the different resin precursors at 90 °C.

Moreover, **Fig. 12** shows an obvious correlation between the evolution of the filament diameter and the distance between the limits of the MWNT fronts during the early stages of interdiffusion by comparing the initial slopes of the curves reported in **Fig. 9** and **Fig. 11**. Actually, before precursor diffusion is hindered, the rate of apparent migration of the phenoxy macromolecules toward the epoxide or diamine precursor is proportional to infiltration of the precursors in the phenoxy filament. This observation

suggests that the thermoplastic movement is more controlled through swelling of the outer part of the filament by the diffusing monomers than by disentanglement and dissolution of the polymer chains. Diffusion kinetics being considerably lower for the large size thermoplastic macromolecules than for the precursors should be responsible for this behavior. Favored diffusion of the precursor molecules into the swollen thermoplastic as compared to their diffusion into the inner core of the filament can also be deduced since the experimental measurements have evidenced that apparent thermoplastic migration due to swelling is faster than infiltration of the resin precursors into the glassy filament.

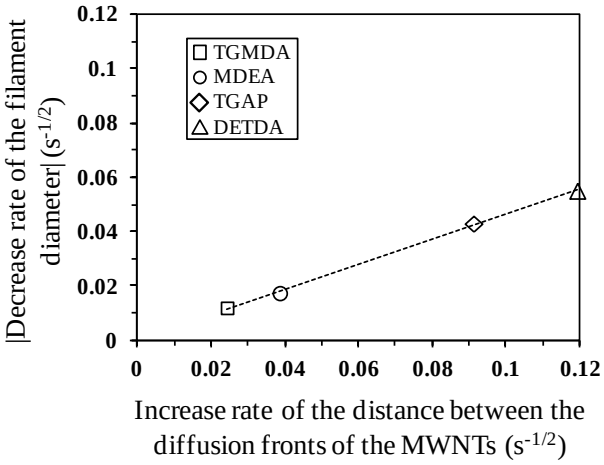

Fig. 12. Correlation between the initial variation rate of the diameter of a phenoxy filament (slope Fig. 9) and the distance between the MWNT fronts (slope Fig. 11) for a phenoxy-MWNT filament in the different resin precursors at 90 °C.

To summarize, the correlation between the respective locations of the diffusion fronts of the epoxy resin precursors and the thermoplastics leads to the conclusion that swelling of the thermoplastic by the epoxide or diamine precursor is the main mechanism explaining its spatial distribution after thermal treatment. A considerably faster diffusion of the low molecular weight precursors compared to the thermoplastic chains should be responsible for this observation while the role of disentanglement and diffusion of the macromolecules on the apparent thermoplastic migration should remain limited. Of course, larger swelling rates of the thermoplastics are observed for lower size precursors penetrating preferentially in the

thermoplastic and contributing to solubilization. The lower dissolution temperatures of the thermoplastics in TGAP and DETDA revealed by DSC is explained by the improved diffusion kinetics of these precursors in the thermoplastic powder. Similarly, the faster diffusion of epoxy resin precursors in phenoxy than in PES should be due to a higher mobility of the lower T_g phenoxy chains. This result supports the dissolution heat flows measured by DSC occurring at lower temperatures for phenoxy than for PES. Beyond the higher mobility of phenoxy chains due to lower T_g, preferential interactions between the phenoxy macromolecules and the resin precursors can potentially contribute to their better diffusion in phenoxy. In order to confirm these conclusions, numerical simulations were performed on the thermoplastic-precursor systems as detailed in the following section.

4. Molecular dynamics simulations

In the experimental section, it has been assumed that thermoplastic dissolution is driven by the epoxy resin precursor mobility. The goal of this section is now to provide an understanding of the mechanisms that control the behaviors of PES and phenoxy thermoplastics at a molecular level and more specifically to quantify the effects of the compatibility between the thermoplastics and the precursors on the mobility of the molecules. These systems were analyzed via the molecular dynamics technique which models, at the same time, the interactions between the atoms (force field), i.e. their compatibility and the effect of the temperature (velocity), i.e. their mobility. The main goal is to calculate the diffusion coefficients of both the thermoplastics and epoxy precursors to improve the understanding of the diffusion mechanisms. It must be emphasized that the resin crosslinking [41-43] was not considered in the model. Every simulation investigated the interaction between a thermoplastic and one precursor of the epoxy resin. The Materials Studio package (Amorphous Cell, Discover, and COMPASS modules) from Accelrys was used to run the simulations. The analyses were performed using the BTCL scripting language provided with this software.

4.1. Methodology

The method consists in generating successive configurations (frames) of a molecular system by applying Newton's second law of motion to each atom $\vec{F}_i^{\alpha} = m_i \vec{a}_i^{\alpha}$ where $\vec{F}_i^{\alpha}$ is the force on atom *i* in the direction α *(x, y, or z),*

m_i is the mass of atom *i*, and $\vec{a}_i^{\alpha}$ its acceleration along the α axis. The force $\vec{F}_i^{\alpha}$ derives from a force field $\vec{U}_i^{\alpha}$ which is here COMPASS (Condensed phase optimized molecular potentials of atomic simulation studies) [44]. The choice of the force field is a key parameter as it defines how the atoms interact with one another. The second generation COMPASS force field was selected because it has already been applied, with success, to model epoxy resin [42], PES [29,45], and a phenoxy monomer (bisphenol A glycerolate dimethacrylate) [40] whose formulation is close to the one used in the present study. For that reason, this force field seems adequate to model the systems described in the experimental section. The non-bonded van der Waals (Lennard-Jones model) and electrostatic (Coulombic model) interactions were calculated using respectively an atom-based method with a cutoff radius of 9.5 Å and a group based method with a cutoff radius of 11.5 Å. The velocities and positions of the atoms were calculated from successive integrations via a Verlet Velocity algorithm [47]. The time step for the integration was 1 fs. When needed, the Andersen thermostat [48] and Berendsen barostat [49] were used to control respectively the temperature and the pressure. The successive positions of the atoms were generated by the Discover module. To start the dynamics, initial positions of the atoms had to be prescribed. The atoms were put in a three dimensional box with periodic boundary conditions in the three directions to avoid side artifacts according to the Theodorou-Suter method [50] implemented in the Amorphous Cell module. It was followed by a short period of relaxation of the structure to relieve constraints involved in the construction step and find a state of minimum potential energy. Even if this model is rather simplistic, it contains all the basic ingredients to mimic a real system. Moreover, to make sure the dynamics were not biased by the initial configuration of the atoms and to enable calculations of averages and standard deviations, at least three different starting configurations were generated.

4.2. Validation: T_g calculations

To validate the method described above, T_g were calculated for the PES and phenoxy models and were compared to the experimental values presented in **Table 1**. It was first required to assess the minimum number of monomers needed to mimic a real polymer chain [42]. 3D cells composed of

thermoplastic oligomers (5 chains) with increasing length were then constructed and submitted to a series of dynamics (100 ps) in the NPT ensemble (constant number of atoms, pressure and temperature) at various temperatures. The density of each cell was calculated and considered as a parameter showing the consistency of the calculation. It was found that for a chain length of 5 phenoxy monomers and 6 PES monomers, the density leveled off. These numbers were therefore used as references for the modeling of the thermoplastics. A transition [46,51-52] in the behavior of the density boxes versus temperature can be distinguished in **Fig. 13**. This transition defining the thermoplastic T_g for the simulation occurs respectively at 90.8 °C and 206.9 ° for phenoxy and PES. These results are consistent with the T_g of the commercial grades (92 °C and 220 °C), and therefore validate the phenoxy and PES models to further investigate the mobility of these oligomers.

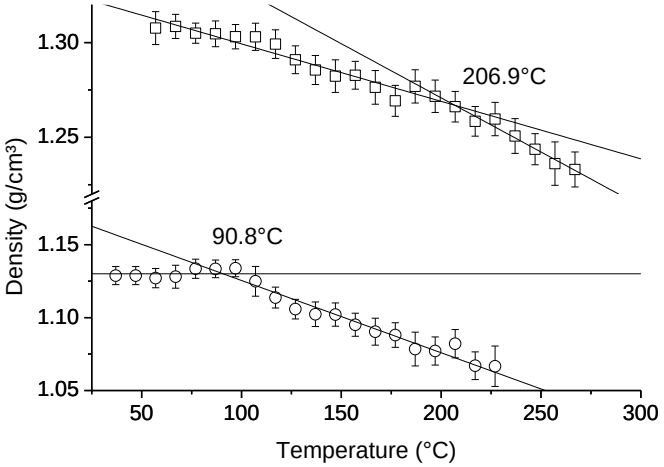

Fig. 13. Density of a 3D cell composed of either phenoxy (circle) and PES (square) oligomers, made respectively of 5 and 6 monomers, versus temperature.

4.3. Results: Diffusion coefficient calculations

To investigate the dynamic behavior of the thermoplastic oligomers in epoxy resin precursors, systems composed of a thermoplastic oligomer and one epoxide or diamine precursor were constructed. One initial structure was typically made of 25 wt % phenoxy or PES consisting in 5 oligomers

together with a resin precursor, i.e. from 50 TGMDA up to 119 DETDA molecules (**Fig. 14**). The choice of the thermoplastic oligomer concentration is a balance between the constraints that impose a large number of atoms to avoid size effects and the need to minimize the duration of the calculations, i.e. to restrict the size of the system. The cells were composed of 3494 atoms for the MDEA-PES system while they contained 4748 atoms for the DETDA-phenoxy system. The temperature was varied between 90 °C and 170 °C with an increment of 10 °C. A NPT dynamics (100 ps) was first run to determine the equilibrium density of the system for each temperature and was followed by a NVT (constant number of atoms, volume and temperature) dynamics (100 ps) during which the trajectories of the molecules were recorded and used to calculate their mean square displacement (MSD). The time required to investigate the dynamics of one type of molecule with a thermoplastic at a given temperature was equal to 3 hours (both NPT and NVT calculations) on an Intel QuadCore 3 Ghz computer running in parallel mode with 3 cores.

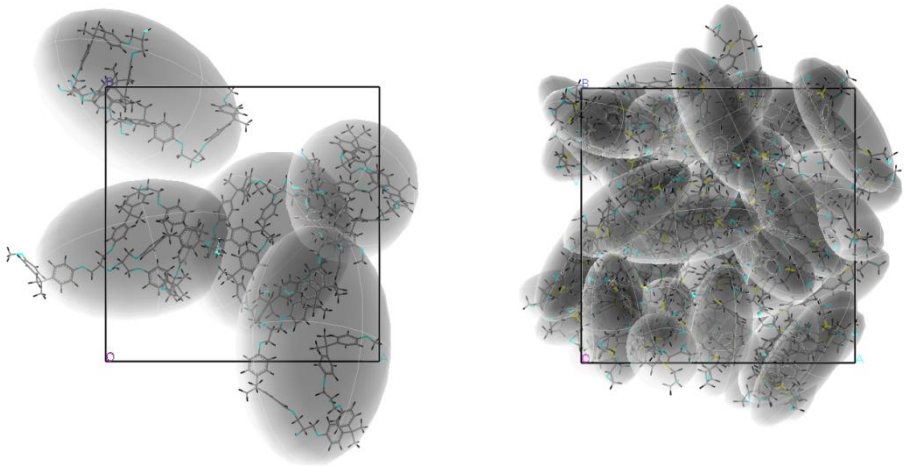

Fig. 14. Illustration of a 3D cell made of phenoxy oligomers (left side) and of TGMDA monomers (right side). The envelopes around each molecule represent the van der Waals volume occupied by a molecule.

The Einstein method was used to calculate the diffusion coefficient [53-54], *D*, defined as

$$D = \frac{1}{6N} \lim_{t \to \infty} \frac{d}{dt} \left\langle \sum_{i=1}^{N} \left[r_i(t) - r_i(0) \right]^2 \right\rangle$$

where $r_i(0)$ is the position of the molecule i at one starting time and $r_i(t)$ its position at a given time t, and N the number of atoms in the molecule. The relation inside the bracket represents the MSD. The brackets must be interpreted as averages over several starting times. The equation shows that D is proportional to the slope of the mean-square displacement at long times. Instead of calculating the diffusion coefficients for every atom of a molecule, the diffusion of the centre of mass of each molecule was measured. **Fig. 15** shows the typical behavior of the different precursors versus time. The linear regime is clearly established before the end of the dynamics so that the calculation of D is appropriate. The oligomer show the same trend with a linear regime reached after 50-60 ps depending on the precursor molecule in the cell. The coefficients of the molecules of the same type were then averaged.

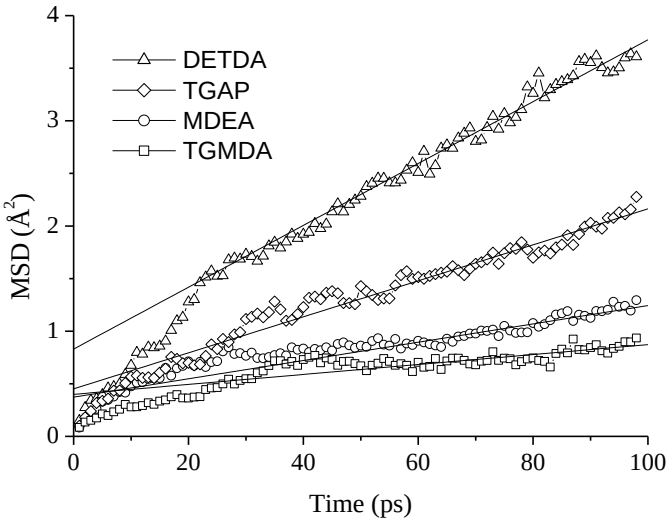

Fig. 15. MSD of the resin precursors in the phenoxy oligomers-precursor systems at 160°C and its best linear fit (full line).

As systems are composed of phenoxy or PES oligomers and precursor molecules, both the diffusions of the resin precursors (**Fig. 16**) and the phenoxy (**Fig. 17**) and PES oligomers surrounded by the precursor molecules can be calculated. For PES, the large size of the error bars does not allow to draw conclusions and to establish a comparison with phenoxy. A reason why the PES system does not provide fully usable results may be due to the fact that, in the temperature range studied, this thermoplastic is in the glassy state and therefore less sensitive to the diffusion process. For

phenoxy, it shows that the TGMDA and MDEA precursors have lower diffusivities than the TGAP and DETDA precursors. When the phenoxy oligomer diffusion is considered, a clear trend is evidenced for the diamine hardeners, showing a larger diffusion of this oligomer in DETDA than in MDEA despite larger error bars (averaging is made only over 5 chains). When the TGMDA and TGAP epoxide are considered, phenoxy oligomer shows a better diffusion in TGAP from 140 °C to 170 °C.

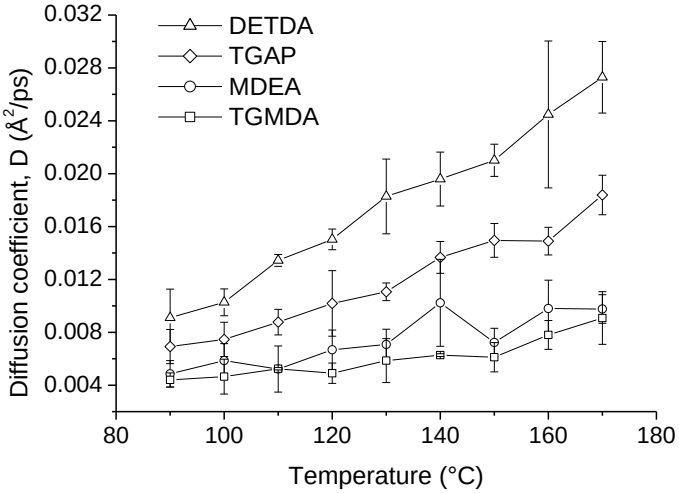

Fig. 16. Diffusion coefficients of the resin precursors in the different phenoxy oligomer-precursor systems.

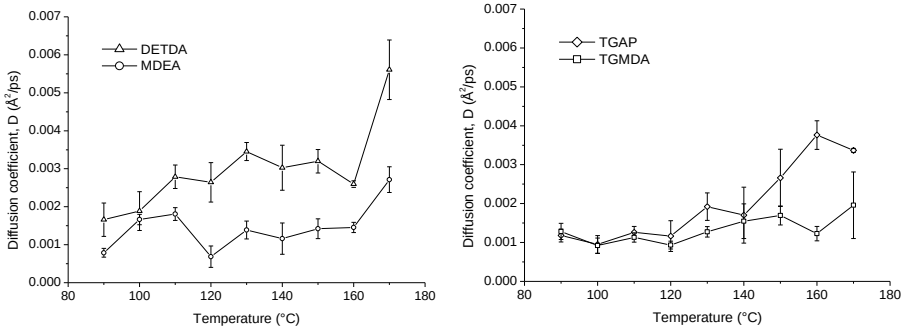

Fig. 17. Diffusion coefficients of the phenoxy oligomers in the different phenoxy-precursor systems.

When comparing these results, it is clear that diffusion of the low size resin monomers is favored compared to diffusion of the thermoplastic oligomers

and that very low diffusion coefficients are expected on basis of the Einstein method for high degrees of thermoplastic polymerization. It justifies the assumption that swelling of the thermoplastics driven by the diffusion of the epoxide or diamine precursors is dominant in comparison with the diffusion of the thermoplastic chains. **Fig. 18** evidences, at the same time, the quicker diffusion of the resin precursors compared to the phenoxy oligomers and the linear correlation existing between the diffusion coefficients calculated for the precursor molecules and the phenoxy oligomer. It also illustrates the improvement of the precursor diffusion in the phenoxy oligomers for the epoxide and diamine monomers with the lowest molecular volume. These results are in good agreement with the trend shown in **Fig. 12** and therefore confirms that the mobility of the diffusing precursors is the key parameter controlling thermoplastic solubilization.

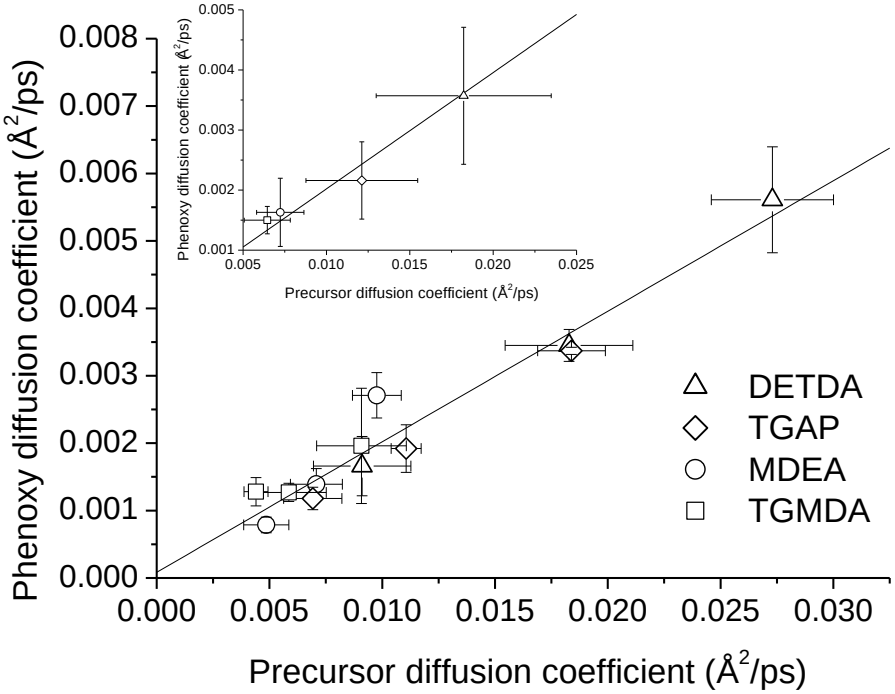

Fig. 18. Correlation between the diffusion coefficients of the precursors and phenoxy in the different phenoxy-precursor systems for temperatures of 90, 130 and 170 °C. Insert: Average values over the temperatures.

Moreover, the diffusion coefficients are proportional to the initial slopes of the curves measuring evolution of the phenoxy filament diameter due to precursors diffusion as a function of the square root of the time (**Fig. 9**).

Considering a one-dimensional fickian diffusion, the diffusion distances ($x = \sqrt{2Dt}$) of the precursors in phenoxy predicted on basis of the diffusion coefficients assessed by molecular dynamics at 90 °C are also in the same order of magnitude than diffusion distances observed experimentally with thermoplastic filaments. Indeed, a DETDA precursor reach the filament center (x = 50 µm) after approximately 300 s at 90 °C while the predicted distance of diffusion after 300 s is about 20 µm.

5. Conclusions

This chapter investigates interdiffusion at the interface between epoxide or diamine precursors and PES or phenoxy polymers. The higher mobility of the lower weight resin precursors as well as the higher mobility of phenoxy macromolecules as compared to higher T_g PES chains improve dissolution thanks to a favored penetration of the precursor into the thermoplastic. Therefore, TGAP triepoxide and DETDA monoaromatic diamine are promising resin precursors to dissolve the poorly soluble PES at lower temperatures than in TGMDA and MDEA precursors composing partially the RTM6 resin like shown by DSC measurements.

It has been demonstrated that swelling of thermoplastics is a function of the precursor diffusion with thermoplastics containing small amounts of carbon nanotubes used as tracers. Moreover, the limited diffusion of polymer macromolecules compared to the dominant effect of the precursor diffusion has been confirmed using simulation by molecular dynamics. Indeed, low values of the diffusion coefficients have been determined for thermoplastic oligomers compared to the resin monomers. For the latter, the calculated values correlate well with the experimental data measured during interdiffusion.

Although the simulation approach needs to be adapted to increase the level of accuracy for high T_g PES and to determine the influence of thermoplastic type on interdiffusion, the molecular dynamics technique presents a real interest to evaluate the diffusion of other potential resin precursors and to orient the choice of new epoxy resin formulations promoting thermoplastic dissolution. Moreover, the modeling of resin cure is another possible development that should help to understand solubilization mechanisms in reactive resins and to determine combinations of thermoplastic and epoxy

resin formulation adapted for in situ dissolution during the cure cycle applied in RTM process. In that case, the resin crosslinking should considerably influence interdiffusion since the formation of oligomers greatly reduces the system mobility. Moreover, because of their different diffusion coefficients, segregation between the epoxide and diamine precursors should occur, leading to stoichiometric imbalances in the resin composition and modification of the thermosetting network properties [21-23]. Effect of the crosslinking reaction on interdiffusion between a thermoplastic and a reactive resin and the induced composition gradients are therefore experimentally investigated in the next chapter.

References

[1] Min HS, Kim SC. Fracture toughness of polysulfone/epoxy semi-IPN with morphology spectrum. Polymer Bulletin 1999;42(2):221-27.
[2] Martinez I, Martin MD, Eceiza A, Oyanguren P, Mondragon I. Phase separation in polysulfone-modified epoxy mixtures. Relationships between curing conditions, morphology and ultimate behavior. Polymer 2000;41(3):1027-35.
[3] Bucknall CB, Partridge, IK. Phase separation in epoxy resins containing polyethersulphone. Polymer 1983;24(5):639-44.
[4] Raghava RS. Development and characterization of thermosetting-thermoplastic polymer blends for applications in damage-tolerant composites. Journal of Polymer Science: Polym. Phys. Ed. 1988;26(1):65-81.
[5] Mimura K, Ito H, Fujioka H. Improvement of thermal and mechanical properties by control of morphologies in PES-modified epoxy resins. Polymer 2000;41(12):4451-59.
[6] Cho JB, Hwang JW, Cho K, An JH, Park CE. Effects of morphology on toughening of tetrafunctional epoxy resins with poly(ether imide). Polymer 1993;34(23):4832-36.
[7] Hourston DJ, Lane JM, Zhang HX. Toughening of Epoxy Resins with Thermoplastics: 3. An Investigation into the Effects of Composition on the Properties of Epoxy Resin Blends. Polymer International 1997;42(4):349-355.
[8] Park JM, Kim DS, Kong JW, Kim SJ, Jang JH, Kim M, Kim W, Devries KL. Interfacial evaluation and self-sensing on residual stress and microfailure of toughened carbon fiber/epoxy-amine terminated (AT)-polyetherimide (PEI) composites. Composites Part B: Engineering 2007;38(7-8):833-46.
[9] Teng KC, Chang FC. Single-phase and multiple-phase thermoplastic/thermosetting polyblends: 2. Morphologies and mechanical properties of phenoxy/epoxy blends. Polymer 1996;37(12):2385-94.

[10] Siddhamali SK, Kyu T. Toughening of thermosetting/thermoplastic composites via reaction-induced phase separation: Epoxy/phenoxy blends. Journal of Applied Polymer Science 2000;77(6):1257-68.
[11] Yun NG, Won YG, Kim SC. Toughening of carbon fiber/epoxy composite by inserting polysulfone film to form morphology spectrum. Polymer 2004;45(20):6953-8.
[12] Thanomsilp C, Hogg PJ. Interlaminar fracture toughness of hybrid composites based on commingled filament fabrics. Composites Science and Technology 2005;65(10):1547-63.
[13] LoFaro C, Abusafieh A, Webb WE and Doyle M, Resin-soluble thermoplastic veil for composite materials. US Patent 0252334 (2006).
[14] Naffakh M, Dumon M, Gérard JF. Study of a reactive epoxy-amine resin enabling in situ dissolution of thermoplastic films during resin transfer molding for toughening composites. Composites Science and Technology 2006;66(10):1376-84.
[15] Mortimer S and Cawse JL, A thermoplastic toughening material and related method. WO Patent 110617 (2007).
[16] Beier U, Wolff-Fabris F, Fischer F, Sandler JKW, Altstädt V, Hulder G, Schmachtenberg E, Spanner H, Weimer C, Roser T, Buchs W. Mechanical performance of carbon fibre-reinforced composites based on preforms stitched with innovative low-melting temperature and matrix soluble thermoplastic filaments. Composites Part A: Applied Sc. and Manufact. 2008; 39(9):1572-81.
[17] Beier U, Sandler JKW, Altstädt V, Spanner H, Weimer C. Mechanical performance of carbon fiber-reinforced composites based on stitched and bindered preforms. Composites: Part A 2009;40(11):1756-63.
[18] Wong DWY, Lin L, McGrail PT, Peijs T, Hogg PJ. Improved fracture toughness of carbon fiber/epoxy composite laminates using dissolvable thermoplastic fibers. Composites Part A: Applied Science and Manufacturing 2010;41:759-67.
[19] Lestriez B, Chapel JP, Gérard JF. Gradient interphase between reactive epoxy and glassy thermoplastic from dissolution process, reaction kinetics, and phase separation thermodynamics. Macromolecules 2001;34(5):1204-13.
[20] Bonnaud L, Bonnet A, Pascault JP, Sautereau H, Riccardi CC. Different parameters controlling the initial solubility of two thermoplastics in epoxy reactive solvents. Journal of Applied Polymer Science 2002;83(6):1385-96.
[21] Oyama HT, Lesko JJ, Wightman JP. Interdiffusion at the interface between poly(vinylpyrrolidone) and epoxy. Journal of Polymer Science: Part B: Polymer Physics 1997;35(2):331-46.
[22] Rajagopalan G, Gillespie Jr. JW., McKnight SH. Diffusion of reacting epoxy and amine monomers in polysulfone: a diffusivity model. Polymer 2000;41(21):7723-33.

[23] Immordino KM, McKnight SH, Gillespie Jr. JW. In-situ evaluation of the diffusion of epoxy and amine in thermoplastic polymers. The Journal of Adhesion 1998;65(1):115-29.
[24] Munz M, Strum H, Stark W. Mechanical gradient interphase by interdiffusion and antiplasticisation effect--study of an epoxy/thermoplastic system. Polymer 2005;46(21):9097-112.
[25] Jawalkar SS, Adoor SG, Sairam M, Nadagouda MN and Aminabhavi TM. Molecular modeling on the binary blend compatibility of poly(vinyl alcohol) and poly(methyl methacrylate): An atomistic simulation and thermodynamic approach. Journal of Physical Chemistry B 2005;109(32):15611-20.
[26] Zhang M, Choi P, Sundararaj U. Molecular dynamics and thermal analysis study of anomalous thermodynamic behavior of poly (ether imide)/polycarbonate blends. Polymer 2003;44(6):1979-86.
[27] Eichinger BE, Rigby D, Stein J. Cohesive properties of Ultem and related molecules from simulations. Polymer 2003;43(2):599-607.
[28] Choi P. Molecular dynamics studies of the thermodynamics of HDPE/butene-based LLDPE blends. Polymer 2000;41(24):8741-7.
[29] Prathab B, Subramanian V, Aminabhavi TM. Molecular dynamics simulations to investigate polymer–polymer and polymer–metal oxide interactions. Polymer 2007;48(1): 409-16.
[30] Madkour T. A combined statistical mechanics and molecular dynamics approach for the evaluation of the miscibility of polymers in good, poor and non-solvents. Chemical Physics 2001;274(2-3):187-98.
[31] Kiuna N, Lawrence CJ, Fontana QPV, Lee PD, Selerland T, Spelt PDM. A model for resin viscosity during cure in the resin transfer moulding process. Composites Part A: Applied Science and Manufacturing 2002;33(11):1497-503.
[32] Araldite® MY 721 datasheet (Huntsman).
[33] Araldite® MY 0510 datasheet (Huntsman).
[34] Lonzacure® DETDA 80 datasheet (Lonza).
[35] Lonzacure® M-DEA kr datasheet (Lonza).
[36] http://www.phenoxy.com/products/pkhp-200.html.
[37] Radel A datasheet (Solvay Advanced Polymers).
[38] Dumont D, Daoust D, Sclavons M and Devaux J. Thermoplastic yarns filled with carbon nanotubes for reinforcement of composite matrices based on epoxy resin. Proceedings of the 14th European Conference on Composite Materials (ECCM14), Budapest (2010).
[39] Mohan R, Lorenz H, Myerson AS. Solubility measurement using differential scanning calorimetry. Industrial and Engineering Chemistry Research 2002;41(19):4854-62.
[40] Ueberreiter K, The Solution Process, in Diffusion in Polymers, ed by Crank J and Park GS. Academic Press, New York, pp 219-257 (1968).
[41] Yarovsky I, Evans E. Computer simulation of structure and properties of crosslinked polymers: application to epoxy resins. Polymer 2002;43(3):963-9.

[42] Wu C and Xu W. Atomistic molecular modeling of crosslinked epoxy resin. Polymer 2006;47(16):6004-9.
[43] Wunderle B, Dermitzaki E, Hölck O, Bauer J, Walter H, Shaik Q, Rätzke K, Faupel F, Michel B, Reichl H. Molecular dynamics approach to structure–property correlation in epoxy resins for thermo-mechanical lifetime modeling. Microelectronics Reliability 2010;50(7):900-9.
[44] Sun H. COMPASS: An ab Initio Force-Field Optimized for Condensed-Phase Applications ─ Overview with Details on Alkane and Benzene Compounds. Journal of Physical Chemistry B 1998;102(38):7338-64.
[45] Wu H, Zhang X, Xu D, Li B, Jiang Z. Enhancing the interfacial stability and solvent-resistant property of PDMS/PES composite membrane by introducing a bifunctional aminosilane. Journal of Membrane Science 2009;337(1-2):61-9.
[46] Song X, Sun Y, Wu X, Zeng F, Molecular dynamics simulation of a novel kind of polymer composite incorporated with polyhedral oligomeric silsesquioxane (POSS). Computational Materials Science 2011;50(12):3282-9.
[47] Verlet L. Computer "experiments" on classical fluids. I. Thermodynamical properties of Lennard-Jones molecules. Physical Review 1967;159:98-103.
[48] Andersen H. Molecular dynamics simulations at constant pressure and/or temperature. Journal of Chemical Physics 1980;72:2384-93.
[49] Berendsen HJC, Postma JPM, Van Gunsteren F, DiNola A, Haak JR. Molecular dynamics with coupling to an external bath. Journal of Chemical Physics 1984;81:3684-90.
[50] Theodorou DN and Suter UW. Detailed molecular structure of a vinyl polymer glass. Macromolecules 1985;18(7):1467-78.
[51] Fan HB and Yuen MMF. Material properties of the cross-linked epoxy resin compound predicted by molecular dynamics simulation. Polymer 2007;48(7):2174-8.
[52] Soldera A, Metatla A. Glass transition of polymers: Atomistic simulation versus experiments. Physical Review E 2006;74(6):061803-1-6.
[53] Allen MP and Tildesley DJ, Computer Simulation of liquids, Oxford University Press, New-York (1991).
[54] Rapaport DC, The art of molecular dynamics simulation, Cambridge University Press, Cambridge (1995).

Chapter 3

SWELLING OF PHENOXY AND POLY(ETHER SULFONE) IN EPOXY RESIN: RESULTING COMPOSITION AND MICROSTRUCTURE GRADIENTS

Abstract

Due to limited resin viscosities imposed by liquid composite molding, toughening of composite matrices by simultaneous injection of high molecular weight thermoplastic with epoxy resin cannot be considered. Therefore, in order to incorporate a ductile polymer phase in complex thermoset composites processed by Resin Transfer Molding (RTM), in situ dissolution of the thermoplastic introduced in the composite preform is required.

The aim of the chapter is to demonstrate that solubility of poly(ether sulfone) (PES) and phenoxy amorphous thermoplastics in epoxide-diamine formulations is exploitable to reinforce thermoset composite matrices while preserving processability. The first step of this work consists in evaluating evolution of PES and phenoxy filaments into HexFlow® RTM6 resin and other resin formulations containing epoxide and diamine precursors having

demonstrated in the previous chapter their ability to improve thermoplastic solubility like triglycidyl p-aminophenol (TGAP) and diethyltoluenediamine (DETDA). In a second step, thermoplastic distributions generated by further interdiffusion between resin precursors and thermoplastic macromolecules are assessed by means of Raman spectroscopy considering the same model systems with a single filament in contact with a reactive resin. The local thermoplastic content is related to microstructures resulting from reaction induced phase separation. Finally, a composite panel with a preform interleaved with a thermoplastic film is investigated.

The lower glass transition temperature (T_g) phenoxy shows a preferential dissolution in the different epoxy resins compared to PES. Moreover, selection of resin formulations and thermal conditions favoring interdiffusion by a good compromise between diffusion and crosslinking kinetics appears as essential considerations to improve thermoplastic distribution into the resin. Residual composition gradients leading to local variation of the blend microstructure are evidenced after curing with both thermoplastics. Nevertheless, while phase inversion can easily be avoided for appropriate phenoxy amounts and adapted temperature profiles, larger composition inhomogeneities subsist for PES introduction in epoxy resin and induce a broad range of microstructures with even pure PES remaining in some cases. Transposition to processing of composites by liquid composite molding using soluble thermoplastic films is validated.

1. Introduction

Toughening of prepregs using an epoxy resin-thermoplastic blend [1-4] or by interleaving thermoplastic particles being soluble [5-6] or insoluble [7] in the uncured resin has demonstrated potential benefits in terms of interlaminar toughness improvement of composites. However, transposition of these toughening methods to a liquid composite molding process like Resin Transfer Molding (RTM) or Liquid Resin Infusion (LRI) is difficult. Indeed, these out-of-autoclave technologies, which are emerging cost effective alternatives to prepreg in order to manufacture composite parts in an automated and versatile way, require injectable resins with low viscosity to ensure infiltration throughout the fabric and preform impregnation, which are essential for a final structure free of voids. Therefore, only small amounts of high molecular weight thermoplastic toughеners can be dissolved into the resin prior to infusion without sacrificing the flowability due to an important viscosity increase of the blend as compared to the neat resin. Moreover, if solid thermoplastic particles dispersed in the epoxy resin are considered, thermoplastic filtration forming agglomerates at undesirable locations during infusion becomes a critical issue.

In order to maintain a low resin viscosity during injection, reinforcement of composite materials can be achieved by the introduction of solid thermoplastic additives into the preform without changing processing conditions. Some studies have highlighted enhanced performance in mode I crack opening, the dominant failure mode in compression after impact (CAI), by means of thermoplastic yarns that either melt or soften in the epoxy matrix formulation during the liquid molding process. Insoluble thermoplastic in the fibrous form, commingled with the structural fibers of the laminate [8-9] or stitched onto the preform [10-11], inhibits crack propagation in these fiber hybrid composites during CAI testing. Fiber bridging with fiber pullout and extensive plastic deformation of the individual thermoplastic fibers contribute to the toughening mechanism. Similar improvements have been observed when thermoplastic veils [9,11] or films [12] are interposed as interleaf layers in the laminate.

However, such thermoplastic reinforcements, insoluble in the epoxy matrix, have minor effect on the initial formation of delamination during impact dominated by mode II shear cracking. The interfaces created by thermoplastic yarns or interleaving binder can also reduce hot-wet

mechanical properties and resistance to fluids of the composite. For these reasons, amorphous thermoplastics being adapted for dissolution in the epoxy resin formulation during the liquid molding process have been selected in many cases as toughening agents of the curable resin in the form of yarns commingled with the structural fibers of the laminate or stitched onto the preform [8,10-11,13] or chopped fibers [14], films [15-17], membranes [18] and non woven mats [9,11,19] interposed as interleaf layers in the laminate. In addition to the potential stabilization of the dry preform improving its handling, the blend microstructure generated by phase separation can provide a localized toughening of the matrix hybrid composite by improving mode I fracture toughness and by delaying the initial formation of delamination during impact dominated by mode II shear cracking. Moreover, dissolution of the thermoplastic incorporated into the composite preform prevents macroscopic interfaces and reduces kinking and misalignment of structural fibers compared to insoluble thermoplastic elements. Fiber break is therefore hampered such as the formation of brittle resin-rich regions that affect in-plane properties of the composite.

Initially, the thermoplastic modifier is intended to remain insoluble during resin infusion to prevent thermoplastic flushing by the resin flow and to avoid consecutive viscosity increase and reduction of the preform wettability. After complete mold filling by the injectable resin and as a result of the temperature increase applied to the system, the thermoplastic becomes subsequently miscible and is distributed in the epoxy resin prior to substantial onset of curing and gelation. From a mechanistic point of view, thermal dissolution occurs through swelling of the amorphous thermoplastic by the diffusing resin monomers and dissolution of the disentangled polymer chains into the epoxide-diamine reactive solution. The thickness of the gel layer with swollen thermoplastic results from the balance between penetration velocity of the resin precursors and dissolution rate induced during mutual diffusion at the glassy thermoplastic-resin precursor interface. It has been suggested that compatibility with the thermoplastic is not the main factor influencing the respective locations of the diffusion fronts of the epoxide and diamine monomers but that molecular dynamics driven by the increased mobility of the smaller molecules had a stronger effect on interdiffusion [20-21]. Finally, phase separation induced by the curing reaction generates a morphology gradient with a microstructure distribution being function of the local blend composition resulting from the interdiffusion between the thermoplastic and the resin precursors.

Interdiffusion coupled with dissolution and miscibility of poly(phenylene ether) (PPE) and poly(ether imide) (PEI) with epoxy resins has been studied by observing the structure of the interfaces/interphases between these high T_g thermoplastics and the epoxide-diamine networks at different conversions [21]. A morphology spectrum with a gradual change of the microstructure feature has been evidenced. Local stoichiometry imbalances in the resin composition due to differences between diffusivities of the epoxide and the diamine hardener during interdiffusion have also been demonstrated [22-24]. This interface induced-segregation, which results in epoxide-diamine concentration gradients, has shown influence on spatial variation of the morphology and related properties of the cured system [25]. The microstructure gradient has also been studied in the case of a polysulfone (PSf) film modified epoxy resin [26] and a PSf film modified epoxy composite [16]. For the same global PSf concentration, a higher improvement of the fracture toughness has been measured for the epoxy resin with morphology spectrum than for the resin with a uniform PSf distribution. This higher capacity for absorbing fracture energy has been attributed to plastic deformation of the continuous PSf rich phase induced by high PSf concentrations generated locally by the films. Although phase inverted morphology improves the fracture toughness more efficiently, it can result in a local decrease of other properties as the high crosslinked epoxy resin is no more the continuous phase everywhere in the blend. Therefore, lower thermoplastic concentrations assuring sea-island or cocontinuous morphologies for all the material can be preferred even if to the detriment of the toughness increase.

As the matrix morphology and consequently the overall properties of a composite depend on both thermoplastic global content in the epoxy resin matrix and local blend composition, thermal dissolution and interdiffusion between the polymer macromolecules and the epoxy resin precursors are primordial considerations to use periodic thermoplastic structures as effective means to reinforce composites. The work reported here specially examines the possibility to dissolve a high T_g amorphous thermoplastic, i.e. poly(ether sulfone) (PES) and a lower T_g thermoplastic poly(hydroxyether of bisphenol A) (phenoxy) in several epoxy resins during time windows limited by the crosslinking reaction. Effect of the resin formulation is explored by comparing RTM6 resin qualified for aeronautic applications to epoxy resins composed of a triepoxide and a liquid monoaromatic diamine. These reactive resins are investigated due to their modulus at least equivalent to the one of

the RTM6 resin and their lower viscosities reported in Chapter 1 such as for their precursors diffusing preferentially into thermoplastics [20] like shown in Chapter 2. The thermoplastic distributions and the residual microstructures inhomogeneities of the thermoplastic-resin blends induced by filaments swelling are investigated in order to determine systems adapted for a transposition to liquid composite molding.

First, epoxy resin-thermoplastic combinations favoring dissolution are discussed on basis of the diameter evolution of single thermoplastic filaments during thermal treatment in the various reactive resin formulations. Then, PES and phenoxy distributions resulting from the filament introduction in the different resins are reported. Concentration profiles of the cured samples determined using Raman spectroscopy reflect the extent of interdiffusion between the resin precursors and the thermoplastic chains before resin crosslinking. The composition gradients evidenced in this way are related to the resulting blend morphology. Finally, the subsisting microstructure gradient is illustrated for a composite panel with a thermoplastic film interleaved in the preform processed by LRI.

2. Experimental

2.1. Materials

2.1.1. Neat resins

HexFlow® RTM6 resin from Hexcel, which is qualified for aeronautic applications, was compared to other epoxy resin formulations prepared by stirring stoichiometric amounts of epoxide monomers and diamine hardener (two oxirane rings for one amine group reacting two times) at ambient until homogeneous mixtures were obtained. These resins are on the one hand, a formulation similarly composed of tetraglycidyl-4,4'-methylenedianiline (TGMDA, Araldite® MY 721 from Huntsman) but crosslinked with a liquid hardener, diethyltoluenediamine (DETDA, Lonzacure® DETDA 80 from Lonza) and on the other hand, a formulation based on a lower viscosity triepoxide, triglycidyl para-aminophenol (TGAP, Araldite® MY 0510 from Huntsman) and the same monoaromatic DETDA diamine.

2.1.2. Thermoplastic filaments and films

The phenoxy (InChemRez® Phenoxy Resin PKHB from InChem Corporation, T_g = 84 °C) and PES (Radel® A-200 NT from Solvay Advanced Polymers, T_g = 220 °C) thermoplastics previously dried during 24 hours at 80 °C under vacuum were respectively melt-processed at 220 °C and 340 °C in a DSM Xplore 15 ml micro-compounder. The residence time in the mixing chamber equipped with a side channel, which allows continuous recycling of the polymer, was set to 5 minutes and the rotation speed of the co-rotating twin screws was 150 rpm. Subsequently, filaments were drawn by winding and stretching the softened thermoplastic exiting a circular die (0.5 mm diameter) using a DSM Xplore Fiber Spin Line. Films were processed with a slit die (0.5 mm thickness) and the DSM Xplore Micro Film Device. Polymer flow, spinning speed and torques were adjusted to control the filament and film dimensions.

2.1.3. Resin-thermoplastic blends

Blends of RTM6 resin with 10, 15 and 20 wt% PES were prepared by dissolution at room temperature in dichloromethane solvent (unstabilized grade for HPLC from BioSolve BV). Dissolution and homogenization of 10 wt % phenoxy in the RTM6 resin were achieved without use of solvent during 10 minutes at 100 °C to limit resin crosslinking. For the TGAP-DETDA and TGMDA-DETDA resins, thermoplastic (up to 30 wt % phenoxy or PES) was first dissolved in the epoxide monomer at 140 °C before mixing with the DETDA curing agent at 80 °C. For morphology observations of the phase separated blends, samples were subsequently cured during 120 minutes at 140 °C.

2.1.4. LRI panel

The production of a RTM6 resin matrix composite panel (A4 size) reinforced with glass fiber fabrics (approximately 60 wt %) interleaved with a PES film was performed by LRI. The composite preform was made of 32 plies of 4H satin E glass fabric HexForce® 00120 M from Hexcel (0.08 mm thick, 105 g/m^2) and a PES film (average thickness of 35 µm) disposed in the central interlayer. A transverse infusion process was used to saturate the panel with RTM6 resin degassed for 60 minutes at 80 °C. Curing was completed under a 1°C/min temperature ramp from 80 to 180 °C with an

intermediate isotherm of 30 minutes at 120 °C and was followed by post-cure for 4 hours at 180 °C.

2.2. Characterization techniques

2.2.1. Hot stage microscopy

An Olympus BX51 optical microscope equipped with a ColorviewI camera was used to observe the dissolution of phenoxy and PES filaments in the epoxy resins during isotherms between 80 °C and 140 °C. Hot stage microscopy was performed by placing a 100 µm diameter fiber (diameter between 95 and 105 µm) of approximately 1 cm length in 50 mg epoxy resin between two microscope glass slides fitted into a Mettler FP82HT hot stage monitored by a Mettler FP90 central processor connected to the microscope.

2.2.2. Raman spectroscopy

After dissolution of the thermoplastic filament and further interdiffusion between thermoplastic chains and precursors of the epoxide-diamine formulation, Raman spectra of the phase separated samples were acquired with a spectrometer DXR SmartRaman from Thermo Scientific operating in the microscopic mode with a 2048 pixel charge-coupled device (CDD) detector. The laser, with an incident excitation wavelength of 780 nm, was focused between the two microscope glass slides, in the plane of the initial location of the filament center with the maximal intensity of the thermoplastic signal. Spectra were acquired perpendicularly to the filament direction every 10 µm on a distance of 2 mm in order to monitor the evolution of the local PES and phenoxy concentrations. Recorded spectra were the average of 5 spectra accumulated for 60 s. The spectral resolution was of about 3 cm^{-1}. The pinhole aperture was set to 50 µm and a 50 times magnification objective was used, resulting in the analysis of a spot diameter of 1,27 µm. A calibration for prediction of the phenoxy concentration in the TGMDA-DETDA resin was also performed by acquisition of spectrum in crosslinking blends containing up to 50 wt % phenoxy using a 50 µm slit aperture and a 10 times magnification objective.

2.2.3. Scanning electron microscopy (SEM)

SEM analyses were performed on cryofractured surfaces of the cured epoxy resin-thermoplastic blends using a LEO 982 (Zeiss) operating at 1 kV after

etching of the thermoplastic phase to reveal the blend microstructure. Tetrahydrofuran (THF) and dichloromethane solvents (unstabilized grades for HPLC from BioSolve BV) were used during 24 hours respectively for phenoxy and PES etching. The etched cross sections of the LRI panel were likewise examined. The morphology gradient generated at the interface between a PES filament and the TGMDA-DETDA resin by an isothermal curing at 120 °C was observed with a VEGA TS 5130 from Tescan operating at 10 kV on a surface dressed in the radial direction.

3. Results and discussion

3.1. Thermoplastic filament dissolution into epoxy resin

The need to exploit in situ dissolution of PES and phenoxy in order to conserve injectable resins for liquid composite molding process has been demonstrated in Chapter 1. Several requirements are associated to this toughening concept preventing difficulties related to injection of high viscosity polymers by disposing initially the thermoplastic modifier in the composite preform. On the one hand, the thermoplastic must remain insoluble in the epoxy resin during its injection to avoid thermoplastic flushing by the resin flow. On the other hand, rapid thermoplastic dissolution in the epoxy resin must be achieved once the mold is completely filled and the preform is impregnated by the low viscosity resin. A compromise between the diffusion kinetics of the resin precursors into the thermoplastic and the cure reaction kinetics must be found by applying an adapted temperature profile. Indeed, crosslinking hampers diffusion due to mobility of the thermoplastic chains drastically reduced and to diffusion coefficients of larger oligomers in the glassy polymers being orders of magnitude lower than those of the resin monomers that lead to thermoplastics swollen by monomers only. Diffusivity models [27-28] describe theoretically this competition between the mutual diffusion process and the crosslinking reaction. In addition to the epoxy network formation that reduces mobility of the diffusing molecules after the initial interdiffusion regime, the dissolution process becomes also inhibited by reduction of the concentration gradient at the resin-thermoplastic interface as the resin precursors and thermoplastic macromolecules diffuse and therefore, alter the conditions for further interdiffusion.

Therefore, an experimental system based on a single thermoplastic filament placed in an epoxy resin droplet was proposed to determine systems and conditions favoring in situ dissolution of PES and phenoxy used as tougheners of composite matrices. The evolution of a filament during dissolution at 120°C is illustrated in **Fig. 1** for a 100 µm diameter PES filament in TGAP-DETDA resin followed by hot stage microscopy. Interdiffusion leading to swelling of the glassy thermoplastic by the resin precursors is responsible for the reduction of the distance between the visible interfaces delimiting the filament and consequently for the apparent dissolution of the filament discussed here. Nevertheless, this apparent filament dissolution is not only due to transition of thermoplastic from the glassy state to macromolecules in solution but also to formation of gel phase containing polymer swollen by the resin precursors. The image sequence shows that the diameter decreases quite regularly all along the fiber and that the filament is completely dissolved in these conditions well before the gel time of the resin of 75 minutes assessed in Chapter 1 by rheometry. Later, as the heating continues and the curing reaction proceeds, phase separation is initiated and becomes progressively detectable as differences between the refractive indexes of the blend phases produce interfaces observable by this technique.

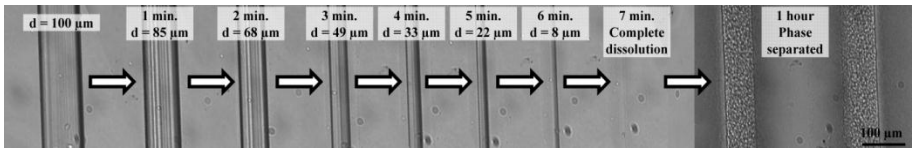

Fig. 1. Images from hot stage microscopy of a 100 µm diameter PES filament in TGAP-DETDA resin at 120 °C.

3.1.1. Influence of epoxy-resin-thermoplastic combination on dissolution

The progress of the apparent dissolution of 100 µm diameter PES and phenoxy filaments in the TGAP-DETDA, TGMDA-DETDA and RTM6 resins during an isothermal treatment at 100 °C is reported in **Fig. 2**. This temperature is a good compromise to compare evolutions of the filament diameters because thermoplastic swelling leading to apparent filament dissolution is total, partial or not initiated depending on the resin formulation and the thermoplastic nature before being significantly hindered by crosslinking. Indeed, gel times evaluated in Chapter 1 are around three hours

and four hours respectively for the TGAP-DETDA and TGMDA-DETDA resins at 100 °C and more than 10 hours for the RTM6 resin.

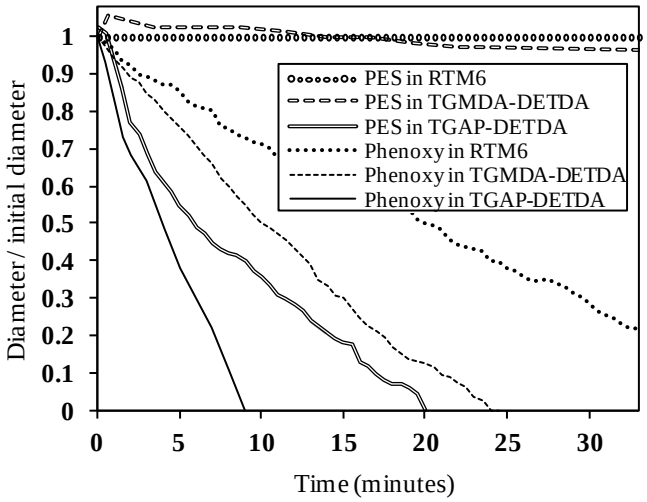

Fig. 2. Evolution of PES and phenoxy filament diameter (initially 100 µm) in TGAP-DETDA, TGMDA-DETDA and RTM6 resins at 100 °C.

The faster reduction of the phenoxy filament diameter in TGAP-DETDA resin than in TGMDA-DETDA formulation is easily explained by the favored diffusion of the lower size TGAP molecules compared to TGMDA epoxide in glassy phenoxy [20] evidenced in Chapter 2. Similarly, the dissolution kinetics of the phenoxy filament is slower in the RTM6 resin than in TGMDA-DETDA resin due to the higher mobility of the DETDA monoaromatic diamine compared to the diaromatic diamines (4,4'-methylenebis-(2-isopropyl-6-methyl)-aniline and 4,4'-methylenebis-(2,6-diethyl)-aniline) contained in the formulation of the RTM6 resin. In addition to the strong effect of the resin composition, the molecular structure of the thermoplastic reveals an obvious influence on the filament dissolution time in epoxy resins. Although both thermoplastics have close average molecular weights, the dissolution kinetics of the phenoxy filament is mainly improved thanks to its inferior T_g (84 °C against 220 °C for PES) that promote chain mobility by transition of the thermoplastic-resin precursor blend from the glassy to the rubbery state at lower temperature or for lower mass fractions of penetrating resin precursors. Phenoxy filaments of 100 µm diameter are totally dissolved in the RTM6 resin at 100 °C unlike PES filaments, which remain insoluble. In order to dissolve a PES filament in these conditions, another resin formulation like TGAP-DETDA resin is required. Indeed, the

lower molecular size of both diamine and epoxide moieties of the TGAP-DETDA resin compared to the RTM6 precursors contributes to preferential dissolution.

3.1.2. Influence of temperature treatment on dissolution

Fig. 3 shows the reduction of the dissolution time period induced by improved mobility of the molecules when temperature is increased. The dissolution kinetics of the filaments was not investigated at temperatures superior to 140 °C. Indeed, significant crosslinking of the resin occurs before reaching higher temperatures during composite processing due to limited heating rates imposed by thermal inertia and in order to prevent excessive heat release by the exothermal reaction.

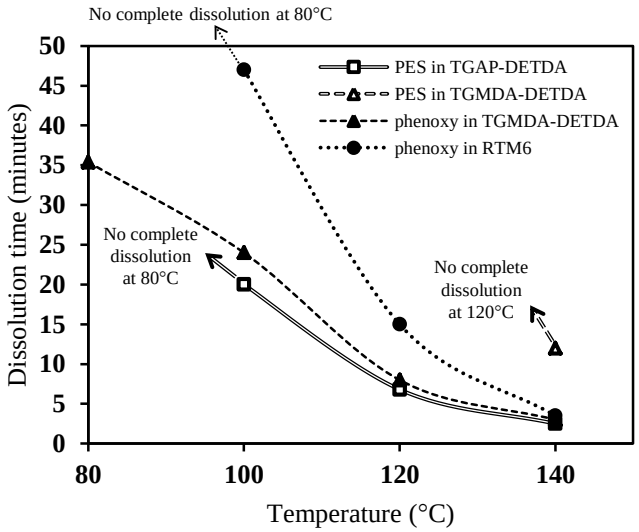

Fig. 3. Dissolution time of a 100 µm diameter filament at 80 °C, 100 °C, 120 °C and 140 °C: PES filament in TGAP-DETDA and TGMDA-DETDA resins and phenoxy filament in TGMDA-DETDA and RTM6 resins.

Phenoxy filaments are completely soluble in each epoxy resin formulation between 100 °C and 140 °C such as PES filaments in TGAP-DETDA resin. In TGMDA-DETDA resin, apparent dissolution of 100 µm diameter PES filaments is only slightly initiated at 100 °C but can be completed by increasing the temperature to 140 °C although gel time (43 minutes at 140 °C vs 4 hours at 100 °C) and consequently time window for dissolution are considerably reduced. However, the complete swelling of a 100 µm diameter

PES filament in the RTM6 is prevented in this temperature interval. Nearly complete insolubility of PES in RTM6 resin at 100 °C is confirmed by the practically unaffected thermoplastic filament shown in **Fig. 4.a** after resin gelation.

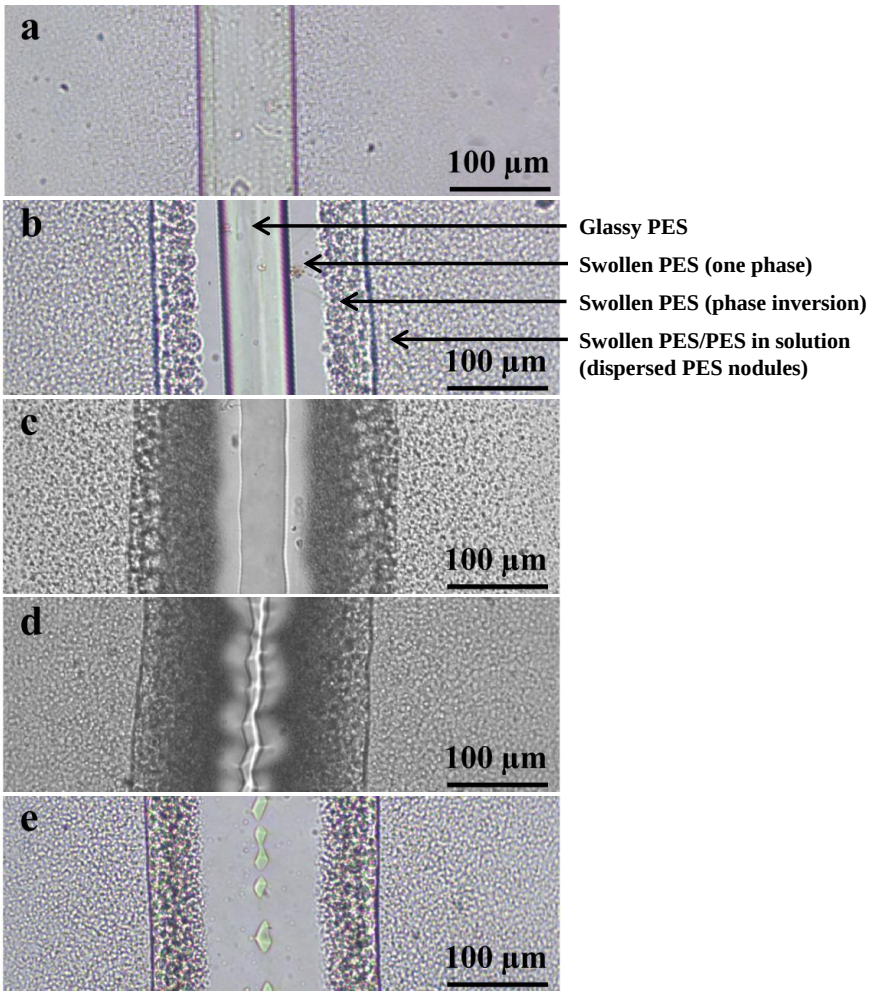

Fig. 4. Images from hot stage microscopy of a PES filament (initial diameter of 100 µm) in RTM6 resin after isothermal treatment at (a) 100 °C (b) 120 °C (c) 140 °C until gel time and after temperature ramp from 80 °C to 180 °C at (d) 1 °C/min (e) 2 °C/min. from toexplain

The residual core of the original PES filament in RTM6 resin cured at 120 °C and 140 °C is observable in **Fig. 4.b** and **c** that also evidence the microstructure gradient resulting from reaction induced phase separation

(RIPS). For these isothermal treatments, apparent dissolution of the 100 µm diameter PES filament is initiated but is too slow to be completed before the molecular weight increase of the RTM6 resin becomes so large as to prevent further diffusion of the reacting resin precursors. Similarly to isothermal diffusion, temperature ramps lead to partial swelling of the PES filament in the RTM6 resin but manage to reduce the PES part remaining in the glassy state (**Fig. 4.d** and **e**). Thanks to thermoplastic swelling initiated at low temperatures limiting the resin crosslinking followed by a rapid diffusion of the precursors at higher temperature, a 2 °C/min heating ramp from 80 °C to 180 °C in RTM6 resin achieves the largest decrease of the pure PES fraction. Only some inclusions of the original filament unaltered by the resin subsist.

3.1.3. Influence of thermoplastic content on dissolution

Since dissolution slows down at increasing times due to crosslinking initiation and reduction of the composition gradient at the resin-thermoplastic interface, the size of the thermoplastic elements added to a composite preform such as the global thermoplastic content, which depends on the thermoplastic modifier distribution, must remain limited to ensure a complete thermoplastic swelling by the resin precursors. The influence of an additional thermoplastic amount on the dissolution time period of thermoplastic filaments is presented in **Fig. 5**. On the one hand, variation of the filament diameter is considered and on the other hand, effect of thermoplastic-modified resins is investigated. Apparent dissolution of a 100 µm diameter PES filament is completed in TGAP-DETDA resin at 120 °C after a time period much shorter than the resin gel time (75 minutes) at this temperature when interdiffusion is very likely since the viscosity is still low. Similarly, total dissolution of a 100 µm diameter phenoxy filament is rapidly achieved in RTM6 resin at 120 °C (gel time > 4 hours). Nevertheless, due to viscosity increase and depletion of precursor molecules close to the interface with the glassy thermoplastic as interdiffusion proceeds, higher dissolution times are observed for larger filaments and can lead to partial insolubility beyond a diameter threshold of approximately 130 µm for phenoxy in RTM6 resin and 150 µm for PES in TGAP-DETDA resin at 120 °C. The dissolution kinetics is likewise rapidly hindered when increasing thermoplastic concentrations have been previously dissolved in the resins. Such results underline the need to limit the thermoplastic content added to epoxy resin and to control distribution and dimensions of the thermoplastic additives in order to fulfill dissolution and prevent residual interface

boundaries, which are deleterious for resistance to environmental stress cracking.

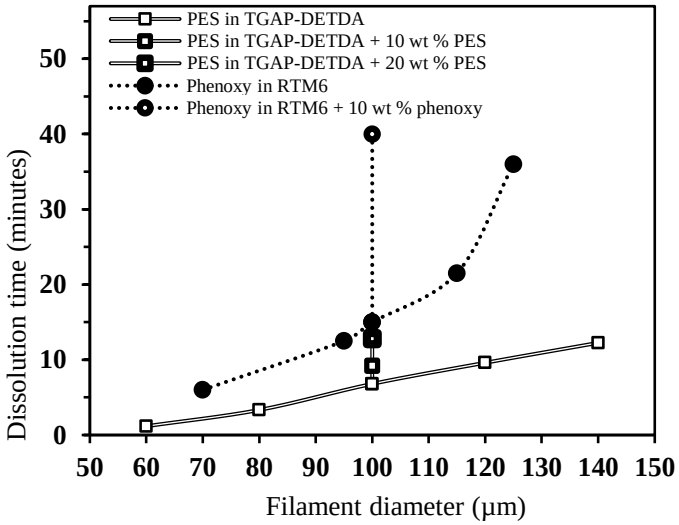

Fig. 5. Influence of filament diameter and thermoplastic amount in the resin on the dissolution time of a PES filament in TGAP-DETDA resin and of a phenoxy filament in RTM6 resin at 120 °C.

3.2. Composition gradient induced by a thermoplastic filament in epoxy resin

Local composition of the epoxy resin-thermoplastic blend induced by in situ dissolution of thermoplastic is also drastically affected by resin crosslinking as the interdiffusion mechanism between the thermoplastic and the resin precursors is rapidly hindered when viscosity starts to rise. As concentration gradient is the only driving force for thermoplastic swelling and distribution in epoxy resin, the interdiffusion time period before significant crosslinking of the reactive resin has primordial effect on inhomogeneities of the blend composition and a residual thermoplastic concentration gradient subsists after resin crosslinking. As a result, soluble thermoplastic additives periodically incorporated into the preform of a composite processed by RTM should lead to local variations of the thermoplastic-epoxy resin matrix composition. Moreover, the microstructure gradient generated by RIPS during the resin curing also depends on the competition between cure reaction and interdiffusion.

Therefore, in addition to demonstrating diffusion of the resin precursors towards the thermoplastic by monitoring decrease of the filament diameter, the model samples containing a single PES or phenoxy filament are intended to underline extent of the apparent thermoplastic migration through swelling of the filament by epoxide and diamine moieties. Concentration profiles evaluated on crosslinked samples enable to evidence composition gradient and to determine if important local inhomogeneity should be expected in the thermosetting-thermoplastic blends resulting from in situ dissolution of a thermoplastic element in reactive resin. Epoxy resin formulations and temperature profiles improving PES or phenoxy distribution resulting from thermoplastic introduction in a composite matrix can be consequently defined. Moreover, study of the resin-thermoplastic interphase composition and induced morphology is necessary to adapt the global thermoplastic content such as shape and distribution of the toughening elements in order to generate the desired microstructure type.

3.2.1. Evaluation of local thermoplastic content in epoxy resin by Raman spectroscopy

Thermoplastic distribution induced by in situ dissolution of a single filament and further swelling by epoxy resin during interdiffusion can be assessed by exploiting Raman spectroscopy. Since PES and phenoxy are characterized by intense spectral bands centered respectively at 1148 cm^{-1} and 1111 cm^{-1} and no Raman band of the epoxide-diamine formulations appears in this region of the spectrum, evolution of the thermoplastic concentration can be followed on the basis of the variation of the intensity of these thermoplastic characteristic bands.

Raman spectra acquired at increasing distances from a 100 µm diameter PES filament after swelling in TGMDA-DETDA resin during a 120 °C isotherm are reported in **Fig. 6**. The evolution of the sulfone band intensity (1144-1148 cm^{-1}) used as reference for PES quantification, which depends on the distance from the initial location of the PES filament center, confirms the presence of a residual concentration gradient. Whatever the resin formulation and the thermal treatment applied are, similar evidence of the residual blend inhomogeneities is observable for phenoxy and PES filaments like described in Chapter 1.

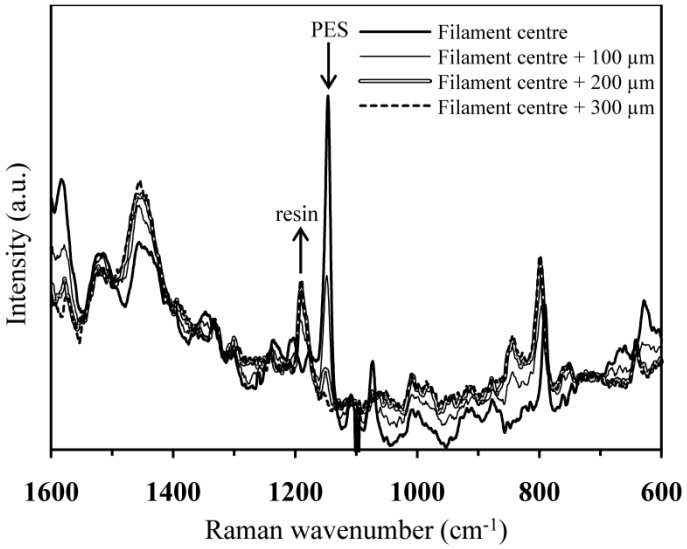

Fig. 6. Raman spectra at increasing distances from the initial location of the center of a 100 µm diameter PES filament after dissolution and interdiffusion at 120 °C in TGMDA-DETDA resin.

The thermoplastic concentration profiles induced by PES and phenoxy filaments in the epoxy resins are determined by applying a baseline subtraction to remove the fluorescence background from the spectra. Limited overlapping between the peaks allows the exploitation of the Raman spectra without decomposition treatment. A linear relation between the intensity of the thermoplastic characteristic band and the thermoplastic content in the epoxy resin is assumed to estimate the concentration profiles.

The PES concentration profile resulting from a 2 °C/min temperature ramp from 80 to 180 °C applied to a 100 µm diameter PES filament into the RTM6 resin shown in **Fig. 7** highlights the potential of Raman spectroscopy to examine the thermoplastic distribution (**Fig. 7.b**). The 600 µm width interval where PES is detected corresponds approximately to the distance on which phase separation can be observed in the polymer blend using hot stage microscopy (**Fig. 7.a**). Moreover, a PES concentration around 20 wt % can be attributed to the interface located beyond 100 µm from the position of the filament center. As evidenced by SEM on PES-RTM6 resin blends (**Fig. 7.c**), a transition from a continuous epoxy resin-rich phase with dispersed PES nodules to a phase inverted morphology occurs at this PES concentration. Therefore, the PES content in RTM6 resin remains too high to

obtain a continuous epoxy phase on a 200 µm wide interval surrounding the initial location of the 100 µm diameter filament.

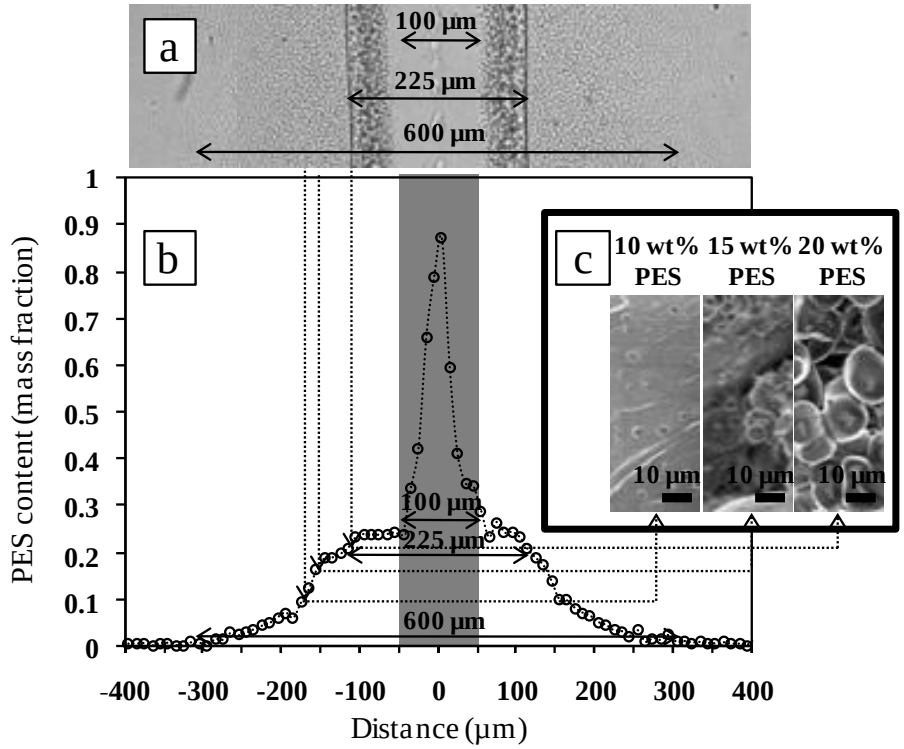

Fig. 7. (a) Image from hot stage microscopy of a 100 µm diameter PES filament after interdiffusion and phase separation during a 2 °C temperature ramp from 80 °C to 180 °C in RTM6 resin, (b) corresponding PES concentration profile determined by Raman spectroscopy and (c) SEM micrographs of the 10-15-20 wt % PES-RTM6 resin blends.

3.2.2. Influence of resin formulation and thermoplastic type on composition gradient

The PES distributions resulting from a 100 µm diameter filament in the different epoxy resin formulations at 120 °C are compared in **Fig. 8**. The samples were analyzed after 120 minutes interdiffusion under isothermal conditions. At this stage of curing, the mobility of the diffusing moieties is too low to further influence the concentration gradient subsisting in the phase separated blend. Concentration profiles determined on basis of the Raman mappings evidence that introduction of a PES filament in TGAP-

DETDA resin induces the lower composition gradient with PES detected on an interval of about 1 mm after the 120 °C isotherm. The high diffusivities of the TGAP and DETDA resin precursors evidenced in Chapter 2 promotes mutual diffusion at the interface with the thermoplastic filament and results in an improved PES distribution in the epoxy resin despite faster crosslinking kinetics of the TGAP-DETDA formulation demonstrated in Chapter 1 that reduces the time period available for diffusion. For TGMDA-DETDA and RTM6 formulations, the larger molar volume of the resin precursors prevents similar diffusion efficiency during the initial stages of the isotherm and reduces filament swelling, which is the dominant phenomenon contributing to the apparent thermoplastic migration. Important composition inhomogeneities with high residual PES concentrations and even pure PES in the RTM6 resin, located near the filament center, are therefore obtained in these resins. After phase separation, the composition gradient in the polymer blend lead to a large morphology spectrum going from sea-island morphology to phase inversion with the thermoplastic forming the continuous phase since the PES concentration remains locally higher than the critical composition. The SEM micrograph of the interphase induced by the PES filament in TGMDA-DETDA resin evidences this microstructure gradient.

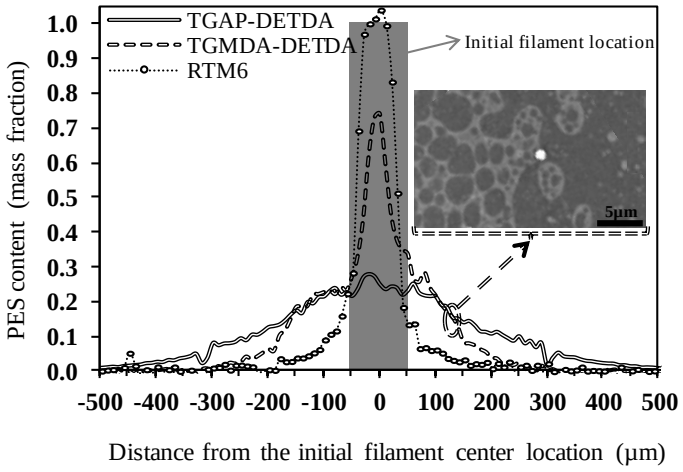

Fig. 8. PES distribution in TGAP-DETDA, TGMDA-DETDA and RTM6 resins after dissolution of a 100 µm diameter PES filament and interdiffusion at 120 °C determined by Raman spectroscopy and SEM micrograph of the induced interphase between the PES filament and the TGMDA-DETDA resin.

Influence of the thermoplastic molecular structure on the composition profile is shown in **Fig. 9** after isothermal treatment of a 100 µm diameter filament in TGMDA-DETDA and RTM6 resins until interdiffusion is prevented by crosslinking. The broader distribution profiles observed for phenoxy reflect a thicker thermoset-thermoplastic interphase with lower local phenoxy contents. Phenoxy appears thus as an alternative to PES that allows improving the thermoplastic distribution into TGMDA-DETDA and RTM6 resins. Indeed, besides the faster apparent dissolution of the phenoxy filaments revealed previously, the preferential diffusion of the epoxy resin precursors into phenoxy [20] (cfr Chapter 2), which leads to a favored swelling of the filament, induces apparent phenoxy migration in the epoxy resins on a larger distance. Moreover, the maximal phenoxy concentration remaining below 30 wt % near the initial filament location, no phase inversion is expected (cfr Chapter 1) after interdiffusion at 120 °C unlike for 100 µm diameter PES filaments in the same conditions.

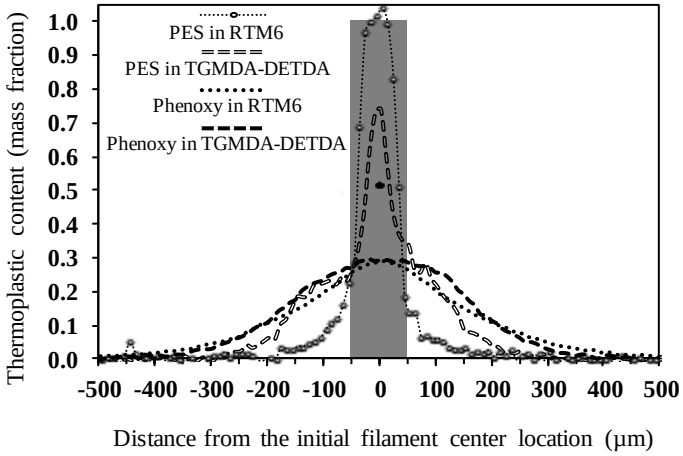

Fig. 9. PES and phenoxy distributions in TGMDA-DETDA and RTM6 resins from Raman spectroscopy after dissolution of a 100 µm diameter filament and interdiffusion at 120 °C.

3.2.3. Influence of temperature treatment on composition gradient

Since both diffusion coefficients and crosslinking kinetics of the epoxy resin are governed by the thermal conditions, control of the temperature during interdiffusion plays also a crucial role on the thermoplastic concentration profile. Therefore, a good compromise between a fast thermoplastic swelling by the epoxide and diamine precursors and a sufficient time window before

significant crosslinking of the resin is required to limit the local thermoplastic concentration and reduce the final composition gradient. Whereas a temperature increase from 100 °C to 140 °C limits the PES distribution in TGAP-DETDA resin (**Fig. 10.a**), it contributes to improve the phenoxy distribution in RTM6 resin (**Fig. 10.b**).

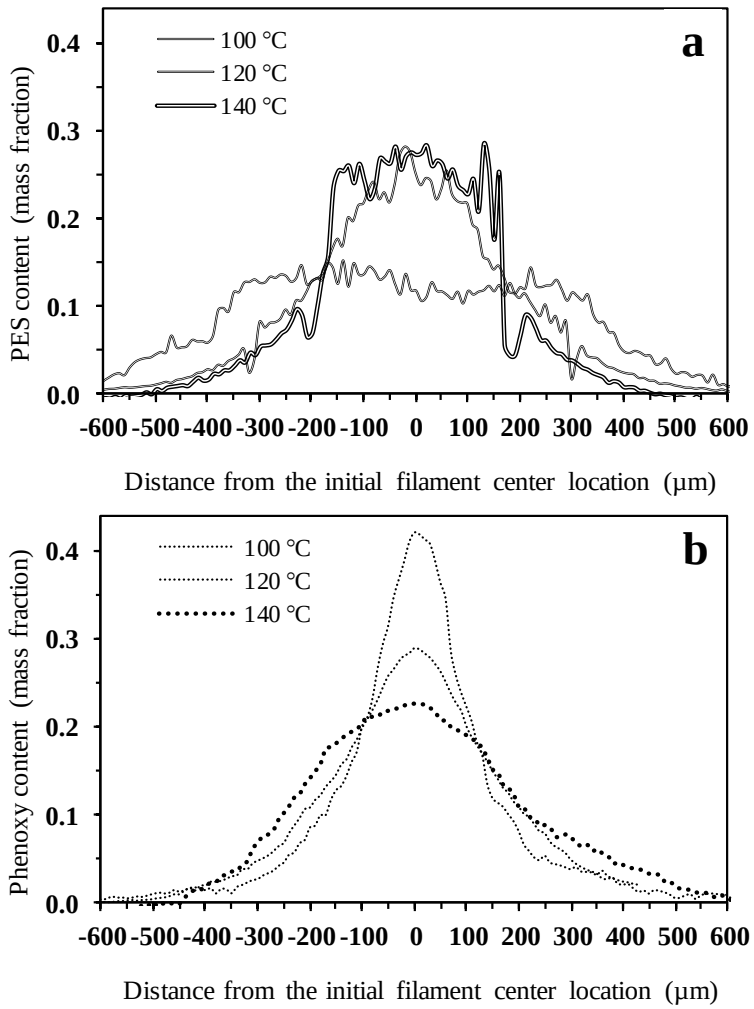

Fig. 10. (a) PES distribution in TGAP-DETDA resin and (b) phenoxy distribution in RTM6 resin after dissolution of a 100 µm diameter filament and interdiffusion at 100 °C, 120 °C and 140 °C.

The wider concentration profile observed at lower temperature into the TGAP-DETDA resin results from the low molar volume of the TGAP

epoxide and DETDA diamine monomers combined with the high reactivity of the resin. Indeed, a high mobility of the diffusing resin precursors subsists at 100 °C while interdiffusion is rapidly hindered at 140 °C by the fast crosslinking reaction leading to a resin viscosity doubled in approximately 10 minutes at this temperature (gel time of about 30 minutes) against more than one hour at 100 °C (gel time of more than 3 hours) as presented in Chapter 1. The limiting factor to interdiffusion is thus crosslinking for the TGAP-DETDA resin. In contrast, higher temperatures are required to favor the thermoplastic distribution in the RTM6 resin due to the lower diffusivities of the resin precursors. Moreover, the slower crosslinking kinetics of the RTM6 resin at 140 °C (gel time of 95 minutes) prevents too fast viscosity increase and therefore, diffusion doesn't slow down so quickly than into the TGAP-DETDA resin. In this case of the RTM6 resin, the limiting factor is no more crosslinking but the epoxide and diamine precursor diffusion. These results indicate that the temperature profile achieving the optimal thermoplastic distribution depends on the epoxy resin-thermoplastic combination. Monitoring of the evolution of the composition profile at several time intervals during the cure reaction should allow to highlight these different behaviors for the various systems.

3.3. Investigation of applicability to composite processing

3.3.1. Thermoplastic concentration profile resulting from two interacting filaments

Beyond influence of carbon fibers fabrics, interactions between neighboring thermoplastic elements must be considered for transposition of the soluble thermoplastic-epoxy resin systems studied in this work to processing of composites allowing in situ dissolution of the thermoplastic modifier in the epoxy matrix. Inspection of the local thermoplastic concentration in a model system containing several filaments disposed in parallel into epoxy resin allow prediction of the residual composition gradient preserved in the polymer blend after curing and can be used to orient the choice of thermoplastic dimensions and layouts adapted for RTM process.

The concentration profile resulting from two parallel phenoxy filaments with diameters of approximately 100 µm and respective centers initially separated by 360 µm is shown in **Fig. 11** after interdiffusion in the TGMDA-DETDA resin at 100 °C. Although a composition gradient subsists, phenoxy contents

varying from around 20 wt % to less than 40 wt % should prevent phase inverted morphologies. The expected blend microstructures mainly consist in a large amount of phenoxy nodules dispersed in a continuous epoxy resin-rich phase like shown for the TGMDA-DETDA resin modified with 30 wt % phenoxy. Such morphologies developed close to the critical composition, largely contribute to toughness improvement and preserve high T_g of the continuous thermoset phase. As demonstrated previously, phenoxy distribution can even be improved by increasing temperature or enhancing the initial distance between the filaments without generating poor phenoxy region. In contrast, sharper concentration profiles with large zones of phase inversion results from introduction of 100 µm diameter-PES filaments in epoxy resin.

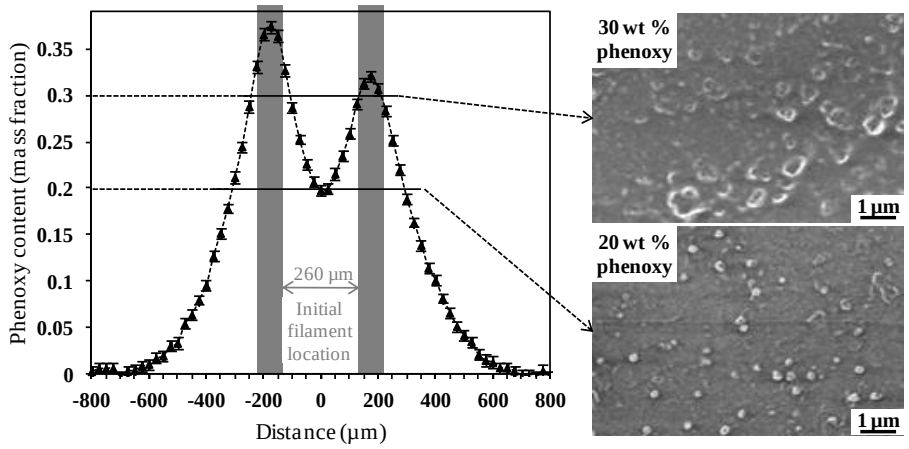

Fig. 11. Phenoxy concentration profile after dissolution of two phenoxy filaments (centers initially separated by 360 µm) in TGMDA-DETDA resin and interdiffusion at 100 °C and corresponding local microstructures shown by SEM micrographs of the TGMDA-DETDA resin modified with 20 and 30 wt % phenoxy.

Chemometrics was chosen in this case as alternative method to classical spectral treatment considering single peak intensities for quantitative evaluation of the phenoxy distribution in the epoxy resin. Indeed, calibration and multivariable treatment of the different spectra with The Unscrambler® X Version 10.0.1 lead to an improved accuracy in the prediction of the local thermoplastic concentration. Such a multivariate analysis provides a relevant procedure for spectrum normalization and is based on the statistical treatment of a large set of spectra and of a broad range of spectral variables

to predict the phenoxy concentration. Partial least square regression (PLS) was applied to perform a data compression in such a way that the extracted latent variables correspond to the directions of largest covariance between the spectral data and the phenoxy concentration. The quantitative calibration model developed to determine this characteristic is created by collecting Raman spectra of TGMDA-DETDA resin blended with phenoxy concentrations up to 50 wt %. In this composition range, limited standard error of prediction enables accurate prediction of the local phenoxy concentration resulting from the adjacent filaments.

3.3.2. Transposition to composite panel with a PES film insert: microstructure examination

Thermoplastic filaments immersed in epoxy resin are suitable specimens to analyze influence of system formulation and temperature cycle on thermoplastic dissolution and distribution but remains very simplified model samples as compared to complex composite structures. Therefore, the concept using soluble thermoplastic for toughening of epoxy resin was transposed to a composite panel processed by LRI in order to take into account features linked to liquid composite molding like the presence of the fiber reinforcement or the different layout of the thermoplastic modifier, which is introduced in the form of a PES film between two glass fiber layers in this case.

The composite panel was produced without perturbation of the process since PES remains insoluble in RTM6 resin during injection at 80 °C. The micrographs of the panel cross section after etching of the PES-rich phase presented in **Fig. 12.** show that the composition gradient in the area of interaction between the PES film and the resin precursors induces important variations of the interphase microstructure depending on the distance from the PES film. Although a limited film thickness of 35 µm, the residual PES content around the initial location of the PES film generates locally a phase inverted microstructure with a continuous thermoplastic-rich phase. Use of thinner film interleaves and faster temperature ramps or modification of the system formulation with resins favoring interdiffusion or with phenoxy can reduce the formation of such morphologies in this area. For increasing distances from the film, the blend morphology evolves to a see-island microstructure with submicron PES-rich nodules dispersed in the continuous RTM6 resin-rich phase up to a distance superior to thickness of the glass

fiber fabrics. The presence of PES nodules on this large distance interval superior to 100 µm evidences passage of thermoplastic macromolecules through the glass fiber layer.

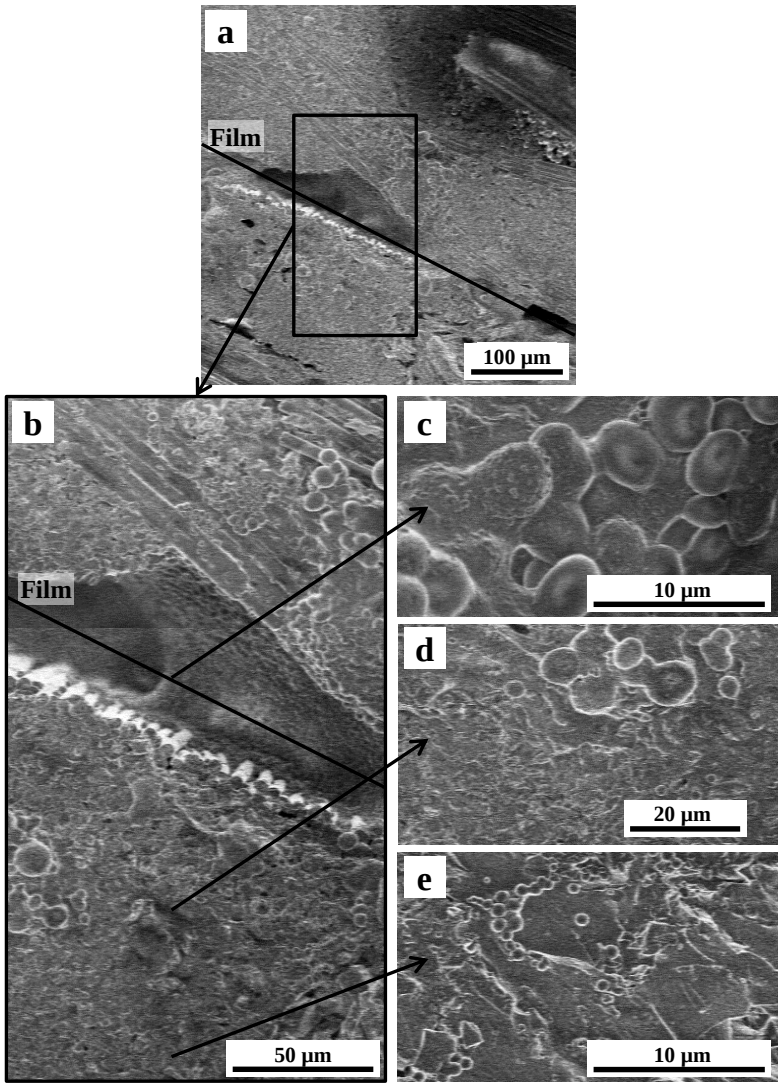

Fig. 12. SEM micrographs of the RTM6 resin-glass fiber composite panel with PES film processed by LRI after etching of the PES-rich phase: (a) overview of the cross section; (b) microstructure gradient around the initial location of the PES film; (c) RTM6 resin-PES blend microstructure near the PES film initial location (d) RTM6 resin-PES blend microstructure between 50 and 100 µm away from the PES film initial location (e) RTM6 resin-PES blend between 100 and 150 µm from the PES film initial location.

4. Conclusions

This study offers several combinations of soluble thermoplastics and reactive epoxide-diamine formulations enabling sufficient time windows for interdiffusion in order to distribute a thermoplastic toughener into an epoxy resin matrix by in situ dissolution during liquid composite molding. Apparent dissolution of 100 µm diameter phenoxy filaments is rapidly completed in RTM6 or TGMDA-DETDA resins. In contrast, total swelling of PES filaments with identical dimensions remains impossible in RTM6 resin. TGAP-DETDA resin based on lower molecular weight epoxide and diamine precursors diffusing preferentially is therefore proposed as alternative formulation for PES dissolution.

Assessment of the composition gradients induced by the filaments in epoxy resin using Raman spectroscopy shows that distribution of phenoxy is achieved on a larger distance than for PES under the same conditions. Similarly, TGMDA-DETDA resin and mainly TGAP-DETDA resin improve thermoplastic distribution as compared to RTM6 resin although their faster crosslinking kinetics reduces the interdiffusion period. Due to the lower residual phenoxy content around the initial filament location and the higher critical composition of the epoxy resin-phenoxy blends, phase inverted microstructure is easier to eliminate with this thermoplastic modifier than with PES, for which it subsists locally if the PES content is not drastically reduced. The thermal profile applied to the system also considerably influences the composition gradient and consequently the morphology variation of the blend since it determines the balance between interdiffusion and crosslinking. While high temperature isotherms and principally fast temperature ramps favor thermoplastic distribution in TGMDA-DETDA and RTM6 resin, isotherm at moderate temperature works best with lower viscosity TGAP-DETDA resin.

The microstructure spectrum created in the model systems by soluble PES and phenoxy filaments can easily be transposed to composite matrices toughened via in situ dissolution of thermoplastic interleaves added to the composite preform as demonstrated when a PES film is introduced between the glass fiber layers of a composite panel processed by LRI.

References

[1] Turmel DJP, Partridge IK. Heterogeneous phase separation around fibers in epoxy/PEI blends and its effect on composite delamination resistance. Composites Science and Technology 1997;57(8):1001-7.
[2] Hayes BS, Seferis JC. Variable temperature cure polyetherimide epoxy-based prepreg systems. Polymer Engineering and Science 1998;38(2):357-70.
[3] Murakami A, Shonaike GO, Ooishi K, Watanabe O, Takezawa M. Fracture toughness of PEI modified epoxy resin CFRP composites. Journal of Reinforced Plastics and Composites 2000;19(2):137-51.
[4] Fernandez B, Arbelaiz A, Diaz E, Mondragon I. Influence of polyethersulfone modification of a tetrafunctional epoxy matrix on the fracture behavior of composite laminates based on woven carbon fibers. Polymer Composites 2004;25(5):480-8.
[5] McGrail PT, Jenkins SD. Some aspects of interlaminar toughening: reactively terminated thermoplastic particles in thermosetting composites. Polymer 1993;34(4):677-83.
[6] Woo EM, Mao KL. Interlaminar morphology effects on fracture resistance of amorphous polymer-modified epoxy/carbon fiber composites. Composites Part A : Applied Science and Manufacturing 1996;27(8):625-31.
[7] Pascal T, Bonneau JL, Biolley N, Mercier R, Sillion B. Approach to improving the toughness of TGMDA/DDS epoxy resin by blending with thermoplastic polymer powders. Polymers for Advanced Technologies 1995;6(4):219-29.
[8] Thanomsilp C, Hogg PJ. Interlaminar fracture toughness of hybrid composites based on commingled filament fabrics. Composites Science and Technology 2005;65(10):1547-63.
[9] Hogg PJ. Toughening of thermosetting composites with thermoplastic fibers. Materials Science and Engineering A 2005;412(1-2):97-103.
[10] Beier U, Wolff-Fabris F, Fischer F, Sandler JKW, Altstädt V, Hulder G, Schmachtenberg E, Spanner H, Weimer C, Roser T, Buchs W. Mechanical performance of carbon fiber-reinforced composites based on preforms stitched with innovative low-melting temperature and matrix soluble thermoplastic filaments. Composites Part A: Applied Sc. and Manufact. 2008; 39(9):1572-81.
[11] Beier U, Sandler JKW, Altstädt V, Spanner H, Weimer C. Mechanical performance of carbon fiber-reinforced composites based on stitched and bindered preforms. Composites: Part A 2009;40(11):1756-63.
[12] Li L, Lee-Sullivan P, Liew KM. The Influence of Thermoplastic Film Interleaving on the Interlaminar Shear Strength and Mode I Fracture of Laminated Composites. Journal of Engineering Materials and Technology 1996;118(3):302-9.
[13] Carter JT, LoFaro C, Maskell RK, McGrail PT. Flexible polymer element as toughening agent in prepregs. U.S. Pat. Appl. Publ. US 2004/0041128 A1, 2004
[14] Wong DWY, Lin L, McGrail PT, Peijs T, Hogg PJ. Improved fracture toughness of carbon fiber/epoxy composite laminates using dissolvable

thermoplastic fibers. Composites Part A: Applied Science and Manufacturing 2010;41:759-67.
[15] An X, Ji S., Tang B, Zhang Z, Yi XS. Toughness improvement of carbon laminates by periodic interleaving thin thermoplastic films. Journal of Materials Science Letters 2002;21:1763-5.
[16] Yun NG, Won YG, Kim SC. Toughening of carbon fiber/epoxy composite by inserting polysulfone film to form morphology spectrum. Polymer 2004;45(20):6953-8.
[17] Naffakh M, Dumon M, Gérard JF. Study of a reactive epoxy-amine resin enabling in situ dissolution of thermoplastic films during resin transfer molding for toughening composites. Composites Science and Technology 2006;66(10):1376-84.
[18] Mortimer S, Cawse JL. A thermoplastic toughening material and related method. PCT Int. Appl. Publ. WO 2007/110617 A1, 2007.
[19] LoFaro C, Abusafieh A, Webb WE, Doyle M. Resin-soluble veil for composite materials. U.S. Pat. Appl. Publ. US 2006/0252334 A1, 2006.
[20] Dumont D, Seveno D, De Coninck J, Bailly C, Devaux J, Daoust D. Interdiffusion of thermoplastics and epoxy resin precursors: investigations using experimental and molecular dynamics methods. Polymer International 2012;61(8):1263-71.
[21] Lestriez B, Chapel JP, Gérard JF. Gradient interphase between reactive epoxy and glassy thermoplastic from dissolution process, reaction kinetics, and phase separation thermodynamics. Macromolecules 2001;34(5):1204-13.
[22] Oyama HT, Lesko JJ, Wightman JP. Interdiffusion at the interface between poly(vinylpyrrolidone) and epoxy. Journal of Polymer Science: Part B: Polymer Physics 1997;35(2):331-46.
[23] Rajagopalan G, Gillespie Jr. JW., McKnight SH. Diffusion of reacting epoxy and amine monomers in polysulfone: a diffusivity model. Polymer 2000;41(21):7723-33.
[24] Immordino KM, McKnight SH, Gillespie Jr. JW. In-situ evaluation of the diffusion of epoxy and amine in thermoplastic polymers. The Journal of Adhesion 1998;65(1):115-29.
[25] Munz M, Strum H, Stark W. Mechanical gradient interphase by interdiffusion and antiplasticisation effect--study of an epoxy/thermoplastic system. Polymer 2005;46(21):9097-112.
[26] Min HS, Kim SC. Fracture toughness of polysulfone/epoxy semi-IPN with morphology spectrum. Polymer Bulletin 1999;42(2):221-27.
[27] Aradian A, Raphaël E, de Gennes PG. A scaling theory of the competition between interdiffusion and cross-linking at polymer interfaces. Macromolecules 2002;35(10):4036-43.
[28] Rajagopalan G, Narayanan C, Gillespie Jr. JW, McKnight SH. Diffusion and reaction of epoxy and amine in polysulfone-transport modeling and experimental validation. Polymer 2000;41(24):8543-56.

CONCLUSIONS PART 1

The first part of the present work aims to investigate the different factors controlling dissolution and distribution of thermoplastic into epoxy resin before significant crosslinking. The main results described in this study involve:

- Characterization of several epoxy resin-thermoplastic systems from thermomechanical, rheological and morphological point of views in blends prepared with fixed thermoplastic contents. The crosslinking reaction of these systems proposed in order to fulfill requirements imposed by RTM process and high performance applications has also been followed by different rheological, thermal and chemical techniques.
- Evaluation of temperature intervals during which thermoplastic dissolution takes place in the epoxide and diamine precursors of the different resins and study of the interdiffusion mechanism leading to thermoplastic dissolution. Measurements performed with a thermoplastic filament in contact with one resin precursor have demonstrated that interdiffusion is governed by the precursor mobility controlling its penetration into the thermoplastic core and extent of thermoplastic swelling. Simulation by molecular dynamics predicting diffusion coefficients of resin monomers and thermoplastic oligomers have confirmed the experimental results.
- Monitoring of thermoplastic filament dissolution in reacting epoxy resins and composition profiles resulting from interdiffusion between thermoplastic and resin precursors. Important disparities of dissolution extent, composition gradient and induced microstructure gradient have been evidenced depending on different parameters like thermoplastic nature, dimensions and distribution, epoxy resin formulation and cure cycle. By selecting two amorphous thermoplastics differing significantly by their molecular structure and by varying the resin formulation, this study presents the originality to investigate the complete range of solubility from thermoplastic being totally insoluble to completely soluble into epoxy resin.

The analyzed samples remain very simplified systems compared to complex composite structures and don’t take into account aspects like presence of carbon fibers. However, a toughening approach for composites processed by RTM using in situ dissolution of thermoplastic elements (filaments, films, veils, membranes, etc) inserted in the composite preform can be developed on basis of the generated results. Indeed, transposition to composite

production by liquid composite molding has been verified for a panel interleaved with a PES film added in the glass fiber preform despite the important composition gradient subsisting through the panel thickness with local phase inverted microstructures. Therefore, the experimental data can be exploited to orient selection of thermoplastic polymers and epoxy resin formulations and to optimize the cure cycle in order to reduce composition inhomogeneities and ensure a continuous epoxy resin-rich phase as polymer matrix of composite parts.

Blends of RTM6 resin with PES have been considered due to the high T_g of this amorphous thermoplastic preventing decrease of thermomechanical properties of the resin. Although improved PES distribution has been measured in RTM6 resin with fast heating ramps as compared to isotherms or slower heating rates, dissolution of PES remains rapidly partial when dimensions of PES filaments increase and phase inverted morphologies appears locally as soon as the PES content exceeds 15 wt %.

Therefore, phenoxy is recommended to toughen composites processed with RTM6 resin. Indeed, its preferential dissolution and swelling by the epoxide and diamine precursors leads to lower composition gradients and to the presence of phenoxy on a larger distance interval. Moreover, epoxy resin remains the continuous phase of the polymer blend for phenoxy contents up to 30 wt %. Since phenoxy distribution in RTM6 resin is favored at higher temperatures, a rapid heating is recommended to optimize thermoplastic distribution but a lower injection temperature is required to prevent a too fast dissolution that could lead to flushing of the phenoxy additive by the resin flow during the injection stage of the RTM process. The only main drawback of phenoxy is its lower T_g and its negative impact on the epoxy resin modulus. Another resin like the TGMDA-DETDA formulation can thus be preferred in this case due to its higher modulus resulting from crosslinking of the TGMDA tetraepoxide with the DETDA monoaromatic diamine characterized by a lower molar mass than the diamines contained in RTM6 resin.

If PES is privileged as thermoplastic modifier, TGAP-DETDA resin is suggested as a convenient alternative to RTM6 resin to complete PES dissolution and reduce the composition gradient since diffusion of both TGAP epoxide and DETDA diamine monomers are promoted through the swollen thermoplastic. Other benefits of the TGAP-DETDA resin are its

modulus at least equivalent to RTM6 resin and its lower viscosity allowing decrease of the injection temperature during RTM process. Due to the faster crosslinking kinetics of this resin and to the rapid PES dissolution, a low temperature is indeed required for injection. During interdiffusion, an intermediate isotherm and limited heating rates should contribute to improve PES distribution in the resin. While the TGAP-DETDA resin seems a good choice for incorporation of PES in a composite, its characteristics prevents toughening of the composite matrix with phenoxy.

On basis of the results from the previous chapters, different temperature cycles suitable for in situ dissolution of PES or phenoxy during composite processing are proposed in **Fig. i** for interesting epoxy resin-thermoplastic combinations. As compared to a classical temperature profile used for processing of composites with a RTM6 resin matrix by RTM, slight adaptations of the thermal cycle are needed to ensure resin injection without thermoplastic dissolution, to optimize thermoplastic distribution or minimize remaining insoluble part and to preserve adapted cure kinetics.

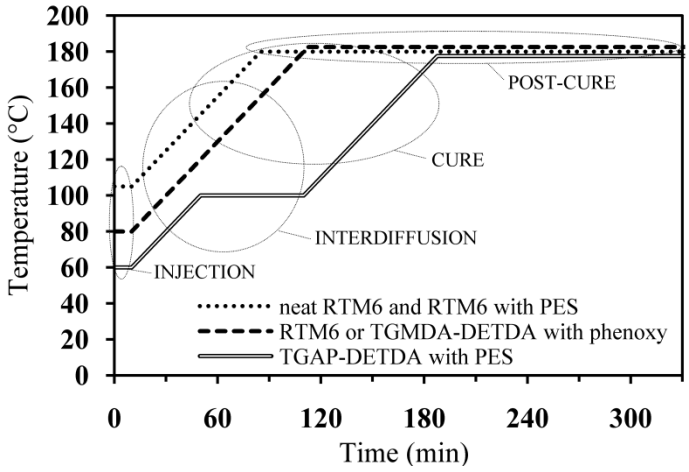

Fig. i. Temperature cycles suggested for processing of composites with neat RTM6 resin matrix or RTM6 resin matrix with in situ dissolution of PES, RTM6 and TGMDA-DETDA resin matrices with in situ dissolution of phenoxy or TGAP-DETDA resin matrix with in situ dissolution of PES.

Part 2

NANOCOMPOSITE MADE OF SOLUBLE THERMOPLASTIC AND CARBON NANOTUBES OR LAYERED CLAY TOWARDS DISPERSION AND DISTRIBUTION OF NANOFILLERS IN EPOXY RESIN

While the first part of this work concentrates on binary blends composed of epoxy resin and soluble thermoplastic, the second part of the study focuses on ternary blends prepared with the same poly(ether sulfone) (PES) and poly(hydroxyether of bisphenol A) (phenoxy) thermoplastics but filled with nanofillers in this case. Different kinds of nanofillers are considered, i.e., unfunctionalized multiwalled carbon nanotubes (MWNTs) and layered clay organomodified or not. An original method is proposed to disperse simultaneously thermoplastic nodules and nanofillers in the HexFlow® RTM6 resin. Two distinct stages are considered to achieve this goal. Nanofillers are first dispersed in the thermoplastic by melt blending and the processed nanocomposites are subsequently blended with the RTM6 resin before significant crosslinking. Curing of the modified resin and reaction induced phase separation should then lead to the desired microstructure with both a thermoplastic phase and nanofillers dispersed in the continuous epoxy resin phase.

The main objective of this part is to demonstrate that this method exploiting nanocomposites to disperse nanofillers into epoxy resin can be transposed to develop a toughening approach of composites processed by RTM. The investigated concept aims thus to take advantage of thermoplastic solublility in the resin precursors reported in Part 1 to use nanocomposites as carrier to disperse and deliver nanofillers in the composite matrix. Depending on the nanocomposite layout in the composite preform and interdiffusion extent before resin crosslinking, nanoparticles are intended to be distributed locally or globally in the polymer matrix.

In order to check the feasibility of the suggested method, microstructures and properties of the nanocomposites prepared by melt blending are first investigated to control if the nanofillers are properly dispersed and homogeneously distributed in the thermoplastics. Then, location of the nanofillers and conservation of their dispersion is verified once nanocomposites are blended with RTM6 resin. Finally, in situ dissolution of nanocomposite filaments in epoxy resin and resulting composition profiles are examined to confirm nanofiller delivery and to evidence the interdiffusion mechanism. Influence of different parameters like nanofiller form (tubular or lamellar) and content, thermoplastic nature and thermal cycle is reported in order to define conditions adapted to limit inhomogeneity in the composite panels.

The second part of the work is divided into three chapters:
- Chapter 4 *"Phenoxy and poly(ether sulfone) filled with carbon nanotubes and layered clay: Preparation and characterization of the nanocomposites"* aims to disperse and homogeneously distribute unfunctionalized MWNTs or organomodified layered clay platelets into phenoxy and PES by melt blending while preventing degradation of the constituents. Microstructures and overall properties of the nanocomposites are inspected to assess the dispersion state of the nanofillers.
- Chapter 5 *"Ternary blends of epoxy resin and phenoxy nanocomposite filled with carbon nanotubes or organomodified layered clay"* demonstrates that nanocomposites described in Chapter 4 can be used for simultaneous dispersion of a ductile thermoplastic phase and nanoparticles in epoxy resin. Microstructures of ternary blends prepared with fixed contents of phenoxy nanocomposites in RTM6 resin are inspected to determine nanofiller location and check their dispersion. The mechanisms controlling location of

the nanoparticles in polymer blends are discussed on basis of thermodynamic predictions and other kinetics considerations

- Chapter 6 *"Soluble thermoplastic for delivery of nanoparticles in epoxy resin"* examines in situ dissolution of nanocomposite filaments in the RTM6 resin. Thermoplastic and nanofiller distributions into epoxy resin resulting from competition between interdiffusion and crosslinking reaction are assessed and correlated to local microstructures. The objective of this chapter is to validate that nanocomposites are exploitable to deliver nanoparticles in epoxy resin and to evidence the mechanism leading to apparent nanofiller migration in epoxy resin.

Chapter 4

PHENOXY AND POLY(ETHER SULFONE) FILLED WITH CARBON NANOTUBES AND LAYERED CLAY: PREPARATION AND CHARACTERIZATION OF THE NANOCOMPOSITES

Abstract

This chapter aims to disperse and homogeneously distribute nanofillers into poly(hydroxyether of bisphenol A) (phenoxy) and poly(ether sulfone) (PES) while preventing degradation of the constituents. Nanocomposites were prepared by melt blending in order to individualize and distribute unfunctionalized multiwalled carbon nanotubes (MWNTs) or layered clay platelets in these thermoplastic matrices.

Fine dispersions and homogeneous distributions of individualized MWNTs were observed in both phenoxy and PES matrices with 1 to 5 wt % MWNTs using processing conditions preserving polymer stability. A rheological percolation threshold attributed to a MWNT content between 1 and 3 wt % MWNTs and improvements in electrical conductivity, thermal stability and

tensile modulus for increasing MWNT concentrations are also reported in this work.

For phenoxy filled with clay, large aggregates subsist after melt processing with sodium montmorillonite. In contrast, mixed intercalated-exfoliated structures with uniform dispersion of thin stacks of clay have been achieved in phenoxy for organomodified clay contents up to 15 wt %. Increase of modulus depending on clay content and nature are also reported.

1. Introduction

Due to their dimensions combined with their outstanding mechanical, electrical and thermal properties, carbon nanotubes (CNTs) have been the subject of multiple expectations since their discovery in 1991 by Sumio Iijima [1], both from a scientific point of view and for industrial applications. Indeed, their high aspect ratio allows the formation of percolating networks of connected nanotubes in polymer matrices at very low volume contents leading to thermal and electric conductivities in the samples approaching the values of the individual carbon nanotubes. Similarly, layered silicates have been widely used as polymer fillers since Toyota researchers have discovered the possibility to produce a nanocomposite from polyamide 6 with organomodified clay improving compatibility with polymer chains [2]. Remarkable improvement of thermal, mechanical and fluid barrier properties have been achieved by well dispersing montmorillonite clay layers throughout polymer matrices to produce nanocomposites with exfoliated or at least intercalated morphologies.

Melt processing appears as an efficient way to produce nanocomposites by bringing the energy required to overcome the inherent thermodynamic drive which leads to the formation of nanotube bundles and to disperse CNTs in thermoplastic matrices. Shear forces likewise promote dispersion of clay tactoids and diffusion of the polymer chains between the clay platelets resulting in intercalated-exfoliated nanocomposites for (organo)clay chemically compatible with the polymer matrix. Under appropriate experimental conditions, good carbon nanotube [3-12] and clay [13-25] dispersions have been reported in various thermoplastic matrices using this process, which is suitable for industrial applications due to its compatibility with extrusion, injection molding or compression molding along with the fact that no solvents are used.

Nevertheless, nanocomposites processed by melt blending of CNTs with PES or phenoxy thermoplastics have been rarely investigated before, apart from Goh and co-workers [26] who have shown that phenoxy composites with 4.8 wt % or more in situ functionalized MWNTs present higher storage modulus than neat phenoxy. Nanocomposites based on phenoxy reinforced with layered clay with different organic modifications have already been melt processed by Gurmendi et al. [27] who have achieved mixed

intercalated-exfoliated structure attributed to the pendent hydroxyl group of the phenoxy chains which is very prone to interact with polar groups.

Therefore, this chapter evaluates if unfunctionalized MWNTs can be properly dispersed and homogeneously distributed in phenoxy and PES by melt blending. Similarly, production of nanocomposites containing pristine or organomodified clay is investigated with phenoxy in the melt state but not with PES requiring processing temperatures superior to 300 °C due to its high glass transition temperature (T_g) leading in many cases to degradation of the organic surfactant intercalated in the modified clay. Several nanofiller contents are considered in order to determine composition ranges on which nanofiller dispersion is preserved. Polymer stability under the applied melt mixing conditions is discussed. MWNT and clay dispersion states achieved in the nanofilled thermoplastics are characterized on basis of observation of local microstructures and evaluation of macroscopic properties. Absence of polymer degradation such as quality of the nanofiller dispersion and homogeneity of the nanofiller distribution in the polymer matrix are indeed essential concerns as they considerably influence properties of the materials.

2. Experimental

2.1. Materials

The amorphous thermoplastic matrices selected to disperse nanofillers are PES (Radel® A-200 NT from Solvay Advanced Polymers) and phenoxy (InChemRez® Phenoxy Resin PKHP-200 or PKHB grades from InChem Corporation), which is a lower T_g poly(hydroxyether) having terminal alpha-glycol groups.

The MWNTs used in this study are Nanocyl™ NC7000 (Nanocyl S.A., Belgium) produced via catalytic carbon vapor deposition (CCVD) process. These unpurified and unfunctionalized MWNTs are synthesized as bundles of highly agglomerated nanotubes [28] with a purity of 90 %. Transmission electron microscopy (TEM) micrographs of the MWNTs are presented in **Fig. 1**. Their aspect ratio is higher than 150 (average diameter of 9.5 nm and average length of 1.5 μm) and their surface area is between 250 and 300 m^2/g [29] while the average number of graphene layers is 8 [30].

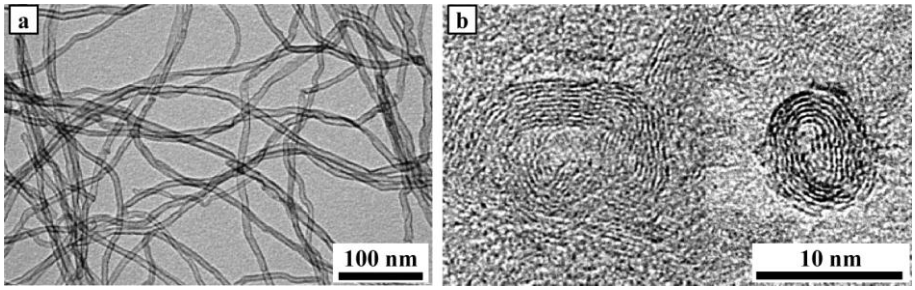

Fig. 1. TEM micrographs of the MWNTs (a) longitudinal view [29] (b) cross-section observed at 200 kV using a JEOL JEM-2100 microscope.

In addition to unmodified MWNTs, pristine and organomodified clays were explored to disperse aluminosilicate layers into the polymer matrices. Chemical structures of Cloisite® Na^+, a natural purified sodium montmorillonite and Cloisite® 30B, a montmorillonite modified by methyl, tallow, bis(2-hydroxylethyl), quaternary ammonium cations (90 meq/100 g) purchased from Southern Clay Products [31-32] are detailed in **Fig. 2**.

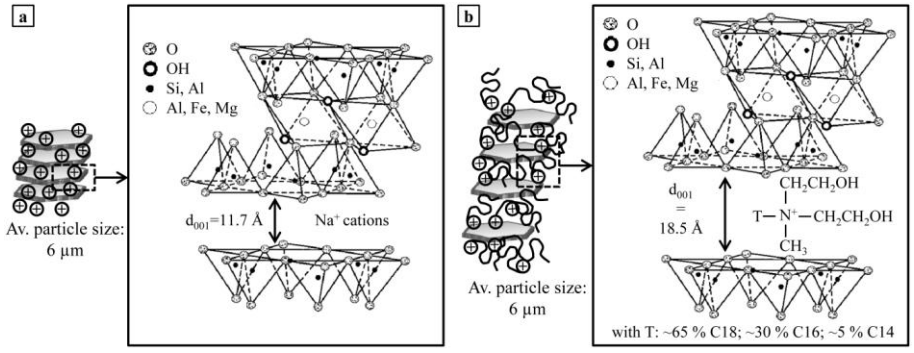

Fig. 2. Chemical structures of (a) pristine clay (Cloisite Na^+) and (b) organomodified clay (Cloisite 30B) [31-32].

2.2. (Nano)composite processing conditions

The PES and phenoxy (PKHP-200) polymers previously dried during 24 hours at 80 °C under vacuum were melt-processed in a DSM Xplore 15 ml micro-compounder without nanofillers and with MWNT concentrations of 1, 3 or 5 wt %. The temperatures applied during the process were respectively 220 °C and 340 °C for the phenoxy and PES polymers. In order to disperse MWNTs in the thermoplastic matrix, the speed of the corotating twin screws was set to 150 rotations per minute (rpm) and a residence time of 5 minutes

in the mixing chamber equipped with a side channel was used. After this recirculation period, the nanofilled compound was expelled through a 5 mm diameter circular die.

Co-rotating extruder Krupp WP ZSK25 WLE from Coperion was used to prepare composites based on phenoxy (PKHP-200) and 5 wt % Cloisite Na^+ or Cloisite 30B. Dried phenoxy and clay were introduced by the feeder in the melting zone of the extruder where a temperature profile of 120 °C-180 °C-180 °C-200 °C-200 °C-220 °C-220 °C-220 °C-220 °C-220 °C from hopper to die was applied. The screw speed was 300 rpm yielding to a residence time in the extruder of about 1 minute. Moreover, a water-assisted compounding technique developed on this extruder [20] was tested since water injection at high pressure and high temperature has been evidenced to favor diffusion of polymer chains inside the clay galleries and to help clay dispersion. The water was pumped into the extruder at 50 ml/min and was compounded with polymers and the clay in the high compression zone at barrel temperature of 220 °C. The screw is designed to increase the pressure in this zone up to 125 bars in order to keep the water liquid at the processing temperature. The water is then degassed in the transport zone of the screw and the vapour is removed by a vacuum pump. On the one hand, addition of water lowers viscosity and increase polarity of the polymer phase. On the other hand, water increases intergallery distance by diffusion between the aluminosilicate layers and adsorption on their surface. Combination of these two effects creates ideal conditions for diffusion and adsorption of polymer chains onto clay surface. Clay dispersion in PKHB was also investigated with different Cloisite Na^+ and Cloisite 30B amounts (5, 10 and 15 wt %) by extrusion at 200 rpm with water injection at 40 ml/min.

For further morphological and thermo-mechanical characterization, injection molded specimens were prepared with nanofilled phenoxy previously dried for 24 hours at 80 °C under vacuum to remove moisture. The samples of phenoxy filled with MWNTs (20 x 4 x 2 mm) were processed at 220 °C using a HAAKE MiniJet from Thermo Electron Corporation by applying a 0.08 MPa pressure during 5 s (ISO 527 type 5). For the extruded phenoxy filled with clay, standard tensile dog-bone specimens according to ASTM D638 type 1/2 norm were processed using a Bühler Rover 63B. The barrel temperature was maintained at 220 °C and the mold at 30 °C during injection taking place for 5 s under a 20 MPa pressure kept up during 1 s before that injection-molded specimens were cooled during 10 s.

2.3. Characterization methods

2.3.1. Size exclusion chromatography (SEC)

In order to determine influence of melt blending on the molar mass distribution, SEC measurements were carried out on the thermoplastics before and after melt processing. For phenoxy, a set of four Waters Styragel HR5, HR4, HR3 and HR2 columns was used with tetrahydrofuran (THF, unstabilized grade for HPLC from BioSolve BV) as mobile phase at a 1 ml/min flow rate. For PES, two PSS Gram columns (porosity of 100 Å and 1000 Å) were used and the carrier solvent (0.5 ml/min, 35 °C) was N,N-dimethylformamide (HPLC grade from BioSolve BV) with 5 mM ammonium hexafluorophosphate. In both cases, the detector was a Waters 410 differential refractometer (DRI). Relative calibration of the columns was obtained with 12 narrow polystyrene (PS) standards ($\overline{M}_w$ ranging between 3 x 10^3 and 1 x 10^6 g/mol).

2.3.2. Thermogravimetric analysis (TGA)

Thermal stability of the processed thermoplastics and nanocomposites was measured by TGA using a Mettler Toledo TGA/SDTA 851e. The weight loss of samples of about 15 mg heated at 20 °C/min was followed from 25 to 800 °C under dry air with a flow rate of 50 ml/min. Weight loss of Cloisite 30 B was controlled in the same way at a heating rate of 10 °C/min.

2.3.3. Transmission electron microscopy (TEM)

Nanofiller dispersion in the thermoplastic matrices was examined by means of TEM by cutting ultrathin sections of approximately 95 nm in thickness with a Reichert Microtome using a histodiamond knife with a cut angle of 45 ° from Diatome at ambient temperature. The ultrathin sections were subsequently collected on 300 mesh copper grids and inspected with a LEO 922 transmission electron microscope operating at 200 kV.

2.3.4. Rheometry

Shear rheology was performed using a Bohlin Gemini II rheometer from Malvern Instruments with a 25 mm diameter parallel-plate geometry and a

gap of 1 mm on neat thermoplastics and nanofilled compounds. The measurements were respectively carried out at 200 and 290 °C on samples based on phenoxy and PES with a shear stress of 100 Pa and an angular frequency varying from 940 to 0.3 rad/s.

2.3.5. Electrical conductivity measurements

Samples for electrical characterization (50 x 30 x 0.8 mm) were prepared by compression molding of neat phenoxy and nanocomposites filled with MWNTs at 220 °C during 1 minute under 10 tons on an aluminum sheet, which acts as a zero potential. A 1.5 mm width microstrip line of copper was added on the top of the sample. The alternating current (AC) electrical properties were measured at room temperature with a Wiltron Model 360B Vector Network Analyzer (VNA) in a wide-band frequency range from 40 MHz to 40 GHz using a line-line (LL) characterization technique applied to CNT-composite in microstrip-line configuration [33].

2.3.6. X-ray diffraction (XRD)

The interlayer spacing of the layered silicates dispersed in phenoxy was studied using a θ-2θ goniometer (Siemens D5000, 30 cm radius). The cooper rotating anode (Cu Kα, λ=1.5418 Å) used as X-ray source was fitted with a graphite secondary monochromator and a scintillation counter.

2.3.7. Traction test

Tensile tests were performed on injection-molded specimens at room temperature using a Zwick Z010 tensile machine with a crossed-head speed of 1 mm/min. Modulus values were calculated by linear regressions for elongation between 0.05 % and 0.5 % from the load-displacement curves.

3. Results and discussion

The stability of PES and phenoxy polymers under the selected processing conditions is initially checked by SEC and TGA. Subsequently, quality of the MWNT dispersion is locally assessed in these thermoplastic matrices on basis of TEM micrographs. Moreover, the global dispersion state of the MWNTs is confirmed by evaluation of macroscopic properties of the nanocomposite samples by rheological and electrical analyzes leading to

assessment of percolation thresholds and by tensile modulus measurements. Similarly, morphological state of phenoxy-clay composites is examined on basis of TEM observations, XRD analysis and tensile modulus values.

3.1. Thermoplastic stability under melt mixing conditions

The preparation of nanocomposites based on thermoplastics and unfunctionalized MWNTs requires a combination of shear and residence time into the extruder to break the nanotube aggregates and to minimize the opportunity of reaggregation. Clay dispersion and separation of the aluminosilicate layers is likewise promoted by shear forces for polymer-clay blends enabling intercalation and exfoliation thanks to favorable interactions. Nevertheless, the process conditions must be carefully selected in order to avoid degradation of the nanofillers and of the polymer matrix that would affect the quality of the desired nanocomposites.

To assess degradation of the thermoplastic matrices under melt mixing, SEC measurements were performed on as received polymers and on polymers submitted to the compounding conditions used for nanocomposite processing. No significant change of the molar mass distribution is revealed by this technique as summarized in **Table 1** comparing the number average molar mass ($\overline{M}_n$), the weight average molar mass ($\overline{M}_w$) and the polydispersity index (PDI) of the pure phenoxy and PES thermoplastics before and after processing.

Table 1. Molar mass characteristics of phenoxy and PES before and after melt blending.

Thermoplastic / process conditions		PS equivalent $\overline{M}_n$ (g/mol)	PS equivalent $\overline{M}_w$ (g/mol)	PDI
Phenoxy (PKHP-200)	Before processing	11100	51500	4.6
	After extrusion 1 min at 220 °C - 300 rpm	11400	51300	4.5
PES	Before processing	24700	49400	2.0
	After compounding 5 min at 340 °C - 150 rpm	22900	50600	2.2

Even if effect of the nanofillers on possible polymer degradation is not taken into account by these measurements, the selected mixing conditions seem thus to guarantee thermoplastic stability during processing. Moreover, thermal decomposition of neat thermoplastics and nanocomposites was investigated by TGA to determine influence of MWNT and clay addition on thermal degradation. **Fig. 3** shows that the weight loss is initiated at temperatures much higher (around 200 °C higher) than the temperatures used for melt processing of the thermoplastics. For composites filled with Cloisite 30B, potential degradation of the quaternary alkylammonium surfactant of the clay during high temperature processing has also to be taken into account. Onset of the weight loss of the organomodified clay remains limited below 1 wt % during heating at 10 °C/min until 220 °C. Processing of Cloisite 30B with a phenoxy matrix is thus possible without significant degradation of the organic modifier but is prevented in PES requiring more severe processing conditions.

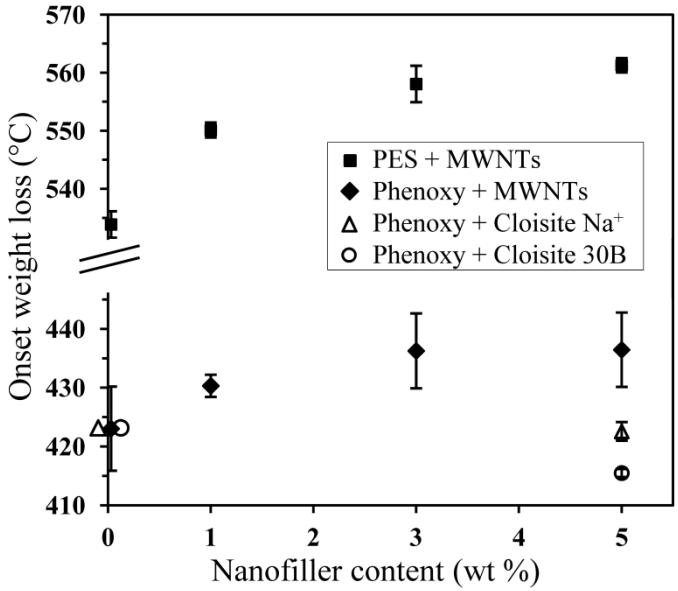

Fig. 3. TGA's onset temperature of weight loss as a function of nanofiller content dispersed in phenoxy (PKHP-200) and PES (pure thermoplastics, 1, 3 and 5 wt % MWNTs in both thermoplastics and 5 wt % pristine or organomodified clay in phenoxy).

Thermal stability of the nanocomposites filled with MWNTs is slightly enhanced compared to the neat thermoplastics. An increase of the onset temperature of weight loss, which reaches more than 15 °C in PES, is

observed by addition of 1 wt % MWNTs in both thermoplastics. Further increase of the onset temperature is observed when increasing the MWNT content to 3 or 5 wt %. Decomposition influenced by radical or radical-promoting species located on crushed nanotube surfaces and enhanced thermal stability of polymer matrices have been reported [34]. Moniruzzaman et al. [35] have suggested several explanations to justify the delay of degradation. The carbon nanotubes can hinder the flux of degradation products or the higher thermal conductivity in the nanocomposites can degrade the polymer more slowly near carbon nanotubes due to facilitated heat dispersion.

Clay also contributes to improve thermal stability in phenoxy nanocomposites [36] by reducing rate of heat release and by delaying its maximum value to higher temperatures. Indeed, diffusion of the volatile decomposition products out of the material is hindered by the layered silicates due to the tortuous path formed in the nanocomposite and due to enhanced performance of the char layer, which acts as an insulator and mass transport barrier. However, no increase of the initial decomposition temperature measured by TGA is evidenced with 5 wt % clay.

3.2. Dispersion state of MWNTs into phenoxy and PES

First, morphologies of the nanofilled phenoxy and PES in the form of pellets are presented in **Fig.4**, which shows TEM micrographs of the nanocomoposites at different MWNT concentrations (1, 3 and 5 wt %). A fine dispersion with individual MWNTs and a homogeneous distribution of the MWNTs in the polymer matrix are observed for all concentrations in both thermoplastics. The processing conditions are therefore suitable to overcome the strong attractive forces between MWNTs having both enthalpic and entropic origins and to disentangle native MWNTs synthesized as bundles. The entropy contribution to attraction between CNTs results from increase of the total conformational entropy for the bundle arrangements as compared to individualized carbon nanotubes due to the reduced number of conformational states for the macromolecules close to CNTs. The enthalpy contribution is due to high van der Waals (VDW) attractive forces between CNTs. For identical geometries of the MWNTs, interaction between two nanotubes depends only on the Hamaker constant, which is governed by the polarizability of the carbon nanotubes and the surrounding polymer matrix. Based the Lifshitz theory [37], the Hamaker

constant (*A*) can be expressed in terms of dielectric constant (ε) and refractive index (*n*) differences between MWNTs and polymer matrix as:

$$A = \frac{3}{4} k_B T \left(\frac{\varepsilon_{MWNTs} - \varepsilon_{polymer}}{\varepsilon_{MWNTs} + \varepsilon_{polymer}} \right)^2 + \frac{3h\nu_e}{16\sqrt{2}} \frac{\left(n^2_{MWNTs} - n^2_{polymer}\right)^2}{\left(n^2_{MWNTs} + n^2_{polymer}\right)^{3/2}}$$

where k_B is the Boltzmann constant, *T* is the temperature, *h* is the Planck constant, ε_{MWNTs} and $\varepsilon_{polymer}$ are the static dielectric constants of the MWNTs and the polymer, ν_e is the main electronic absorption frequency in the UV typically around $3*10^{15}$ s^{-1}, n_{MWNTs} and $n_{polymer}$ are the refractive indexes of the MWNTs and the polymer.

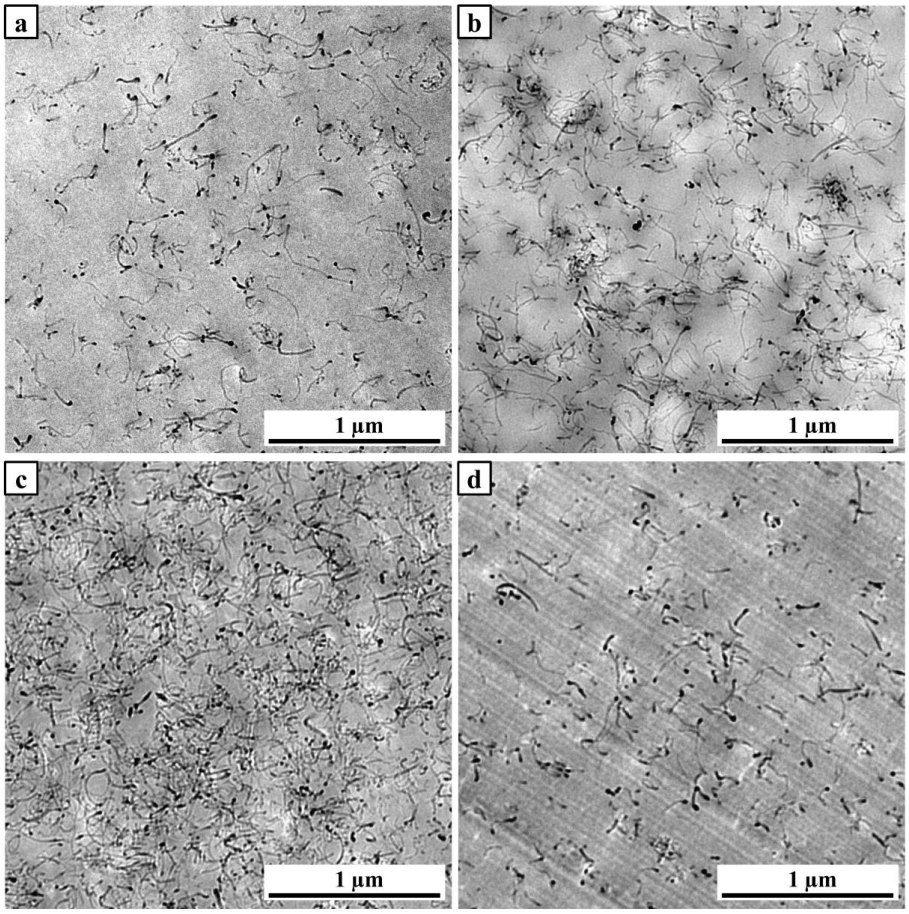

Fig. 4. TEM micrographs illustrating the dispersion of (a) 1 wt %, (b) 3 wt %, (c) 5 wt % MWNTs in phenoxy and (d) 1 wt % MWNTs in PES.

In order to disperse properly MWNTs in a polymer matrix, the value of the Hamaker constant has to be minimized to decrease the interaction energy between MWNTs. According to relatively high values of the transverse dielectric constant and refractive index of MWNTs [30], the VDW interactions between MWNTs are thus reduced in phenoxy or PES presenting dielectric constants and refractive indexes respectively of 3.8 and 1.6 for phenoxy [38] and 3.5 and 1.65 for PES [39-40] higher than other thermoplastic matrices like polyolefins. Therefore, the excellent dispersions of MWNTs observed in phenoxy and PES matrices are explained by these thermodynamic considerations combined with an adequate choice of moderate processing conditions providing the mixing energy required to disperse MWNTs while limiting reduction of their aspect ratio. Suitable screw rotation speed and mixing time along with adapted compounding temperature allow infiltration of the polymer chains into MWNTs agglomerates leading to MWNT dispersion by mechanisms of rupture and erosion of MWNT agglomerates [41].

The good dispersion state of MWNTs in both thermoplastics is also confirmed by the rheological analysis of the nanocomposites. The frequency dependence of the shear storage modulus *G'* and the damping factor $tan\ \delta = G''/G'$ are shown in **Fig. 5** for the neat thermoplastics and the nanocomposites, respectively at 200 °C for phenoxy and 290 °C for PES.
At high frequency, the response is not sensitive to the filler concentration. The short-range polymer dynamics remains unaffected since the local behavior of the macromolecules is not influenced by MWNTs. On the contrary, for low frequencies, the storage modulus increases in presence of MWNTs, particularly for high MWNTs contents, indicating a transition from a liquid-like viscoelastic behavior to a solid-like or gel-like behavior when *G'* becomes nearly independent of the frequency. This transition is also highlighted by the presence of a maximum for $tan\ \delta$.

In order to clearly evaluate the rheological percolation threshold, Van Gurp-Palmen plots, displaying the phase angle δ as a function of the complex modulus G* are presented in **Fig. 6**. For neat thermoplastic matrices, the phase angle approaches 90 ° at low complex modulus, indicating that the polymer acts like a viscous fluid. Comparatively, the significant decrease in phase angle observed for the nanocomposites containing 3 and 5 wt % MWNTs reveals an increasing elastic behavior (with a corresponding

equilibrium modulus of the elastic solid that can be determined by extrapolation of the phase angle to 0 °).

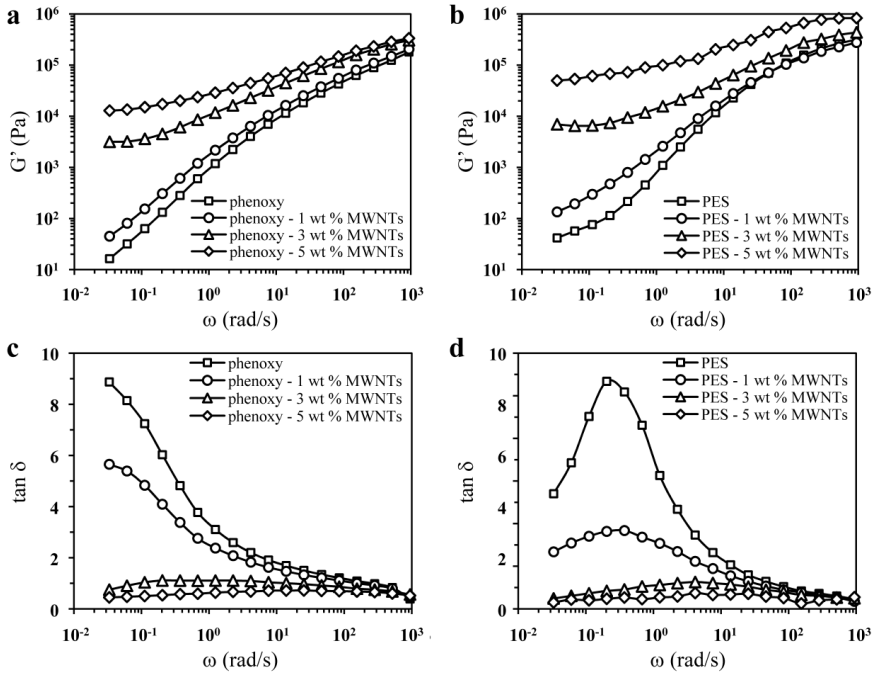

Fig. 5. Rheological properties of thermoplastics and nanocomposites filled with 1, 3 and 5 wt % MWNTs, respectively at 200 °C and 290 °C for phenoxy and PES matrices. Storage modulus (*G'*) of (a) phenoxy and (b) PES compounds and damping factor (*tan δ*) of (c) phenoxy and (d) PES compounds depending on angular frequency.

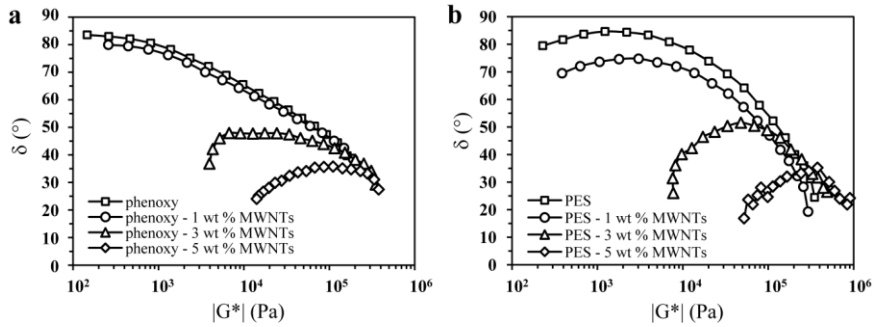

Fig. 6. Phase angle δ as a function of the absolute value of the complex modulus $|G^*|$ measured by shear rheometry (van Gurp-Palmen plot) for neat extruded thermoplastic and nanocomposite (1, 3 and 5 wt % MWNTs); (a) phenoxy compounds at 200 °C and (b) PES compounds at 290 °C.

The transition of the nanocomposite behavior above 3 wt % MWNTs is attributed to the formation of a three-dimensional percolating structure as in the case of polycarbonate and polyethylene matrices reinforced by CNTs [42-43]. Therefore, it can be concluded that the rheological percolation threshold under the selected process conditions is reached for a MWNT concentration comprised between 1 and 3 wt %, for which the MWNTs can hinder the polymer motion when the distance between two of them becomes lower than twice the gyration radius of the macromolecules.

The distance between MWNTs is shorter to reach the electrical percolation threshold than the rheological percolation threshold since a higher density of the MWNT network is required to allow the flow of electrons and achieve high conductivity levels [44]. Therefore, in order to determine electrical percolation threshold, electrical conductivity of the phenoxy-MWNT nanocomposites was measured in the microwave frequency range (40 MHz–40 GHz) using microstrip transmission lines. At low frequency, there is no physical contact between MWNTs for low amounts of MWNTs. The conductivity level remains therefore low as shown in **Fig. 7** presenting the real part of the conductivity (σ') depending on the frequency.

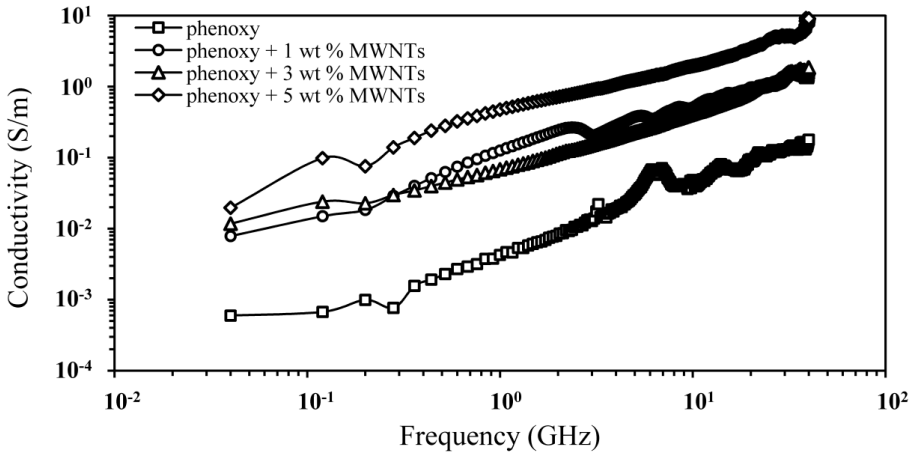

Fig. 7. Real part of the AC conductivity as a function of the MWNT concentration in phenoxy at 25 °C.

At high frequency, even in absence of a physical contact between MWNTs, electrical conductivity increases due to the capacitive coupling between carbon nanotubes when the distance between MWNTs is small as compared to the wavelength [33]. Whereas conductivity is approximately similar for 1

and 3 wt % MWNTs, the increase of conductivity observed for 5 wt % MWNTs on a wide range of frequencies means that electrons are permitted to flow through the sample due to the creation of a conductive pathway. The electrical percolation threshold seems thus to be reached between 3 and 5 wt % but the relatively high conductivity values measured for pure phenoxy prevent the presence of a sharp transition. Measurements at lower frequencies could be tested to evidence the percolation threshold with more accuracy by increasing the conductivity gap.

The low rheological and electrical percolation thresholds are due to the fine and homogeneous dispersion of the unmodified MWNTs into PES and phenoxy. Indeed, no reduction of the aspect ratio of the fillers due to agglomeration of the MWNTs was observed. Moreover, the dispersion was achieved without chemical functionalization, therefore avoiding disruption of the extended л conjugation and maintaining the electrical conductivity of individual CNTs [45].

The significant increase of the Young modulus of the nanocomposites reported in **Fig. 8** (28 % increase of the tensile modulus calculated from linear regression of the load-displacement curve for elongation between 0.05 % and 0.5 % when 5 wt % MWNTs are added to phenoxy) also derives from the fine MWNT dispersion.

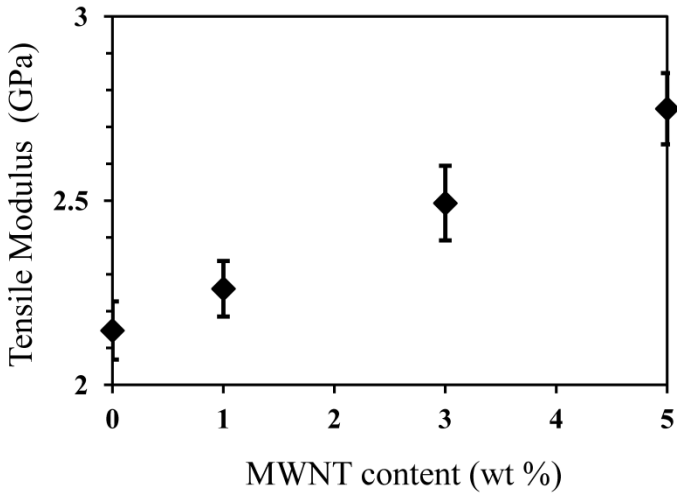

Fig. 8. Tensile modulus of phenoxy depending on the MWNT content dispersed by melt blending.

Indeed, due to their very high elastic modulus, it is well known that CNTs enhance the stiffness of nanocomposites [46-47]. The tensile modulus of polymers filled with CNTs generally increases with loading, dispersion and alignment of the CNTs and with interfacial interactions between the nanotubes and the matrix [35]. Therefore, the large interface created between thermoplastics and nanotubes by the good MWNT dispersion state in phenoxy and PES favors increase of the nanocomposite modulus.

3.3. Morphological state of pristine and organomodified clay into phenoxy

The morphologies of phenoxy extruded with 5 wt % clay are compared in **Fig. 9.a** and **Fig. 9.b** for composites containing Cloisite Na^+ and Cloisite 30B. Ineffective fragmentation of Cloisite Na^+ primary particles achieved in phenoxy is evidenced by a coarse dispersion of large aggregates. Only a moderate amount of tactoids or intercalated stacks composed of a large number of clay layers is sheared off from the primary particles during the extrusion process leading to formation of microcomposites. Some intercalation is evidenced by silicate layers peeling off from one end indicating diffusion of polymer macromolecules into clay galleries. Dispersion improved to some extent and slightly smaller stacks of Cloisite Na^+ are obtained thanks to water injection under high pressure and high temperature contributing to burst the clay aggregates into their tactoid subunits during the extrusion process. As compared to sodium montmorillonite, dispersion of the organomodified clay is clearly improved in the phenoxy matrix thanks to the strong interaction between Cloisite 30B and the polar phenoxy. A uniform dispersion of thin intercalated stacks containing few clay platelets and even of some exfoliated platelets of Cloisite 30 B is reached without use of important shear rate. The present study confirms thus results of Gurmendi et al. [27] having observed the same behavior. In the same way, **Fig. 9.c** and **Fig. 9.d** exhibit that mixed intercalated-exfoliated structures are achieved for phenoxy containing 10 and 15 wt % Cloisite 30B. These results show that phenoxy is an adequate matrix for producing polymer nanocomposite even with higher contents of modified clay. Mixing dynamics, injection of water during extrusion and molar mass of phenoxy were not found to have a significant role on dispersion of Cloisite 30B in phenoxy.

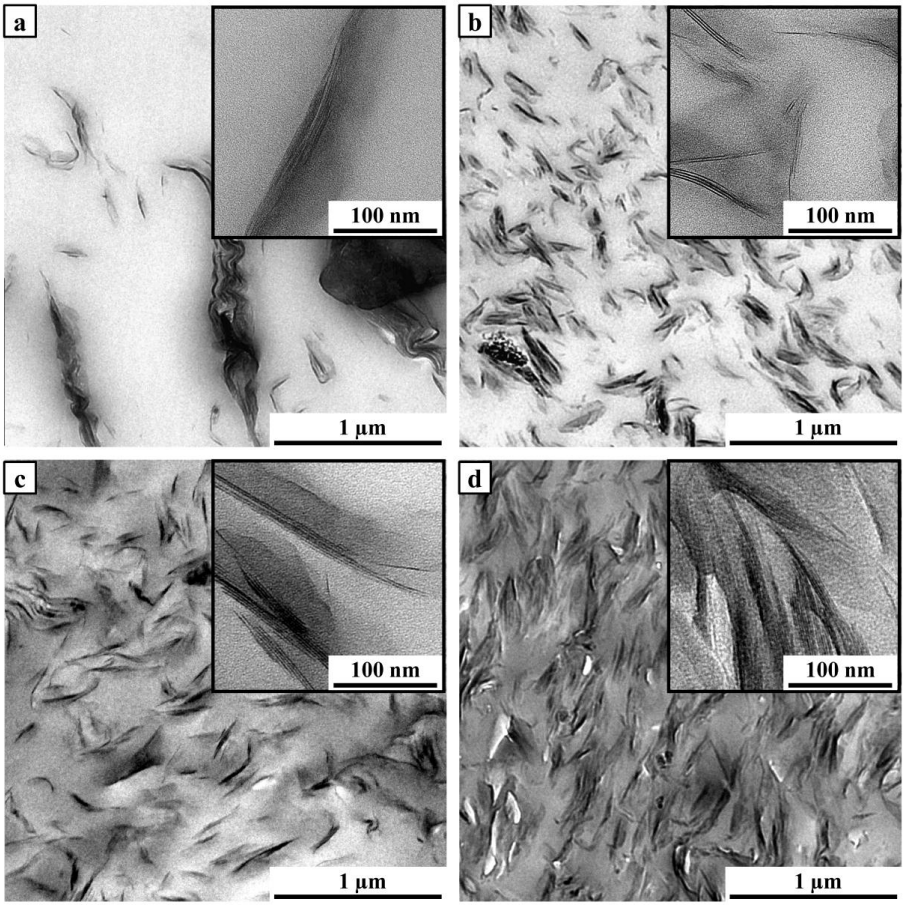

Fig. 9. TEM micrographs illustrating the dispersion of clays in phenoxy achieved by extrusion; (a) 5 wt % Cloisite Na^+ and (b) 5 wt % Cloisite 30B in PKHP-200, (c) 10 wt % and (d) 15 wt % Cloisite 30B in PKHB.

Cloisite Na^+ and Cloisite 30B were analyzed as received from the supplier by XRD such as phenoxy composites filled with 5 wt % of both clay types in order to determine the extent of phenoxy intercalation into the clay galleries. XRD patterns presented in **Fig. 10** show that sodium montmorillonite has a smaller basal spacing d_{001} than Cloisite 30B since no surfactant fills in the galleries between the silicate platelets of Cloisite Na^+. The diffraction peaks at 7.3 ° for Cloisite Na^+ and 4.8 ° for Cloisite 30B indicates that gallery distances are respectively around 12.1 Å and 18.4 Å before extrusion. The measured values are close to the supplier data of 11.7 Å and 18.5 Å [31-32]. Results from XRD characterization of the phenoxy-clay composites are in accordance with TEM observations. Indeed, the weak increase of the clay

interlayer spacing from 12.1 Å to 15.1 Å (2θ = 5.8) for Cloisite Na^+ into phenoxy is attributed to intercalation. Nevertheless, its extent remains limited because of the lack of affinity between the polymer matrix and the hydrophilic layers of the sodium montmorillonite making phenoxy little prone to intercalation in the clay galleries. For Cloisite 30B, the spectra display a shift of the first order peak from 4.8 ° to 2.8 ° upon melt processing corresponding to an increase of the clay interlayer spacing from 18.4 Å to 31 Å. This observation confirms the ability of phenoxy to produce intercalated structures like demonstrated by Gurmendi et al. [27]. The presence of second and third order diffraction peaks denotes an ordered morphology of the organoclay in phenoxy. Such an extent of phenoxy intercalation in the Cloisite 30B galleries is principally explained by the thermodynamic affinity between the phenoxy macromolecules and the polar modification of the clay layers presenting a structure with two hydroxyethyl groups, the preexisting increase of gallery height and the absence of collapse into the clay galleries during the process thanks to the selection of adapted process conditions preventing surfactant degradation. It can also be noticed that use of water injection during extrusion has not shown any effect on the intercalation extent of both clay types.

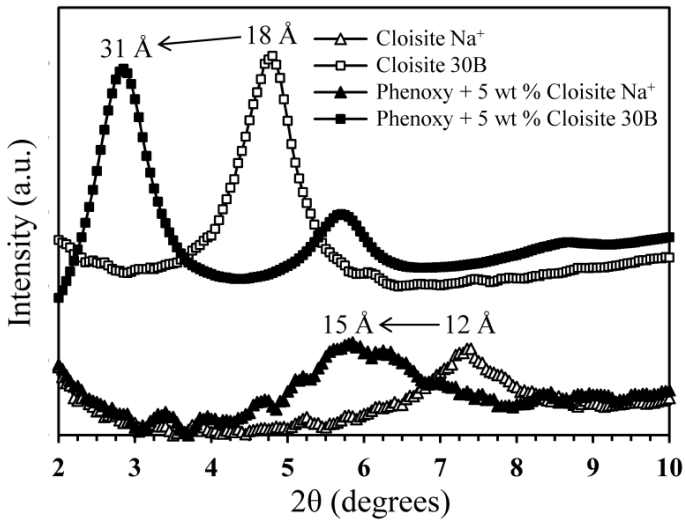

Fig. 10. XRD patterns of Cloisite Na^+, Cloisite 30B and phenoxy filled with 5 wt % of these clays.

Indirect evaluation of the clay dispersion in the phenoxy matrix was also performed as complement to TEM observations by measuring the modulus

of elasticity of the melt processed composites. Improved clay dispersion contributes to enhance the modulus as a large interfacial area increases the opportunity of clay particle-thermoplastic matrix interactions and reduces the mobility of the surrounding polymer [48] with as consequence higher stress being required to deform the material. The tensile modulus measured on injection-molded dog-bone specimens of phenoxy composites based on 5 wt % Cloisite Na^+ and Cloisite 30B are compared to neat phenoxy in **Fig. 11.a**. Higher tensile modulus of neat phenoxy measured for these specimens as compared to specimens exploited to assess MWNTs influence can be due to different process conditions that could lead to a stronger orientation of the polymer chains. The slight increase of the storage modulus with sodium montmorillonite reflects the poor quality of its dispersion in phenoxy. In contrast, 5 wt % Cloisite 30B are responsible for a substantial increase (around 50 %) of tensile modulus previously reported by Gurmendi et al. [27]. This result suggests an improved dispersion of the organomodified clay in phenoxy corroborating the morphologies observed by TEM.

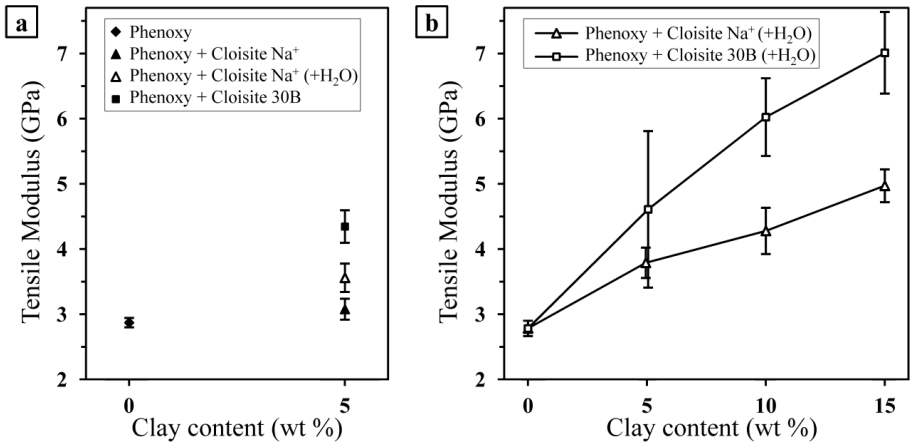

Fig. 11. Tensile modulus of (a) extruded phenoxy (PKHP-200) and composites with 5 wt % clay (Cloisite 30B and Cloisite Na^+ with and without water injection during extrusion at 300 rpm) and of (b) extruded phenoxy (PKHB) and composites (with water injection during extrusion at 200 rpm) depending on Cloisite Na^+ and Cloisite 30B concentration (0, 5, 10 and 15 wt %).

While influence of water injection during the extrusion process on the morphological state of Cloisite 30B presenting already an excellent dispersion is limited, the positive effect of water-assisted processing on

dispersion of Cloisite Na^+ in the phenoxy matrix is clearly verified by the tensile modulus measurements. Nevertheless, even with water injection, the modulus remains significantly lower for composites processed with sodium montmorillonite than with organomodified clay as confirmed in **Fig. 11.b** for filler concentrations up to 15 wt %. Despite the lower inorganic content (0.68 wt % of the total clay mass) of Cloisite 30 B dispersed in phenoxy, the elastic modulus of 7 GPa (more than 2.5 times higher than for neat phenoxy) reached with 15 wt % Cloisite 30B (around 10 wt % inorganic part) is considerably higher than the modulus around 5 GPa obtained with 15 wt % Cloisite Na^+.

4. Conclusions

This chapter demonstrates that nanocomposite can be prepared by dispersing unfunctionalized MWNTs or organomodified layered clay either in phenoxy for both nanofillers or in PES in the case of MWNTs.

Phenoxy and PES nanocomposites with homogeneous and fine MWNT dispersions were prepared with MWNT contents up to 5 wt % by melt blending. Soft melt mixing seems to be really promising for an industrial scale up as this process allows to overcome VDW attractive forces between MWNTs in these thermoplastic matrices without significant degradation of the constituent integrity. Beyond TEM observations, rheological and dielectric analyzes were performed on the nanocomposites such as tensile modulus measurements in order to confirm quality of the MWNT dispersion. Rheological percolation threshold has been identified between 1 and 3 wt % MWNTs in both polymers on basis of the transition in elastic melt properties while electrical percolation has been attributed to MWNT contents higher than 3 wt % in the phenoxy matrix.

Dispersion of pristine and organomodified clays achieved by melt processing in phenoxy has been likewise evaluated by TEM. Dispersion of organomodifed clay is clearly improved thanks to increase gallery height and interactions with the polar phenoxy as compared to sodium montmorillonite characterized by a coarse dispersion of large aggregates in the phenoxy matrix even if favored by water-assisted processing. Uniform dispersions of thin stacks of Cloisite 30B were achieved thanks to shear forces promoting dispersion of clay tactoids. Intercalation of phenoxy into the organomodified clay galleries has also been demonstrated by XRD. Mixed intercalated-

exfoliated structures were obtained for Cloisite 30B contents up to 15 wt % showing that phenoxy is an adequate matrix for nanocomposite production. Indirect measurements of clay dispersion leading to the same conclusions than for TEM observations have also been performed by evaluation of the tensile modulus of the melt processed composites.

Thanks to quality of the processed nanocomposite presenting excellent dispersion and homogeneous distribution of the nanofiller combined with solubility of phenoxy and PES matrices in epoxide-diamine formulations demonstrated in Chapter 2 and 3, dispersion of MWNTs or clay in epoxy resin simultaneously with thermoplastic incorporation in the resin could be considered by exploiting these nanofilled thermoplastics. Therefore, the next chapters aim to investigate ternary blends prepared by nanocomposite dissolution in epoxy resin and delivery of nanoparticles associated to interdiffusion between thermoplastic and resin precursors.

References

[1] Iijima S. Helical microtubules of graphitic carbon. Nature 1991;354:56-8.
[2] Usuki A, Kojima Y, Kawasumi M, Okada A, Fukushima Y, Kurauchi T, Kamigaito O. Synthesis of nylon 6-clay hybrid. Journal of Materials Research 1993;8(5):1179-84.
[3] Jin Z, Pramoda KP, Xu G, Goh SH. Dynamic mechanical behavior of melt-processed multi-walled carbon nanotube/poly(methyl methacrylate) composites. Chemical Physics Letters 2001;337:43-7.
[4] Zeng J, Saltysiak B, Johnson WS, Schiraldi DA, Kumar S. Processing and properties of poly(methyl methacrylate)/carbon nano fiber composites. Composites Part B: Engineering 2004;35:173-8.
[5] Haggenmueller R, Gommans HH, Rinzler AG, Fischer JE, Winey KI. Aligned single-wall carbon nanotubes in composites by melt processing methods. Chemical Physics Letters 2000;330:219-25.
[6] Chen L, Pang XJ, Yu ZL. Study on polycarbonate/multi-walled carbon nanotubes composite produced by melt processing. Materials Science and Engineering: A 2007; 457:287-91.
[7] Pötschke P, Fornes TD, Paul DR. Rheological behavior of multiwalled carbon nanotube/polycarbonate composites. Polymer 2002;43:3247-55.
[8] Pötschke P, Bhattacharyya AR, Janke A. Melt mixing of polycarbonate with multiwalled carbon nanotubes: microscopic studies on the state of dispersion. European Polymer Journal 2004;40:137-48.

[9] Pegel S, Pötschke P, Petzold G, Alig I, Dudkin SM, Lellinger D. Dispersion, agglomeration, and network formation of multiwalled carbon nanotubes in polycarbonate melts. Polymer 2008;49:974-84.
[10] Hasan MM, Zhou Y, Jeelani S. Thermal and tensile properties of aligned carbon nanofiber reinforced polypropylene. Materials Letters 2007;61:1134-6.
[11] Liu TX, Phang IY, Shen L, Chow SY, Zhang WD. Morphology and mechanical properties of multiwalled carbon nanotubes reinforced nylon-6 composites. Macromolecules 2004;37:7214-22.
[12] Tang W, Santare MH, Advani SG. Melt processing and mechanical property characterization of multi-walled carbon nanotube/high density polyethylene (MWNT/HDPE) composite films. Carbon 2003;41(14):2779-85.
[13] Lepoittevin B, Devalckenaere M, Pantoustier N, Alexandre M, Kubies D, Calberg C, Jérôme R, Dubois P. Poly(ε-caprolactone)/clay nanocomposites prepared by melt intercalation: mechanical, thermal and rheological properties. Polymer 2002;43(14):4017–23.
[14] Yoon PJ, Hunter DL, Paul DR. Polycarbonate nanocomposites. Part 1. Effect of organoclay structure on morphology and properties
Polymer 2003;44(18):5323–39.
[15] Zheng X, Wilkie CA. Nanocomposites based on poly (ϵ-caprolactone) (PCL)/clay hybrid: polystyrene, high impact polystyrene, ABS, polypropylene and polyethylene. Polymer Degradation and Stability 2003;82(3):441-50.
[16] Pegoretti A, Kolarik J, Peroni C, Migliaresi C. Recycled poly(ethylene terephthalate)/layered silicate nanocomposites: morphology and tensile mechanical properties. Polymer 2004;45(8):2751–9.
[17] Tanoue S, Utracki LA, Garcia-Rejon A, Tatibouet J, Cole KC, Kamal MR. Melt compounding of different grades of polystyrene with organoclay. Part 1: Compounding and Characterization. Polymer Engineering and Science 2004;44(6):1046–60.
[18] Utracki LA. Clay-Containing Polymeric Nanocomposites. Rapra Technology Limited: Shawbury, UK, 2004.
[19] Dhakal HN, Zhang ZY, Richardson MOW. Nanoindentation behaviour of layered silicate reinforced unsaturated polyester nanocomposites. Polymer Testing 2006. 25(6):846-52.
[20] Fedullo N, Sclavons M, Bailly C, Lefebvre JM, Devaux J. Nanocomposites from untreated clay: A myth? Macromolecular Symposia 2006;233(1):235-45.
[21] Lei SG, Hoa SV, Ton-That MT. Effect of clay types on the processing and properties of polypropylene nanocomposites. Composites Science and Technology 2006;66(10):1274-9.
[22] Peprnicek T Kalendova A, Pavlova E, Simonik J, Duchet J, Gerard JF. Poly(vinyl chloride)-paste/clay nanocomposites: Investigation of thermal and morphological characteristics. Polymer Degradation and Stability 2006;91(12):3322-9.

[23] Samyn F, Bourbigot S, Jama C, Bellayer S, Nazare S, Hull R, Fina A, Castrovinci A, Camino G. Characterisation of the dispersion in polymer flame retarded nanocomposites. European Polymer Journal 2008;44(6):1631-41.
[24] Mainil M, Urbanczyk L, Calberg C, Germain A, Jerome C, Bourbigot S, Devaux J, Sclavons M. Morphology and properties of SAN-clay nanocomposites prepared principally by water-assisted extrusion. Polymer Engineering and Science 2010;50(1):10-21.
[25] Rousseaux DDJ, Sallem-Idrissi N, Baudouin AC, Devaux J, Godard P, Marchand-Brynaert J, Sclavons M. Water-assisted extrusion of polypropylene/clay nanocomposites: A comprehensive study. Polymer 2011;52(2):443-51.
[26] Goh HW, Goh SH, Xu GQ, Pramoda KP, Zhang WD. Dynamic mechanical behavior of in situ functionalized multi-walled carbon nanotube/phenoxy resin composite. Chemical Physics Letters 2003;373:277-83.
[27] Gurmendi U, Eguiazabal JI, Nazabal J. Structure and properties of a new polymer nanocomposite based on poly (hydroxy ether of bisphenol A) matrix. Composites Science and Technology 2006;66(10):1221-8.
[28] Villmow T, Kretzschmar B, Pötschke P. Influence of screw configuration, residence time, and specific mechanical energy in twin-screw extrusion of polycaprolactone/multi-walled carbon nanotube composites Composites Science and Technology 2010;70:2045-55.
[29] Nanocyl^{TM} NC 7000 technical datasheet (Nanocyl).
[30] Baudouin AC. Dispersion of carbon nanofillers in mono- and biphasic polymer matrices. Thermodynamic versus kinetic control and influence on high-frequency electrical properties. PhD Thesis Université catholique de Louvain 2011.
[31] Cloisite® Na^+ product bulletin (Southern Clay Products).
[32] Cloisite® 30B product bulletin (Southern Clay Products).
[33] Saib A, Bednarz L, Daussin R, Bailly C, Lou X, Thomassin, JM, Pagnoulle C, Detrembleur C, Jerome R, Huynen I. Carbon nanotube composites for broadband microwave absorbing materials. IEEE Transactions on Microwave Theory and Techniques 2006;54:2745-54.
[34] Schartel B, Braun U, Knoll U, Bartholmai M, Goering H, Neubert D, Pötschke P. Mechanical, thermal, and fire behavior of bisphenol A polycarbonate/multiwall carbon nanotube nanocomposites, Polymer Engineering and Science 2008;48:149-58.
[35] Moniruzzaman M, Winey KI, Polymer nanocomposites containing carbon nanotubes, Macromolecules 2006;39:5194-205.
[36] Cordenier F, Bailly C, Berben R, Dumont D, Henry E, Sclavons M, Van Velthem P, Daoust D. Phenoxy nanocomposites with improved mechanical, fire, and electrical performance. Poster JEC Composites show Paris 2011.
[37] Lifshitz EM. The theory of molecular attraction forces between solid bodies. Journal of Experimental and Theoretical Physics 1955;29:94-110.
[38] http://www.phenoxy.com/technical-data/inchem_properties.html.
[39] Radel® A datasheet (Solvay Advanced Polymers).

[40] http://www.goodfellowusa.com/A/Polyethersulfone.html.
[41] Kasaliwal GR, Pegel S, Göldel A, Pötschke P, Heinrich G. Analysis of agglomerate dispersion mechanisms of multiwalled carbon nanotubes during melt mixing in polycarbonate. Polymer 2010;51(12):2708-20.
[42] Pötschke P, Abdel-Goad M, Alig I, Dudkin S, Lellinger D. Rheological and dielectrical characterization of melt mixed polycarbonate-multiwalled carbon nanotube composites. Polymer 2004;45:8863-70.
[43] Nobile MR, Simon GP, Valentino O, Morcom M. Rheological and structure investigation of melt mixed multi-walled carbon nanotube/PE composites. Macromolecular Symposia 2007;247:78-87.
[44] Du F, Scogna RC, Zhou W, Brand S, Fischer JE, Winey KI. Nanotube networks in polymer nanocomposites: rheology and electrical conductivity. Macromolecules 2004; 37:9048-55.
[45] Tjong SC, Liang GD, Bao SP. Effects of cristallization on dispersion of carbon nanofibers and electrical properties of polymer nanocomposites. Polymer Engineering and Science 2008;48:177-83.
[46] Thostenson ET, Ren Z, Chou TW. Advance in the science and technology of carbon nanotubes and their composites: a review. Composites Science and Technology 2001;61:1899-912.
[47] Coleman JN, Khan U, Blau WJ, Gun'ko YK. Small but strong: A review of the mechanical properties of carbon nanotube-polymer composites. Carbon 2006;44:1624-52.
[48] Chisholm BJ, Moore RB, Barber G, Khouri F, Hempstead A, Larsen M, Olson E, Kelley J, Balch G, Caraher J. Nanocomposites derived from sulfonated poly(butylene terephtalate). Macromolecules 2002;35:5508-16.

Chapter 5

TERNARY BLENDS OF EPOXY RESIN AND PHENOXY NANOCOMPOSITES FILLED WITH CARBON NANOTUBES OR ORGANOMODIFIED CLAY

Abstract

This chapter demonstrates that nanocomposites processed with unfunctionalized multiwalled carbon nanotubes (MWNTs) or organomodified layered clay and a thermoplastic soluble in epoxide and diamine resin precursors like poly(hydroxyether of bisphenol A) (phenoxy) can be used for simultaneous dispersion of a ductile polymer phase and nanoparticles in epoxy resin. After nanofiller predispersion achieved in phenoxy by melt blending (see Chapter 4), the investigated concept aims to dissolve the produced nanocomposite in epoxy resin in order to obtain a homogeneous blend and afterwards the projected microstructure, once reaction induced phase separation (RIPS) takes place.

First, microstructures of ternary blends prepared by thermal dissolution of phenoxy filled with MWNTs into RTM6 resin are inspected. Location of MWNTs in the epoxy resin-rich phase and preservation of the MWNT

dispersion are evidenced in the different blends. The mechanism leading to location of MWNTs exclusively in the epoxy rich phase of the ternary blend is then discussed on basis of thermodynamic predictions and other kinetic considerations like adsorption of phenoxy chains on the MWNT surface. Finally, the possibility to similarly exploit phenoxy as nanocomposite matrix for dispersion of other nanofillers such as organomodified clay platelets in epoxy resin is demonstrated as well as its positive impact on blend modulus.

1. Introduction

Phenoxy has already demonstrated a positive effect on properties of epoxy resin. As a result of the blend microstructure generated by the phase separation induced during resin curing by the thermoplastic, toughening of the thermoset network has been evidenced without compromising other characteristics of the crosslinked resin for adapted thermoplastic concentrations [1-4].

Nevertheless, additional improvements of epoxy resin performances have also been largely researched by dispersion of nanoparticles in the reactive resin formulation. Due to their high aspect ratio combined with their outstanding properties, carbon nanotubes discovered in 1991 by Sumio Iijima [5] have demonstrated their benefit on fracture toughness [6-11] or electrical conductivity [6,12-14] of epoxy resin even at very low content for optimized dispersion. Similarly, since researchers have discovered the possibility to produce a nanocomposite with layered silicates [15], remarkable improvement of thermal stability [16-17], mechanical performances [9,18-22] and fluid barrier properties [23-24] have been achieved for nanocomposites with exfoliated or at least intercalated morphologies as compared to neat epoxy resin or conventional composites by well dispersing montmorillonite clay layers in the thermoset matrix.

The present work aspires thus to simultaneously introduce nanofillers and a thermoplastic phase into epoxy resin in order to benefit from effects of both additives on the system properties. Ternary blends based on epoxy resin and both nanofiller and thermoplastic additives have been rarely considered previously. Asif et al. [25] have studied a toughened epoxy resin prepared by mixing successively poly(ether sulfone) (PES), clay and diamine hardener in difunctional epoxide but epoxy resin blended with nanofillers and phenoxy has not been examined. Therefore, an innovative method is investigated in this chapter to prepare ternary blends by dissolution of a phenoxy-matrix nanocomposite into epoxy resin. This two-step procedure requires preparation of a nanocomposite prior to its dissolution in epoxy resin. The potential of this original approach to disperse individualized lamellar or tubular nanoparticles together with a thermoplastic phase generated by RIPS is evaluated into a widespread epoxy resin like HexFlow® RTM6 resin developed for aerospace applications. The selected thermoplastic is phenoxy since it enables proper dispersion and homogeneous distribution of both

unfunctionalized MWNTs and organomodified clay by melt blending (see Chapter 4) and allows blend preparation by thermal dissolution into epoxide-diamine resin formulations (see Chapters 1 to 3). An additional advantage of this processing method combining nanofiller and thermoplastic incorporation into epoxy resin is that difficulty to disperse directly nanoparticles in low viscosity resin is prevented thanks to predispersion in phenoxy.

This chapter first explores location and dispersion state of MWNTs in ternary blends produced by thermal dissolution of a phenoxy nanocomposite into RTM6 resin. The mechanism controlling MWNT location in the phenoxy-epoxy resin blend is then discussed on basis of thermodynamic predictions and kinetics limitations. Finally, microstructures of ternary blends prepared with nanocomposites filled with organomodified clay dissolved into RTM6 resin are presented and influence of the nanocomposite content on the blend modulus is described.

2. Experimental

2.1. Materials

Nanocomposites prepared with phenoxy are considered to disperse nanofillers into HexFlow® RTM6 monocomponent epoxy resin from Hexcel specifically developed to fulfill the requirements of the aerospace industry in advanced RTM process.

The first kind of nanocomposite investigated is phenoxy (InChemRez® Phenoxy Resin PKHP-200 from InChem Corporation) filled with 3 or 5 wt % unfunctionalized MWNTs Nanocyl™ NC7000 (Nanocyl S.A., Belgium). These unpurified MWNTs produced via catalytic carbon vapor deposition are synthesized as bundles of highly agglomerated nanotubes with a purity of 90 %, an average diameter of 9.5 nm and average length of 1.5 μm (aspect ratio higher than 150). Their surface area is between 250 and 300 m^2/g [26] and their average number of graphene layers is 8 [27]. The chemical nature of the MWNT surface determined by X-ray photoelectron spectroscopy (XPS) [27] is reported in **Table 1**. The analysis has evidenced that MWNTs are almost exclusively composed of carbon while the presence of oxygen is very weak and consequently, prevents evaluation of the chemical functions located on the MWNT surface. Moreover, presence of aluminum indicates that at least part of oxygen is linked to it and that functional groups are

nearly absent on the MWNT surface. Phenoxy previously dried during 24 hours at 80 °C under vacuum was melt-processed with MWNTs in a DSM Xplore 15 ml micro-compounder at 220 °C with a speed of the corotating twin screws of 150 rotations per minute (rpm). After the 5 minute recirculation period, the nanofilled compound was expelled through a 5 mm diameter circular die. A fine dispersion of individualized MWNTs and their homogeneous distribution in phenoxy has been shown in Chapter 4.

Table 1. Chemical composition of the MWNT surface (XPS analysis) [27].

Element	Electronic level	Energy (eV)	Molar fraction (%)
O	O 1s	533.2	0.5
C	C 1s	284.8	99.2
Al	Al 2p	76.9	0.3

The second kind of nanocomposites used for RTM6 resin modification was prepared with dried phenoxy (InChemRez® Phenoxy Resin PKHB from InChem Corporation) and 10 wt %. organomodified clay (Cloisite® 30B from Southern Clay Products), a montmorillonite modified by methyl, tallow, bis(2-hydroxylethyl), quaternary ammonium cations (90 meq/100 g). The average distance between aluminosilicate layers of Cloisite 30B is 18.5 Å and the average particle size is 6 µm [28]. A co-rotating extruder Krupp WP ZSK25 WLE from Coperion was used to prepare nanocomposites at 220 °C with water injection at 40 ml/min. The screw speed was 200 rpm yielding to a residence time in the extruder of about 1 minute. The dispersion of clay platelets and the intercalated-exfoliated structure of the nanocomposites have been reported in chapter 4.

2.2. Preparation of ternary blends (RTM6 resin and nanocomposite)

Preparation of ternary blends based on RTM6 resin, phenoxy and nanofillers was achieved by solvent-assisted or thermal dissolution and homogenization of nanocomposite powder obtained by mechanical grinding in reactive resin. For phenoxy filled with MWNTs, thermal dissolution of the nanocomposite was performed into RTM6 resin without use of solvent at 140 °C before important resin crosslinking for 20 and 30 wt % of phenoxy filled with 3 wt % MWNTs and with 50 wt % phenoxy filled with 5 wt % MWNTs. Curing of the modified resin samples was then continued at this temperature until

gel time of the resin (95 minutes). For phenoxy filled with organomodified clay, dissolution of the nanocomposite in RTM6 resin was achieved at room temperature under stirring in tetrahydrofuran (THF, unstabilized grade for HPLC from BioSolve BV) with various contents (10, 20 and 30 wt %) of phenoxy filled with 10 wt % Cloisite 30B. Reference blends without filler were similarly produced with neat phenoxy. Curing of these samples was then completed after solvent evaporation and resin degassing at 90 °C following a thermal cycle adapted to RTM process at a 1 °C/min heating rate from 80 to 180 °C with an intermediate isotherm of 30 minutes at 120 °C and a post-cure of 120 minutes at 180 °C. Thermal dissolution was preferred in the first case to evidence effect of thermal treatment on the MWNTs location in ternary blends without interference due to use of solvent even if to the detriment of blend homogeneity. In contrast, a solvent-assisted dissolution was chosen in the second case to optimize the homogenization stage before curing of the samples filled with clay.

A Soxhlet device was used in order to determine the MWNT location in such polymer blends by extracting the phenoxy-rich phase from the blend of 50 wt % epoxy resin and 50 wt % phenoxy filled with 5 wt % MWNTs. The extraction was performed at 50 °C during 24 hours using 200 ml dichloromethane (unstabilized grade for HPLC from BioSolve BV) for 500 mg of crushed sample deposited in the glass fiber thimble.

2.3. Characterization methods

2.3.1. Transmission electron microscopy (TEM)

Blend morphologies were examined by means of TEM by cutting ultrathin sections of approximately 95 nm in thickness with a Reichert Microtome using a histodiamond knife with a cut angle of 45 ° from Diatome at ambient temperature. The ultrathin sections were subsequently collected on 300 mesh copper grids and inspected with a LEO 922 transmission electron microscope operating at 200 kV.

2.3.2. Thermogravimetric analysis (TGA)

MWNTs were extracted from nanocomposites filled with 5 wt % MWNTs with the help of a Soxhlet device with boiling dichloromethane operating during 24 hours. TGA measurements were then performed at a heating rate

of 5 °C/min on the extracted MWNTs and phenoxy such as on pristine MWNTs. The weight loss of samples of about 15 mg was followed from 25 to 800 °C under dry air with a flow rate of 50 ml/min using a Mettler Toledo TGA/SDTA 851e.

2.3.3. Dynamic mechanical analysis (DMA)

Samples of RTM6 resin modified with 10, 20 and 30 wt % phenoxy containing 10 wt % Cloisite 30B were analyzed in three-point bending mode on a DMA/STDA 861e from Mettler Toledo. Specimens were cured in silicone molds (Elastomould 90 mm x 48 mm x 30 mm from de Buyer) under a 1°C/min temperature ramp from 80 to 180 °C with an intermediate isotherm of 30 minutes at 120 °C. After post-curing during 2 hours at 180 °C, rectangular bars measuring approximately 60 mm × 10 mm x 2 mm were cut by a diamond saw and subsequently analyzed at an oscillation frequency of 1 Hz. Data were collected from room temperature to 250 °C at a scanning rate of 3 °C/min and results were averaged on 5 samples. A 3 N pre-stressing was applied to the specimens (45mm) and maximal 10 µm displacement and 0,1 N force were imposed in order to be located in the linear stress-strain domain.

3. Results and discussion

Ternary blends prepared with RTM6 resin and nanocomposites filled with MWNTs are first examined. Location of MWNTs in the polymer blend is inspected and microstructures are observed in order to determine if dissolution of the produced nanocomposites allows dispersion of both thermoplastic phase and MWNTs in epoxy resin. Mechanisms controlling MWNT location in the ternary blends are then discussed. Finally, influence of a nanocomposite filled with organomodified clay on the blend morphology and modulus is also investigated.

3.1. RTM6 resin-phenoxy-MWNTs ternary blends

3.1.1. Blend morphology

The fine dispersion and the homogeneous distribution of MWNT achieved in phenoxy makes the nanocomposites prepared by melt blending suitable for testing as a means to incorporate a thermoplastic phase in epoxy resin

simultaneously with dispersion of the MWNTs in the resulting polymer blend. Indeed, thanks to MWNT predispersion in phenoxy combined to swelling and dissolution of the phenoxy matrix into epoxide-diamine formulations during thermal treatment (see Chapters 2 and 3), the processed nanocomposites should allow dissemination of individualized MWNTs in the epoxy resin-thermoplastic blend prior to reaction induced phase separation (RIPS). Moreover, MWNT location in the immiscible blend once phase separation has taken place is undeniably an important feature for exploitation of the nanocomposite since it plays a considerable role on the resulting system properties. Therefore, in order to determine MWNT location and dispersion state in ternary blends, solvent extractions and TEM observations were performed on blends composed of RTM6 resin, phenoxy and MWNTs obtained by thermal dissolution of the nanocomposites.

MWNT location was examined for RTM6 resin blended with 50 wt % phenoxy filled with 5 wt % MWNTs after curing at 140 °C. Since such a phenoxy content leads to phase inverted morphologies (see Chapter 1), dissolution of the continuous phenoxy phase in the dichloromethane solvent occurs during extraction with the help of a Soxhlet device. In contrast with pristine MWNTs migrating rapidly towards the bottom of a flask filled with dichloromethane (**Fig. 1.a**), MWNTs from the ternary blend remain at the top, in insoluble epoxy resin inclusions (**Fig. 1.b**) while the phenoxy phase precipitated in methanol doesn't show presence of MWNTs (**Fig. 1.c**). These results evidence that MWNTs initially dispersed in phenoxy are located in the epoxy resin-rich phase of the blend after RIPS.

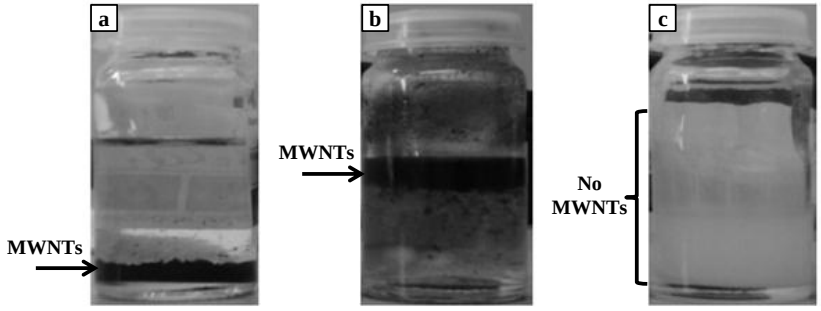

Fig. 1. Images of (a) pristine MWNTs in dichloromethane, (b) insoluble part of a ternary blend (50 wt % epoxy resin and 50 wt % phenoxy filled with 5 wt % MWNTs) in dichloromethane after Soxhlet extraction with boiling dichloromethane and (c) soluble part of the ternary blend precipitated in methanol.

TEM observations of ternary blends aim on the one hand to confirm the preferential location of MWNTs in the epoxy resin-rich phase and on the other hand to determine if dispersion of the MWNTs is maintained. TEM micrographs of RTM6 resin blended with nanocomposite based on phenoxy filled with 3 wt % MWNTs are presented in **Fig. 2**. Below the critical composition of the RTM6 resin-phenoxy blend, for phenoxy contents around 20 wt %, both phenoxy inclusions and MWNTs are dispersed in the continuous epoxy resin matrix. The presence of some larger phenoxy-rich inclusions with secondary phase separation subsisting locally in the blend should be due to lack of composition homogeneity in this kind of high viscosity specimens prepared with nanocomposite in the form of powder. A selective location of individualized MWNTs in the RTM6 resin-phenoxy blend is clearly evidenced when higher nanocomposite concentrations are incorporated in the reactive resin producing a continuous phenoxy phase like in the case of the co-continuous morphology generated with around 30 wt % nanofilled phenoxy. Indeed, the MWNTs initially dispersed in phenoxy are exclusively located in the darker phase of the blend corresponding to the epoxy resin-rich phase after phase separation. Moreover, MWNTs are well dispersed and seems homogeneously distributed in the epoxy resin-rich phase. These results confirm that nanocomposites made of a soluble phenoxy matrix can be exploited to disperse MWNTs in epoxy resin since MWNT dispersion is preserved in the phase separated blends.

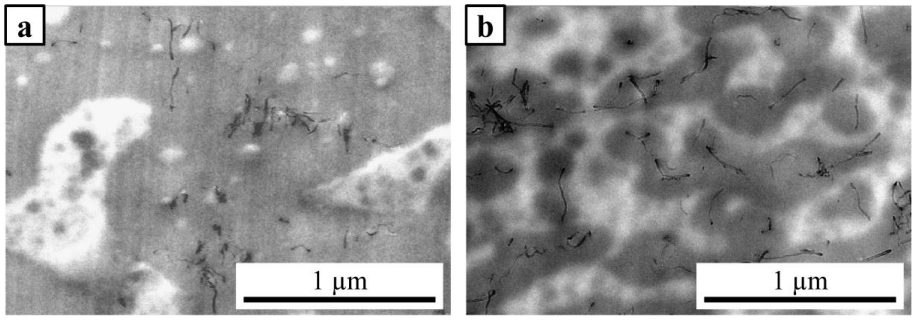

Fig. 2. TEM micrographs of (a) 20 wt % and (b) 30 wt % phenoxy filled with 3 wt % MWNTs blended with RTM6 resin (dark phase: mainly epoxy resin, bright phase: mainly phenoxy).

3.1.2. Mechanisms controlling MWNT location in ternary blends

Location of MWNTs in the epoxy resin-rich phase results from competition between thermodynamic and kinetic factors. Indeed, MWNT location

depends on the one hand on interactions between the nanotubes and both thermoplastic chains and epoxy resin and on the other hand on other considerations like viscosities of both phases or partially irreversible adsorption of thermoplastic on the MWNT surface during the melt blending sequence. The driving force for the apparent MWNT migration is the minimization of the interfacial energy of the blend. Location of MWNTs in immiscible polymer blends is a consequence of convection of the molten thermoplastic chains and mainly of the resin precursors leading to apparent MWNT migration during phase separation while self diffusion of the nanotubes by Brownian motion remains very limited under static conditions.

The equilibrium position of nanofillers in blends of immiscible polymers can be predicted using thermodynamics through evaluation of interactions between the surface of the nanoparticules and the polymers. According to Young's equation [29], the position of MWNTs minimizing interfacial energy depends on the wetting coefficient

$$\omega = \frac{\gamma_{MWNTs-epoxy\,resin} - \gamma_{MWNTs-TP}}{\gamma_{TP-epoxy\,resin}}$$

where $\gamma_{MWNTs-epoxy\,resin}$, $\gamma_{MWNTs-TP}$ and $\gamma_{TP-epoxy\,resin}$ are respectively the interfacial energies between MWNTs and epoxy resin, between MWNTs and thermoplastic and between thermoplastic and epoxy resin. Assuming that dispersive part (γ_d) and polar part (γ_p) of the surface energies ($\gamma = \gamma_d + \gamma_p$) of both polymers and MWNTs are precisely known, interfacial energies and consequently wetting coefficient are assessable [27] and allow consequently theoretical prediction of the equilibrium position of the nanotubes. Depending on the wetting coefficient value, MWNTs will be preferentially located in thermoplastic (ω > 1), in epoxy resin (ω < -1) or at the interface between the two polymer phases (-1 < ω < 1). Total surface energy and polarity (γ_p / γ) of respectively 30.9 mJ m^{-2} and 0.001 have been measured for the MWNTs without surface functionalization (**Table 1**) used in this study [30]. Surface energies of 41.9 mJ m^{-2} (polarity of 0.6) [31] and of 32 mJ m^{-2} (no indication about polarity) [32] have been respectively reported for phenoxy and for RTM6 resin. These few data found in literature allow prediction of the MWNT location in RTM6 resin, which corroborates TEM observations, considering the limited polarity of epoxy resin as compared to phenoxy. Concerning another thermoplastic like PES, its lower

polarity of 0.149 (total surface energy of 47 mJ m^{-2}) [33] should lead to localization of MWNTs in the RTM6 resin phase or at the interface.

Nevertheless, thermodynamical predictions must be handled carefully due to uncertainties on surface tension values of both MWNTs and polymers. On the one hand, accurate measurement of surface tension of nanoparticles is complicated and although MWNTs are apolar objects, very different values are reported in the literature with non-negligible polar contributions [27]. On the other hand, definition of the polymer surface tensions is complex due to difficulty of extrapolation of values measured at room temperature to higher temperature and to polymer phases not composed of pure thermoplastic or epoxy resin. Complexity is further increased for polymer blends composed of a thermoset resin generating RIPS during the cure. Indeed, conversion influences surface tension of epoxy resin [34] and since reactive epoxide-diamine formulations are composed of at least two low molecular weight precursors able to migrate toward the blend interface, local segregation is potentially induced in such systems.

Moreover, thermodynamic predictions based on evaluation of the surface tension of neat polymers and MWNTs are not sufficient to predict location of the latter in polymer blends. Indeed, deviations between the expected morphology, based on the trends provided by wetting coefficient assessment, and the observed microstructure can occur [27]. General mechanism controlling final MWNT location in immiscible polymer blends is far from trivial and depends on many different factors.

Differences with experimental observations can partially be explained by kinetic limitations due to high viscosities of both polymer phases hindering diffusion when phase separation is initiated by the crosslinking reaction in thermoset-thermoplastic blends. As apparent MWNT migration is limited, their location depends thus also on the size of the polymer phases and on the phase separation mechanism by spinodal decomposition or nucleation and growth.

Phenomena of coating and wrapping of the MWNTs by thermoplastic chains during the melt blending sequence must also be taken into account as at least partially irreversible polymer adsorption can modify surface energy of the MWNTs. Baskaran et al. [35] have highlighted that non-covalent and non-specific adsorption occurs irrespective of the polymer nature through

interaction of polymer methyl groups with the MWNT surface. Electrostatic and/or van der Waals (VDW) forces induce polymer wrapping around MWNTs through CH-π interactions and, for polymer containing aromatic rings like phenoxy and PES, π–π stacking formed with the graphitic sidewalls of MWNTs [36-37].

In order to demonstrate phenoxy adsorption at the MWNT surface, extraction was performed on nanocomposite filled with 5 wt % MWNTs using a Soxhlet device with boiling dichloromethane during 24 hours. Adsorption of phenoxy on the unfunctionalized MWNTs is evidenced in **Fig. 3** presenting evolution of the relative mass of MWNTs extracted from the nanocomposite and of its derivative measured by TGA during heating at 5 °C/min under air atmosphere. Comparison with the weight loss of extracted phenoxy and of as produced MWNTs allows to attribute the two transitions occurring around 320 °C and 550 °C for extracted MWNTs respectively to degradation of phenoxy not extracted from the MWNT surface and to MWNT oxidation. The phenoxy fraction not removed from the nanocomposite demonstrates the presence of phenoxy adsorption in a partially irreversible way onto the MWNT surface by successive contacts between MWNT and phenoxy chains during melt blending.

Due to phenoxy adsorption, interfacial thermodynamics based on the surface properties of the neat components do not predict exactly MWNT location. Actually, phenoxy macromolecules should first be desorbed from the nanotube surface and then be replaced by resin precursors in order to transfer a nanotube from the phenoxy-rich phase to the epoxy resin-rich phase. Therefore, MWNTs are able to migrate inside epoxy resin on condition that MWNTs are not fully covered with phenoxy chains and that an important part of the adsorbed chains desorbs. This adsorption-desorption process has already been explained for carbon black particules [38] and MWNTs [39] in immiscible polymer blends. For the epoxy resin-phenoxy blends considered, it seems that resin precursors can however diffuse towards the MWNT surface since morphological observations have confirmed their location in the epoxy resin-rich phase. The small dimension of the epoxide and diamine precursors should contribute to their possible access to MWNT surface despite its partial coating by phenoxy in an irreversible way.

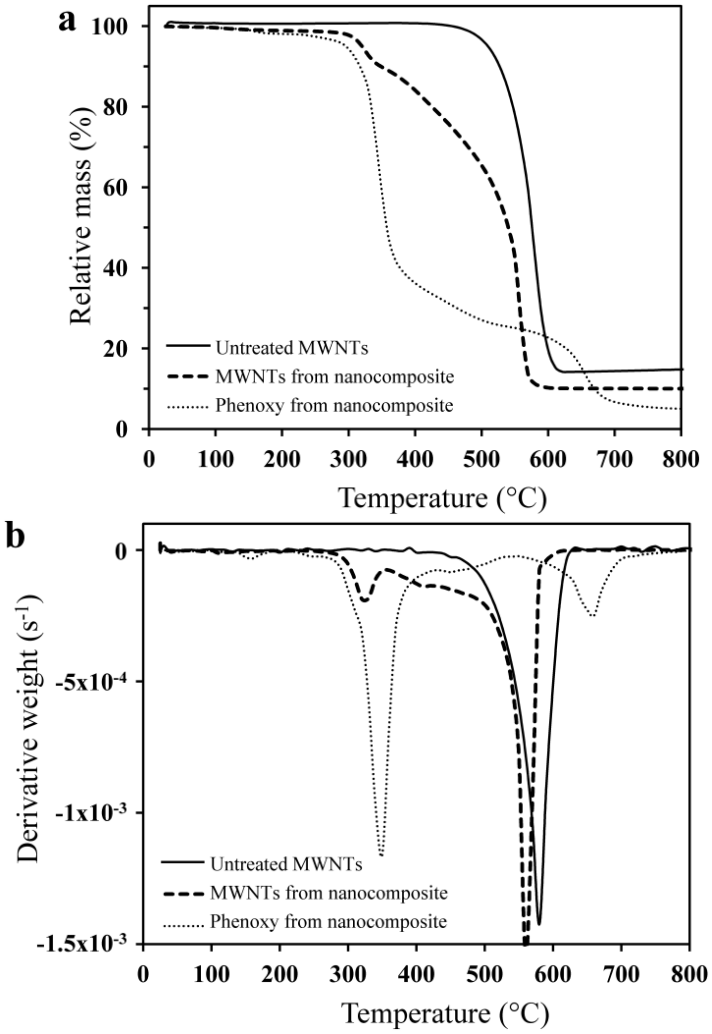

Fig. 3. Weight loss curves measured by TGA: (a) relative mass and (b) its derivative versus temperature for pure MWNTs and for phenoxy and MWNTs extracted from a phenoxy nanocomposite filled with 5 wt % MWNTs.

3.2. RTM6 resin-phenoxy-clay ternary blends

3.2.1. Blend morphology

Nanocomposites processed by melt blending of phenoxy with 10 wt % Cloisite 30B were also tested for dispersion of clay platelets into RTM6 resin as organomodified clay has been successfully dispersed in a uniform

way into phenoxy with intercalated and even exfoliated morphological states (see Chapter 4). In this case, solvent assisted dissolution was used to maximize composition homogeneity of the blends. Therefore, morphological observations must be interpreted carefully because solvent could influence the microstructure to some extent by modifying the process of adsorption and desorption of polymer at the nanofiller surface, the polymer intercalation between the clay layers or even the crosslinking kinetics by residual solvent subsisting in the blend [40]. Microstructures of RTM6 resin blended either with 20 wt % pure phenoxy or with 20 wt % nanocomposite filled with 10 wt % Cloisite 30B are displayed in parallel in **Fig. 4** after curing at 140 °C. For such phenoxy content added to RTM6 resin, the blend composition remaining below the critical point induces a microstructure with phenoxy-rich nodules from 100 to 200 µm dispersed in the continuous phase mainly composed of epoxy resin (**Fig. 4.a**). Similar microstructures have been observed using SEM for samples prepared by thermal dissolution (see Chapter 1). **Fig. 4.b** illustrates the microstructure of blends prepared with the nanocomposite. It can be observed that small stacks of organomodified clay are dispersed in the continuous epoxy matrix as second additive and have no important influence on morphology of the thermoplastic phase. This result lead to the conclusion that phenoxy can be exploited to combine incorporation of a thermoplastic phase in the epoxy resin network along with dispersion of several nanofiller types like not only MWNTs but also organomodified clay.

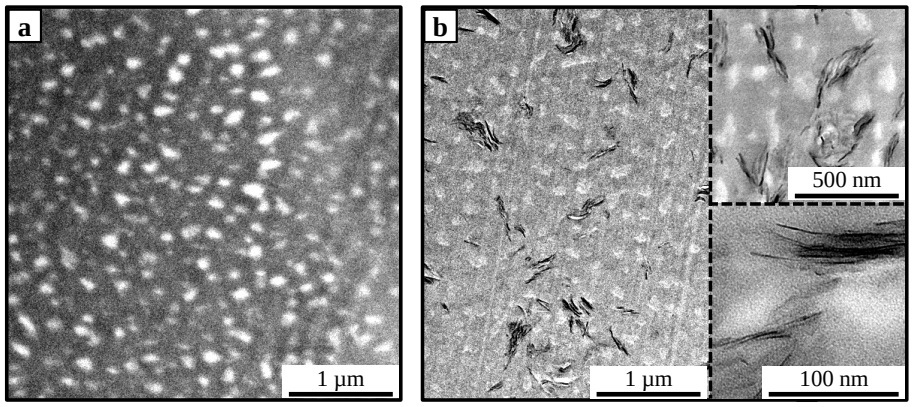

Fig. 4. TEM micrographs of RTM6 resin blended with (a) 20 wt % phenoxy and (b) 20 wt % phenoxy filled with 10 wt % Cloisite 30B [41].

3.2.2. Blend modulus

Although phenoxy is an appropriate thermoplastic to introduce predispersed nanofillers in epoxy resin whilst generating a microstructure toughening the crosslinked resin [1-4], its low T_g remains an important drawback for applications requiring high thermomechanical performances. Whereas no significant evolution of the flexural modulus measured at room temperature takes places when RTM6 resin is modified with phenoxy contents from 10 to 30 wt %, a considerable reduction of the modulus in blends containing more than 10 wt % phenoxy occurs at temperatures higher than the phenoxy T_g (84 °C [42]), as reported in **Fig. 5** at 125 °C.

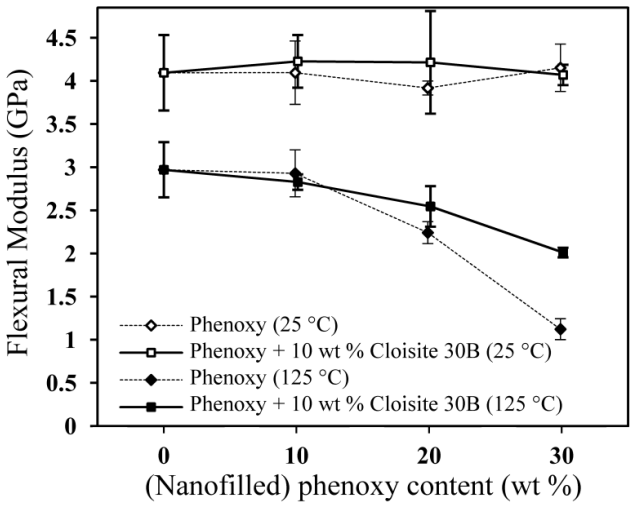

Fig. 5. Flexural modulus of RTM6-phenoxy and RTM6-phenoxy-Cloisite 30B blends measured by DMA in 3 point bending mode at 25 and 125 °C as a function of the content of neat phenoxy or phenoxy filled with 10 wt % Cloisite 30B [43].

Therefore, introduction of a nanocomposite in epoxy resin in place of pure phenoxy so as to combine formation of phenoxy nodules with dispersion of clay platelets could present a significant interest to compensate modulus decrease. Indeed, the positive effect of layered clay on Young's modulus of epoxy resin has been demonstrated by several authors [19-22]. For nanocomposite composed of 10 wt % Cloisite 30B dispersed in phenoxy, the organomodified clay has no significant effect on the flexural modulus of the RTM6 resin-phenoxy blend at 25 °C. The limited clay amount contained in the ternary blend (content of inorganic part around 2 wt % with 30 wt %

nanocomposite) can explain this behavior. Nevertheless, at 125 °C, clay plays on the contrary an important role on the modulus of blends with phenoxy contents equivalent or higher to 20 wt %. Indeed, for these compositions causing considerable reduction of the blend modulus above the phenoxy T_g, the organomodified clay counteracts partially the effect of phenoxy and limits the modulus decrease even for moderate clay contents. Nevertheless, flexural modulus of the polymer matrix is not the main parameter to consider for application to composite since this property depends mainly on the fiber fabric characteristics in composite laminates. Determination of a potential positive effect of clay addition on other properties principally controlled by the composite matrix is more essential to promote clay incorporation in the polymer blend.

4. Conclusions

The method developed in the frame of this work was intended to disperse nanoparticles, i.e. carbon nanotubes or organomodified clay, and a thermoplastic phase in RTM6 resin by dissolution of nanocomposites in the reactive resin before important crosslinking and successive phase separation. Dispersion and distribution of both tubular and lamellar nanofillers in the phase separated-blend has been evidenced using phenoxy as nanocomposite matrix. Therefore, phenoxy appears as an excellent choice to combine dispersion of different types of nanofillers in epoxy resin networks with incorporation of a thermoplastic phase thanks to its good solubility in epoxy resin (see Chapter 2 to3) and its potential to disperse nanofillers during processing by melt blending (see Chapter 4). The mechanism leading to location of MWNTs exclusively in the epoxy resin-rich phase of ternary blends has been discussed. Even if desorption of phenoxy chains from the MWNT surface remains partial, thermodynamic predictions are respected since MWNT location in epoxy resin minimizes interfacial energy in the blend. The interest of clay dispersion in epoxy resin-phenoxy blends to balance modulus decrease above T_g of phenoxy has also been suggested.

Additional developments could be achieved by using phenoxy to disperse other categories of nanofillers or various additives in epoxy resin. Moreover, its remarkable distribution obtained by thermal treatment in epoxide-diamine formulations (see Chapter 3) makes phenoxy an ideal candidate for delivery of dispersed MWNTs or organomodified clay in epoxy resin. The concept exploiting thermoplastic as nanofiller carrier for their distribution in epoxy

resin is therefore investigated in the next chapter. Transposition to composite manufacturing by RTM process can also be considered since in situ dissolution of phenoxy should increase fracture toughness of composites [2-4] while dispersing and distributing nanoparticles in the composite matrix without difficulties related to injection of nanofillers or stability of the dispersion in epoxy resin.

References

[1] Teng KC, Chang FC. Single-phase and multiple-phase thermoplastic/thermoset polyblends: 2. Morphologies and mechanical properties of phenoxy/epoxy blends. Polymer 1996;37(12):2385-94.
[2] Siddhamali SK, Kyu T. Toughening of thermoset/thermoplastic composites via reaction-induced phase separation: Epoxy/phenoxy blends. Journal of Applied Polymer Science 2000;77(6):1257-68.
[3] Beier U, Wolff-Fabris F, Fischer F, Sandler JKW, Altstädt V, Hulder G, Schmachtenberg E, Spanner H, Weimer C, Roser T, Buchs W. Mechanical performance of carbon fibre-reinforced composites based on preforms stitched with innovative low-melting temperature and matrix soluble thermoplastic filaments. Composites Part A: Applied Sc. and Manufact. 2008; 39(9):1572-81.
[4] Wong DWY, Lin L, McGrail PT, Peijs T, Hogg PJ. Improved fracture toughness of carbon fiber/epoxy composite laminates using dissolvable thermoplastic fibers. Composites Part A: Applied Science and Manufacturing 2010;41:759-67.
[5] Iijima S. Helical microtubules of graphitic carbon. Nature 1991;354:56-8.
[6] Thostenson ET, Chou TW. Processing-structure-multi-functional property relationship in carbon nanotube/epoxy composites. Carbon 2006;44(14):3022-9.
[7] Gojny FH, Wichmann MHG, Fiedler B, Schulte K. Influence of different carbon nanotubes on the mechanical properties of epoxy matrix composites - A comparative study. Composites Science and Technology 2005;65:2300-13.
[8] Yu N, Zhang ZH, He SY. Fracture toughness and fatigue life of MWCNT/epoxy composites. Materials Science and Engineering: A 2008;494:380-4.
[9] Ganguli S, Aglan H, Dean D. Microstructural origin of strength and toughness of epoxy nanocomposites. Journal of Elastomers and Plastics 2005;37(1):19-35.
[10] Ganguli S, Bhuyan M, Allie L, Aglan H. Effect of multi-walled carbon nanotube reinforcement on the fracture behavior of a tetrafunctional epoxy. Journal of Materials Science 2005;40(13):3593-5.
[11] Karapappas P, Vavouliotis A, Tsotra P, Kostopoulos V, Paipetis A. Enhanced fracture properties of carbon reinforced composites by the addition of multi-wall carbon nanotubes. Journal of Composite Materials 2009;43(9):977-85.
[12] Sandler J, Shaffer MSP, Prasse T, Bauhofer W, Schulte K, Windle AH. Development of a dispersion process for carbon nanotubes in an epoxy matrix and the resulting electrical properties. Polymer 1999;40:5967-71.

[13] Gojny FH, Wichmann MHG, Fiedler B, Kinloch IA, Bauhofer W, Windle AH, Schulte K. Evaluation and identification of electrical and thermal conduction mechanisms in carbon nanotube/epoxy composites Polymer 2006;47:2036-45.
[14] Song YS, Youn JR. Influence of dispersion states of carbon nanotubes on physical properties of epoxy nanocomposites. Carbon 2008;43(7):1378-85.
[15] Usuki A, Kojima Y, Kawasumi M, Okada A, Fukushima Y, Kurauchi T, Kamigaito O. Synthesis of nylon 6-clay hybrid. Journal of Materials Research 1993;8(5):1179-84.
[16] Park SJ, Seo BS, Lee JR, Surface modification of montmorillonite on surface acid-base characteristicsof clay on thermal stability of epoxy/clay nanocomposites. Journal of Colloid and Interface Science 2002;251:160-5.
[17] Lakshmi MS, Narmadha B, Reddy BSR, Enhanced thermal stability and structural characteristics of different MMT-Clay/epoxy-nanocomposite materials. Polymer Degradation and Stability 2008;93(1):201-13.
[18] Lan T, Pinnavaia TJ. Clay-reinforced epoxy nanocomposites. Chemistry of Materials 1994;6(12):2216-9.
[19] Kornmann X, Lindberg H, Berglund LA, Synthesis of epoxy-clay nanocomposites. Influence of the nature of the curing agent on structure. Polymer 2001;42(10):4493-9.
[20] Becker O, Varley, Simon G. Morphology, thermal relaxations and mechanical properties of layered silicate nanocomposite based upon high functionality epoxy resins. Polymer 2002;43:4365-73.
[21] Qi B, Zhang QX, Bannister M, Mai YW. Investigation of the mechanical properties of DGEBA-based epoxy resin with nanoclay additives. Composite Structures 2006;75(1-4):514-9.
[22] Ha SR, Ryu SH, Park SJ, Rhee KY. Effect of clay surface modification and concentration on the tensile performance of clay/epoxy nanocomposites. Materials Science and Engineering: A 2007. 448(1-2):264-8.
[23] Wang Z, Massam J, Pinnavaia TJ. Epoxy-clay nanocomposites. In: Pinnavaia TJ, Beall GW, editors. Polymer clay nanocomposites. Chichester:Wiley;2000:127-48.
[24] Becker O, Varley RJ, Simon GP. Thermal stability and water uptake of high performance epoxy layered silicate nanocomposites. European Polymer Journal 2004;40:187-95.
[25] Asif AA, Bibin J, Rao VL, Ninan KN, Surface morphology, thermomechanical and barrier properties of poly(ether sulfone)-toughened epoxy clay ternary nanocomposites. Polymer International 2010;59:986-97.
[26] Nanocyl™ NC 7000 technical datasheet (Nanocyl).
[27] Baudouin AC. Dispersion of carbon nanofillers in mono- and biphasic polymer matrices. Thermodynamic versus kinetic control and influence on high-frequency electrical properties. PhD Thesis Université catholique de Louvain 2011.
[28] Cloisite® 30B product bulletin (Southern Clay Products).
[29] Wu S. Polymer Interface and Adhesion. Marcel Dekker Inc, New York 1982.

[30] Stöckelhuber KW, Das A, Jurk R, Heinrich G. Contribution of physico-chemical properties of interfaces on dispersibility, adhesion and flocculation of filler particles in rubber. Polymer 2010;51:1954-63.
[31] Huang HL, Goh SH, Lai DMY, Huan CHA, Wee ATS. Surface properties of miscible poly(1,1,1,3,3,3-hexafluoroisopropyl methacrylate)/phenoxy blends. Journal of Applied Polymer Science 2004;91:1798-805.
[32] Hautier M, Lévêque D, Huchette C, Olivier P. Réparation des composites par infiltration de résine. Investigation of a composite repair method by liquid resin infiltration. Proceeding JNC 16, Toulouse (France), 2009.
[33] Cho JS, Han S, Kim KH, Han YG, Lee JH, Lee CS, Sung JW, Beag YW, Koh SK. Surface modification of polymers by ion-assisted reactions: An overview. In Adhesion aspects of thin films, Volume 2, Mittal KL, ed. VSP, Utrecht (Netherlands), 2005:105-121.
[34] Page SA, Mezzenga R, Boogh L, Berg JC, Månson JAE. Surface energetics evolution during processing of epoxy resins. Journal of Colloid and Interface Science 2000;222:55-62.
[35] Baskaran D, Mays JW, Bratcher MS. Noncovalent and nonspecific molecular interactions of polymers with multiwalled carbon nanotubes. Chemistry of Materials 2005;17:3389-97.
[36] Hill DE, Lin Y, Rao AM, Allard LF, Sun YP. Functionalization of carbon nanotubes with polystyrene. Macromolecules 2002;35:9466-71.
[37] Tasis D, Tagmatarchis N, Bianco A, Prato M. Chemistry of carbon nnotube. Chemical Reviews 2006;106:1105-36.
[38] Zaikin AE, Karimov RR, Arkhireev VP. A study of the redistribution conditions of carbon black particles from the bulk to the interface in heterogeneous polymer blends. Colloid Journal 2001;63:53-9.
[39] Baudouin AB, Devaux J, Bailly C. Localization of carbon nanotubes at the interface in blends of polyamide and ethylene-acrylate copolymer. Polymer 2010;51:1341-54.
[40] Mondragon I, Bucknall CB. Effects of residual dichlormethane solvent on the cure of expoxy resin. Plastics, Rubber and Composites Processing and Applications 1994;21:275-81.
[41] Berben R. Contribution à l'élaboration d'un matériau composite aux performances améliorées destiné au secteur aéronautique. Travail de fin d'étude Haute Ecole Lucia de Brouckere - Institut Meurice - Université catholique de Louvain 2010.
[42] http://www.phenoxy.com/technical-data/inchem_properties.html.
[43] Debleser R. Incorporation d'un thermoplastique nanochargé dans des composites aéronautiques produits par "Resin Transfer Moulding". Travail de fin d'études Université catholique de Louvain 2011.

Chapter 6

SOLUBLE THERMOPLASTIC FOR DELIVERY OF NANOPARTICLES IN EPOXY RESIN

Abstract

This chapter aims to validate that thermoplastic matrix-nanocomposites are exploitable to deliver nanoparticles in epoxy resin. Nanocomposites prepared by melt blending of unfunctionalized multiwalled carbon nanotubes (MWNTs) or organomodified layered clay in poly(hydroxyether of bisphenol A) (phenoxy) and poly(ether sulfone) (PES) are investigated as they have previously demonstrated to combine several advantages. Indeed, the thermoplastic matrices are at least partially soluble in the RTM6 resin precursors (see Chapter 2 and 3) and additionally, such nanocomposites present a fine dispersion and homogenous distribution of the nanofillers (see Chapter 4). Therefore, these nanocomposites are intended to lead to nanofiller distribution in the epoxy resin-thermoplastic blend thanks to interdiffusion between the thermoplastic macromolecules and the resin precursors. Moreover, a good dispersion of the nanofillers in the polymer blend and their preferential location in the epoxy resin-rich phase has been demonstrated in ternary blends prepared with RTM6 resin and a phenoxy nanocomposite after phase separation occurring during cure of the reactive resin (see Chapter 5).

Model systems consisting of a single nanocomposite filament in contact with RTM6 resin are first considered in the present study. Inspection of the filament morphology shows that the nanofiller dispersion is preserved despite a strong orientation effect of the nanofiller. Dissolution of the filament is investigated during thermal treatment in epoxy resin and the resulting nanofiller and thermoplastic distributions are evaluated by Raman spectroscopy. MWNTs and thermoplastic exhibit the same spatial distributions in the epoxy resin. No effect of the nanofiller on the thermoplastic distribution is observed with both tubular or lamellar nanoparticles. These results suggest that the nanoparticles remain entangled within the swelled thermoplastic during the interdiffusion process and that the same mechanism controlled by the thermoplastic swelling explains their delivery into epoxy resin. Phenoxy is thus more adapted than PES to distribute nanofiller on a large distance interval since its swelling in the RTM6 resin precursors is favored. Finally, the microstructure gradient induced by the composition gradient is discussed. Using phenoxy as nanocomposite matrix, both thermoplastic nodules and nanofillers can be dispersed in the continuous phase made of epoxy resin. The soluble thermoplastic acts thus as carrier of nanofillers for their dispersion and distribution in the epoxy resin matrix.

After validation of the concept using thermoplastic for delivery of nanofiller in model systems, transposition to process of composite interleaved with nanocomposite films by RTM is also reported in the present chapter. The produced composite panels show that MWNT dispersion and distribution is achieved in the interlaminar area thanks to thermoplastic swelling but that even if thermoplastic can migrate through the carbon fabrics, a filtering effect of the fibers prevents MWNTs to penetrate in the fabric core. Incorporation of phenoxy films in the composite preform increases the energy required for mode I crack propagation but PES and MWNTs have not the same positive influence.

1. Introduction

Added to preform of thermoset composites, soluble amorphous thermoplastics have already demonstrated a positive effect on properties of laminate composites processed by liquid composite molding (LCM) technologies like Resin Transfer Molding (RTM) [1-11]. As a result of the blend microstructure generated by the phase separation induced during resin crosslinking, toughening of epoxy resin matrices has been evidenced without compromising thermomechanical performances of the epoxy network for adapted thermoplastic concentrations. Moreover, the concept using in situ dissolution of a thermoplastic modifier into reactive resin maintains processability without modification of the processing conditions being required.

Nevertheless, sectors requiring high performance materials like the aerospace industry are still looking for additional property improvement by introduction of nanoparticles in the composite parts. Different ways to incorporate nanofillers into FRPs processed by LCM have been investigated. Dispersion of carbon nanotubes (CNTs) in the injectable resin followed by infusion of the nanophased matrix through the composite preform has been studied [12-21]. However, dispersion of unmodified CNTs in polymers remains a critical challenge due to their high intermolecular van der Waals interactions and physical entanglements. Several methods [22] among which mechanical stirring, high shear mixing through calendering and sonication have been tested to break aggregates and properly disperse CNTs in thermosetting resin formulations. Solvents, surfactants and functionalization of CNTs have also been largely examined in order to achieve stable dispersions. Injection of epoxy resin filled with layered clay has also been considered [23-24]. Beyond challenge to disperse nanofillers in epoxy resin, injection of a nanofilled resin presents other drawbacks. Indeed, the resin viscosity is considerably increased by nanofillers and consequently, good impregnation of the preform can be prevented or can require more severe process conditions. Moreover, a potential filtering effect can be caused by the composite preform during injection of the nanofilled resin [23,25-26] and can lead to an inhomogeneous nanofiller distribution in the composite matrix depending on permeability of the fibrous porous medium. Therefore, other methods are explored to disperse nanofillers in the epoxy resin matrix of composites processed by LCM like growth or coating of CNTs on the

preform fibers [27-34] and dispersion of CNTs in the sizing agent of the fibers [35-40].

The present study intends to develop an alternative route to deliver nanoparticles in the polymer matrix of composite laminates. The concept investigated here [10,41-42] aims to use a nanofilled thermoplastic placed in the composite preform as carrier for in situ distribution of
dispersed nanoparticles into an epoxy matrix during composite processing. Nanocomposites prepared by melt blending of the nanofillers with a thermoplastic soluble into the epoxy resin precursors are exploited for this purpose. The proposed method present several advantages since preliminary nanofiller dispersion is achieved in the thermoplastic matrix, difficulties related to injection of stable dispersion of nanofillers in epoxy resin are avoided and positive effects of the thermoplastic and the nanofillers on the composite properties are combined.

The potential of two different amorphous thermoplastics, poly(hydroxyether of bisphenol A) (phenoxy) and poly(ether sulfone) (PES) to distribute multiwalled carbon nanotubes (MWNTs) or organomodifed layered clay into HexFlow® RTM6 epoxy resin is tested in the present work. Indeed, swelling by the resin precursors and further interdiffusion before important crosslinking have been previously demonstrated for both thermoplastics (see Chapter 2 and 3). Moreover, excellent dispersion and distribution of MWNTs in both thermoplastics have been obtained and intercalated-exfoliated nanocomposites have been produced with phenoxy and organomodified clay (see Chapter 4). Last but not least, it has been shown that phenoxy filled with both types of nanofillers can lead to microstructures with phenoxy nodules and nanoparticles dispersed in a continuous phase made of epoxy resin when blended with RTM6 resin (see Chapter 5).

This chapter investigates model systems based on a single nanocomposite filament in RTM6 resin to evidence delivery of nanofillers in epoxy resin. The nanofiller dispersions achieved in nanocomposite filaments are first examined. Evolution of the nanocomposite filament resulting from isothermal temperature treatment into the resin is then reported and both thermoplastic and nanofiller concentration profiles evaluated by Raman spectroscopy are presented. Influence of the thermoplastic nature on nanofiller distribution is inspected by comparing behavior of PES and phenoxy nanocomposites. Two different kinds of nanofillers are also

considered in order to determine if the mechanism leading to their delivery in epoxy resin is similar for tubular and lamellar nanoparticles. Subsequently, blend microstructures resulting from reaction induced phase separation are discussed and correlated to the composition profiles. Finally, the proposed concept exploiting soluble thermoplastic as carrier for distribution of nanofillers into epoxy resin is transposed to production of composites interleaved with nanocomposite films processed by RTM. Effect of carbon fabrics and film thickness on the panel microstructures is discussed and influence of the films on mode I crack propagation is evaluated.

2. Experimental

2.1. Materials

Nanocomposites were successfully prepared by dispersing unfunctionalized MWNTs Nanocyl™ NC7000 from Nanocyl S.A. or organomodified clay Cloisite® 30B from Southern Clay Products in amorphous thermoplastic matrices using a melt mixing process (see chapter 4). On the one hand, 1 to 5 wt % MWNTs were dispersed in poly(ether sulfone) (PES, Radel® A-200 NT from Solvay Advanced Polymers) and phenoxy (InChemRez® Phenoxy Resin PKHP-200 or PKHB from InChem Corporation) and on the other hand, intercalated-exfoliated nanocomposites were processed with Cloisite 30B contents from 5 to 15 wt % in phenoxy.

The behavior of the nanocomposites in the form of filament was tested into HexFlow® RTM6 resin from Hexcel. Another epoxy resin formulation prepared with stoichiometric amounts of tetraglycidyl-4,4'-methylenedianiline (TGMDA, Araldite® MY 721 from Huntsman) and diethyltoluenediamine (DETDA, Lonzacure® DETDA 80 from Lonza) was also used to determine the microstructure induced by a filament of phenoxy filled with MWNTs.

2.2. Spinning of nanocomposite filaments

Filaments were drawn by stretching and winding the nanocomposites melt processed in a DSM Xplore 15 ml micro-compounder respectively at 220 °C and 340 °C for phenoxy and PES matrices. A DSM Xplore Fiber Spin Line was used to produce 100 µm-diameter filaments (diameter varying between

95 and 105 µm) with the nanocomposite exiting the mixing chamber through a 0.5 mm diameter die. Filaments were subsequently embedded in cold-setting resin Epofix from Electron Microscopy Sciences to prepare ultrathin sections of approximately 95 nm in thickness (cut with a Reichert Microtome using a histodiamond knife with a cut angle of 45 ° from Diatome) for transmission electron microscopy (TEM) characterization. Micrographs were imaged with a LEO 922 transmission electron microscope operating at 200 kV.

2.3. Thermal treatment of nanocomposite filaments in epoxy resin and investigation of the resulting composition gradient

Nanocomposite filaments of about 1 cm length were placed into 50 mg RTM6 epoxy resin between two microscope glass slides and fitted into a Mettler FP82HT hot stage monitored by a Mettler FP90 central processor to apply an isothermal temperature treatment. An Olympus BX51 optical microscope equipped with a ColorviewI camera was used to follow the interdiffusion process.

The samples were removed from the hot stage after gelification of the resin for analysis by Raman spectroscopy to determine composition gradient induced by the filament in the epoxide-diamine formulation. Local MWNT and thermoplastic contents were assessed on basis of spectra acquired perpendicularly to the initial filament direction at intervals of 10 µm using a Raman spectrometer DXR SmartRaman from Thermo Scientific operating in the microscopic mode. The laser, with an incident excitation wavelength of 780 nm was focused between the two microscope glass slides, in the plane of the filament center. The power of the laser was reduced to 4 mW and the exposure time limited to prevent sample degradation during sample exposition. The pinhole aperture was set to 50 µm in combination with a 50 times magnification objective. Reference spectra of the polymers and nanofillers were acquired with the same device using a 50 µm slit aperture and a 10 times magnification objective.

2.4. Examination of microstructures induced by thermoplastic and nanocomposite in epoxy resin

Preparation of RTM6 resin-thermoplastic blends with various contents of PES (10, 15 and 20 wt %) or phenoxy (20, 30 and 40 wt %) was achieved to

observe microstructures of the phase separated blends depending on their composition. Dissolution and homogeneization of the thermoplastic in the reactive resin were respectively completed at 140 °C before important resin crosslinking for phenoxy and at room temperature in dichloromethane solvent (unstabilized grade for HPLC from Biosolve) for PES. The modified resin samples were then cured during 120 minutes at 140 °C, after solvent elimination for the blend containing PES. SEM analyses were performed on cryofractured surfaces of the cured epoxy resin-thermoplastic blends using a LEO 982 (Zeiss) operating at 1 kV after etching of the PES- or phenoxy-rich phase using respectively dichloromethane or tetrahydrofuran (THF, unstabilized grade for HPLC from BioSolve BV) solvents during 24 hours.

Ternary blends containing epoxy resin, phenoxy and MWNTs were likewise produced by thermal dissolution of 20 and 30 wt % nanocomposite powder (phenoxy filled with 3 wt % MWNTs) into RTM6 resin under stirring. TEM was exploited to evidence morphologies of these blends using the same device and experimental conditions than for observation of nanocomposite filaments.

Microstructures located in the morphology spectrum induced by a 100 µm diameter filament of phenoxy filled with 1 wt % MWNTs in epoxy resin at 140 °C were also locally observed on thin sections prepared by ultramicrotomy with a JEM-1400 transmission electron microscope from JEOL operating at 120 kV.

2.5. Process and characterization of composite panels interleaved with thermoplastic or nanocomposite films

Composite panels (420 mm x 300 mm x 4.4 mm) containing 12 layers (around 67 wt %) of HexForce® G0926 carbon fabrics supplied by Hexcel Composites with a quasi-isotropic $[(+45/-45)/(0/90)]_{3S}$ lay-up were processed using vacuum-assisted resin transfer molding (VARTM). A reference panel composed of RTM6 resin and carbon fibers without additves was produced such as panels modified with thermoplastic or nanocomposite films added to the preform. These composite panels were interleaved with 40 µm thick films of pure PES or phenoxy inserted between each carbon fabric layer or with 80 µm thick films of pure phenoxy or phenoxy filled with 3 wt % MWNTs placed in the mid-plane and every two interlayers in the preform. Moreover, an additional panel was processed with 80 µm thick films of pure

phenoxy placed every two interlayers in the preform but without phenoxy film in the mid-plane. The nanocomposite films were previously casted with a DSM Xplore Micro Film Device after 5 minutes recirculation (screw speed of 150 rpm) in the DSM Xplore 15 ml micro-compounder used for melt-processing. For all panels, film thickness and stacking sequence were chosen to reach a global thermoplastic fraction in the polymer matrix around 16 wt %. A polyimide insert was also placed in the preform mid-plane of each panel in order to initiate crack propagation during double cantilever beam (DCB) test.

All composite panels were manufactured using the same process conditions allowing transverse infiltration of the injected resin even with films placed in each interlayer. After complete impregnation of degassed RTM6 resin at 100 ml/min, a dwell pressure of 6.5 bars was applied for 120 min to minimize porosity. A temperature cycle recommended for processing of RTM6 resin (1°C/min ramp from 80°C to 180°C followed by a 180°C isotherm for 2 hours) was applied. Injection of the RTM6 resin was achieved at 80 °C without difficulty related to preform impregnation or thermoplastic flushing by the resin flow since limited viscosity and absence of significant thermoplastic dissolution are ensured at this temperature. Non destructive testing (NDT) was performed on the processed panels to control their quality. Ultrasonic C-scan inspection has shown that the proposed process conditions allow production of composite panels without any defect like porosity or area with dry fibers. The carbon fiber contents and conversion rates were also checked respectively by TGA and ADSC methods like the absence of flushing by FTIR spectroscopy.

DCB tests were performed according to ASTM D5528-01 on composite specimens cut to size 25 mm x 150 mm including two round notches at the end of the sample allowing attachment of piano hinges via small screws were loaded in tensile mode at 1 mm/min using a Zwick Universal testing machine. Crack growth was observed using a magnifying lens and the measurements of load and displacement at corresponding crack length were recorded.

The polished cross sections of the composite panels and their failure surfaces resulting from DCB test were inspected by SEM using a LEO 982 (Zeiss) operating at 1 kV before and after etching of the thermoplastic-rich phase with tetrahydrofuran and dichlormethane solvents (unstabilized grades for

HPLC from BioSolve BV) respectively for phenoxy and PES during 24 hours.

3. Results and discussion

This section describes first influence of stretching on morphology of nanocomposite filaments. Dissolution of nanocomposite filaments in RTM6 resin due to phenoxy swelling by the resin precursors is then compared to dissolution of a neat phenoxy filament. Subsequently, thermoplastic and MWNT distributions resulting from interdiffusion between the resin precursors and the thermoplastic macromolecules are evaluated. Finally, local compositions are correlated to ternary blend microstructures.

3.1. Morphology of the nanocomposite filaments

In contrast with MWNTs randomly oriented in nanocomposite pellets (see Chapter 5), MWNT orientation in the axial direction of the nanocomposite filaments was observed. TEM micrographs of a phenoxy filament filled with 3 wt % MWNTs presented in **Fig. 1** evidence that the morphology is identical at the filament surface and within the filament core. The MWNT orientation results from the process conditions leading to important shear during flow of the nanocomposite through the compounder die and to stretching applied to nanocomposites during filament winding. Influence of the process conditions on MWNT orientation in a PES matrix has been previously quantified [43].

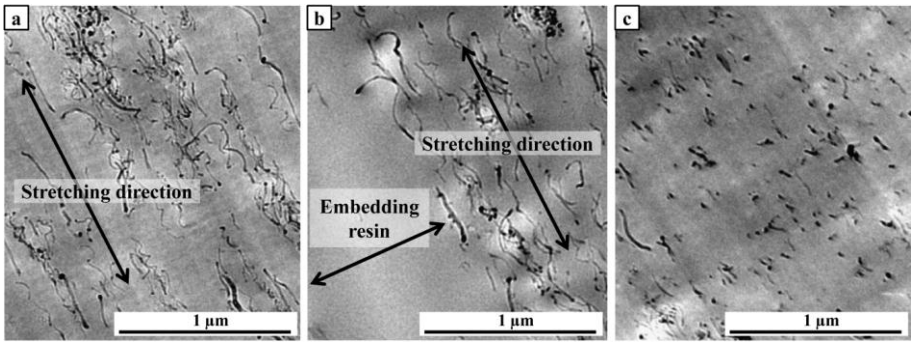

Fig. 1. TEM micrographs of a phenoxy filament filled with 3 wt % MWNTs (a) in the filament core and (b) at the filament surface (in contact with embedding resin used to prepare ultrathin sections) in the stretching direction and (c) in the filament core transversally to the filament axis.

Whereas orientation of the MWNTs in the thermoplastic matrix is considerably influenced by the spinning process, TEM micrographs of the nanocomposite filaments show that good dispersion and rather homogeneous distribution of the MWNTs are maintained throughout the filament. The observed morphologies demonstrate conservation of the MWNT dispersion achieved during melt blending and few agglomeration of nanotubes during the filament production, which are essential considerations to take advantage of the nanocomposite filaments to distribute nanofillers in epoxy resin.

Similarly to MWNTs, organomodified clay platelets are mainly oriented in the direction of the filament axis. This anisotropy of the filament morphology is observable in **Fig. 2** showing TEM micrographs of a nanocomposite filament of phenoxy with 10 wt % Cloisite 30B. Moreover, the good clay dispersion and the mixed intercalated-exfoliated structure of the nanocomposite pellets are maintained in filaments of phenoxy filled with organomodified clay.

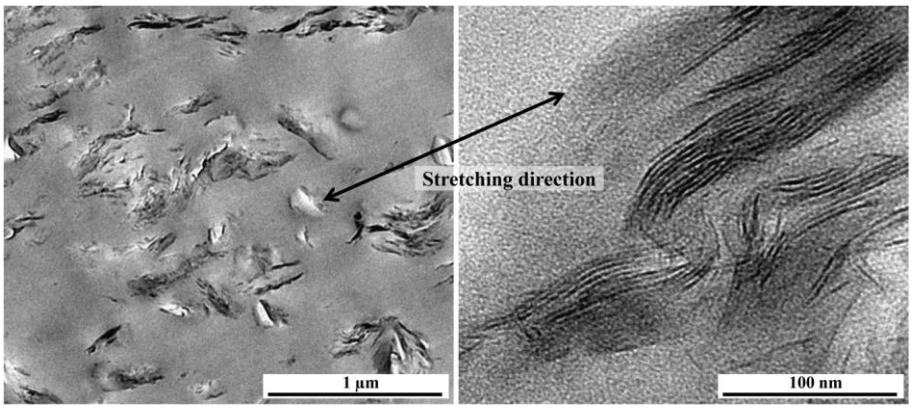

Fig. 2. TEM micrographs of a phenoxy filament with 10 wt % Closite 30B in the stretching direction.

Since dispersions of MWNTs and organomodified clay in phenoxy are excellent and remain stable when filaments are manufactured, this thermoplastic is suitable as matrix to process nanocomposite filaments that can be subsequently tested in order to deliver nanoparticles in epoxy resin. Indeed, thermal dissolution of phenoxy in epoxy resin, which has been previously demonstrated (see Chapters 2 and 3), is expected to allow distribution of nanofillers in the polymer blend, more specifically in the epoxy resin-rich phase once phase separation takes place (see Chapter 5).

Therefore, dissolution of nanocomposite filaments and composition gradients resulting from interdiffusion are studied in the following subsections.

3.2. Influence of nanofillers on filament dissolution in RTM6 resin

Filaments of neat phenoxy and phenoxy nanocomposite were used to highlight influence of the nanofillers on the filament dissolution. Evolution of a filament (initially 100 µm diameter) into RTM6 resin during thermal treatment at 120 °C is illustrated in **Fig. 3** comparing the behavior of filaments of pure phenoxy and phenoxy filled with 10 wt % Cloisite 30B or 1 wt % MWNTs. For phenoxy filled with organoclay (**Fig. 3.a**) like for neat phenoxy (**Fig. 3.b**), the rapid dissolution is evidenced on the image succession by the decrease of the distance between the visible interfaces delimiting the filament. The interfaces detectable by this optical technique can be considered as the diffusion fronts of the epoxy resin precursors and delimit the thermoplastic or nanocomposite layer still unaffected by the resin. In both cases, the residual glassy layer of the filament completely disappears before 20 minutes of isothermal treatment at 120 °C much before gel time of RTM6 resin (more than four hours, see Chapter 1) as a result of interdiffusion between the low molar mass resin precursors and the polymer chains. In contrast to organoclay, MWNTs prevent detection of the interface between the inner core of the filament and its gel layer containing swollen nanocomposite (**Fig. 3.c**). Nevertheless, for these nanocomposite filaments filled with MWNTs, apparent migration of the nanotubes is observable. Thanks to the important contrast between the MWNTs and the polymer matrix, their front of apparent migration in the epoxy resin can be easily followed.

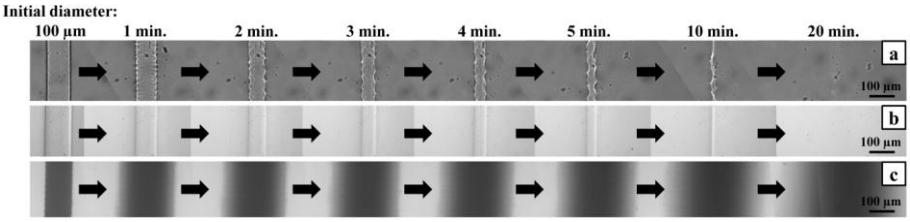

Fig. 3. Images from hot stage microscopy of a 100 µm diameter filament of (a) pure phenoxy, (b) phenoxy filled with 10 wt % Cloisite 30B and (c) phenoxy filled with 1 wt% MWNTs in RTM6 resin at 120 °C.

The distance between the visible interfaces of a filament of pure phenoxy is compared to the one of a filament of phenoxy filled with 10 wt % Cloisite 30B in **Fig. 4** as a function of the duration of the heat treatment in RTM6 resin at 80, 100, 120 and 140 °C. A decrease of the diameter of the unswollen part of the filament being slightly faster in the case of the pure phenoxy filament has been measured at all temperatures. The slower dissolution of the filament filled with organomodified clay suggests that clay platelets hinder diffusion of the resin precursors inside the phenoxy core. Nevertheless, the impact of this barrier effect on the interdiffusion extent remains limited and dissolution is completed in both cases much before gelation of the resin between 100 and 140 °C (gel times of more than 1.5, 4 and 10 hours respectively at 140, 120 and 100 °C are reported in Chapter 1).

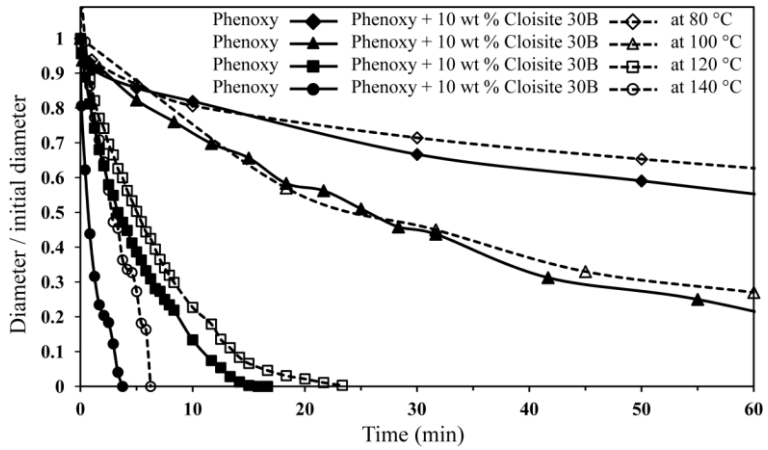

Fig. 4. Evolution of the normalized diameter of phenoxy and nanocomposite (phenoxy filled with 10 wt % Closite 30B) filaments (initially 100 µm) in RTM6 resin during isotherms at 80, 100, 120 and 140 °C.

Initial orientation of the nanofillers in the nanocomposite filament may also affect the interdiffusion extent. Even if some reorientation of the nanoparticles is possible during the interdiffusion process between the nanocomposite and the resin precursors, intensity of the barrier effect limiting dissolution may be modified depending on the initial nanofiller orientation. However, this aspect is not further discussed since a weak effect of the clay platelets on dissolution has been shown for the filaments processed in this work. Moreover, dissolution should be even less influenced by tubular nanofillers like MWNTs due to their shape factor and lower contents dispersed in the nanocomposites.

3.3. Composition gradients induced by a nanocomposite filament in RTM6 resin

Local compositions of ternary blends induced by thermal treatment of a nanocomposite filament in RTM6 resin have been evaluated by Raman spectroscopy after resin gelation once interdiffusion is prohibited. The purpose of these measurements is to establish nanofiller and thermoplastic concentration gradients in order to prove that a nanocomposite processed with a thermoplastic being soluble in epoxy resin precursors is exploitable as carrier to distribute nanofillers in a reactive resin.

First, the possibility to detect PES, phenoxy and MWNTs and to assess their local content by means of Raman spectroscopy is exposed. Then, PES and phenoxy distributions induced by a nanocomposite filament are compared and influence of the nanofiller on the thermoplastic concentration profile is presented. Finally, the potential of soluble thermoplastic to deliver MWNTs in epoxy resin is demonstrated and effects of both MWNT content dispersed in the nanocomposite and temperature on the MWNT distribution are discussed.

3.3.1. Evaluation of PES, phenoxy and MWNT local contents by Raman spectroscopy

The thermoplastic content resulting from the filament swelling and further interdiffusion can be correlated to intensity of spectral bands centered respectively at 1146 cm^{-1} and 1111 cm^{-1} for PES and phenoxy (see Chapter 3). The D peak from disordered graphite due to the breathing modes of sp^2 atoms in rings [44], which is centered at 1312 cm^{-1}, can be exploited to follow variations of the MWNT concentration. Indeed, the evolution of these intense characteristic bands of the filament components can easily be monitored as they are located in spectral regions where no Raman band of the epoxide-diamine formulation is present like shown in **Fig. 5**. In contrast, Raman spectroscopy is not adapted to assess the clay concentration in epoxy resin because no polarizability change of the clay bindings occurs and as consequence no Raman scattering takes place. Even if several bands due to the organic agent of Cloisite 30B are detected on its Raman spectra, their intensity remains too weak in order to quantify the organomodified clay content once dispersed in the polymer matrix. Therefore, a complementary technique like Fourier Transform Infrared (FTIR) spectroscopy has also been

tested to assess the clay content. Nevertheless, below 10 wt % clay, FTIR spectroscopy becomes likewise ineffective to determine the composition due to the decreasing clay absorbance.

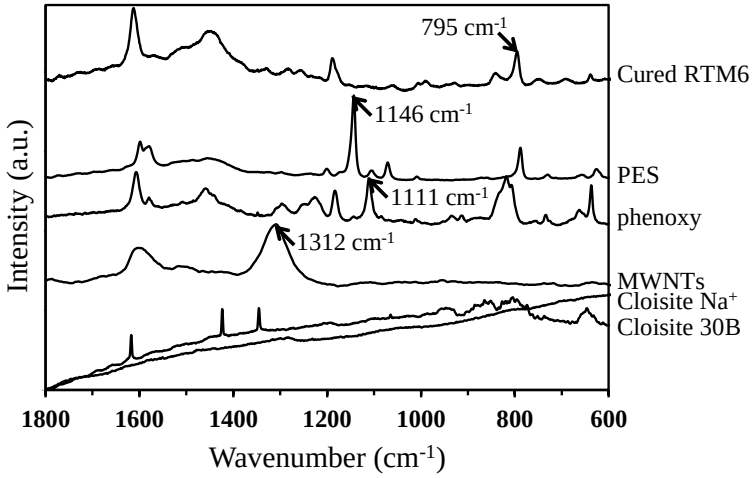

Fig. 5. Raman spectra of RTM6 resin cured at 140 °C, PES and phenoxy thermoplastics and nanofillers (MWNTs, Cloisite Na^+ and Cloisite 30B).

In order to determine thermoplastic and MWNT distributions induced by the filament in epoxy resin, Raman spectra of the samples crosslinked using isothermal conditions were acquired at different distances from the initial location of the filament center (**Fig. 6**)

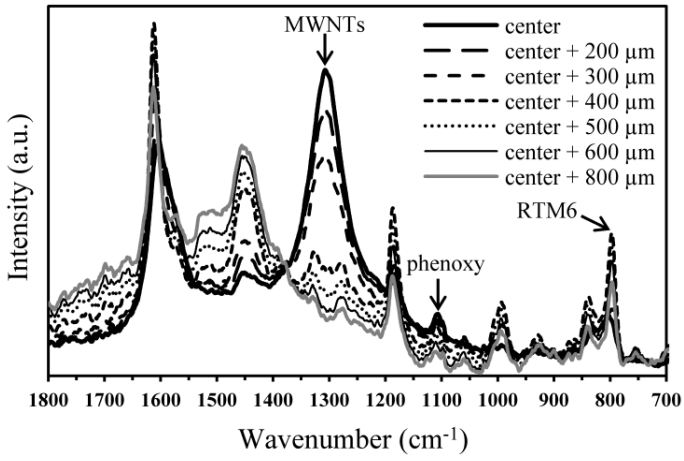

Fig. 6. Raman spectra at increasing distances from the initial location of the center of phenoxy filament filled with 1 wt % MWNTs (diameter of 100 µm) after interdiffusion at 140 °C in RTM6 resin.

Intensity of the band centered at 1312 cm^{-1} depending on the distance from the filament indicates the presence of a MWNT concentration gradient after interdiffusion between the epoxide and diamine precursors of RTM6 resin and a phenoxy filament filled with 1 wt % MWNTs. Similarly, intensity of the phenoxy peak (1111 cm^{-1}) can be followed to evaluate distribution of the thermoplastic carrier.

3.3.2. Thermoplastic distribution

Distributions of PES and phenoxy in RTM6 resin after a 140 °C isotherm applied to a nanocomposite filament containing 1 wt % MWNTs in the epoxide-diamine formulation are compared in **Fig. 7**.

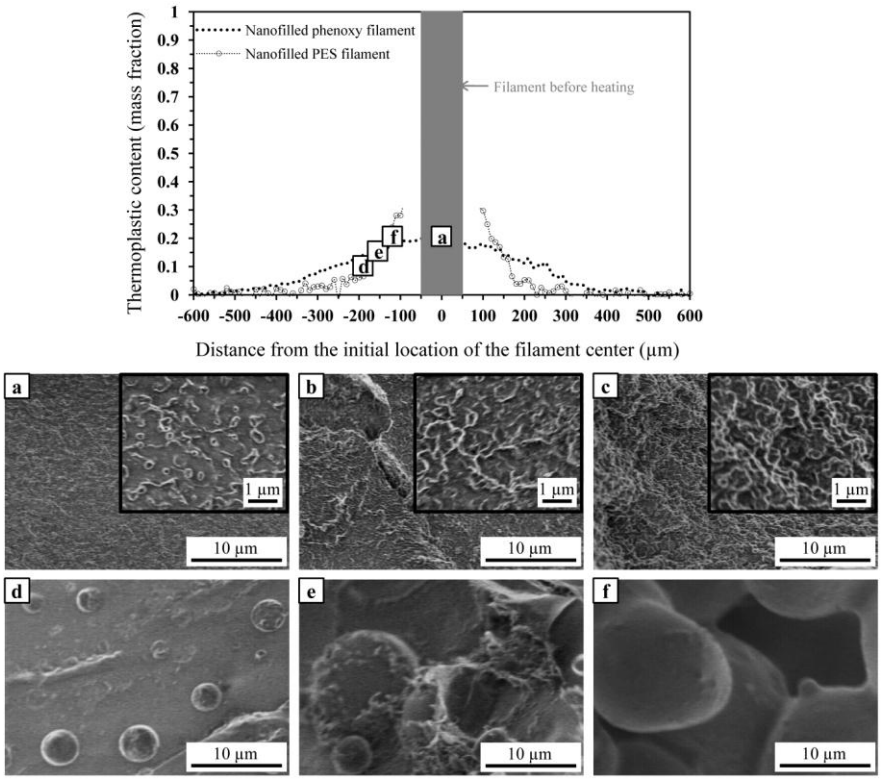

Fig. 7. Phenoxy and PES distributions induced by 100 µm diameter nanocomposite filaments filled with 1 wt % MWNTs after interdiffusion at 140 °C in RTM6 resin determined using Raman spectroscopy; SEM micrographs of RTM6 resin-thermoplastic blends corresponding to the local predicted compositions: (a) 20 wt % phenoxy, (b) 30 wt % phenoxy, (c) 40 wt % phenoxy, (d) 10 wt % PES, (e) 15 wt % PES and (f) 20 wt % PES.

The composition profiles of the polymer blends have been determined according to the evolution of the ratio between intensity of the thermoplastic characteristic band located at 1146 cm^{-1} for PES and 1111 cm^{-1} for phenoxy and the sum of intensities of this band and the epoxy resin band centered at 795 cm^{-1} chosen as reference (**Fig. 5**). An obvious influence of the thermoplastic molecular structure on the distribution profile is evidenced. As expected on basis of the preferential diffusion of epoxide and diamine monomers into phenoxy (see Chapter 2) and consequently the favored swelling of phenoxy into RTM6 resin (see Chapter 3), the composition gradient is very different for the nanocomposite based on a phenoxy matrix as compared to a PES matrix. Considering a 100 µm diameter filament, phenoxy is accordingly detected on a larger distance interval of approximately 1 mm against almost the half for PES.

Despite potential effect of the nanofiller on the morphology induced by phase separation, local thermoplastic concentrations assessed by Raman spectroscopy can be associated to different microstructure types resulting from thermoplastic incorporation in epoxy resin. For PES-matrix nanocomposites, a large morphology spectrum is formed in the interaction zone between the filament and RTM6 resin. Indeed, the higher composition gradient subsisting after interdiffusion is combined with phase inversion occurring at lower concentration (around 15 wt % PES) observed in homogenous epoxy resin-PES blends. Microstructures going from a sea (epoxy resin-rich phase)-island (PES-rich nodules) morphology to a phase inverted morphology with PES forming the continuous phase and even pure PES area are generated by the 100 µm diameter filament. In contrast, the phenoxy-matrix nanocomposite filament induces lower local concentrations of phenoxy remaining below the critical composition (around 30 wt % phenoxy) everywhere through the RTM6 resin-phenoxy interphase. The morphologies created by the nanocomposite filament are thus in this case limited to phenoxy-rich nodules dispersed in the continuous epoxy resin-rich phase, even around the initial location of the filament center where the maximal phenoxy content subsists. Therefore, it confirms that a phenoxy matrix is more adapted than a PES matrix to distribute thermoplastic nodules on a large distance interval into RTM6 resin and to prevent local phase inversion while preserving the epoxy resin as continuous phase. Potential of phenoxy to deliver nanofillers in RTM6 resin is for that reason considered later in this chapter.

Influence of nanofiller on the thermoplastic distribution in the epoxy resin has also been investigated. Very close composition profiles are shown in **Fig. 8** for phenoxy coming from a pure thermoplastic filament or from a nanocomposite filament filled either with 1 wt % MWNTs or with 10 wt % organomodifed clay after a 120 °C isotherm in RTM6 resin. Such similar concentration profiles evidence that both MWNTs and clay platelets do not hinder the filament swelling and interdiffusion processes and that these nanofillers have no important effect on the phenoxy distribution in epoxy resin.

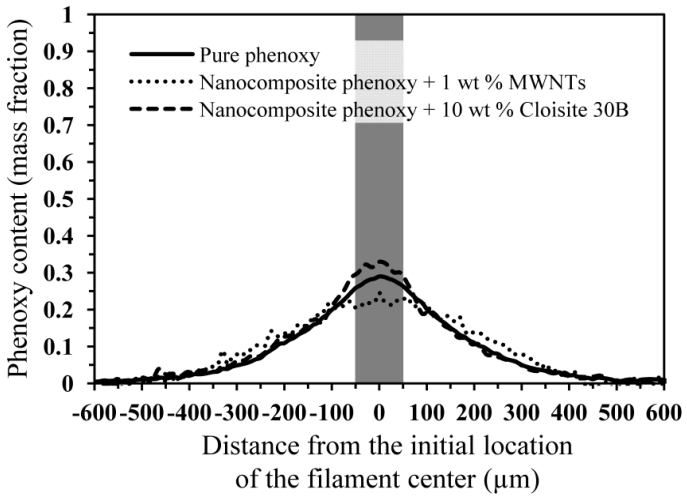

Fig. 8. Phenoxy distribution in RTM6 resin from Raman spectroscopy after dissolution of a 100 µm diameter filament of pure phenoxy, phenoxy filled with 1 wt % MWNTs and phenoxy filled with 10 wt % Cloisite 30B and interdiffusion at 120 °C.

3.3.3. MWNT distribution

Distribution profiles of MWNTs and phenoxy are compared in **Fig. 9.a** after interdiffusion at 120 °C between a filament of phenoxy filled with 1 wt % MWNTs and the RTM6 resin precursors. Assumption of proportionality between the MWNT concentration and the ratio between intensities of the D peak of the MWNT spectrum (1312 cm^{-1}) and a reference peak of RTM6 resin (795 cm^{-1}) has been made for the compositions ranges studied in order to assess the MWNT distribution in the epoxy resin-thermoplastic blend. A baseline subtraction was applied to remove the fluorescence background from the spectra while the limited overlapping between the peaks allows the

exploitation of the Raman spectra without decomposition treatment. Similar shapes of the phenoxy matrix and the MWNT concentration profiles evidence that nanofiller and thermoplastic distributions in the epoxy resin depend on each other. The same behavior has been observed with filaments of PES filled with MWNTs.

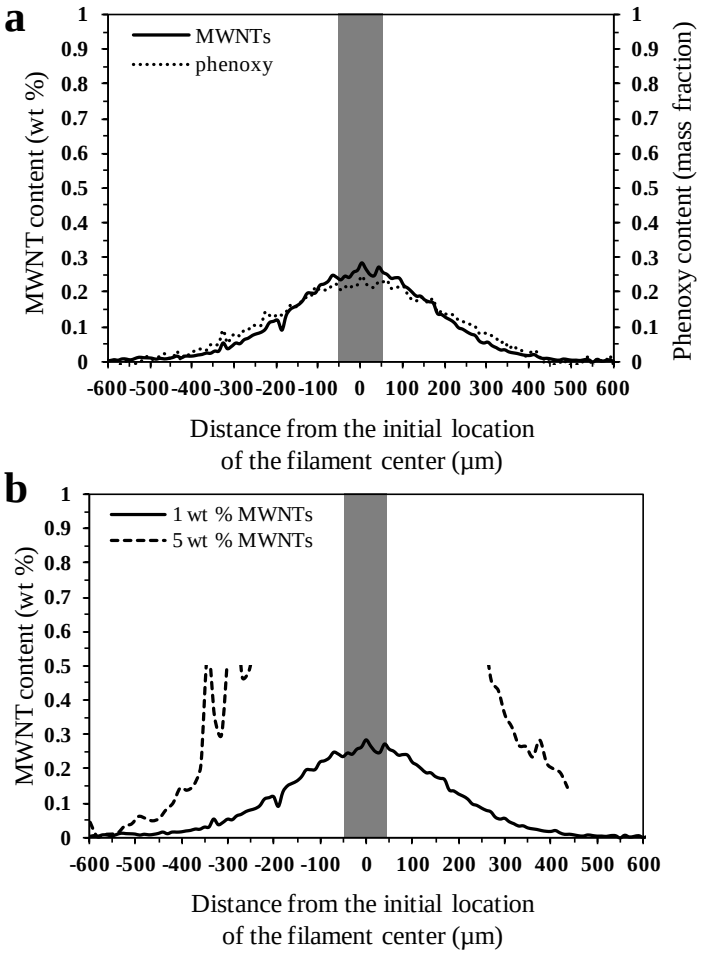

Fig. 9. Composition profiles induced by 100 µm diameter phenoxy filaments filled with MWNTs in RTM6 resin after interdiffusion at 120 °C determined by Raman spectroscopy: (a) phenoxy and MWNT distributions for a nanocomposite filament containing 1 wt % MWNTs; (b) MWNT distribution for nanocomposite filaments containing 1 and 5 wt % MWNTs.

These results suggest that the MWNTs remain entangled within the swelled thermoplastic during the interdiffusion process and that their delivery in

epoxy resin is thus controlled by the thermoplastic swelling.The local MWNT content depends thus on the local thermoplastic concentration in the epoxy resin. Therefore, phenoxy is more suited than PES as soluble thermoplastic carrier to deliver both nanofillers on a large distance interval in the crosslinked epoxy resin. Since identical phenoxy distributions have been observed for phenoxy filled with clay and MWNTs, the same mechanism should explain delivery of lamellar nanoparticles in epoxy resin.

However, on the downside, the concept using phenoxy to distribute MWNTs in RTM6 resin leads to limited nanofiller contents dispersed in the polymer blend after interdiffusion. In the case of the 100 µm nanocomposite filament filled with 1 wt % MWNTs at 120 °C, the maximal MWNT concentration is indeed lower than 0.3 wt %. Nevertheless, transposition of the concept with nanocomposite filaments filled with higher MWNT contents, even superior to the percolation threshold, is possible to increase the local MWNT concentration without reduction of the distance interval containing MWNTs. Although high MWNT contents prevent exploitation of Raman spectra acquired around the filament center due to the too low intensity of the resin reference peaks or to sample degradation during laser exposition, **Fig. 9.b** evidences that the limits of the zone containing MWNTs are approximately the same for a nanocomposite filament with 1 or 5 wt % MWNTs. Indeed, the MWNT characteristic band is detected approximately on the same distance interval. The local MWNT content around the initial location of the filament should thus be significantly increased using phenoxy filled with 5 wt % MWNTs.

Not only the nanocomposite composition but also the thermal profile applied to the system during interdiffusion can be adapted to optimize the final MWNT distribution in the epoxy resin. Influence of the temperature is demonstrated in **Fig. 10** for a filament of phenoxy filled with 1 wt % MWNTs during different isotherms at 100, 120 and 140 °C. The distribution profiles assessed by Raman spectroscopy show that the composition gradient is strongly dependent on the isotherm temperature. The broader MWNT distribution in the RTM6 resin-phenoxy blend is achieved like expected at the higher temperature since swelling of the phenoxy filament by the resin precursors is favored for increasing temperatures (see Chapter 3).

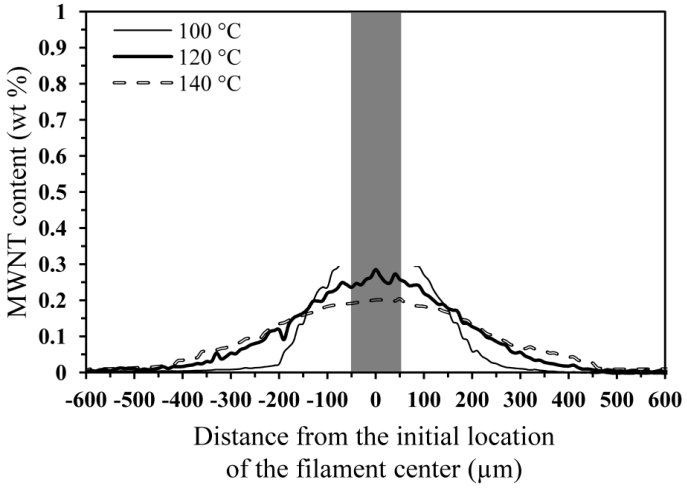

Fig. 10. MWNT distribution into RTM6 resin generated by a 100 µm diameter nanocomposite filament (phenoxy filled with 1 wt % MWNTs) at 100, 120 and 140 °C assessed using Raman spectroscopy.

3.4. Microstructures of ternary blends induced by a nanocomposite filament in epoxy resin

Investigation of phenoxy and MWNT distributions in RTM6 resin resulting from incorporation of a nanocomposite in the unreacted resin has validated that a soluble thermoplastic can be exploited as carrier to deliver previously dispersed nanofillers in the generated polymer blend. However, in order to potentially improve properties of the epoxy network, nanofiller and thermoplastic additives have also to be correctly dispersed in the crosslinked resin. The local microstructures induced by the nanocomposite filament during phase separation in the ternary blend must thus be closely considered. Indeed, the composition gradient due to swelling of the nanocomposite and interdiffusion in the epoxy resin is the source of a microstructure gradient in the phase separated blend.

Therefore, microstructures that can be locally induced by nanocomposite filaments in epoxy resin are presented here to complete the demonstration and show that nanocomposites are adapted to disperse nanofillers and thermoplastic nodules in epoxy resin. For example, **Fig. 11** shows that the local blend morphologies produced by a nanocomposite filament filled with 3 wt % MWNTs in RTM6 resin at 120 °C can be related to the local compositions of the blend evaluated by Raman spectroscopy. Depending on

the distance from the filament center, the blend microstructure varies accordingly with the evolution of its composition. Locally, for a content of 20 wt % nanocomposite in the RTM6 resin, a microstructure with both thermoplastic nodules and MWNTs dispersed in the continuous epoxy resin-rich phase is predicted on basis of TEM observations of blends prepared by thermal dissolution and curing of 20 wt % nanocomposite powder in the resin (see also Chapter 5). The co-continuous morphology obtained with 30 wt % nanocomposite in the RTM6 resin is on the contrary not reached with the 100 µm diameter filament after the 120 °C isotherm and the epoxy resin remains thus the continuous phase everywhere in the sample.

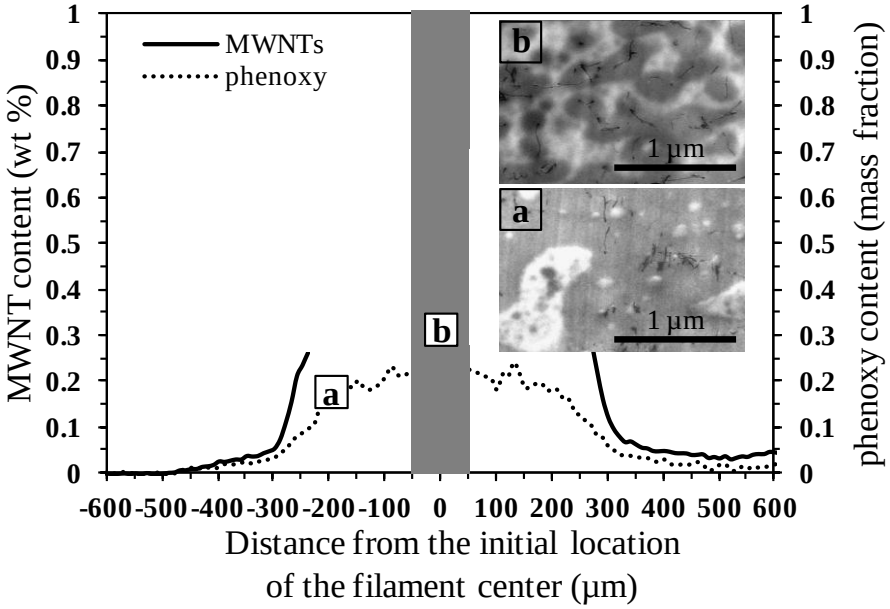

Fig. 11. Phenoxy and MWNT distributions induced by a 100 µm diameter nanocomposite filament containing 3 wt % MWNTs after interdiffusion at 120 °C in RTM6 resin determined using Raman spectroscopy and microstructures (TEM micrographs) of ternary blends corresponding to compositions locally predicted; (a) 20 wt % and (b) 30 wt % nanocomposite.

The morphology indirectly predicted thanks to determination of the composition profile knowing microstructures of blends prepared by thermal dissolution under stirring is confirmed by direct TEM observation of the interphase between the nanocomposite filament and the epoxy resin. The presence of both phenoxy nodules and MWNTs dispersed in the continuous

phase mainly composed of epoxy resin is clearly visible in **Fig. 12** in the interdiffusion region between epoxy resin and a 100 µm nanocomposite filament filled with 1 wt % MWNTs. This result proves that the concept using a soluble thermoplastic as carrier of nanofillers in epoxy resin allows to disperse a thermoplastic phase simultaneously with nanofillers in an epoxy matrix without mechanical stirring. Indeed, apparent migration of the entangled MWNTs results from swelling of the nanocomposite by the resin precursors and interdiffusion. MWNTs contained in the swollen thermoplastic are surrounded by an important amount of resin precursors having diffused towards the filament. When phase separation takes place, dispersion of the MWNTs is achieved in the epoxy resin thanks to partial desorption of phenoxy from the MWNT surface and reduction of the interfacial energy of the blend for MWNT located in the epoxy resin-rich phase (see Chapter 5). Since clay dispersion in the epoxy resin has been previously observed in ternary blends prepared by thermal dissolution under stirring (see Chapter 5), the same microstructure with clay platelets dispersed in the continuous epoxy phase is expected by using a phenoxy filament filled with organomodified clay as nanocomposite carrier.

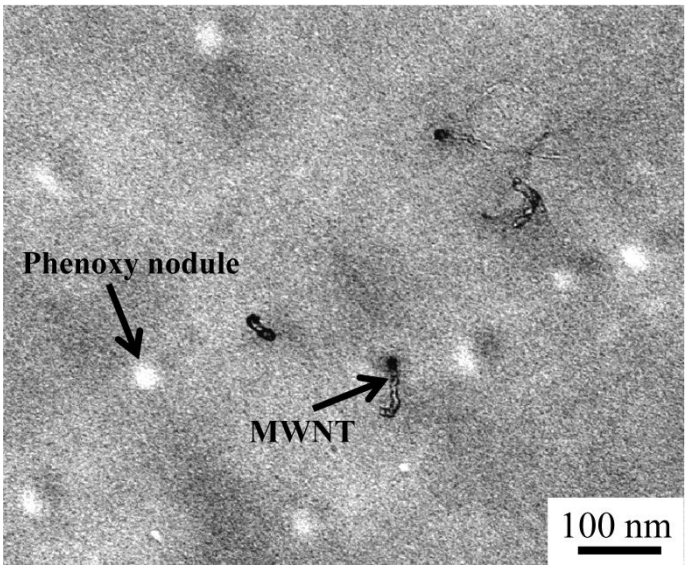

Fig. 12. TEM micrograph of the microstructure induced by a 100 µm diameter phenoxy filament containing 1 wt % MWNTs in epoxy resin after interdiffusion at 140 °C.

3.5. Application to composite processed by RTM interleaved with nanocomposite films

Transposition of the developed concept exploiting thermoplastic as nanofiller carrier in epoxy resin to process of composite panels by RTM was investigated during the APC project by researchers of the IMCN-BSMA laboratory. Films of the produced nanocomposites were introduced between layers of continuous fiber fabrics in the dry preform. Significant differences between composite materials interleaved with nanocomposite films and model systems based on nanocomposite filaments in epoxy resin must be taken into account like the different shapes of nanocomposite, the presence of continuous fibers and the dynamic temperature profile. However, this approach was likewise expected to deliver nanoparticles in the epoxy resin matrix of the composite during a typical thermal cycle applied for RTM processing thanks to swelling of the thermoplastic carrier by the resin precursors.

In order to check this assumption, a first test was achieved by producing a composite panel interleaved with 80 µm thick films of phenoxy filled with 3 wt % MWNTs place in the mid-plane of the panel and every two interlayers. The microstructure of the interlaminar layer containing a nanocomposite film (**Fig. 13**) confirms that interdiffusion between phenoxy and the resin precursors taking place during the initial stages of the curing cycle leads to dispersion and distribution of MWNTs in the RTM6 matrix. Incorporation of nanocomposite films in the composite preform appears thus as an innovative approach to implement the concept developed in this work exploiting thermoplastic to deliver nanoparticles in a composite matrix. However, important inhomogeneities of nanofiller distribution are encountered through the panel thickness due, on the one hand, to impossibility to reach homogeneous distribution of the thermoplastic carrier without input of mixing energy to the system and, on the other hand, to a filtering effect by the carbon fabrics. Indeed, MWNTs are almost exclusively located in a zone of approximately 40 µm in width without carbon fibers around the initial location of the nanocomposite film (**Fig. 13. a**). Presence of MWNTs in this area counterweights absence of carbon fibers due to the insert of phenoxy films in the composite preform and could have a positive effect on the panel properties. Nevertheless, filtration by the low permeability fabrics hindering apparent MWNT migration is a drawback of this approach. Indeed, the MWNT content rapidly decreases with penetration distance in the carbon

fiber layer (**Fig. 13. b**) and inhomogeneities of the MWNT distribution can appear around the fibers (**Fig. 13. c**). Epoxy resin matrix surrounding carbon fibers in the fabric core is thus not easily accessible for nanofillers and receives little benefit from their incorporation.

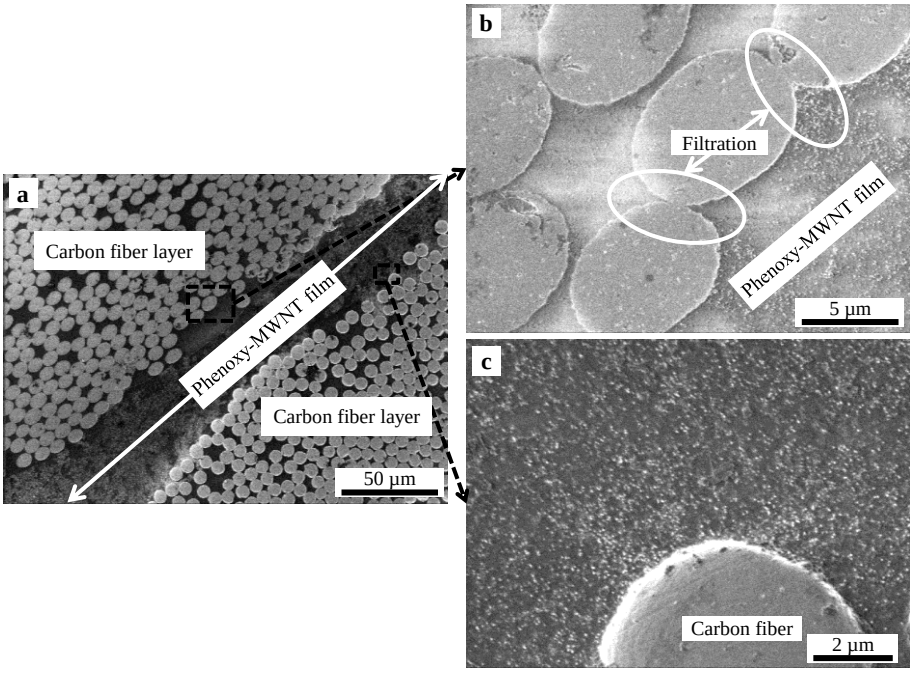

Fig. 13. SEM micrographs of the cross-section of the composite panel interleaved with films of phenoxy filled with 3 wt % MWNTs: (a) Overview of the interlayer area; (b) Interface between carbon fiber fabric and nanocomposite film; (c) MWNT dispersion near a carbon fiber fabric.

After demonstration of processability of composite panels interleaved with nanocomposite films, influence of thermoplastic and MWNTs distributed in the epoxy resin matrix on interlaminar fracture toughness has been evaluated. Incorporation of thermoplastic films in the composite preform plays a crucial role on mode I fracture toughness measured by DCB test. On the contrary to 40 µm thick PES films slightly decreasing the energy release rate required for crack propagation (G_{IC}), the same phenoxy content improves G_{IC} by around 100 % as compared to the reference panel (**Fig. 14**). Crack propagation is still better hindered when thickness of the phenoxy film is increased up to 80 µm (260 % increase of G_{IC}).

Toughening of composites interleaved with phenoxy films is an additional advantage of phenoxy beyond excellent nanofiller dispersion and improved distribution in epoxy resin for its exploitation in place of PES as carrier to disperse nanofillers into the matrix of composites processed by RTM. However, the limited MWNT content subsisting locally after interdiffusion in the matrix of the composite interleaved with nanocomposite films containing 3 wt % MWNTs has no significant additional effect on G_{IC}, which is already considerably increased thanks to phenoxy. Even if G_{IC} is drastically increased by phenoxy, it must be remarked that the same improvement has not been observed for other mechanical properties like CAI or ILSS. Additional measurements of crack propagation in mixed-mode should lead to evaluation of G_{IIC} and better understanding of the involved mechanisms.

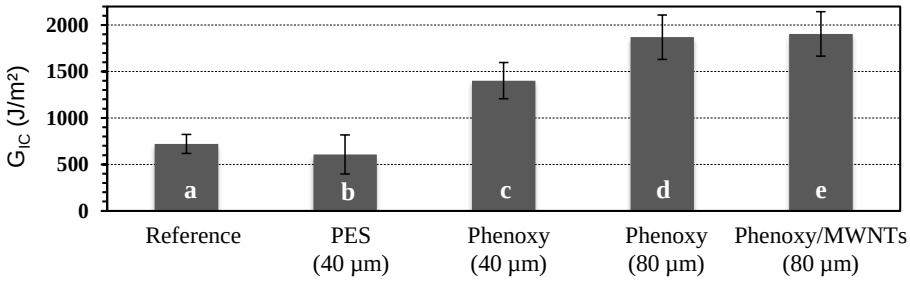

Fig. 14. Energy release rate required for crack propagation in mode I (G_{IC}) of a composite panel (a) without thermoplastic films and with (b) 40 µm thick PES films (c), 40 µm thick phenoxy films, (d) 80 µm thick phenoxy films and (e) 80 µm thick films of phenoxy filled with 3 wt % MWNTs.

It must be also noticed that even if higher phenoxy amounts in the crack propagation plane contribute to increase interlaminar fracture toughness, phase inversion has to remain limited in the interlaminar region in order to preserve thermomechanical and chemical properties of the thermoset network and thinner films could thus be preferred. Even if the global thermoplastic concentration in the composite matrix was fixed to 16 wt % and is below the critical composition generating phase inverted morphologies in phenoxy-RTM6 resin blends, the composition gradient remaining through the panel thickness after interdiffusion is responsible for the presence of a continuous phenoxy-rich phase around the initial location of the 80 µm thick films. The cavity observable along the phenoxy film location after solvent etching (**Fig. 15.a**) evidences this continuous phenoxy-

rich phase subsisting locally over an interval from 10 to 20 µm, which may be due to phase inversion or even pure phenoxy unaffected by the resin precursors.

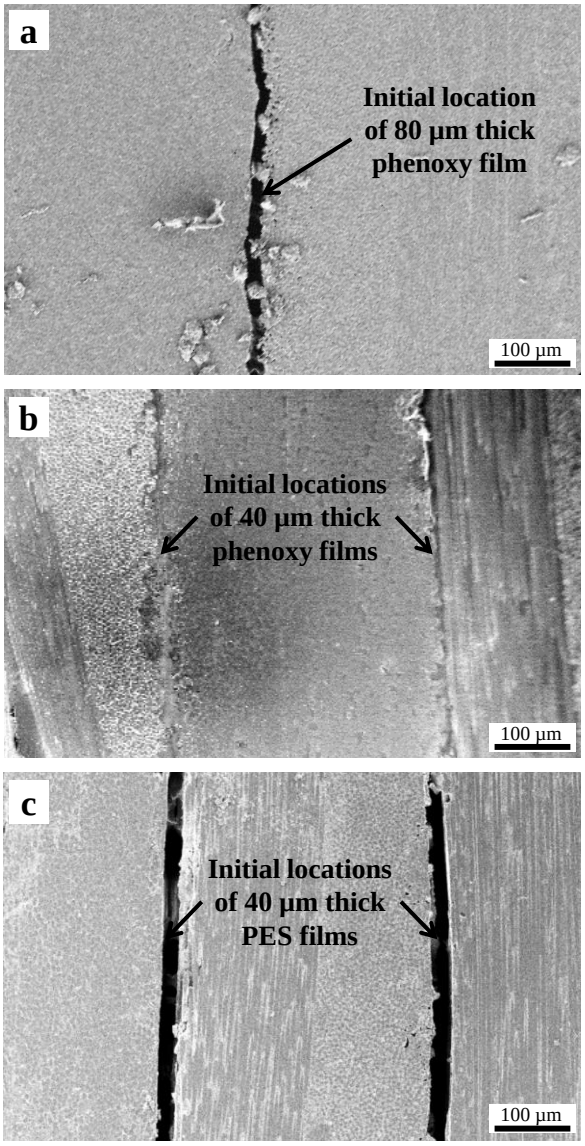

Fig. 15. SEM micrographs of the solvent etched cross-sections of composite panels interleaved with phenoxy films having a thickness of (a) 80 µm (every two interlayers) and (b) 40 µm (each interlayer) and (c) with PES films having a thickness of 40 µm (each interlayer).

The same global phenoxy amount is added to the composite matrix by replacing 80 µm thick films inserted every two layers by 40 µm thick films of phenoxy placed at each interlayer in the preform but the lower local phenoxy content induced by these thinner films ensure a continuous epoxy resin-rich phase everywhere in the panel. Indeed, **Fig. 15.b** shows that solvent etching does not affect specimen integrity and thus that phase inversion is prevented with 40 µm films. In addition to control of film thickness, selection of an adequate thermoplastic is also essential to limit extent of phase inversion like demonstrated by comparing the cross-sections of composites interleaved with 40 µm thick films of phenoxy or PES after solvent etching respectively in **Fig. 15.b** and **Fig. 15.c**. The SEM micrographs reveal that; in contrast with 40 µm thick films of phenoxy, PES films of the same thickness do not lead to a continuous epoxy resin-rich phase through the entire panel but to areas with phase inversion or pure PES due to the limited swelling of PES and the lower critical composition leading to phase inversion in PES-epoxy resin blends.

In order to fully understand the role of fibers on the distribution of the film components into the composite matrix and determine if phenoxy is able to diffuse through the carbon fabrics, an additional panel was processed with 80 µm thick films of pure phenoxy placed every two interlayers in the preform but without phenoxy film in the mid-plane. Indeed, filtering effect of the preform fabrics on apparent MWNT migration has been demonstrated but carbon fiber layers could also potentially influence thermoplastic distribution and thus play a considerable role on composite properties. With the selected stacking sequence, no phenoxy film is present in the crack initiation plane with the polyimide insert. Nevertheless, the failure surface observed by SEM after DCB test and solvent etching is rougher for the composite panel containing phenoxy (**Fig. 16.b**) than for the reference panel (**Fig. 16.a**). Moreover, despite absence of phenoxy film in the initial crack propagation plane, G_{IC} (890 J/m^2) is increased by about 25 % as compared to the reference panel. Such findings seem to indicate presence of phenoxy in the plane without toughener and suggest thus that apparent migration of phenoxy through the carbon fibers is less hindered than in the case of MWNTs and is locally possible through all the fabric thickness. Even if access of nanofiller to the core of the carbon fiber fabrics is prohibited, the composite laminate can thus benefit from the thermoplastic effect in these areas.

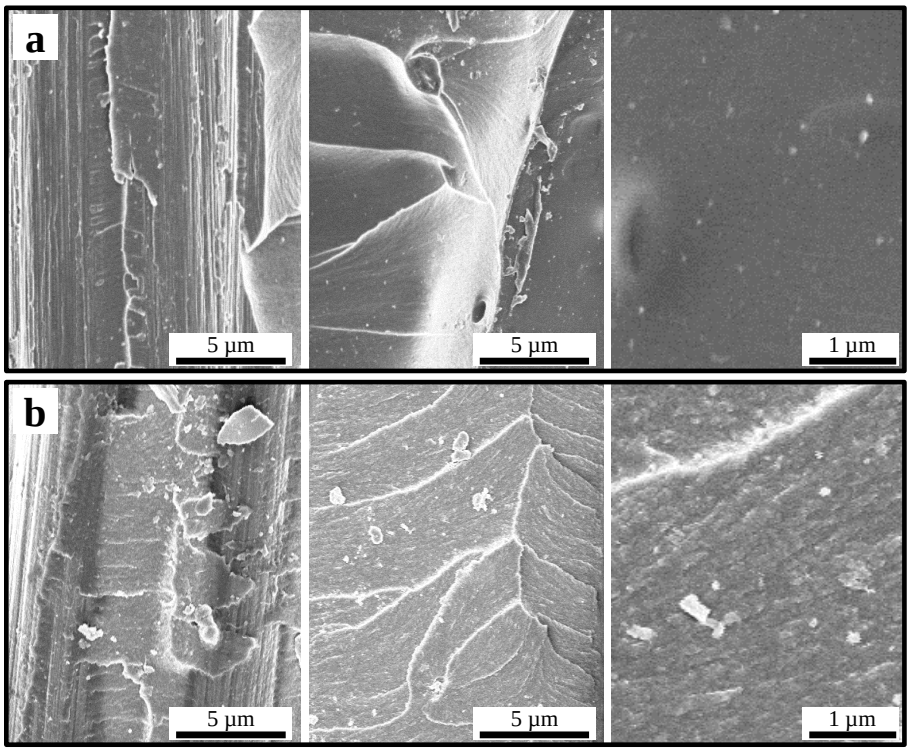

Fig. 16. SEM micrographs of the etched DCB failure surface of (a) the reference panel made of RTM6 resin reinforced with carbon fibers and (b) the composite panel with 80 µm phenoxy interleaves in the plane without phenoxy film.

4. Conclusions

Nanocomposites filaments filled with MWNTs and organomodified clay have demonstrated the potential of thermoplastics being soluble in the RTM6 resin precursors to deliver both tubular and lamellar nanofillers in the epoxy resin before crosslinking. The phenoxy nanocomposites, whatever the nanofiller concentration, allow the delivery of nanoparticles and thermoplastic in the resin on a distance interval of several times the initial filament diameter. Otherwise, the PES nanocomposite generates composition gradients with a larger inhomogeneity due to slower diffusion of the RTM6 resin precursors in the thermoplastic matrix. In both cases, a nanofiller distribution similar to the thermoplastic distribution was observed while no effect of the nanofiller on the thermoplastic distribution was evidenced. A

mechanism controlled by the thermoplastic swelling has been proposed to explain apparent migration of MWNTs and layered clay epoxy resin.

Using phenoxy as matrix for a 100 µm diameter nanocomposite filament, the composition gradient in the RTM6 resin leads to morphologies with nanofillers dispersed in the continuous epoxy phase through the entire interdiffusion zone once phase separation takes place. This morphology is guaranteed by local phenoxy contents below 30 wt % and location of MWNTs being thermodynamically favored into epoxy resin (see Chapter 5). Both nanofillers and phenoxy nodules can thus be distributed and dispersed in the epoxy resin using a nanocomposite as carrier for delivery of nanoparticles. The microstructure gradient induced using PES as nanocomposite matrix is in contrast responsible for local phase inversion or glassy PES subsisting around the location of the filament center. Even if PES is less adapted than phenoxy for nanofiller distribution into RTM6 resin on a large distance interval, both thermoplastics can be exploited as nanocomposite matrices to control the local and global nanofiller contents in the epoxy resin by adjusting the nanofiller concentration, the temperature treatment or the filament diameter.

Moreover, the developed concept is transposable to production of composite interleaved with nanocomposite films processed by RTM like shown for phenoxy filled with MWNTs. The proposed method allows to disperse and distribute nanofillers in the interlaminar region thanks to swelling of the thermoplastic carrier. However, even if thermoplastic can migrate through the carbon fabrics, the filtrating effect of the carbon fibers prevents penetration of MWNTs through the entire fabric layers. Finally, influence of thermoplastic and nanocomposite films on one property of the composite panels, G_{IC}, has been evaluated and has demonstrated the positive effect of phenoxy on mode I interlaminar fracture toughness while PES and MWNTs does not lead to any significant improvement.

References

[1] Thanomsilp C, Hogg PJ. Interlaminar fracture toughness of hybrid composites based on commingled filament fabrics. Composites Science and Technology 2005;65(10):1547-63.
[2] Hogg PJ. Toughening of thermosetting composites with thermoplastic fibers. Materials Science and Engineering A 2005;412(1-2):97-103.

[3] Beier U, Wolff-Fabris F, Fischer F, Sandler JKW, Altstädt V, Hulder G, Schmachtenberg E, Spanner H, Weimer C, Roser T, Buchs W. Mechanical performance of carbon fiber-reinforced composites based on preforms stitched with innovative low-melting temperature and matrix soluble thermoplastic filaments. Composites Part A: Applied Sc. and Manufact. 2008; 39(9):1572-81.
[4] Beier U, Sandler JKW, Altstädt V, Spanner H, Weimer C. Mechanical performance of carbon fiber-reinforced composites based on stitched and bindered preforms. Composites: Part A 2009;40(11):1756-63.
[5] Carter JT, LoFaro C, Maskell RK, McGrail PT. Flexible polymer element as toughening agent in prepregs. U.S. Pat. Appl. Publ. US 2004/0041128 A1, 2004
[6] Wong DWY, Lin L, McGrail PT, Peijs T, Hogg PJ. Improved fracture toughness of carbon fiber/epoxy composite laminates using dissolvable thermoplastic fibers. Composites Part A: Applied Science and Manufacturing 2010;41(6):759-67.
[7] An X, Ji S., Tang B, Zhang Z, Yi XS. Toughness improvement of carbon laminates by periodic interleaving thin thermoplastic films. Journal of Materials Science Letters 2002;21(22):1763-5.
[8] Yun NG, Won YG, Kim SC. Toughening of carbon fiber/epoxy composite by inserting polysulfone film to form morphology spectrum. Polymer 2004;45(20):6953-8.
[9] Naffakh M, Dumon M, Gérard JF. Study of a reactive epoxy-amine resin enabling in situ dissolution of thermoplastic films during resin transfer molding for toughening composites. Composites Science and Technology 2006;66(10):1376-84.
[10] Mortimer S, Cawse JL. A thermoplastic toughening material and related method. PCT Int. Appl. Publ. WO 2007/110617 A1, 2007.
[11] LoFaro C, Abusafieh A, Webb WE, Doyle M. Resin-soluble veil for composite materials. U.S. Pat. Appl. Publ. US 2006/0252334 A1, 2006.
[12] Gojny FH, Wichmann MHG, Fiedler B, Bauhofer W, Schulte K. Influence of nano-modification on the mechanical and electrical properties of conventional fibre-reinforced composites. Composites Part A: Applied Science and Manufacturing 2005;36(11):1525-35.
[13] Bekyarova E, Thostenson ET, Yu A, Itkis ME, Fakhrutdinov D, Chou TW, Haddon RC. Functionalized single-walled carbon nanotubes for carbon fiber-epoxy composites. Journal of Physical Chemistry C 2007;111(48):17865-71.
[14] Fan Z, Santare MH, Advani SG. Interlaminar shear strength of glass fiber reinforced epoxy composites enhanced with multi-walled carbon nanotubes. Composites Part A: Applied Science and Manufacturing 2008;39(3):540-554.
[15] Zhou Y, Pervin F, Lewis L, Jeelani S. Fabrication and characterization of carbon/epoxy composites mixed with multi-walled carbon nanotubes. Materials Science and Engineering A 2008;475(1-2):157-65.
[16] Fernberg P, Nilsson G, Joffe R. Piezoresistive performance of long-fiber composites with carbon nanotube doped matrix. Journal of Intelligent Material Systems and Structures 2009;20(9):1017-1023.

[17] Gao L, Thostenson ET, Zhang Z, Chou TW. Sensing of damage mechanisms in fiber-reinforced composites under cyclic loading usin carbon nanotubes. Advanced Functional Materials 2009;19(1):123-30.
[18] Kim M, Park YB, Okoli OI, Zhang C. Processing, characterization, and modeling of carbon nanotube-reinforced multiscale composites. Composites Science and Technology 2009;69(3-4):335-42.
[19] Chandrasekaran VCS, Advani SG, Santare MH. Role of processing on interlaminar shear strength enhancement of epoxy/glass fiber/multi-walled carbon nanotube hybrid composites. Carbon 2010;48(13):3692-9.
[20] Wang S, Qiu J. Enhancing thermal conductivity of glass fiber/polymer composites through carbon nanotubes incorporation. Composites Part B: Engineering 2010;41(7):533-6.
[21] De Greef N, Gorbatikh L, Godara A, Mezzo L, Lomov SV, Verpoest I. The effect of carbon nanotubes on the damage development in carbon fiber/epoxy composites. Carbon 2011;49(14):4650-64.
[22] Rana S, Alagirusamy R, Joshi M. A review on carbon epoxy nanocomposites. Journal of Reinforced Plastics and Composites 2009;28(4):461-87.
[23] Lin LY, Lee JH, Hong CE, Yoo GH, Advani SG. Preparation and characterization of layered silicate/glass fiber/epoxy hybrid nanocomposites via vacuum-assisted resin transfer molding (VARTM). Composites Science and Technology 2006;66(13):2116-25.
[24] Schubel PJ, Johnson MS, Warrior NA, Rudd CD. Characterisation of thermoset laminates for cosmetic automotive applications: Part III – Shrinkage control via nanoscale reinforcement. Composites Part A: Applied Science and Manufacturing 2006;37(10):1757-72.
[25] Fan Z, Hsiao KT, Advani SG. Experimental investigation of dispersion during flow of multi-walled carbon nanotube/polymer suspension in fibrous porous media. Carbon 2004;42(4):871-6.
[26] Baets J, Godara A, Devaux J, Verpoest I. Toughening of polymerized cyclic butylene terephthalate with carbon nanotubes for use in composites. Composites Part A: Applied Science and Manufacturing 2008;39(11):1756-61.
[27] Bekyarova E, Thostenson ET, Yu A, Kim H, Gao J, Tang J, Hahn HT, Chou TW, Itkis ME, Haddon RC. Multiscale carbon nanotube-carbon fiber reinforcement for advanced epoxy composites. Langmuir 2007;23(7):3970-4.
[28] Zhu J, Imam A, Crane R, Lozano K, Khabashesku VN, Barrera EV. Processing a glass fiber reinforced vinyl ester composite nanotube enhancement of interlaminar shear strength. Composites Science and Technology 2007;67(7-8):1509-17.
[29] Garcia EJ, Wardle BL, Hart AJ, Yamamoto N. Fabrication and multifunctional properties of a hybrid laminate with aligned carbon nanotubes grown *In Situ*. Composites Science and Technology 2008;68(9):2034-41.
[30] Qian H, Bismarck A, Greenhalgh ES, Kalinka G, Shaffer MSP. Hierarchical composites reinforced with carbon nanotube grafter fibers: The potential assessed at the single fiber level. Chemisty of Materials 2008;20(5):1862-9.

[31] Wardle BL, Saito DS, Garcia EJ, Hart AJ, Guzmán de Villoria R, Verploegen EA. Fabrication and characterization of ultrahigh-volume-fraction aligned carbon nanotube–polymer composites. Advanced Materials 2008;20(14):2707-14.
[32] Cebeci H, Guzman de Villoria R, Hart AJ, Wardle BL. Multifunctional properties of high volume fration aligned carbon nanotube polymer composites with controlled morphology. Composites Science and Technology 2009:69(15-16):2649-56.
[33] Sager RJ, Klein PJ, Lagoudas DC, Zhang Q, Liu J, Dai L, Baur JW. Effect of carbon nanotubes on the interfacial shear strength of T650 carbon fiber in an epoxy matrix. Composites Science and Technology 2009;69(7-8):898-904.
[34] Lomov SV, Gorbatikh L, Kotanjac Z, Koissin V, Houlle M, Rochez O, Karahan M, Mezzo L, Verpoest I. Compressibility of carbon woven fabrics with carbon nanotubes/nanofibres grown on the fibres. Composites Science and Technology 2011;71(3):315-25.
[35] Godara A, Gorbatikh L, Kalinka G, Warrier A, Rochez O, Mezzo L, Luizi F, van Vuure AW, Lomov SV, Verpoest I. Interfacial shear strength of a glass fiber/epoxy bonding in composites modified with carbon nanotubes. Composites Science and Technology 2010;70(9):1346-52.
[36] Mezzo L, Godara A, Rochez O, Luizi F, Warrier A, Verpoest I, Lomov S. Method for the preparation of a reinforced thermoset polymer composite. PCT Int. Appl. WO 2010/007163 A1, 2010.
[37] Warrier A, Godara A, Rochez O, Mezzo L, Luizi F, Gorbatikh L, Lomov SV, VanVuure AW, Verpoest I. The effect of adding carbon nanotubes to glass/epoxy composites in the fibre sizing and/or the matrix. Composites Part A: Applied Science and Manufacturing 2010;41(4):532-8.
[38] Gao L, Chou TW, Thostenson ET, Zhang Z, Coulaud M. *In situ* sensing of impact damage in epoxy/glass fiber composites using percolating carbon nanotube networks. Carbon 2011;49(10):3382-5.
[39] Gorbatikh L, Lomov SV, Verpoest I. Nano-engineered composites: a multiscale approach for adding toughness to fibre reinforced composites. Procedia Engineering 2011;10:3252-8.
[40] Kamae T, Drzal LT. Carbon fiber/epoxy composite property enhancement through incorporation of carbon nanotubes at the fiber–matrix interphase – Part I: The development of carbon nanotube coated carbon fibers and the evaluation of their adhesion. Composites Part A: Applied Science Manufacturing 2012;43(9):1569-77.
[41] Song YS. Multiscale fiber-reinforced composites prepared by vacuum-assisted resin transfer molding. Polymer Composites 2007;28(4):458-61.
[42] Luinge H, Wachinger G. Method for the production of a fiber composite component, and semifinished textile product therefor. PCT Int. Appl. WO 2010/020237 A2, 2010.

[43] Osterrieth C. Polyéthersulfone chargé en nanotubes de carbone dans une résine époxy. Observations morphologiques et propriétés électriques résultantes. Travail de fin d'études. Université catholique de Louvain, 2011.
[44] Ferrari AC, Robertson J. Raman spectroscopy of amorphous, nanostructured, diamond-like carbon, and nanodiamond. Philosophical Transactions of the Royal Society A: Mathematical, Physical and Engineering Sciences 2004;362,2477–512.

CONCLUSIONS PART 2

The second part of the present work demonstrates that a thermoplastic like phenoxy can be used to deliver nanofillers into epoxy resin thanks to its good solubility in epoxide and diamine precursors and favored interdiffusion shown in Part 1. Different stages have been considered to validate the proposed method:

- Nanocomposites have first been processed by dispersing MWNTs or organomodified clay into thermoplastic by melt compounding. Fine dispersion and homogeneous distrubtions of both tubular and lamellar nanofillers have been obtained and intercalated-exfoliated nanostructures have been achieved with organoclay.
- Microstructures induced by curing of ternary blends prepared with the nanocomposite and RTM6 resin have then been controlled and have shown that both thermoplastic nodules and nanofillers can be dispersed in epoxy resin. Dispersion of the nanofillers conserved in the phase-separated blends and their location in the epoxy resin-rich phase have been observed.
- Finally, local thermoplastic and MWNTs contents resulting from thermal treatment of a nanocomposite filament in RTM6 resin have been evaluated. Distribution of MWNTs in epoxy resin has been evidenced on basis of the composition gradients assessed in these model systems while no important effect of nanoparticle structure and concentration on the composition profiles has been identified.

The mechanisms responsible for nanofiller dispersion and distribution in epoxy resin have been discussed. Delivery of nanofillers in epoxy resin has been explained by interdiffusion between thermoplastic macromolecules and resin precursors leading to swelling of the nanocomposite and consequently to apparent migration of the entangled nanoparticles. Exclusive location of MWNTs in the epoxy resin-rich phase of the blend has been attributed to desorption of thermoplastic chains from the MWNT surface by the resin precursors resulting in dispersion of MWNTs in epoxy resin, which minimizes interfacial energy when phase separation takes place.

The concept developed in this study exploiting soluble thermoplastic as nanofiller carrier is transposable to distribute nanofillers in the matrix of composites processed by RTM. Although delivery of nanoparticles is

hindered due to a filtering effect by the fabrics, nanocomposite interleaves disposed into the composite preform ensure dispersion of thermoplastic and nanofillers through the interlayer thickness. Depending on the nanocomposite assembly included in the preform, a local action of the nanofillers or a global effect in the entire composite structure can be priviledged. Phenoxy is recommended as nanocomposite matrix to reduce composition inhomogeneities through the thickness of composite laminates and to maintain a continuous epoxy resin phase. Even if nanofiller delivery is also possible with PES, larger composition gradients subsist and phase inversion is more probable with this thermoplastic matrix. An adapted thermal cycle is also needed to optimize thermoplastic and nanofiller distributions. A limited injection temperature is required to prevent nanocomposite dissolution during resin injection and avoid thermoplastic and nanofiller flushing by the resin flow leading to important composition inhomogeneity between resin inlet and outlet. Then, once the mold is filled, a rapid temperature increase is advised to improve thermoplastic and nanofiller distributions into RTM6 resin. Several parameters like thermal profile, thermoplastic choice, nanocomposite content and assembly or amount of nanofiller dispersed in thermoplastic allow thus to control nanofiller distribution in epoxy resin. Moreover, soluble thermoplastics are not only suitable as carrier for delivery of MWNTs and layered clay in composite matrices but also of other kinds of fillers and additives. The concept investigated is thus a promising method to produce customized composites by LCM.

Overall conclusions and prospects

The present study intended to develop a method to incorporate additives, more particularly a thermoplastic polymer and nanoparticles, in the brittle matrix of composite laminates processed by RTM. Therefore, a method using thermoplastic to disperse nanofillers by melt blending prior to incorporation of the produced nanocomposite in the composite preform has been proposed. This approach aims to combine delivery of a thermoplastic phase and nanofillers in epoxy resin used in aeronautical structures like the RTM6 resin.

The objective of this work was to demonstrate that soluble thermoplastics can act as carrier for dispersion and distribution of nanoparticles like carbon nanotubes and layered clay into epoxy resin. This original concept exploited for nanofiller delivery into epoxy resin has been investigated for model systems based on nanocomposite filaments in contact with the reactive resin formulation. Influence of thermoplastic dissolution and interdiffusion with the resin precursors on nanofiller distribution in epoxy resin has been examined like microstructures generated by RIPS during the cure cycle.

The main results of the different stages that have been required to validate the concept, to understand the involved mechanisms and to perfect the method are first summarized in the final section of this document. Then, perspectives of this work are presented and possible developments are suggested.

1. Concept development and validation

The study has been divided in two main parts to evidence that PES or phenoxy can be exploited as nanofiller carrier in epoxy resin. The behavior of these thermoplastics has been first investigated in epoxide and diamine precursors and in reactive resins. Both amorphous thermoplastics were selected for their singular chemical structures leading to important disparities in terms of in situ dissolution, interdiffusion with resin precursors, composition gradient and morphology spectrum induced by a thermoplastic filament in epoxy resin. Then, a two-stage method has been proposed to deliver nanofillers in the epoxy resin-rich phase of the blend by dispersion of nanoparticles in thermoplastic followed by thermal treatment of the produced nanocomposite in epoxy resin and has been explored. Since thermoplastic-epoxy resin blends and interdiffusion mechanisms have already been previously studied for several systems, originality of this work

lies mainly in this second part of the study inspecting incorporation of nanofillers. Indeed, dispersion, distribution and location of carbon nanotubes and layered clay have been examined and explained in the ternary blend resulting from thermoplastic swelling during interdiffusion between resin precursors and a nanocomposite filament and phase separation during resin crosslinking.

In the first part of the study, different epoxy resin formulations adapted to applications requiring high thermomechanical performances and blends of these resins with phenoxy and PES have been characterized. The mechanisms driving interdiffusion between epoxy resin precursors and both thermoplastics have then been investigated by a combination of experimental and numerical simulation methods (**Fig. 1**). Thermoplastic filaments in contact with epoxide and diamine precursors have been used to monitor diffusion of resin precursors into thermoplastic while apparent migration of thermoplastic chains outwards the filament core has been followed with filament filled with MWNTs used as markers (**Fig. 1.a**). A favored penetration of the low molecular weight resin monomers has been demonstrated as well as a higher mobility of the lower T_g phenoxy as compared to PES. Apparent migration of thermoplastic macromolecules controlled by precursor diffusion leading to thermoplastic swelling has been experimentally evidenced and confirmed by diffusion coefficients evaluated by molecular dynamics (**Fig. 1.b**).

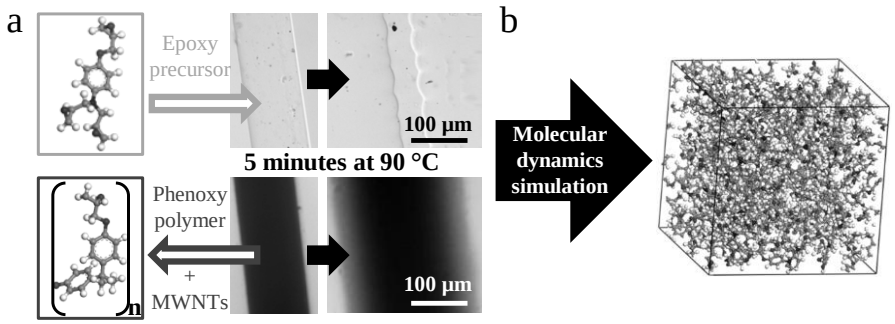

Fig. 1. Illustration summarizing the study of interdiffusion between a resin precursor and a thermoplastic: (a) Experimental study evaluating diffusion of resin precursors and apparent migration of thermoplastic with model systems containing respectively a thermoplastic filament and a nanocomposite filament filled with MWNTs; (b) 3D cell with thermoplastic oligomers and epoxide or diamine monomers used for molecular dynamics simulation.

Important disparities of interdiffusion range in the various thermoplastic-precursors systems allow to explain differences of temperature intervals during which thermoplastic dissolution takes place in a resin precursor determined on basis of heat flows measured during dynamic heating. Since interdiffusion between epoxy resin and thermoplastic has also to take into account the crosslinking reaction, dissolution of PES and phenoxy filaments and composition profiles induced by their thermal treatment have also been considered in reactive resins. Faster dissolution has been observed with phenoxy due to its favored swelling by resin precursors. Distribution of phenoxy on larger distances and thus lower local phenoxy contents have also been evidenced once interdiffusion is stopped by the cure reaction like displayed in **Fig. 2** comparing phenoxy and PES concentration gradients induced by a 100 µm diameter filament into RTM6 resin at 120 °C and the corresponding local microstructures. By choosing this filament dimension, a poor distribution of PES macromolecules achieved in epoxy resin with the inner core of the PES filament remaining unaffected by the RTM6 resin precursors has been demonstrated while phenoxy has shown dissolution rapidly completed with local phenoxy contents lower than 30 wt % subsisting in the resin. A microstructure with phenoxy-rich nodules dispersed in the continuous epoxy resin-rich phase is thus conserved for higher global phenoxy contents added in the resin as compared to PES. Moreover, blend microstructures have shown that phase inversion occurs at higher phenoxy concentration (more than 30 wt % against around 15 wt % for PES). Nevertheless, PES distribution can also be improved in some extent by adapting the resin formulation and optimizing the cure cycle.

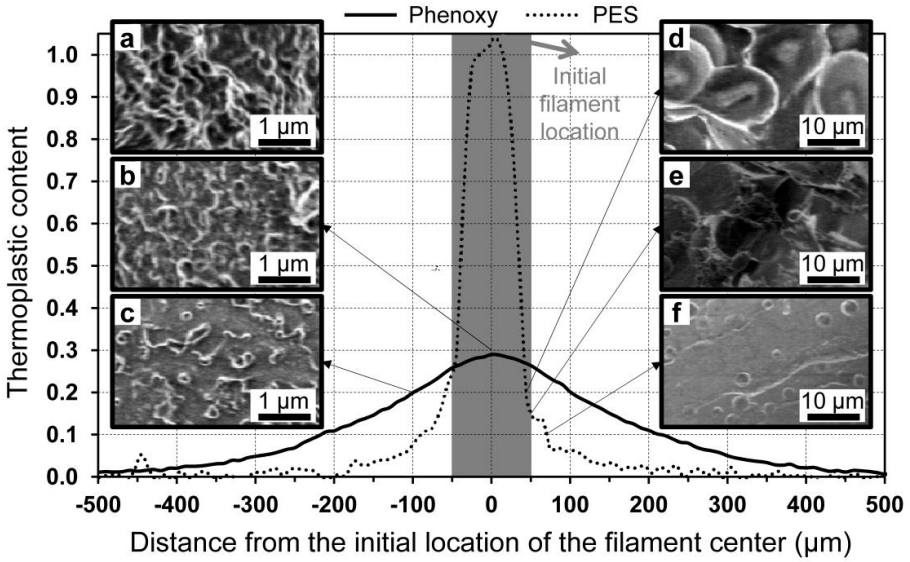

Fig. 2. PES and phenoxy concentration profiles in RTM6 resin determined by Raman spectroscopy after a 120 °C isotherm applied to a 100 µm diameter filament and blend microstructures corresponding to local compositions: (a) 20 wt %, (b) 30 wt % and (c) 40 wt % phenoxy; (d) 10 wt %, (e) 15 wt % and (f) 20 wt % PES.

Since phenoxy presents the faster dissolution and the best distribution in the crosslinked resin, this thermoplastic appears as an ideal choice for delivery of nanoparticles in epoxy resin and has consequently been further tested as nanocomposite matrix in the second part of the study. Unfunctionalized MWNTs and organomodified clay have been successfully dispersed in phenoxy by melt processing. Fine dispersion of individual MWNTs homogenously distributed in the phenoxy matrix has been obtained (**Fig. 3.a**) like dispersion of layered clay with a mixed intercalated-exfoliated morphology (**Fig. 3.b**). Global nanocomposite properties have confirmed the quality of the nanofiller dispersion and distribution in phenoxy.

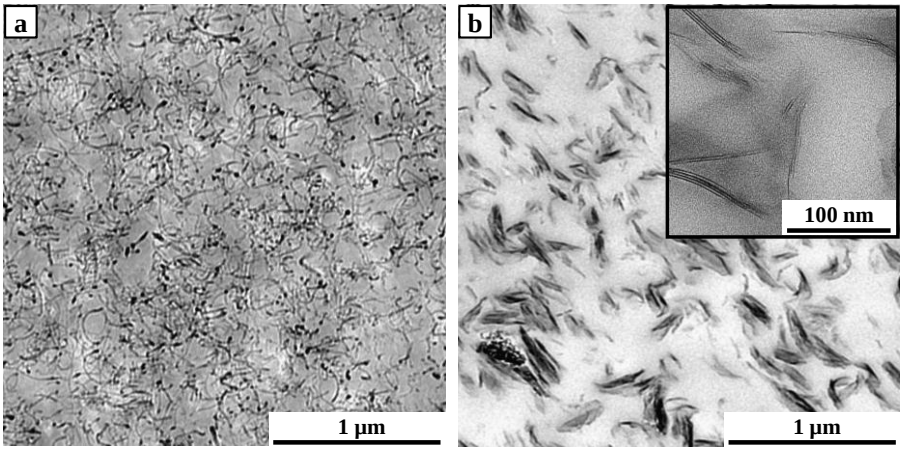

Fig. 3. TEM micrographs illustrating the dispersion of 5wt % (a) MWNTs and (b) organomodified clay (Cloisite 30B) in phenoxy.

This work has then studied composition gradients and microstructures induced by the processed nanocomposites in epoxy resin. Delivery of MWNTs has been examined in model systems based on a nanocomposite filament in RTM6 resin and compared to thermoplastic distribution. The composition profiles determined by Raman spectroscopy have revealed that nanofillers have no influence on thermoplastic distribution (**Fig. 4.a**) and that MWNT and phenoxy concentration gradients have similar shapes (**Fig. 4.b**). Delivery of nanofillers in epoxy resin by in situ dissolution of nanocomposite and interdiffusion has been verified on basis of these results and has been explained by swelling of the thermoplastic carrier by resin precursors with nanoparticles remaining entangled with the polymers macromolecules. The same behavior has been observed for tubular and lamellar nanofillers since both kinds of nanoparticles present at least one dimension several orders of magnitude larger than the gyration radius of the thermoplastic macromolecules and are thus not able to migrate in the swollen thermoplastic. Finally, transposition of the concept to process of composite by RTM has been demonstrated by interleaving their preform with nanocomposite films.

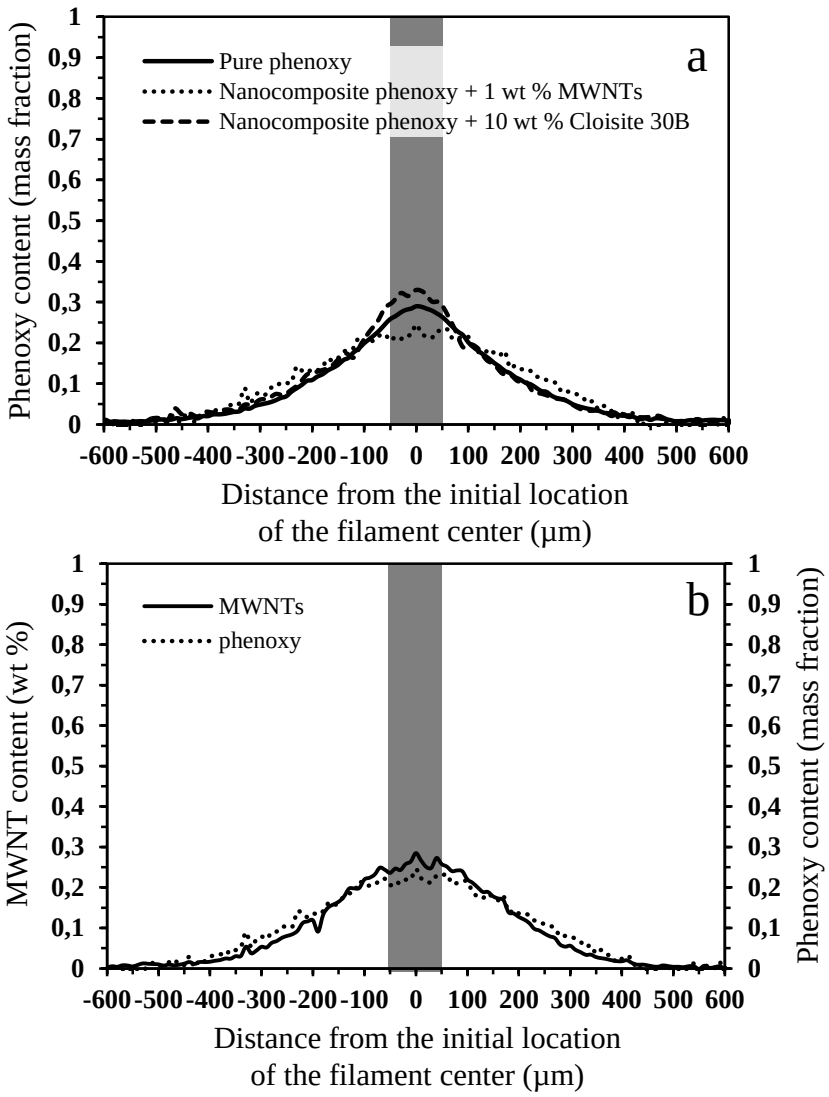

Fig. 4. Composition profiles induced by a 100 µm diameter filament in RTM6 resin after interdiffusion at 120 °C determined by Raman spectroscopy: (a) Phenoxy distribution for a filament of pure phenoxy, phenoxy filled with 1 wt % MWNTs and phenoxy filled with 10 wt % Cloisite 30B; (b) phenoxy and MWNT distributions for a nanocomposite filament containing 1 wt % MWNTs.

Once phase separation takes place in the ternary blends induced by interdiffusion due to resin crosslinking, dispersion of MWNTs is conserved and MWNTs are exclusively located in the epoxy resin-rich phase (**Fig. 5.a**).

These microstructures have been explained by desorption of phenoxy chains from the MWNT surface and adsorption of resin precursors decreasing interfacial energy. Similarly, clay dispersion is maintained in ternary blends and can lead to microstructures with both phenoxy nodules and intercalated or exfoliated clay platelets dispersed in a continuous epoxy resin network (**Fig. 5.b**).

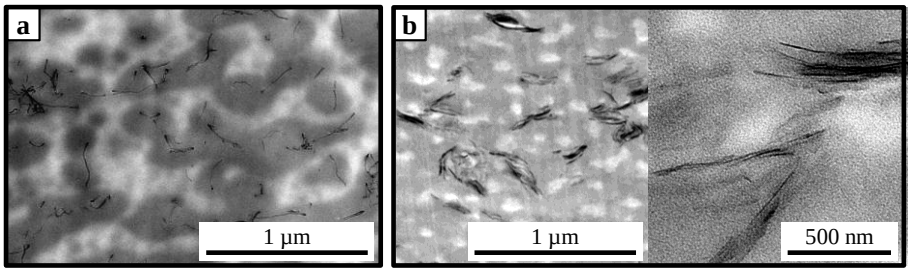

Fig. 5. TEM micrographs of RTM6 resin blended with (a) 30 wt % phenoxy filled with 3 wt % MWNTs and (b) 20 wt % phenoxy filled with 10 wt % Cloisite 30B.

2. Perspectives

This work has demonstrated that phenoxy or PES can be exploited to disperse and distribute MWNTs or, in the case of the phenoxy carrier, organomodified clay into epoxy resin. Transposition of the concept to RTM-processed composites containing a preform made of carbon fiber fabrics interleaved with nanocomposite films has evidenced a joined delivery of a phenoxy phase and MWNTs in the epoxy resin matrix. Consequently, contribution of both thermoplastic and nanofillers for improvement of physical or mechanical properties of the composite was desired. Nevertheless, evaluation of G_{IC} has shown that even if phenoxy films increases interlaminar fracture toughness, the opposite effect is obtained with PES while influence of MWNTs remains limited. Therefore, several developments are proposed in this sub-section to apply the concept to other systems and potentially improve fracture toughness or other properties by modifying the thermoplastic carrier, the nanofillers, the epoxy resin matrix, the content and form of nanocomposite elements, the preform structure or the process conditions. All these prospects detailed hereafter shows that the present work opens the door to production of customized composites.

Concerning thermoplastic carriers, only two amorphous thermoplastics have been considered in the study. Nevertheless, other thermoplastics, amorphous or even semi-crystalline, are all potential carriers that can lead from narrow to wide distributions of the filler depending on their ability to be dissolved into epoxy resin, which can vary from total insolubility to complete solubility. Phenoxy has effectively proved its benefit on G_{IC} like its excellent distribution into epoxy resin and presents thus remarkable attributes to be used as thermoplastic carrier in composites despite its limited T_g. In contrast, G_{IC} has not been enhanced with PES interleaves and has even been reduced with this amorphous thermoplastic, which had been selected for its high T_g and its excellent performances. Indeed, thin and weak thermoset-thermoplastic interfaces propagating fracture in composite panels are created by the PES with chlorinated chain ends used in the present study due to its poor affinity with epoxy resin and its low mobility, which are unfavorable for interdiffusion and chemical interactions. Other grades of PES with potentially reactive chain ends, PES functionalized with chemical groups improving its affinity with the epoxy network other high T_g-thermoplastics more miscible and interacting preferentially with epoxy resin should be more adapted as nanofiller carriers preventing G_{IC} drop and could thus be tested in a future work.

Concerning nanofillers, dispersion of MWNTs in phenoxy films incorporated in the composite preform has not conducted to a significant additional increase of G_{IC} as compared to neat phenoxy for a content of 3 wt % MWNTs in the nanocomposite. However, the global MWNT concentration in the composite matrix remains limited to less than 0.5 wt % with the stacking sequence used in this work. Dispersion of higher MWNT amounts in the ternary blend generated in the polymer matrix could be necessary to obtain the desired effect. Therefore, further investigations with nanocomposite films containing higher MWNT contents could be interesting developments even if nanoparticle concentration is limited to preserve a good nanofiller dispersion. Furthermore, even if only fracture toughness has been examined in the present study, other properties of the processed composite panel like electrical and thermal conductivities could also take advantage from the dispersed MWNTs and supplementary tests should be achieved in this direction. Further works could also focus on a wide range of other properties by dispersing different additives in the thermoplastic carrier. A composite panel interleaved with films of phenoxy filled with organomodified clay should similarly be produced and characterized to

determine the impact of layered clay on its mechanical performances but also on other properties of the composite potentially improved like barrier properties. Indeed such lamellar nanofillers could possibly reduce water uptake or sensitivity to solvent and enhance fire resistance. Delivery of MWNTs and layered clay in epoxy resin by a thermoplastic carrier has been demonstrated in this study but the concept could also be extended to other nanofillers or additives. In addition to study of composites modified with tubular and lamellar nanoparticles, influence of other fillers with different nature, shape or size could likewise be explored. Likelihood to obtain a synergistic effect by combining different kinds of particles, like for example nano- and micro-tougheners, is another avenue to prospect. Other toughening agents incorporated in the thermoplastic like core-shell particles, block copolymers or elastomers are also interesting additives able to increase impact properties or fracture toughness of composites.

Concerning epoxy resin, RTM6 resin has been chosen to produce composite panels due to its specifications allowing process of composite structures qualified for aeronautic applications by RTM. Although this resin formulation induces good phenoxy distribution for moderate film thickness, dissolution of PES becomes rapidly incomplete in RTM6 resin for increasing dimensions of thermoplastic elements. Therefore, other resin formulations fulfilling requirements of high performance applications and more adapted than RTM6 resin for dissolution and distribution of PES or thermoplastic necessitating higher mobility of the resin precursors to promote interdiffusion have been suggested in this work. These epoxy resins formulated with a monoaromatic diamine as low molecular weight hardener could thus also be assessed as matrices of composite interleaved with PES films by adapting the thermal cycle used during RTM process. Indeed, higher reactivity of these resin imposes a reduction of the injection temperature easily achievable with these low viscosity resin.

Concerning content and form of thermoplastic or nanocomposite additives, selection of an optimal thickness of the nanocomposite films is required to boost effect of thermoplastic and nanofiller additives on the composite properties while limiting the formation of large areas with phase inversion or pure thermoplastic. Moreover, besides influence of nanocomposite content, it must also be remarked that narrow tapes (60 mm width) processed by melt compounding and film casting have been placed side by side in the interlayers between carbon fiber fabrics. This way of incorporation of home-

made thin films has been selected due to technical limitations but presents several disadvantages. Indeed, discontinuity and thickness inhomogeneity of the generated thin films can influence crack propagation and absence of porosity hinders diffusion of resin precursors to the thermoplastic core and decreases preform permeability. Therefore, insertion of continuous films or other elements presenting different shapes in the composite preform could be tested in order to determine if better methods can be proposed for nanocomposite introduction. Alternative forms of nanocomposite could be for example veils, non-woven fabrics, membranes or filaments stitched through the carbon preform or commingled with the carbon fibers.

Concerning the preform structure, in place of a global action of both thermoplastic and nanofillers on the composite properties thanks to periodic incorporation of nanocomposite everywhere in the preform, a local effect can be privileged. Nanocomposite insertion can indeed be focused towards locations of the laminate requiring specific performances by conceiving complex preforms. Moreover, only bulk properties of composite laminates processed by RTM have been evoked so far. However, potential improvement of surface properties is also a critical aspect that can take a leading role on composite performances in many cases. In this context, nanocomposite films placed at the preform surface could play a positive role on several properties like fire resistance by formation of a protective char layer during combustion, electrical conductivity by creation of a surface conductive pathway or shock resistance by absorption of impact energy. Thermoplastic or nanocomposites added to the surface of thermoset matrix laminates could also be exploited for welding of composite structures.

Concerning process conditions, different cure cycles adapted for RTM process could be tested to define the more appropriate thermal profile for optimization of composite properties and determine its correlation with thermoplastic and nanofiller distributions and the interlaminar microstructure. Finally, it can be noticed that transposition of the studied concept to process of composite by LRI and RTM has been demonstrated but could also be extended to other LCM technologies increasingly used nowadays like same qualified resin transfer molding (SQRTM) by introduction of nanocomposite in the prepreg.

Further investigations are planned in these directions with the goal to produce tailored carbon fiber laminates adapted to the desired application.